Contribution to the implementation of a process control system for continuous powder mixing

Xiaojuan Zhao

Université de Toulouse

THÈSE

En vue de l'obtention du

DOCTORAT DE L'UNIVERSITÉ DE TOULOUSE

Délivré par :

École Nationale Supérieure des Mines d'Albi-Carmaux conjointement avec l'INP Toulouse

---

Présentée et soutenue par :
Xiaojuan ZHAO

le mardi 26 novembre 2013

Titre :

Contribution to the implementation of a process control system for continuous powder mixing

---

École doctorale et discipline ou spécialité :
ED MEGEP : Génie des procédés et de l'Environnement

Unité de recherche :
Centre Rapsodee, CNRS - UMR 5302, Ecole des Mines d'Albi-Carmaux

Directeur(s) de Thèse :

Henri BERTHIAUX
Michel CABASSUD

Jury :

Francis COURTOIS, Professeur, AgroParisTech, Rapporteur
Khashayar SALEH, Professeur, Université de Technologie de Compiègne, Rapporteur
Bernard CUQ, Professeur, Université de Montpellier SupAgro, Président
Jean-Louis DIRION, Maître-Assistant HDR, Ecole des Mines d'Albi-Carmaux, Examinateur
Henri BERTHIAUX, Professeur, Ecole des Mines d'Albi-Carmaux, Directeur
Michel CABASSUD, Professeur, Université Paul Sabatier - Toulouse, Co-Directeur
Cendrine GATUMEL, Maître-Assistante, Ecole des Mines d'Albi-Carmaux, Invitée

ACKNOWLEDGEMENTS

My first and sincerely acknowledgement goes to both my supervisors Henri Berthiaux and Michel Cabassud for their guidance, continuous advice and encouragement during my PhD study. I'm grateful to Henri for his patience, motivation, knowledge and words that inspire and bring me to finish my thesis step by step. I thank Michel for his travels from Toulouse for my thesis meetings in Albi and his inspiring suggestions to my thesis research.

I would like to express my special thank to my tutor Jean-Louis Dirion for his help, support and encouragement especially at the end of my thesis. I would also like to thank my tutor Cendrine Gatumel for her help, support and kindness during my PhD study.

I would like to give gratitude to the technicians Denis, Laurent and Philippe of the laboratory Rapsodee who have helped me. I would like to thank my best friends Sarah, Nibal, and David for their spiritual support. I would like to thank Madame Fabienne Espitalier, Madame Anne-Marie Fontes, Madame Claudine Sablayrolles and Madame Rita Franco for their help and kindness to me. I would also like to thank the director of laboratory Rapsodee, Ange Nzihou, who has offered me extra two months' finance to let me finish my thesis. I would like to thank Fanny, William, Graciela, Jacqueline, Pierre-Marie, Baptiste and all other PhD students with whom I've had the pleasure to work.

Last but not least, I would like to thank my parents and sisters for their love and support.

ABSTRACT

Powder mixing is an essential operation in various industrial fields, such as pharmaceuticals, agro-food, cements, etc. Continuous powder mixing, as an alternative to conventional batch mixing, has attracted a lot of interest mainly due to its capacity in handling high volume manufacturing. This work aims at the contribution to the implementation of process control applications for powder mixing in a pilot-scale continuous mixer. Prior to developing process control strategies, new developments have been presented for better understanding continuous mixing of two components. Hold-up weight and relative hold-up weight distribution of each component in the whole mixer have been experimentally investigated under different operating conditions. An improved Markov chain model has been finally presented to predict the mean concentration of the mixtures obtained at the mixer's outlet. The implementation of a proportional-integral-derivative (PID) controller has been experimentally performed as an initial attempt to real-time control the homogeneity of the mixture produced. The rotational speed of the stirrer, identified as an important deciding factor towards the mixer's efficiency, has been considered as the manipulated variable. The closed-loop control is based on either the mean concentration or the relative standard deviation. The performances of the proposed closed-loops have been evaluated for continuous mixing subjected to step changes in feed rates of the mixer. Four case studies have been defined and presented. The main challenge in the process control system is the tuning of PID parameters. The performance of closed-loop control of either the mean concentration or the relative standard deviation has been compared to open-loop operation.

Key words: Continuous powder mixing, Implementation, Process control, Markov chain, PID controller, Closed-loop control

TITRE: Contribution à l'implémentation d'un système de contrôle-commande pour mélange de poudres en continu

RESUME

Le mélange de poudres est une opération essentielle dans divers domaines industriels, tels que les produits pharmaceutiques, agro-alimentaires, ciments, etc. Le mélange de poudres en continu, comme alternative intéressante au mélange conventionnel en batch, suscite beaucoup d'intérêt surtout en raison de sa capacité à gérer de grands volumes de production. Ce travail vise à contribuer à l'implémentation des applications de contrôle-commande. Avant de développer des stratégies de contrôle-commande, de nouveaux développements ont été présentés pour mieux comprendre le mélange continu de deux composants. La masse retenue et la répartition relative de la masse retenue de chaque composant dans le mélangeur ont été étudiées et prédites sous les différentes conditions opératoires. L'amélioration d'un modèle basé sur les chaînes de Markov a été finalement présentée pour prédire la concentration moyenne des mélanges obtenus à la sortie du mélangeur. L'implémentation d'un contrôleur PID a été expérimentalement réalisée comme une première tentative pour contrôler en temps réel l'homogénéité du mélange produit. La vitesse de rotation du mobile d'agitation, identifiée comme un facteur important influençant l'efficacité du mixer, a été considérée comme la variable manipulée. La commande en boucle fermée est basée soit sur la concentration moyenne, soit sur le coefficient de variation. Les performances des boucles fermées proposées ont été évaluées pour le mélange continu subi à des changements d'échelon dans les débits d'alimentation du mélangeur. Quatre études de cas ont été définies et présentées. Le défi principal dans le système de contrôle-commande est le réglage des paramètres PID. La performance de commande en boucle fermée soit de la concentration moyenne, soit du coefficient de variation a été comparée à l'opération en boucle ouverte.

Mots clés: Mélange de poudres en continu, Implémentation, Contrôle-commande, Chaînes de Markov, Contrôleur PID, Commande en boucle fermée

TABLE OF CONTENTS

GENERAL INTRODUCTION

Powder mixing is a very common unit operation in many industries, including pharmaceuticals, food, cements, etc. This operation is intended to ensure a uniform distribution of all components in the end product. It can be either a batch or continuous process. Continuous mixing offers several advantages over traditional batch mixing, such as larger volume manufacturing, easier scale-up, and lower segregation risk due to the absence of the intermediate storage and handling. While for continuous process, continuous real-time quality control is indispensable. Like in the pharmaceutical and food processing, the implementation of closed-loop control system is strongly encouraged by important regulatory authorities (e.g., Food and Drug Administration, FDA and European Medicine Agency, EMA, etc.), hence ensuring the quality of each end product, in turn eliminating product waste due to manufacturing failure.

In recent years, intensive research efforts have mainly focused on the understanding of continuous powder mixing processes using both experimental and computational approaches. The measurements of powder mixing homogeneity have been able to perform non-invasively or in real-time with the development of online/inline monitoring techniques (e.g. near infrared spectroscopy, Raman spectroscopy, etc.). However, continuous powder mixing processes are still difficult to be characterized or predicted due to complicated effects of operating conditions (feed rate, impeller speed, etc.) and geometric designs (mixer size, impeller types, etc.) on the mixing efficiency and throughput of mixers. To date, little work has been published on the development of control strategies for continuous powder mixing.

This manuscript is in continuity with previous thesis defended in the laboratory [1,2]. This work aims to contribute to the implementation of a process control system for continuous powder mixing.

An effective design and implementation of continuous powder mixing typically consists of a feeding system, a continuous mixer and a monitoring and control system as follows.

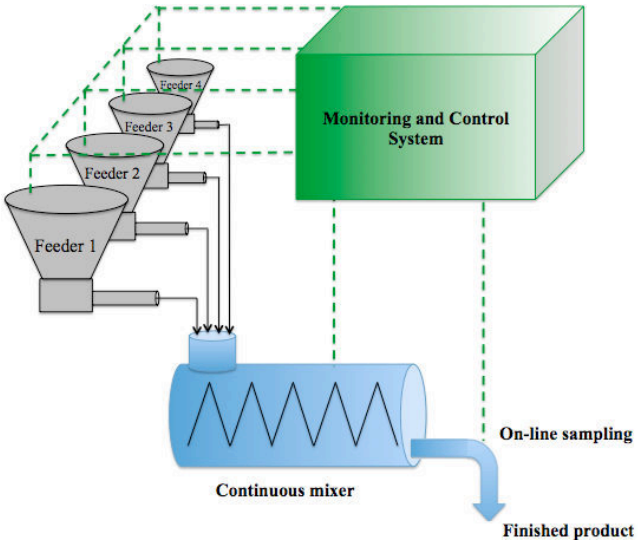

Figure 1: General framework for a well-controlled continuous powder mixing process.

The manuscript is structured as follows:

Chapter I presents a review on the continuous mixing of powders. The review is organized into five parts. The first part presents the fundamental powder mixing and segregation mechanisms, a general classification of mixers, and the main features of powder mixing in batch mode and continuous mode, respectively. The second part presents the definition and indexes of mixture homogeneity as well as currently available homogeneity monitoring techniques, particularly for continuous mixing. The third part focuses on experimental studies to characterize the effects of key design and process parameters on the performance of continuous powder mixing. The fourth part illustrates various modelling approaches that are mainly used to describe powder flow behaviour in continuous mixers. The fifth part first presents two main control strategies proportional-integral-derivative (PID) control and model predictive control (MPC), which are widely used in various process industries. Very few examples found in the literature on model-based control for continuous powder mixing are then illustrated.

Chapter II describes the materials and the experimental setting used for continuous powder mixing. Two materials (component A and B, respectively), fine couscous and medium couscous are used. Critical material properties (e.g. particle size distribution, bulk density, flowability, etc.) have been measured experimentally. For the experimental set-up, the feeding

system, the continuous mixer and the on-line image analysis for mixture homogeneity are first described as three individual units and then combined together by operating systems based on the Labview platform.

Chapter III presents a new development in the understanding of continuous powder mixing. Hold-up weight and relative hold-up weight distribution in the whole mixer, virtually divided into 5 compartments, are experimentally investigated under different operating conditions (e.g. mixing formulation, total feed rate and rotational speed of the mixer). Based on the empirical expressions determined for hold-up weight and relative hold-up weight distribution, an improved Markov chain model is finally obtained to predict the process behaviour over a much wider range of operating conditions. The reliability of the model is also verified by additional mixing experiments.

Chapter IV presents the design an implementation of PID controllers in the continuous powder mixing process. The process is first analysed based on a “black-box” model. The rotational speed of the mixer is finally selected as the manipulated variable (or actuator). The controlled variables are the mean concentration and the relative standard deviation, respectively. A PID controller is designed for closed-loop control of either of two controlled variables. The implementation of PID controllers in the real plant is realised using PID Control Toolkit in Labview software package. Two performance criteria and the PID tuning procedure are proposed to obtain satisfactory control performance.

Chapter V presents the experimental results of the proposed PID control in four possible industrial cases, which correspond to four different step changes in flow rates of the two powder components.

CHAPTER I: Background on powder mixing process

1 Generality on powder mixing process

Powder mixing is an operation aiming to achieve a uniform distribution of different powder ingredients or powders of the same nominal composition but having different particles sizes. In some industrial fields, it is called blending. The adverse effect tending to be present in powder mixing is segregation or demixing, which makes the production of an ideal or random mixture difficult. When segregation occurs, the final state reached in the mixer is an equilibrium between mixing and segregation. The final mixture quality will be determined by the relative importance of each mechanism but segregation should be minimized in favor of the mixing operation. Depending on the extent of mixing, the distribution of powders after the process can be perfectly mixed, or randomly mixed, or partially segregated, or even completely segregated [3,4] as depicted in Figure I-1 picturing these possibilities for two components. A perfect mixture of two types of particles is one in which any group of particles taken from any position in the mixture will contain the same proportions of each particle, the nominal one. In practice, a perfect mixture cannot be obtained. Generally, the aim is to produce a random mixture, in which the probability of finding a particle of any component is the same whatever the location in the mixture.

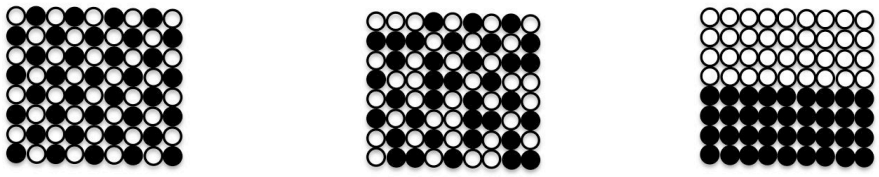

(a) (b) (c)

Figure I-1: Types of mixture adapted from [3,4]: (a) Perfectly mixed; (b) Randomly mixed; (c) Completely segregated.

1.1 Mixing mechanisms

Mixing of powders is accomplished within the flowing three types of particle transport mechanisms:

(a) ***Diffusive mixing.*** This refers to random motions of individual particles resulting in micromixing as individual particles randomly dispersed through the mixture.

(b) ***Convective mixing.*** Convection is related to the movement of groups of particles from one position to another within the mixture, resulting in macromixing.

(c) ***Shear mixing.*** In shear mixing, shear stress give rise to slip zones and mixing takes place by interchange of particles between layers within the slip zone.

1.2 Segregating mechanisms

In industrial practice, particles to be mixed almost always have some different physical properties and tend to segregate. Segregation occurs due to differences in particulate properties such as particle size, shape, density, etc. Of these, size difference is by far the most important factor driving to segregation. Four mechanisms of segregation according to size are identified [4–6], as illustrated in Figure I-2.

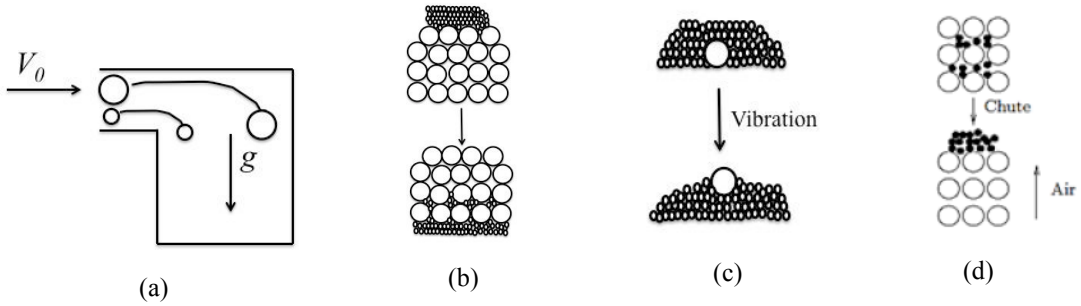

Figure I-2: Illustration of the mechanisms of segregation, adapted from [4–6]: (a) Trajectory segregation; (b) Percolation segregation; (c) Vibration segregation; (d) Elutriation segregation.

(a) ***Trajectory segregation.*** The term trajectory segregation is used to describe separation of coarse and fine particles projected from the end of a chute or fast-moving belt.

(b) ***Segregation by percolation.*** Finer particles trickle down through the gaps between the larger ones. These gaps act like a sieve. Percolation is the most commented segregation effect and percolation occurs even when there is a very small difference in particle size. Percolation of fine particles usually occurs in charging and discharging storage hoppers.

(c) ***Segregation by vibration.*** If a mixture of particles of different size is vibrated, the coarser particles moves upwards and collect near the open surface area.
(d) ***Elutriation segregation.*** When a powder is poured into the top of a hopper, a large volume of air is displaced. The upward velocity of air may exceed the terminal free-fall velocity of some of the finer particles, in turn causing the fines to elutriate while the coarse particles settle down.

1.3 Equipment for powder mixing

A large number of equipment is available on the market to suit the multiplicity of mixing tasks. An appropriate mixer tends to minimize the segregation effect. Most mixers for powder mixing can be broadly classified into the following categories [4–7] :

- ***Tumbler mixers***

Tumbler mixers are the simplest and the most common type of batch mixers. A tumbler mixer comprises a closed vessel rotating around an axis. It is generally attached to a drive shaft and supported on one or two bearings. Mixing is achieved dominantly by diffusion. Three of the most common geometries used are the V-mixer, the double cone mixer and the bin blender, sketched in Figure I-3. One of the main disadvantages of this type of mixer is the demixing possibility due to the funnel flow pattern formation that occur upon discharging.

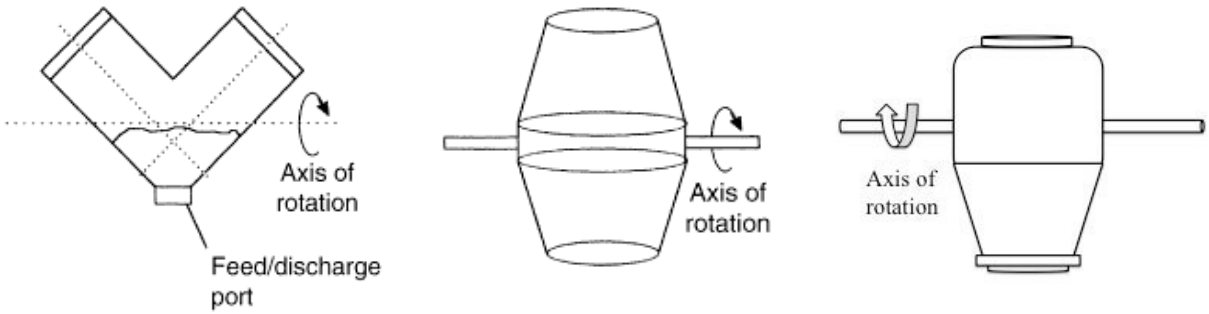

(a) (b) (c)

Figure I-3: Tumbler mixers, adapted from [4]: (a) V-mixer; (b) Double cone mixer; (c) Bin mixer.

- ***Convective mixers***

In convective mixers, mixing is strongly convective and segregation is far less pronounced than in tumbler mixers. Most convective mixers have a rotating impeller within a stationary vessel, and moves groups of particles from one location to another, thus creating mixing. The stationary mixing chamber may be conical, cylindrical, or trough-shaped, and impeller designs range from ribbons to paddles to screws. There are four common types of convective mixers: the ribbon mixer, the paddle mixer, the orbital screw (Nauta) mixer and the vertical screw mixer, as illustrated in Figure I-4. The greatest attraction is that many convective mixers can be designed to accommodate continuous rather than batch processing, further adding to their utility.

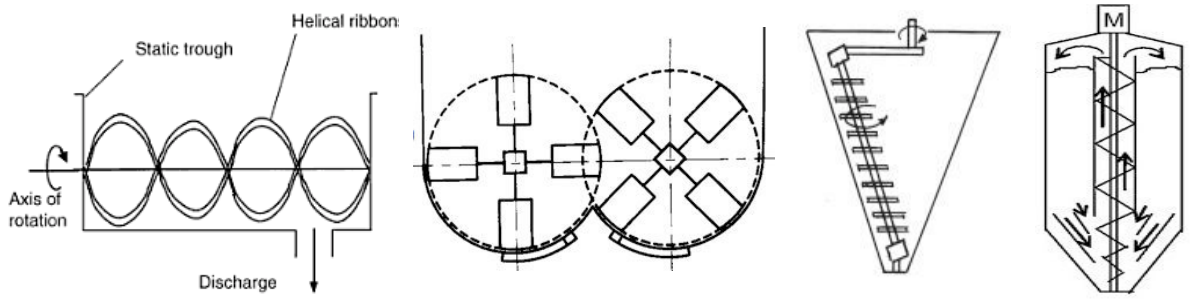

Figure I-4: Convective mixers, adapted from [4,7]: (a) Ribbon mixer; (b) Paddle mixer; (c) Nautamix; (d) Vertical screw mixer.

- ***Fluidized mixers***

Powders can also be mixed by aeration using a fluidized mixer. Fluidization is caused by the passage of air through a bed of particles. Excellent mixing can be produced if there is considerable turbulence within the bed and the combination of turbulence and particle mobility. An important feature of the fluidized bed mixer is that several processing steps (mixing reaction, coating, drying, etc.) may be carried out in the same vessel [4], thus avoiding transportation and contamination problems.

- ***Other types of mixers***

There are many other kinds of mixer, such as hopper mixers, high shear mixers, etc. Among these, the high shear mixers emphasize breaking down agglomerates of cohesive powders rather than breaking individual particles.

1.4 Batch and continuous powder mixing processes

Powder mixing can be carried out either in batch or continuous mode [5].

- ***Batch (or discontinuous) powder mixing***

In batch mode, the mixer is filled with ingredients then started and after a certain time ("mixing time") the mixture is discharged. The filling, mixing and discharging operations are performed one after another.

- ***Continuous powder mixing***

In a continuous mixing process, the ingredients are continuously fed into the mixer, mixed, preparing the product for the next processing stage. The operations of feeding, mixing and discharging follow each other locally but contemporaneously. The mixers in process industries are generally selected based on different aspects, such as process requirements, mixture quality, mixing costs, etc.

2 Assessment of powder mixtures

2.1 Mixture homogeneity

The evaluation of the homogeneity of a powder mixture is key to ensure that the product is satisfactory for its end-use, which imposes a scale of scrutiny on the mixture.

2.1.1 Scale of scrutiny

Danckwets [8] defined a "scale of scrutiny" for a mixture to describe the minimum size of the regions in a particular mixture which would cause it to be regarded as insufficient mixed. An identification of the scale of scrutiny for a product fixes the size of the sample to be taken from the mixture and assessed for mixture quality. In pharmaceutical applications, for a tablet or capsule formulation, the appropriate sample size is that of dosage form (tablet or capsule). The homogeneity for a powder mixture can be determined once a suitable scale of scrutiny is set.

2.1.2 Scale and intensity of segregation

Two important concepts related to mixture homogeneity have been proposed by Danckwerts [8] such as scale and intensity of segregation.

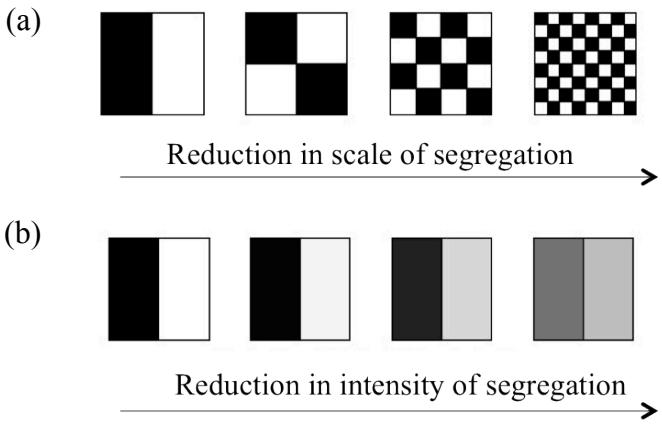

Figure I-5: Schematic representation of scale and intensity of segregation: (a) reduction in scale of segregation; (b) reduction in intensity of segregation.

- ***Scale of segregation***

The scale of segregation is a measure of the size of regions of segregation in the mixture, as depicted in Figure 1-5 (a). It is a function of space for batch mixing systems and a function of time for continuous mixing systems. The smaller the scale of segregation is, the better the mixture is.

- ***Intensity of segregation***

The intensity of segregation is a measure of the spread of the concentration of the component of interest in the mixture, as depicted in Figure I-5 (b). The lower the intensity of segregation is, the better the mixture is. The role of a mixture is to reduce the scale and intensity of segregation within the mixture.

2.1.3 Homogeneity for batch or continuous mixing

- ***Homogeneity for batch mixing***

In the case of a batch mixer, the mixture uniformity is usually measured at the end of the operation, known as the end-point. The homogeneity of the mixture can be determined by two methods: (1) the estimation of mixture homogeneity by taking randomly distributed samples across the whole mixture (2) the examination of mixture homogeneity by taking all samples from the mixture flow, which is formed by continuously discharging the mixture from the mixer.

- ***Homogeneity for continuous mixing***

For continuous mixers, homogeneity must be defined at the level of the mixture flowing out of the mixer, and falling down to a conveyor or any other transportation equipment.

2.1.4 Statistical estimation of homogeneity

Typically, the degree of homogeneity of a mixed product can be measured by statistical analysis of a number of samples of the mixture. The statistics relevant to a mixture of two components are summarized below:

- ***Mean composition***

The sample mean $\overline{x}_s$ is given by

$$\overline{x}_s = \frac{1}{n}\sum_{i=1}^{n} x_i \qquad \text{(I-1)}$$

where x_i is the composition of the key component in the ith sample and n is the number of samples. It is used for estimating the mean composition of a specified mixture.

- ***Variance, standard deviation, and relative standard deviation***

The sample variance s^2 is defined as

$$s^2 = \frac{1}{n-1}\sum_{i=1}^{n}(x_i - \bar{x}_s)^2 \qquad \text{(I-2)}$$

The value of standard deviation s is an estimation of the actual value of the standard deviation of the mixture, σ. Another important measure of blend uniformity is the relative standard deviation (*RSD*), also known as the coefficient of variance (*CV*), defined to be

$$RSD = CV = \frac{s}{\bar{x}_s} \qquad \text{(I-3)}$$

In the pharmaceutical industry, the content uniformity tests are used for proving the uniform distribution of the active ingredient in a production batch. The content uniformity test of United States Pharmacopeia (USP) is performed by measuring the contents of active ingredient in each of 10 dosage units taken at random. The USP acceptance criteria [9] for content uniformity are: (1) the mean content should fall within the range of 92.5% to 107.5% of the content stated on the label; (2) the content of active ingredient in each individual dosage unit should fall within the range of 85% to 115% of the content stated on the label; (3) $RSD \leq 6\%$.

- ***Theoretical limits of variance***

The limiting variance values were calculated for a two components mix in which the particles are of the same size.

(a) upper limit (completely segregated) $\sigma_0^2 = p(1-p)$ (I-4)

(b) lower limit (randomly mixed) $\sigma_R^2 = \frac{p(1-p)}{n_p}$ (I-5)

where p and $(1-p)$ are the proportions of the two components determined from samples and n_p is the number of particles in the sample.

- ***Mixing indices***

The quality of mixing of a real mixture would be between that of the completely segregated and that of the random mixed. Various definitions of mixing indices have been proposed using the three variances σ^2, σ_0^2 and σ_R^2, as shown in Table I-1. For example, the Lacey index [10] is the ratio of "mixing occurred" to "mixing could occur". A Lacey index of zero would represent completely segregated mixture and a value of unity would represent a completely randomized mixture. Practical values of this index, however, are found to be restricted in the range of 0.75 to 1.0, which makes the Lacey index nearly insensitive to mixture quality. Compared to Lacey index, the mixing index suggested by Poole et al. [11] gives better discrimination for practical mixture and approaches unity for fully random mixtures.

Table I-1: Some definitions of mixing indices.

Mixing index definition	Reference
$M = \frac{\sigma_0^2 - \sigma^2}{\sigma_0^2 - \sigma_R^2}$	Lacey [10]
$M = 1 - \frac{\sigma}{\sigma_0}$	Rose [12]
$M = \frac{\sigma}{\sigma_R}$	Poole et al. [11]
$M = \sqrt{\frac{\ln\sigma_0^2 - \ln\sigma^2}{\ln\sigma_0^2 - \sigma_R^2}}$	Ashton and Valentin [13]

2.1.5 Mixture structure

Let us consider a powder mixture flow as a mono-dimensional layer divided into N consecutive "elementary" samples. The global (or macro) analysis of the homogeneity can be determined by the use of statistics (e.g. mean composition and variance). Figure I-6 illustrates two different mixture structures may be observed for the same state of macromixing.

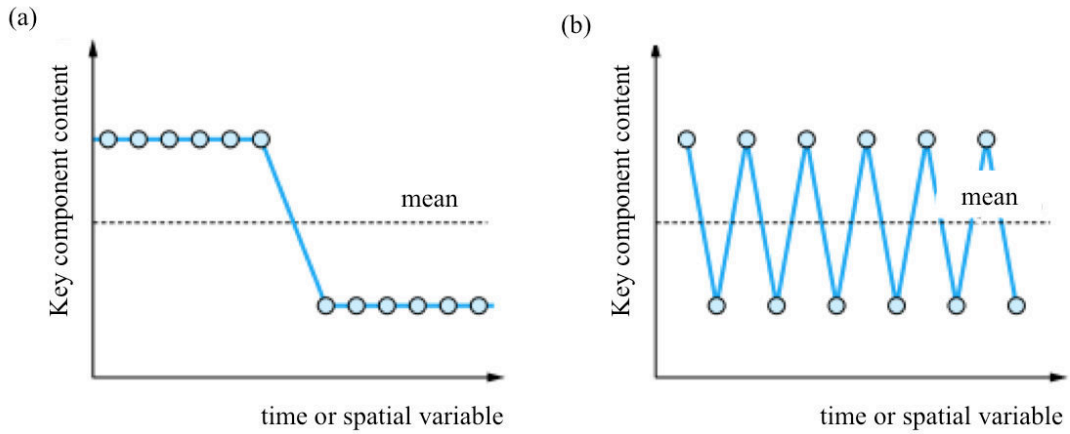

Figure I-6: Two different mixture structures observed in two mixtures of same macromixing state.

Thus, it is necessary to examine the mixing structure. As introduced by Danckwerts [14,15] in the mid-fifties and more recently reviewed by Gyenis [16], the mixing structure can be accounted for by the use of the autocorrelation function $R(r)$. For n consecutive samples, if x_i and x_m are, respectively, the composition of the sample i in a certain component and the mean composition for the n values, the mathematical definition of $R(r)$ is as flows:

$$R(r) = \frac{\sum_{i=1}^{n-r}(x_i - x_m)(x_{i+r} - x_m)}{\sum_{i=1}^{n}(x_i - x_m)^2} \qquad \text{(I-6)}$$

It is used to characterize the interdependence of the composition of two samples separated by a distance (number of samples) r. If no correlation exists, then the value of $R(r)$ is equal to zero, and the mixture can be considered as homogeneous at this scale.

2.2 Methods for measuring mixture quality

Conventional methods for measuring powder-blend uniformity are mainly based on invasive (or manual) sampling and off-line destructive analysis with HPLC or UV spectroscopy [17]. These, however, are often time-consuming, error-prone and may include artifacts, since segregation and contamination may be introduced [18]. Due to advance in effective and fast sensing technologies, at-/in-/on-line monitoring methodologies have been recently developed. It aims at acquiring fast and reliable data with representative or non-invasive sampling and

thus collecting data in real-time [19]. Furthermore, this would facilitate real-time decisions and adjustments during processing by implementing appropriate data analysis and modeling strategy. For instance, in the pharmaceutical industry, the Process Analytical Technology (PAT) [20] system has been proposed by the Food and Drug Administration (FDA) as "a system for designing, analyzing, and controlling manufacturing through timely measurements (i.e., during processing) of critical quality and performance attributes of raw and in-process materials and processes with the goal of ensuring final product quality." The ultimate goal of the PAT initiative is to enhance process understanding, leading to improved control of the manufacturing process.

2.2.1 Image processing techniques

Studies for defining and characterizing homogeneity in powder mixing using image processing techniques have been published by Muerza et al. [21], Realpe and Velazquez [22], Berthiaux et al [23], Obregon and Velazquez [24], and André et al [25]. What they have in common is the use of components of different colors and the analysis of mixtures with a PC-based vision system mainly consisting of a charge-coupled device (CCD) camera, an illumination system, an image acquisition board integrated to a computer and software based on graphical programming. Figure I-7 presents an experimental set-up described by Berthiaux et al [23] for powder mixtures flowing out of a continuous mixing or at the discharge of a batch process.

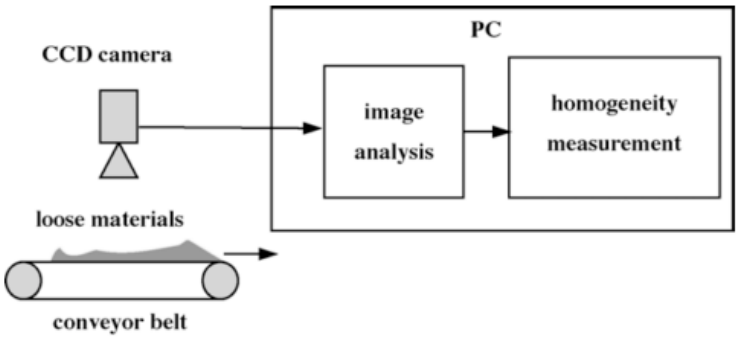

Figure I-7: Experimental set-up for monitoring of powder mixture quality using image analysis from Berthiaux et al. [23].

For image processing, red/green/blue (RGB) color images, gray-level images and binary images were widely used. An RGB color image is an $M \leq N \leq 3$ array of color pixels, where

each color pixel is a triplet corresponding to the red, green and blue components. By eliminating the hue and saturation information while retaining only the luminosity layer, gray-level images can be obtained. The gray-level (8 bit) image is represented as an $M \leq N$ array of pixels, where each pixel has an intensity value from 0 (black) to 255 (white). While the binary image has only two possible values for each pixel: the value 0 corresponding to black and the value 1 corresponding to white. Therefore, binary images are the easiest to process and analyze than the two other types of images. Single or double threshold values can be used for binarising gray-level images.

Demeyre [26] have applied a threshold value to acquire gray-level images in order to distinguish couscous colored in black from the nearly yellow semolina. The couscous proportion was then obtained from the ratio of black pixels to white pixels and a calibration curve was established to convert pixel proportion into mass composition. The image processing was carried out at the emptying stage of a batch mixer Triaxe®.

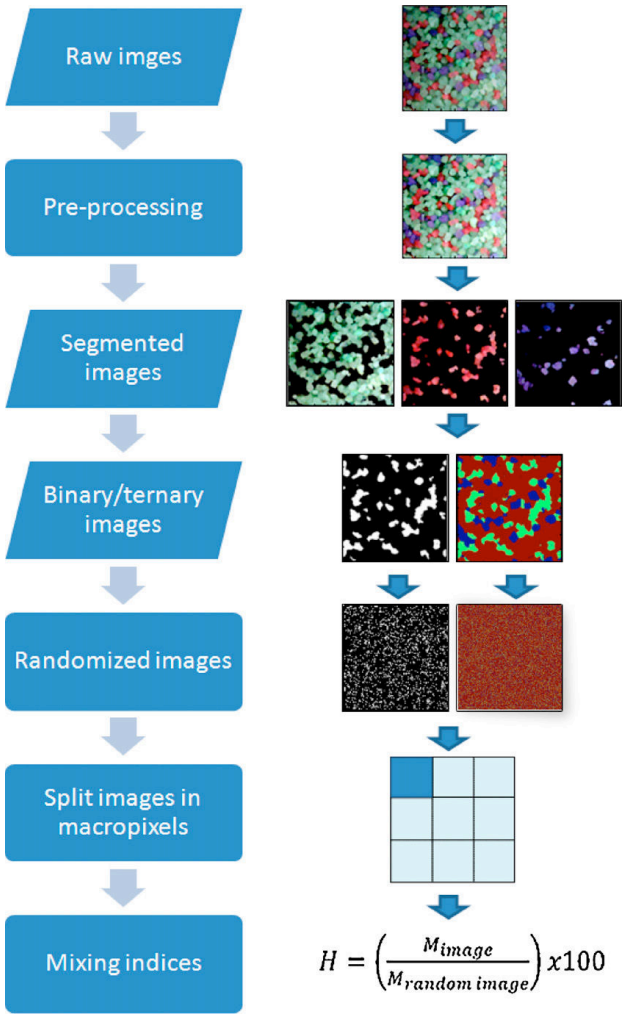

Figure I-8: Steps to determine homogeneity from images from Rosas and Blanco [27].

Recently, Rosas and Blanco [27] have studied either binary mixtures (or mixtures of two components) or ternary mixtures (or mixtures of three components), using colored sand (SiO_2) with three different particles size (small, medium and large). A miniature blender robot and both invasively and non-invasively monitoring systems were used. Labeled images (binary and ternary images) have been introduced by labeling every pixel in the image with its cluster obtained from the result of color segmentation. "Binary images" were denoted for labeled images from binary mixtures and ternary images for labeled images from ternary mixtures. The procedure for assessing image homogeneity is summarized by Figure I-8.

2.2.2 Spectroscopic techniques

Driven by the PAT initiative, spectroscopic techniques like Raman spectroscopy and near infrared (NIR) spectroscopy, were increasingly implemented for non-invasive monitoring of pharmaceutical processes. These spectroscopic methods provide physical as well as chemical information of the active and inactive components in composite mixtures.

(1) Principle of Raman spectroscopy [28]

It is vibrational spectroscopic technique that is based on light scattering phenomena, where scattering occurs due to collision between photons and molecules. When the energy of the incident photon is unaltered after collision with a molecule, the scatter photon has the same frequency as the incident photon. This is elastic or Rayleigh scattering. When energy is transferred from the molecule to the photon or vice versa, the scatter photon has less or more energy than that of incident photon. This is inelastic or Raman scattering. The energy difference between incident photons and scattered photons is called "Raman shift". A Raman spectra is a plot of scattered intensity versus the frequency of the Raman shift. It usually consists of sharp peaks whose position and intensity can be used to characterize the functional chemical groups. This information can be interpreted to determine chemical structure and to identify the compounds present. Since excipients and APIs will exhibit difference in Raman peak intensities and shift positions, it is useful to determine the composition of a pharmaceutical powder mixture.

(2) Principle of NIR spectroscopy [29]

It is based on absorption. The entire near-infrared region (NIR) of the electromagnetic spectra encompasses light with wavelength ranging from 750 to 2,500 nm, lying between the visible

light and the infrared light. NIR spectra predominantly correspond to harmonics of overtones and combination of fundamental vibration transitions more frequently associated with (mid-) infrared spectroscopy. Overton and combination absorptions are principally seen for C-H, O-H, and N-H molecular groups. A NIR spectra is a plot of these absorptions as a function of wavelength or wavenumber.

(3) Preprocessing and quantitative analysis of spectral data

Raman/NIR spectra could be affected by the physical properties of samples and other interferences or noises. Therefore, it is necessary to preprocess (or "correct") Raman/NIR spectral data to reduce, eliminate or standardize the above-mentioned effects. Common preprocessing methods include baseline correction [30], first and second derivative Savitzky Golay [31], Standard normal variate (SNV) [32], and multiple scattering correction (MSC) [33]. The preprocessed spectral data will be then quantitatively analyzed using of multivariate regression methods, such as multiple linear regression (MLR), principal component analysis/regression (PCA/PCR), and partial least squares regression (PLSR), etc. These quantitative models enable prediction of desired quality variable (e.g. API content). A detailed description of quantitative analysis of spectra can be found in [34].

In the pharmaceutical industry, the use of Raman spectroscopy for process analysis is so far limited compared to the use of NIR spectroscopy [35]. This is attributed to two aspects. On one hand, Raman spectroscopy is less sensitive to variations in physical properties (e.g. particle size), which directly influence the product performance. On the other hand, when dealing with small amounts of material and low level of API, low sensitivity of Raman may become an issue.

- ***Application examples for batch mixers***

A binary powder mixture of acetyl salicylic acid (ASA) as an active pharmaceutical ingredient (API) and α-lactose monohydrate (LM) as an excipient in a four-blade mixer were characterized in-line using NIR spectroscopy by Koller et al [36]. The optimal spectral range for API and LM was found to be 6000-10,000 cm^{-1}, including several specific peak regions of ASA (around 6000 cm^{-1} and 8500-9000 cm^{-1}) and LM (6000-7000cm^{-1}), as illustrated in Figure I-9.

Figure I-10 presented the experimental set-up. The fiber optical probe of the spectrometer was placed close to the rotor and at the powder top surface. The spectral data were finally transferred to a computer for data processing and interpretation of the powder composition with validated models. It was proved that the filling level and the filling protocol have strong impact on mixing performance, as powder flow and the blending dynamics depends on both. It was also found that convective mixing is strongest for low filling levels, whereas diffusive mixing dominates the overall process for high fill levels.

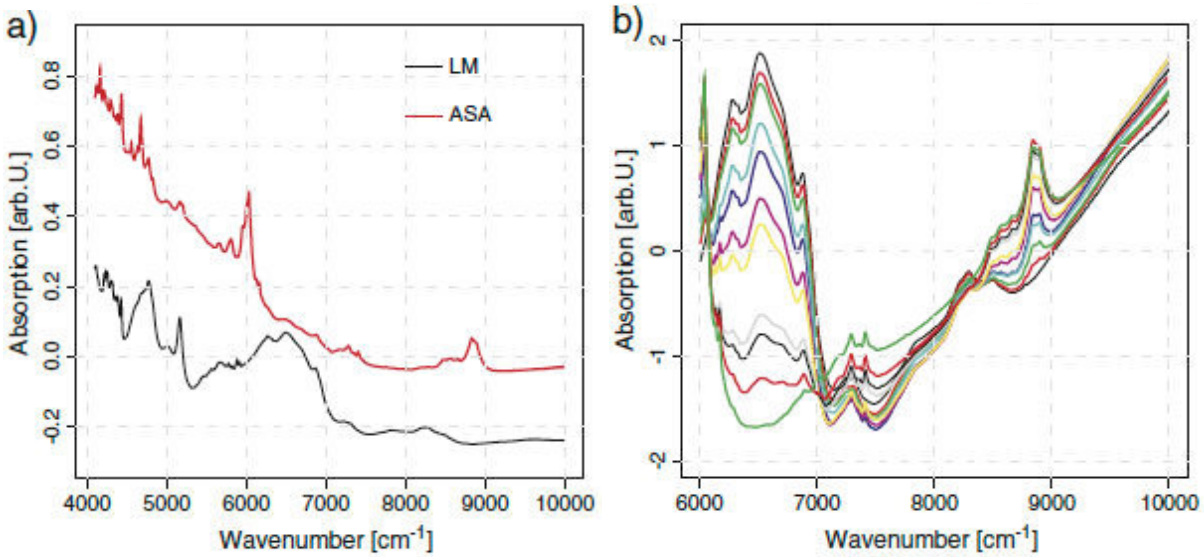

Figure I-9: (a) Raw spectra of pure LM and ASA (b) NIR spectra after data preprocessing for the calibration sets containing 11 samples ranging from 0-100% API content from Koller et al. [36].

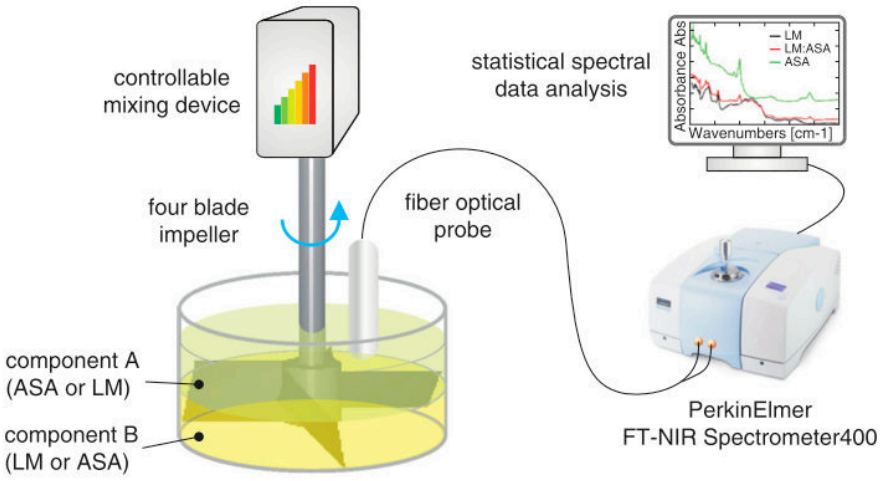

Figure I-10: In-line quantitative monitoring of powder mixing dynamics in a four-blade mixer via NIR from Koller et al. [36].

De Beer et al. [37] demonstrated that Raman spectroscopy can be used for the in-line and real-time endpoint monitoring and understanding of a powder blending process. The powder mixture consisted of diltiazem hydrochloride (API), Avicel PH 102, lactose DCL 21, and silicium dioxide (additives). The blending experiments were performed in a GralTM 10 high shear mixing system from GEA-Collet. The correctness of the Raman endpoint conclusions was assured by comparing with NIR measurements. One blending experiment was monitored using simultaneously Raman and NIR spectroscopy. The Raman immersion probe was placed in a hole on the side of the blender, and the NIR probe was positioned on top of the blender. For each monitoring technique, the blending endpoint referring to the time required to obtain a homogeneous blend was determined using the conformity index (CI) method [38]. The CI versus blending time plots for the Raman and NIR measurements were given in Figure I-11. Similar process end-points (blending time of 300 s) were concluded by both independent monitoring techniques.

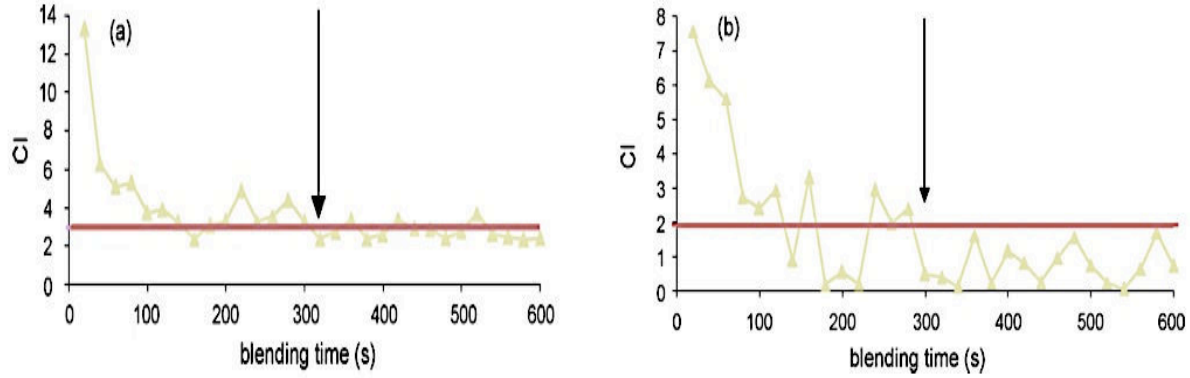

Figure I-11: Homogeneity is reached after about 300 s: (a) CI plot for NIR data; (b) CI plot for Raman data from De Beer et al. [37].

- ***Application examples for continuous mixers***

Martinez et al. [39] developed a partial least square (PLS) model for quantifying the API content in a continuous blending process, which was in-line monitored by NIR. The NIR measurements were performed using a NIR diode array spectrometer with fast data acquisition. The NIR probe was mounted at the outlet of the continuous mixer (see Figure I-12) with Modulomix technology (Hosakawa Micron BV, NL). The formulation studied contains one low dose active (A1), magnesium stearate (MgSt) as lubricant and a granular material. The start-up, steady state, and emptying phases of the continuous mixing process

were identified using three different qualitative tools: principle component analysis (PCA), moving block of standard deviation (MBSD) [40,41], and relative standard deviation (*RSD*).

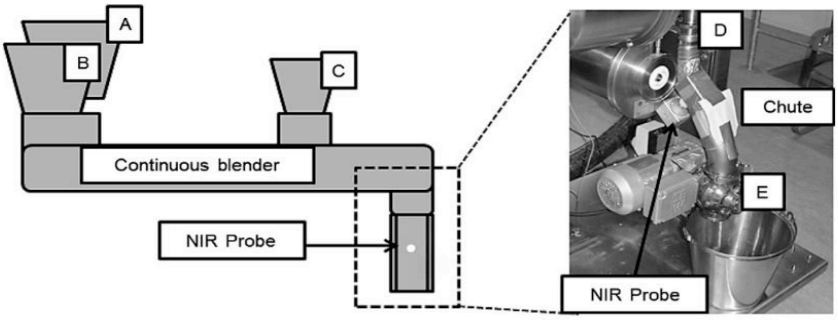

Figure I-12: NIR with a fiber optical probe from Martinez et al. [39].

The influences of the process parameters (e.g. feeding rate and stirring rate) exerted on NIR spectra and PLS model's predictions were also discussed. The predicted A1 concentrations and the *RSD* values were calculated for four different continuous mixing trials (T1, T2, T3 and T4), as shown in Figure I-13.

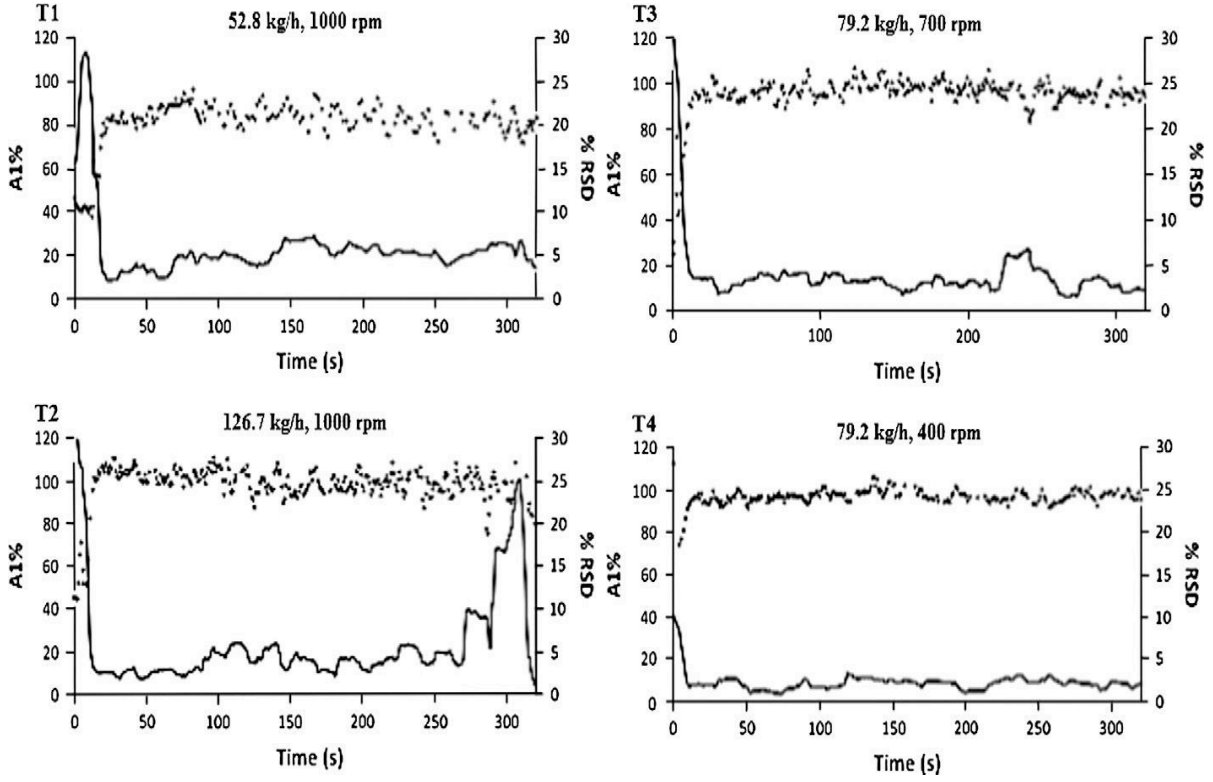

Figure I-13: Predicted NIR values (♦) with *RSD* (continuous line) for the four trials at different feeding rates and stirring rates from Martinez et al. [39].

All trials presented high *RSD* values at the beginning of the process, which was associated with the start-up phase. By comparing mixing dynamics at different stirring rates, it was found that lower stirring rate reduced the fluctuations on the predicted concentration for A1 as well as *RSD* values.

Aditya et al. [42] quantified the error associated with the in-line (NIR) blend uniformity measurements, and compared that with the off-line (UV) measurements. In-line measurements for API concentration were performed by mounting a multi-point fiber optic probe NIR system at the exit of a continuous mixer Gericke GCM 250, where a chute was utilized for discharging powder by gravity, as illustrated in Figure I-14. Off-line measurements were performed by ultraviolet (UV) absorption. The formulation consisted of 3% granulated acetaminophen as API, 96% Avicel PH-200, and 1% magnesium stearate.

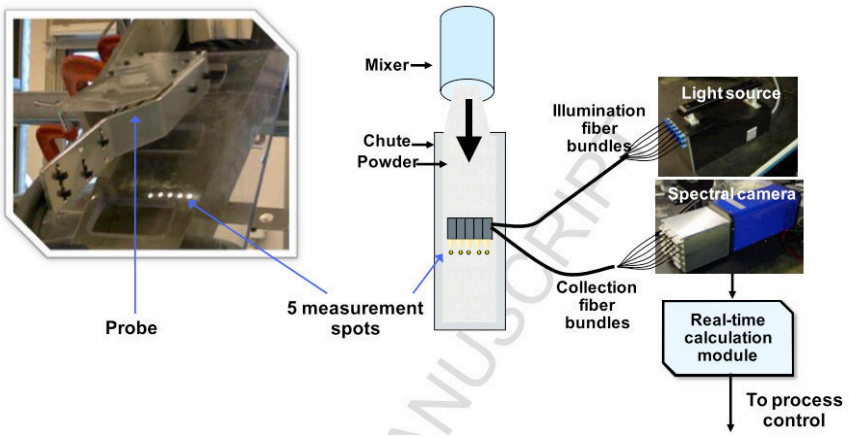

Figure I-14: Schematic of the multipoint NIR measurement system consisting of a fiber-optic lights source, 5 fiber-optic probes and a fiber-optic spectral camera by Aditya et al. [42].

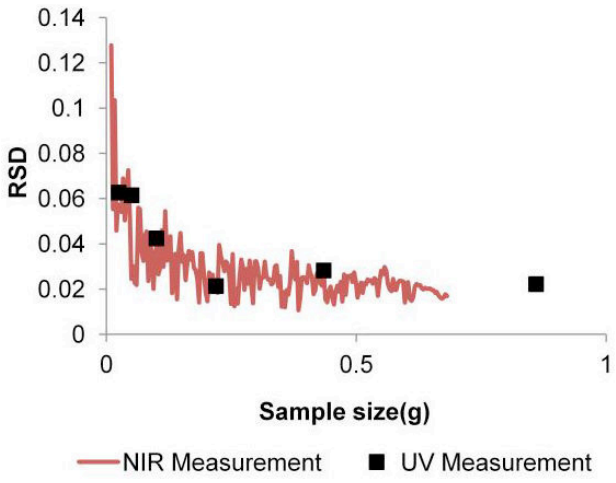

Figure I-15: Blend uniformity (*RSD*) as a function of sample size measured by on-line (NIR) and off-line (UV) methods from Aditya et al. [42].

Comparison of in-line and off-line methods was made at equivalent sample sizes. The sample size being analyzed in the in-line measurements was determined by measuring the velocity of the powder on the chute. Blend uniformity, quantified by the relative standard deviation (*RSD*) was represented as a function of sample size, as shown in Figure I-15. The similar point for both measurements is that *RSD* decrease with increasing sample size and eventually becomes plateaus around 0.02. In addition, mathematical model fitting for both showed that the contribution of the method error was negligible.

2.2.3 Near infrared chemical imaging (NIR-CI) technique

Near infrared chemical imaging (NIR-CI) adds spatial distribution information to the spectral information by combining traditional NIR spectroscopy with digital imaging. It can be used to visualize the spatial distribution of the chemical compounds in a sample (providing a chemical image). In NIR-CI, a NIR spectra is recorded in each pixel of the sample image resulting in a hyperspectral data cube, from which chemical concentrations can be estimated. A detail description of NIR-CI on pharmaceutical solid dosage can be referred in [43]. The use of NIR-CI for the determination of powder blend and tablet homogeneity based on API concentrations has been previously described [44–47].

Recently, Wu et al. [48] demonstrated a novel application of NIR-CI for monitoring the mixing process of Yinhuang powder. The formulation of each Yinghuang tablet included 0.1 g LJE, 0.04 g SBE, and 0.0158 g STA. The mixing process was performed in a micro-blender (Yarong Company, Inc., Shanghai, China). Eight blending experiments were executed at different rotational speeds and ended at various blending time, as shown in Figure I-16 (a). A methodology called basic analysis of correlation between analytes (BARA) [49,50] was introduced to determine the spatial distribution of SBE in the blend. Characteristic wavenumbers were used to generate a RGB image, which indicated the distribution of SBE (red), LJE (green) and STA (black) in each blend sample. The homogeneity of SBE distribution was measured by two methods: the histogram analysis method and the moving block macropixel relative standard deviation (MBMRSTDEV) method [51]. The result of the former showed that the standard deviation varied significantly at the initial stage and overall it decreased with increasing blending time. The latter calculated the relative standard deviation (*RSD*) of the macropixel intensity of the entire image at different blending time, as shown in Figure I-16 (b). The term macropixel refers to a square cluster of pixels whose intensity value equals to the average value of all included pixels. It was found that the *RSD* was dependent on

the size of the macropixel. The MBMRSTDEV value changed dramatically from B1 to B6 and then tended to be steady from B6 to B8. That indicated the trend of the blending process.

(a)

Number	Formulation (g)	Blending time (min)	Rotation velocity (rpm)
B1	LJE (0.1229) + SBE(0.0510) + STA(0.1940)	0.5	40
B2	LJE (0.1262) + SBE(0.0503) + STA (0.1951)	2	40
B3	LJE (0.1308) + SBE(0.0517) + STA (0.1884)	5	40
B4	LJE (0.1259) + SBE(0.0505) + STA (0.1939)	10	80
B5	LJE (0.1255) + SBE(0.0520) + STA (0.1887)	15	80
B6	LJE (0.1247) + SBE(0.0505) + STA (0.1902)	20	80
B7	LJE (0.1241) + SBE(0.0511) + STA (0.1886)	30	120
B8	LJE (0.1278) + SBE(0.0500) + STA (0.1902)	50	120

(b)

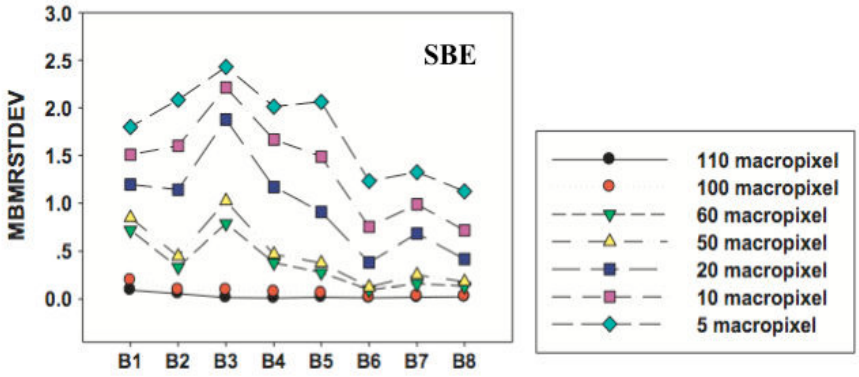

Figure I-16: (a) Process parameters for the mixing of Yinhuang powder; (b) Results of the MBMRSTDEV analysis method applied to the image of the SBE distribution during the blending process from Wu et al. [48].

3 Characterization of continuous powder mixing

For a continuous mixing of powders, the mixing performance can be characterized by mainly two approaches: the determination of mixture homogeneity and the examination of flow behavior in the mixer. To achieve the latter, residence time distribution (RTD), variance reduction ratio (*VRR*), and powder hold-up weight in the mixer were widely utilized in the literature [52–54].

- ***Residence time distribution (RTD)***

The residence time distribution (RTD) was previously proposed by Danckwerts [14]. It was measured using the pulse test method, where a large number of tracer particles were injected

at the entrance of the mixer and the tracer concentration was measured at the mixer outflow. The residence time distribution (RTD) function $E(t)$ is given by:

$$E(t) = \frac{C(t)}{\int_0^\infty C(t)\,dt} \tag{I-7}$$

where $C(t)$ is the concentration of the tracer in the outlet stream over time. It reflects the time spent by the particles within the mixer and captures the non-ideality associated with the flow. Two important parameters derived from the RTD function are the mean residence time <*t*> as

$$< t >= \int_0^\infty tE(t)\,dt \tag{I-8}$$

and the variance σ^2 as

$$\sigma^2 = \int_0^\infty (t - t_m)^2 E(t)dt \tag{I-9}$$

In continuous powder mixing processes, Sen et al. [55], Vanarase et al. [53,56], Gao et al. [57] experimentally investigated RTD as follows. Bulk material was fed in the mixer until steady state is reached. A known mass of (colored) tracer, usually being API particle (e.g. APAP), was then inserted into the inflow stream as an "instantaneous" pulse. The concentration of the tracer at the outlet of the mixer was subsequently determined by collecting samples at various times.

- ***Variance reduction ratio (VRR)***

The earliest variance reduction ratio (*VRR*) was introduced by Beaudry [58] for characterizing the fluctuation of continuous fluid mixers. *VRR* is the ratio of the variance of the concentration fluctuations at the inlet σ_{in}^2 to that at the outlet σ_{out}^2. The higher the value of *VRR*, the better the performance of the mixer. Danckwerts, Williams and Rahman, and Weinekötter and Reh [14,59,60] expressed *VRR* as a function of the auto-correlation coefficient from the feeder fluctuations and the residence time distribution (RTD), as given by Eq. (I-10) and Eq. (I-11).

$$\frac{1}{VRR} = \frac{\sigma_{out}^2}{\sigma_{in}^2} = 2\int_0^\infty R(r)E(t)E(t+r)\,dr \quad \text{(I-10)}$$

$$R(r) = \frac{cov(x_t, x_{t+r})}{var(x_t)} \quad \text{(I-11)}$$

where $R(r)$ stands for the autocorrelation coefficient, x_t is the concentration at input at time t, and r is the window of observation and $E(t)$ is the residence time distribution (RTD) function.

- ***Hold-up***

Powder hold-up in the mixer is important because it determines the geometrical residence time [hold-up (kg)/flow rate (kg.h^{-1})]. As Vanarase and Muzzio [53], Ammarcha et al. [54] illustrated, hold-up can be measured by simultaneously monitoring the weight of the powder collected at the mixer's outlet and that of powder being fed. According to the evolution of powder hold-up weight in the mixer, a common continuous mixing process can be divided into three phases: start-up, steady state and emptying. In preliminary measurements, hold-up is initially zero. In the period of start-up, hold-up increases with time, and finally reaches a plateau. The mixer operating under constant hold-up was considered to be operating at steady state in which the mixer has reached a constant mass inflow and outflow. In the emptying phase, the remaining material is discharged from the mixer.

For bulk medium couscous in a continuous mixer Gericke GCM 500, Ammarcha et al. [54] used a minimum hold-up weight "M_{min}" below which no powder can flow out the mixer during start-up phase, and a maximum hold-up weight "M_r"representing the constant value at steady-state, as shown in Figure I-17 (a). On the other hand, it was observed that the hold-up weight obtained at steady state depends experimentally on the feed rate and the rotation speed, as shown in Figure I-17 (b).

(a)

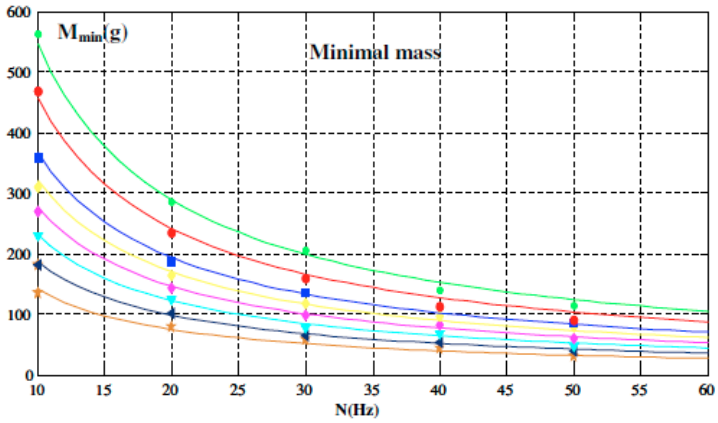

(b)

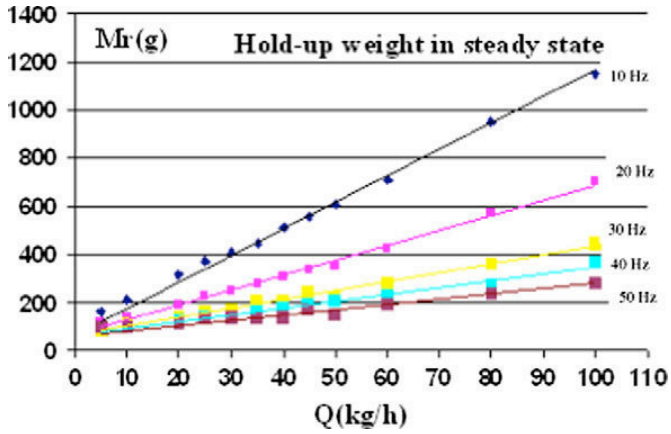

Figure I-17: Hold-up weight of bulk powder in the mixer: (a): minimum hold-up weight with inflow rates at 10, 20, 30, 40, 50, 60, 80 and 100 kg.h-1 (from bottom to top); (b): hold-up weight at steady state from Ammarcha [54].

By means of RTD and hold-up measurements, the effects of various factors, such as particulate properties (size distribution, powder cohesion, etc.), operating conditions (feed rate, impeller rotation rate) and geometric designs (mixer size, blade configuration, etc.) have been examined.

3.1 The effects of particulate properties

As mentioned above, the physical properties of the particles are known to have an effect on the mixing and segregation of powders. The segregation of powders mainly occurs due to a particle size difference between the individual components of powder mixtures. Since powder flowability is dominantly influenced by the particle size, powders can be generally categorized into two groups: free-flowing powders and cohesive powders [5]. In general, free flowing powders are ones relatively easy to mix, but the resultant mixture is prone to segregation of the components. Cohesive powders are those for which the constituent fine

particles are aggregated to each other by forces such as electrostatic forces and liquid bridges caused by humidity. Free-flowing powders have been the most commonly studied powders in continuous mixing. Recently, pharmaceutical powders for continuous mixing have been also studied. The active pharmaceutical ingredients (APIs) usually demonstrated very different physical properties in terms of powder flowability.

Portillo et al. [61] have described the effects of powder cohesion in two scale continuous mixers manufactured by GEA Bulk systems (see Figure I-18). The investigation was based on the mixing of milled acetaminophen (30 μm) with two different lactose that varied in cohesion: high cohesion lactose 125 (130 μm) and low cohesion lactose 100 (55 μm). Results showed that the effect of powder cohesion depends geometric parameters of the blender, having a significant effect in the larger mixer. It was also pointed out that the effects of cohesion could be system-dependent. Since cohesion can affect the degree of variability in the flow rate delivered by a powder feeder, it should be expected that cohesion could have impacted the performance of the integrated system, including feeders, mixers, and downstream finishing equipment.

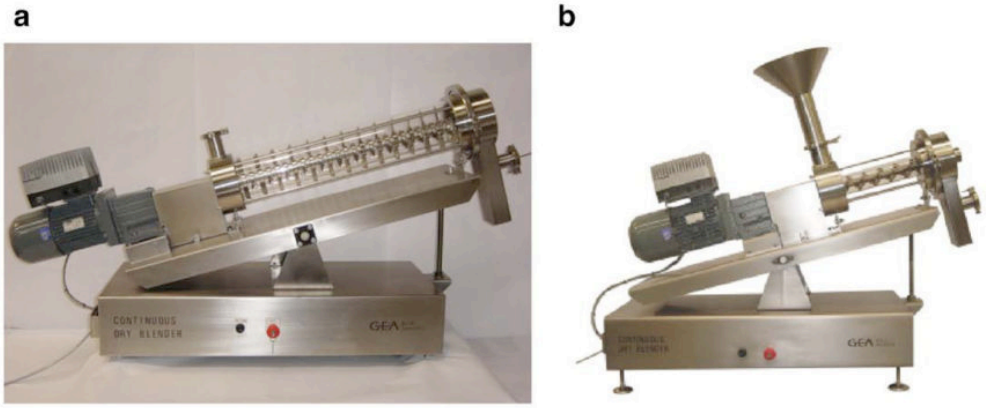

Mixer	Diameter (m)	Length (m)	No. of blades	Blade length (m)	Blade type	Speed (RPM)
1	0.15	0.74	0–34	0.05	Rectangular with a circular tip	16–87
2	0.05	0.31	0–14	0.02	Triangular with a circular tip	16–340

Figure I-18: Continuous mixers in two different geometries: (a): 1st continuous mixer; (b) 2end continuous mixer from Portillo et al. [61].

The effect of cohesion on the particles paths lengths inside a continuous mixer has also been examined by Portillo et al. [62] using positron emission particle tracking (PEPT), where the

impeller rotation speed was adjusted to three different rotational speeds (16, 75, and 170 rpm). It was found that the effect of cohesion was not significant at the highest rotation speed (170 rpm). This means the influence of cohesion will be undermined by higher energy imparted by the impeller on the particles.

3.2 The effects of operating conditions and design parameters

In the continuous mixers considered, feed rate and impeller rotational speed were found to be significant process parameters affecting mixing performance. As Weinekötter and Gericke [5] illustrated, feed rate is a crucial process parameter in continuous powder mixing. It depends on the accuracy and capacity of the powder feeding system employed. Gao et al. [57,63] has experimentally investigated the influence of feed rate variability on the output variance σ_{out}^2. Two loss-in-weight feeders provided by Schenck-Accurate were utilized to feed the mixer. The feed rate variability of API and excipient were separately measured at the corresponding feed rates using a catch-scale that records the weight of powder discharged by the feeders as a function of time.

(a)

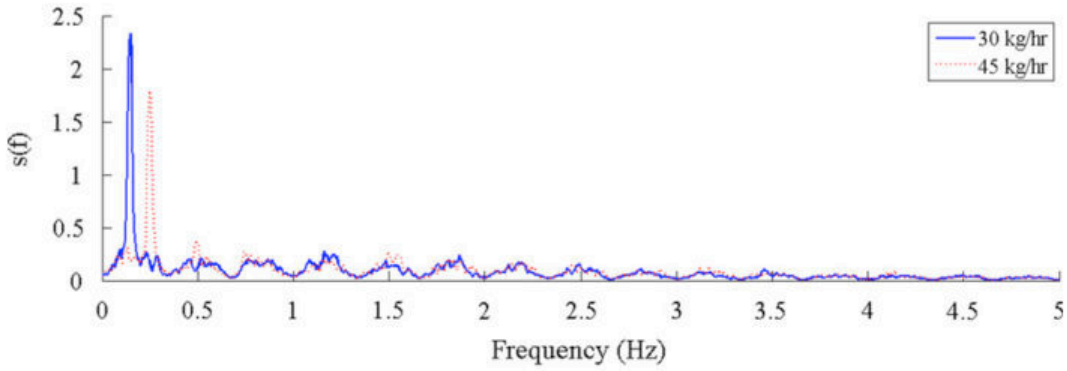

(b)

Feed rate (kg/h)	API%		
	Average value	Standard deviation	RSD (%)
30	3.00	1.09	36
45	3.02	0.64	21

Figure I-19: (a) Feed rate analysis of API; (b) Statistics of feed rate fluctuation of API at the investigated feed rates from Gao et al. [63].

The variance distribution function $s(f)$ of the feed rates are calculated at different frequencies, as shown Figure I-19 (a). It was noticed that the lowest peak of feed rate

fluctuations (peak at the lowest frequency) always corresponds to the rotation frequency of the feeding screw. Better feeding conditions of API were obtained at higher frequency and small relative standard deviation (*RSD*) was observed for the feed rate of 45 $kg.h^{-1}$, as depicted in Figure I-19 (b).

In the literature, the most common continuous mixers studied are convective mixers, in which there is usually a stirring device consisting of several impeller blades attached to a rotating shaft. The stirring speed is a key factor that affects material dispersion throughout the mixer. The effect of impeller rotational speed was generally investigated under various inflow rates, and design parameters (e.g. stirrer type, mixer configuration, etc.).

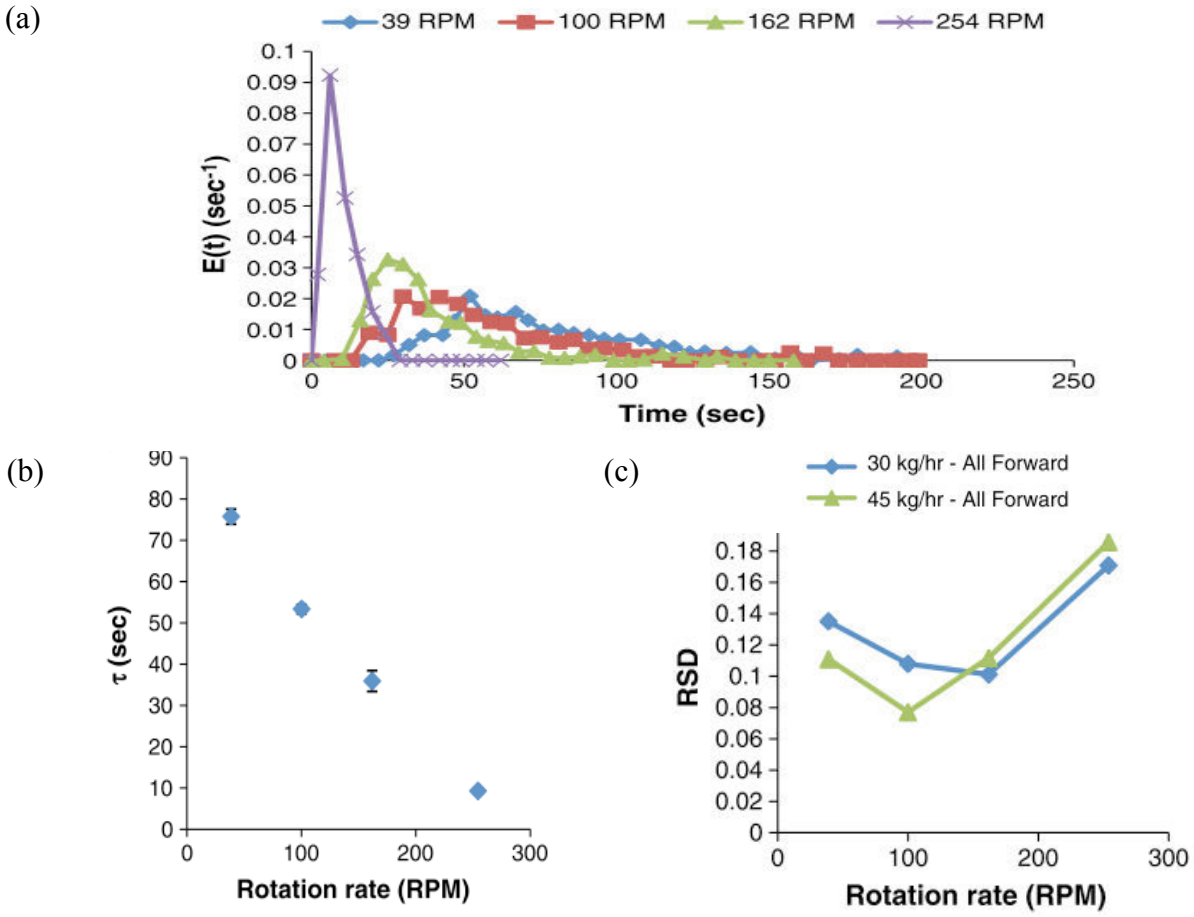

Figure I-20: Effect of rotation rate on RTD with flow rate-30 $kg.h^{-1}$ and blade configuration – All forward from Vanarase and Muzzio [53]: (a) residence time distribution; (b) mean residence time; (c) relative standard deviation.

Vanarase and Muzzio [53] examined the effect of rotational speed on the residence time distribution (RTD), as shown in Figure I-20 (a), using a stirring device composed of all blades directing forward with a single blade angle of 20°. Figure I-20 (b) showed that the mean

residence time <*t*> decreased as the rotational speed increased. This indicated that higher rotational speed decreases the time available for mixing (lower residence time). Figure I-20 (c) plotted the relative standard deviation (*RSD*) versus the rotational speed. A higher *RSD* was observed at the highest rotational speed of 254 rpm owing to an extremely low mean residence time.

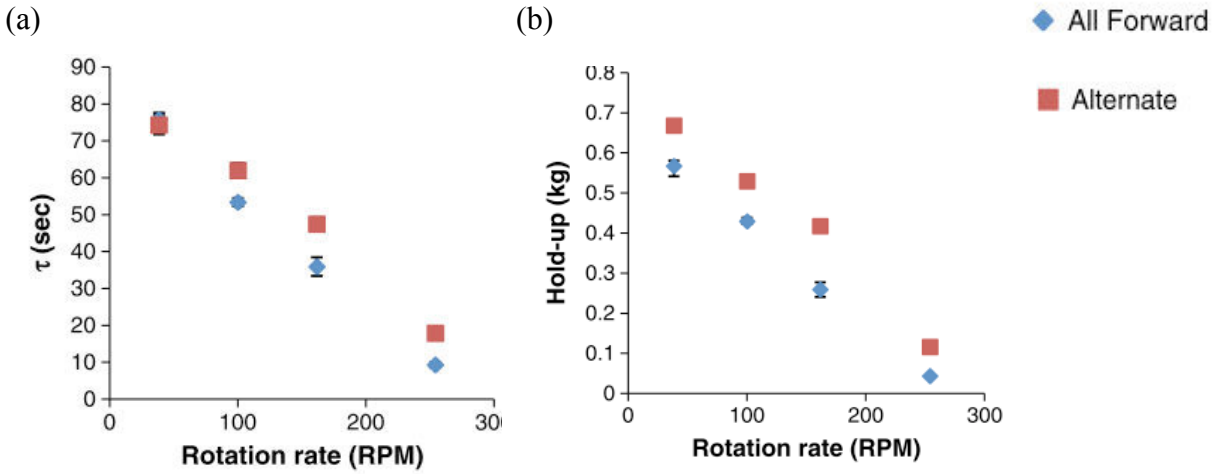

Figure I-21: Effect of blade configuration on (a) mean residence time; (b) hold-up at steady stage from Vanarase and Muzzio [53].

In addition, this "All forward" blade configuration of stirring device has also been compared with " Alternate" blade configuration consisting of alternate blades directing in forward and backward with blade angle of 20°. Figure I-21 concluded that the effect of blade configuration was not very significant at lower rotational speed, while the mean residence and hold-up were greater for the "Alternate" blade configuration at higher rotational speed. This implied that there is powder recirculation in the mixer when using the "Alternate" blade configuration.

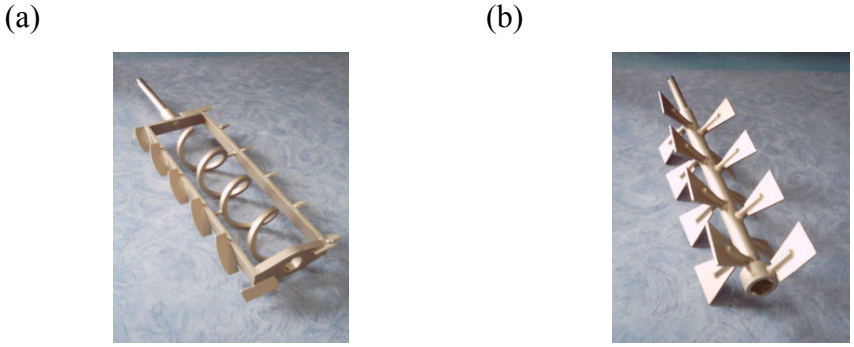

Figure I-22: Two stirrers design studied by Marikh et al. [52]: (a) stirrer A; (b) stirrer B.

Marikh et al. [52] have reported the impact of stirrer type on mixture homogeneity in a pilot-scale continuous mixer Gericke GCM 500, using two different types of stirrers (see Figure I-22): stirrer A consisting of 14 blades installed on a frame with an internal transporting screw and stirrer B consisting of 15 blades on a shaft.

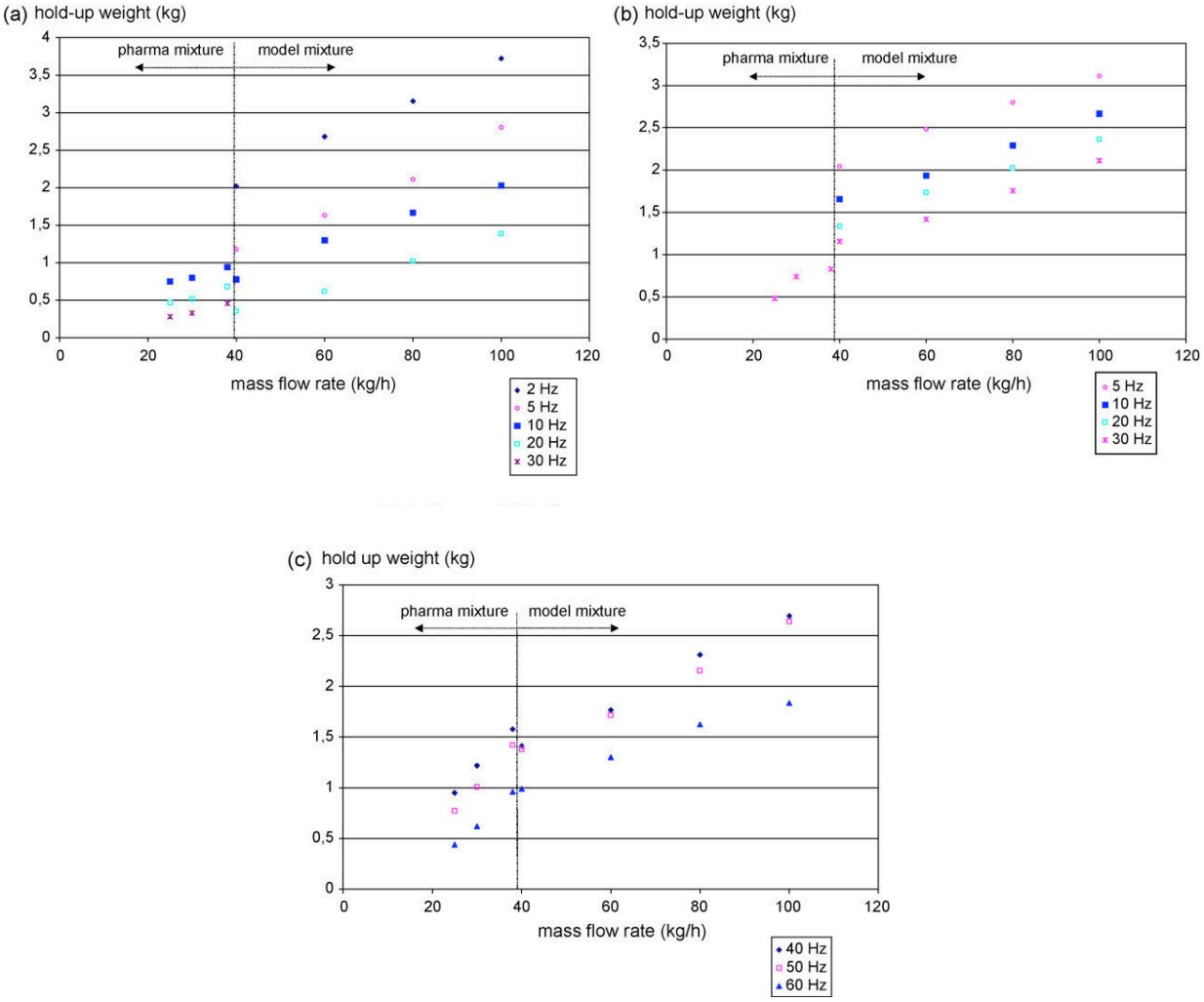

Figure I-23: Hold-up measured as a function of mass flow rate and mixture types for: (a) stirrer A; (b) stirrer B under dense phase flow regime; (c) stirrer B under fluidized flow regime from Marikh et al. [52].

Two different flow regimes were discussed: the dense phase regime obtained at rotational speeds less than 35 Hz and the fluidized regime obtained at higher rotational speeds. Stirrer A was used up to 30-35 Hz, because no fluidization occurs at higher rotational speeds, whereas stirrer B was used up to 60 Hz. Experiments were done for two types of mixtures: a real pharmaceutical mixture containing a low dosage in active ingredient A_3 and a model mixture consisting of semolina and couscous. The pharmaceutical mixture was processed with lower

flow rates (≤ 40 kg.h^{-1}), while the model mixture was processed with higher flow rates. The hold-up against the flow rate was plotted for both stirrers at different rotational speeds, as shown in Figure I-23. It was observed that, under dense phase flow regime, the increase in the rotational speed of both stirrer devices provokes a decrease in the hold-up mass. But the comparison of Figure I-23 (b) and (c) concluded that the hold-up mass with stirrer B rises quietly sharply to slow down against increasing rotational speed when transiting from the dense phase regime to the fluidized regime. Moreover, the study of mixture homogeneity showed that stirrer A is more efficient in reducing feeding fluctuations. An excessive rotational speed of stirrer B can lead to worse mixtures since higher hold-up may be provoked under fluidized flow regime.

4 Powder mixing models

Several modeling approaches exist in the literature for powder mixing process. The current modeling approaches can be mainly categorized into Markov chain models, discrete element method (DEM) models, convection-diffusion models, convection-dispersion models and population balance models (PBM).

4.1 Markov chain model

A Markov chain is a probabilistic model that exhibits a special type of dependence, that is, where the state of the system on the (n+1) th observation depends only on the state of the system on the n th observation. This means that, given the present state of the process, the future state is independent of the past. This property is usually referred as the Markov property [64].

The theory of Markov chains has been early applied for batch mixing processes [65,66], static mixing processes [67,68] and powder mixing in fluidized beds and a hoop mixer [69–71]. More recently, Markov chain-based models have been used to describe continuous convective bulk flow and mixing of powders. Berthiaux et al. [72] have first introduced a one-dimensional (or 1D) Markov chain model to describe continuous convective mixing of two components A and B. The basic of one-dimensional Markov chain is show in Figure I-24.

(a)

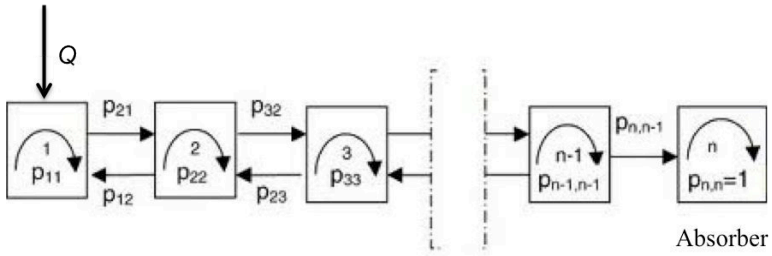

(b)

$$\boldsymbol{S} = \begin{bmatrix} S_1 \\ S_2 \\ \dots \\ S_n \end{bmatrix} = [S_1 \quad S_2 \quad \dots \quad S_n$$

(c)

$$\mathbf{P} = \begin{bmatrix} P_{11} & P_{12} & 0 & \dots & 0 & 0 \\ P_{21} & P_{22} & P_{23} & \dots & 0 & 0 \\ 0 & P_{32} & P_{33} & \dots & 0 & 0 \\ \dots & \dots & \dots & \dots & \dots & \dots \\ 0 & 0 & 0 & \dots & P_{n-1,\,n-1} & 0 \\ 0 & 0 & 0 & \dots & P_{n,\,n-1} & P_{nn} \end{bmatrix}$$

Figure I-24: One-dimensional Markov chain proposed by Berthiaux et al. [72] for modeling the particle flow inside a continuous powder mixer: (a) graphical presentation; (b) state vector $\boldsymbol{S}$; (c) $\boldsymbol{P}$ matrix of transition probabilities.

The mixer has been presented by a series $(n-1)$ of interconnected cells. It was assumed that the exchange of material inside the mixer through zones are perfectly mixed. The last cell (n^{th}) corresponds to the absorbing state: a collector of particles of outflow, which is not part of the mixer. The chain composed of these n cells is observed in discrete intervals, which are called system states. The set of probabilities to occupy all the cells forms, in the sample space, the state vector $\boldsymbol{S}$ with elements S_i $(i=1,2,...,n)$, which is shown as a column vector of the size $n \leq 1$. The transition duration Δt is chosen to be small enough so that the particles are allowed to transit only to neighboring cells. It is obvious that the current time is equal to $k\Delta t$ after k transition. If the state vector at the k^{th} moment of time is $\boldsymbol{S}(k)$, then after the current transition it will be $\boldsymbol{S}(k+1)$. The correlation between $\boldsymbol{S}(k)$ and $\boldsymbol{S}(k+1)$ can be described by the matrix formula:

$$\boldsymbol{S}(k+1)=\boldsymbol{P}\boldsymbol{S}(k) \tag{I-12}$$

where $\boldsymbol{P}$ is the matrix of transition probabilities – the basic operator of a Markov chain. Every transition has its own probability. p_{ij} means the probability of particles in the cell j to move to the cell i. If $i=j$, then p_{ii} means the probability of particles in the cell i to remain in the cell.

Further, Markih et al. [73] have developed a two-dimensional (or 2D) Markov chain (see Figure I-25) for taking into account more features of real powder flow, such as crosswise mixing in the sections of a mixer, which is supposed to be perfect for one-dimensional models.

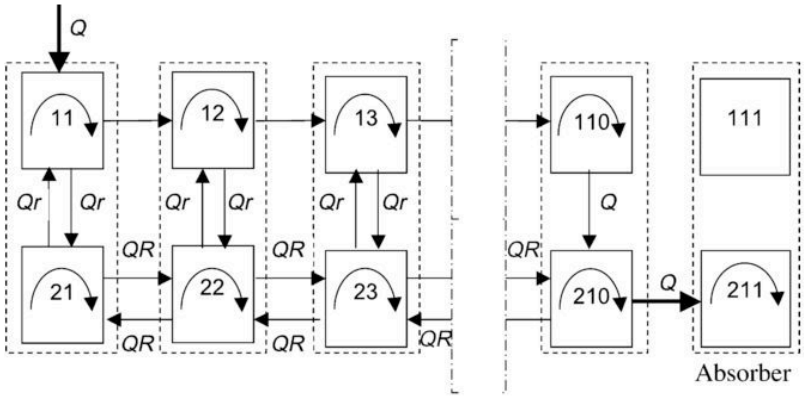

Figure I-25: Two-dimensional Markov chain with two parallel chains proposed by Marikh et al. [73] for continuous powder mixing.

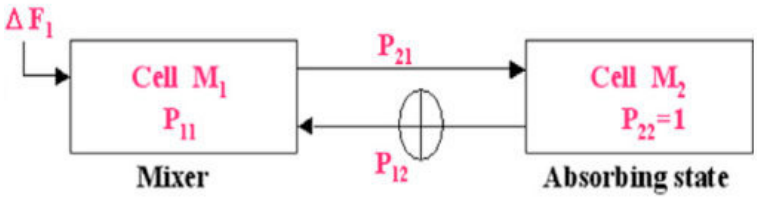

Figure I-26: A simple Markov chain model for describing the macroscopic behavior of bulk powder flow in a continuous mixer from Ammarcha et al. [54].

As the parameter determinations of both 1D and 2D chain models mentioned above were based on the experimental RTD data obtained by tracer experiments, Ammarcha et al. [54] have described a simple Markov chain model based on experimental measurements of bulk powder hold-up in the continuous mixer, the inflow and outflow rates. As shown in Figure I-26, a cell represents the entire mixer and another cell at the outlet of the mixer corresponds to the absorbing state. In Ammarcha's Ph.D. thesis [2], a Gericke GCM500 mixer has been compartmentalized into five cells of equal axial length for building a Markov chain model (see Figure I-27).

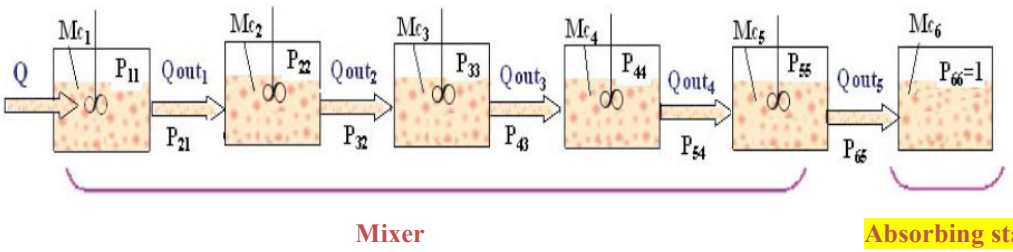

Figure I-27: A Markov chain model for describing the mesoscopic behavior of bulk powder flow in a continuous mixer from Ammarcha [2].

Bulk couscous was fed at Q into the entrance of the mixer. Transitions (or mass flows) were permitted between adjacent cells, and Q_{out_i} represents the difference of forward and backward flow rates of couscous between adjacent cells. The matrix of transition probabilities has been determined by measuring hold-up weight of bulk powder in each cell after each transition. The evolution of the vector of hold-up was expressed by Eq. (I-13), where $M_i(k+1)$ is the hold-up weight of particles in i^{th} cell after k transitions; $p_{ii}(k)$ and $p_{i+1,i}(k)$ are respectively the probabilities of to stay in the i^{th} cell and to move from the i^{th} cell to the $i+1^{th}$ cell for k^{th} transition; $p_{ii}(k)=1-p_{i+1,i}(k)$ and $p_{66}(k)=1$ because there is no backward for the last cell.

$$\begin{bmatrix} M_1(k+1) \\ M_2(k+1) \\ M_3(k+1) \\ M_4(k+1) \\ M_5(k+1) \\ M_6(k+1) \end{bmatrix} = \begin{bmatrix} P_{11}(k) & 0 & 0 & 0 & 0 & 0 \\ P_{21}(k) & P_{22}(k) & 0 & 0 & 0 & 0 \\ 0 & P_{23}(k) & P_{33}(k) & 0 & 0 & 0 \\ 0 & 0 & P_{34}(k) & P_{44}(k) & 0 & 0 \\ 0 & 0 & 0 & P_{45}(k) & P_{55}(k) & 0 \\ 0 & 0 & 0 & 0 & P_{56}(k) & P_{66}(k) \end{bmatrix} \begin{bmatrix} M_1(k)+Q\Delta t \\ M_2(k) \\ M_3(k) \\ M_4(k) \\ M_5(k) \\ M_6(k) \end{bmatrix} \quad \text{(I-13)}$$

It was assumed that the transition probability $p_{i+1,i}(k)$ during the start-up stage varies linearly with the measured hold-up. While it reaches its maximum value and remains constant at steady state and the value depends on the feeding rate Q and the rotational speed of the stirring device N. Thus, the transition probabilities can be calculated as follows:

$$p_{i+1,i}(k) = \begin{cases} 0, & for\ M_i < M_{i,min} \\ \dfrac{P_{i+1,i\,max}}{M_{i,max}-M_{i,min}}(M_i(k)-M_{i,min}), & for\ M_{i,min} \le M_i < M_{i,max} \\ P_{i+1,i\,max}, & for\ M_i = M_{i,min} \end{cases} \quad \text{(I-14)}$$

$$P_{i+1,\,i\,max}(k)=\begin{cases}\dfrac{Q\Delta t}{M_{i,\,max}+Q\Delta t}, & for\ i=1\\ \dfrac{Q\Delta t}{M_{i,\,max}}, & for\ i=2,3,4,5\end{cases} \tag{I-15}$$

$$M_{i+1,\,i\,max}=\begin{cases}f_1(Q,N), & for\ i=1,2,3,4\\ f_2(Q,N), & for\ i=5\end{cases} \tag{I-16}$$

The Markov chain model presented above was used for predicting bulk powder flow dynamics in the continuous mixer. However, in this study, our aim is to model a continuous powder mixing process. For this purpose, it is proposed to modify this previously developed model for simulating a continuous mixing dynamics of two particulate components. The possible way is to determine the matrix of transition probabilities for each individual component.

4.2 Convection-dispersion model and Population balance model

- ***Convection-dispersion model***

The convection-dispersion model is based on the Fokker-Planck equations (FPEs) and it is used to describing mixing in the axial direction, as given by Eq. (I-17).

$$\frac{\partial C}{\partial t}=-v\frac{\partial C}{\partial z}+D\frac{\partial^2 C}{\partial z^2} \tag{I-17}$$

where C is the concentration of particles of one particulate component in a system, z is the axial direction of motion, v is related to particle velocity, and D is a dispersion coefficient.
Sommer [74,75] introduced FPEs for the case of continuous mixers and solved for each component in the mixture. Figure I-28 described a continuous mixing of two components based on the convection and dispersion mechanisms.

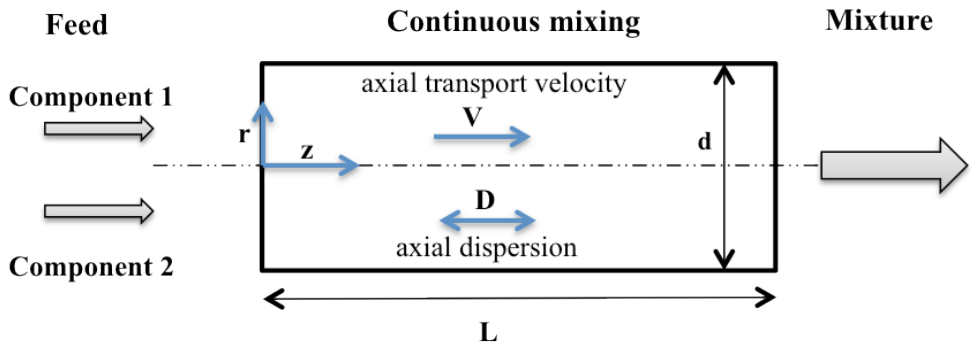

Figure I-28: Schematic of the axial mixing of two components in a continuous mixer.

Weinekötter et al. [60] used this model for a low dosage mixture. Later Kehlenbeck and Sommer [76] later used FPEs to model the dynamics of mixing in a continuous rotary powder blender. Particle streams with merely identical physical properties were used, so that it could be assumed that all the components in the mixture exhibited the same particle velocity and dispersion coefficient. Once FPEs were written, the important issue is to solve FPEs by determining parameters. Results showed that the ratio of the mean residence time to the time period of the fluctuation in the feeder is the most important parameter affecting the variance reduction ratio.

- ***Population balance model***

Population balance models (PBMs) have been frequently applied to model particulate process such as crystallization and granulation but few for powder mixing till recently. It can be expressed as [77] :

$$\frac{\partial}{\partial t}F(\mathbf{x},\mathbf{z},t)+\frac{\partial}{\partial \mathbf{x}}\left[F(\mathbf{x},\mathbf{z},t)\frac{d\mathbf{x}}{dt}\right]+\frac{\partial}{\partial \mathbf{z}}\left[F(\mathbf{x},\mathbf{z},t)\frac{d\mathbf{z}}{dt}\right]=\Re_{formation}-\Re_{depletion} \qquad \text{(I-18)}$$

where $F(\mathbf{x},\mathbf{z},t)$ is the population distribution function, $\mathbf{x}$ is the vector of internal co-ordinates used to characterize the internal distribution, $\mathbf{z}$ is the vector of external co-ordinates used to represent spatial position of the particles and t is the time. The term $(\partial/\partial\mathbf{x})\left[F(\mathbf{x},\mathbf{z},t)d\mathbf{x}/dt\right]$ accounts for the rate of change of particle distribution due to change in particle size. The term $(\partial/\partial\mathbf{z})\left[F(\mathbf{x},\mathbf{z},t)d\mathbf{z}/dt\right]$ accounts for the rate of change of particle distribution with respect to spatial co-ordinates. $\Re_{formation}$ and $\Re_{depletion}$ stand for particles being formed and depleted

respectively. A multi-dimensional population balance model have been formulated to elucidate the dynamics of a continuous powder mixing process by Sen et al. [55]. It has been assumed that particle size could not change, so the rate of particle formation and depletion are zero. The modified population balance equation is thus given as follows:

$$\frac{\partial}{\partial t}F(\mathbf{z},t)+\frac{\partial}{\partial z}\left[F(\mathbf{z},t)\frac{d\mathbf{z}}{dt}\right]=0 \qquad \text{(I-19)}$$

where $\mathbf{z}$ can be expressed by the spatial co-ordinate in the axial direction x and the spatial co-ordinate in radial direction y. The above equation can be written in multi-dimensional form as shown below:

$$\frac{\partial}{\partial t}F(n,x,y,t)+\frac{\partial}{\partial x}\left[F(n,x,y,t)\frac{dx}{dt}\right]+\frac{\partial}{\partial y}\left[F(n,x,y,t)\frac{dy}{dt}\right]=Inflow-outflow \qquad \text{(I-20)}$$

It represent an n multi-dimensional formulation where n=2 to represent the API and excipient components. The effect of important process parameters on flow and mixing (e.g. API composition, *RSD* and RTD) have been investigated by Sen and Ramachandran [78] using the PBM scheme presented above.

4.3 Discrete element model

Till now, considerable reports from the literature have focused on a numerical technique - the discrete element methods (DEM) for modeling the mixing of granular materials [79]. The DEM approach has been originally developed by Cûdall and Strack [80] and has become a useful tool that can provide detailed microscopic information about a given particulate system: particle location, velocity and force acting on each individual particle at any time during the process.

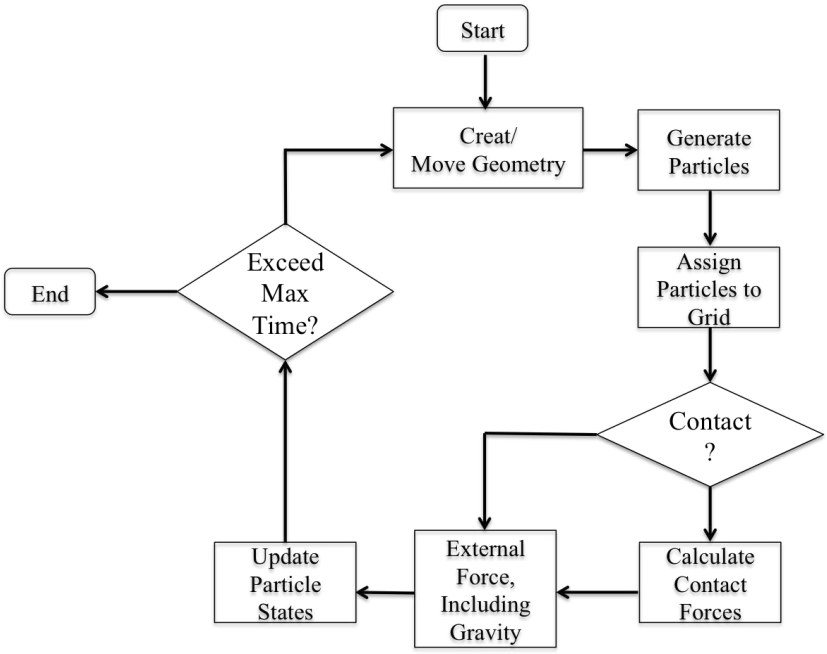

Figure I-29: Principe of DEM analysis from Bharadwaj [81].

Each particle is computationally defined along with its shape, initial position, velocity and other physical properties. Changes in these parameters over time are calculated for each particle as they move around an interact/collide with other particles in the simulation domain. The principle of DEM is illustrated Figure I-29. The essential elements of the algorithm for the DEM simulation are:

(1) the geometries of particles

For the computational simplicity, the majority of DEM models were realized using the simplest geometrical shapes for particles, such as disc-shaped and spherical elements. Some complex shapes were also invented such as ellipse, ellipsoid, polygon, polyhedron and super-quadric particles. However, the implementations of these geometries encounter limitations when a large-scale calculation is essential.

(2) the use of a suitable contact model to resolve any forces acting on a particle in the system

A model is required to evaluate contact force term $\boldsymbol{F}_{c,ij}$ between particles i and j, which is the sum of normal (head-on and tangential (shear) contributions. Many different contact models have been proposed in DEM simulations and the reader can referred to Schafer et al. [82] and Bertrand et al. [83] for more details. The most common representation used in a

DEM simulation is a spring-dashpot model, such as the linear-spring-dashpot (LSD) model of Cûndall and Strack [80] and the non-linear-spring-dashpot model based on the work of Hertz [84]. Recently, a combination of these two models has been proposed by Zhou et al. [85].

(3) the application of Newton's second law of motion to calculate changes in the motion of particles resulting from any unbalanced forces.

The simulation advance using small incremental time steps, and the total force on each particle is determined at every instant of time. The total force is the sum of all mechanical contact and body forces. These forces are then integrated over time to obtain the position and the velocity of each individual particle using Newton's second law of motion as follows:

$$m_i \frac{d\boldsymbol{v_i}}{dt} = \sum_{j=1}^{k_i} (\boldsymbol{F}_{c,ij} + \boldsymbol{F}_{d,ij}) + m_i \boldsymbol{g} + \boldsymbol{F}_i \qquad \text{(I-21)}$$

where m_i is the mass of particle i, $\boldsymbol{v_i}$ is its translation velocity, and k_i is the number of particles in contact with i at time t. The right-hand side of Eq. (I-21) represents the total force acting on the particle, including the contact force $\boldsymbol{F}_{c,ij}$ and contact damping force $\boldsymbol{F}_{d,ij}$ between particles i and j, the gravitational force $m_i \boldsymbol{g}$, any other forces $\boldsymbol{F}_i$ such as fluid drag or cohesion arising from Van der Waals interactions, liquid bridging, or electrostatic or magnetic effects.

Until now, for mixing processes the DEM has been mainly applied for modeling granular flows in various batch mixers [79], such as modeling of a V-blender by Lemieux [86], a double cone mixer by Manickam [87], a paddler mixer by Hassanpour et al. [88], a laboratory scale Turbula mixer by Marigo et al. [89,90], etc. Many of these studies have been validated by comparing with PEPT experimental results and these DEM simulations were generally used for understanding the dependence of mixer performance with varying conditions such as impeller speed and fill level, design parameters such as blade configurations and powder properties such as cohesion.

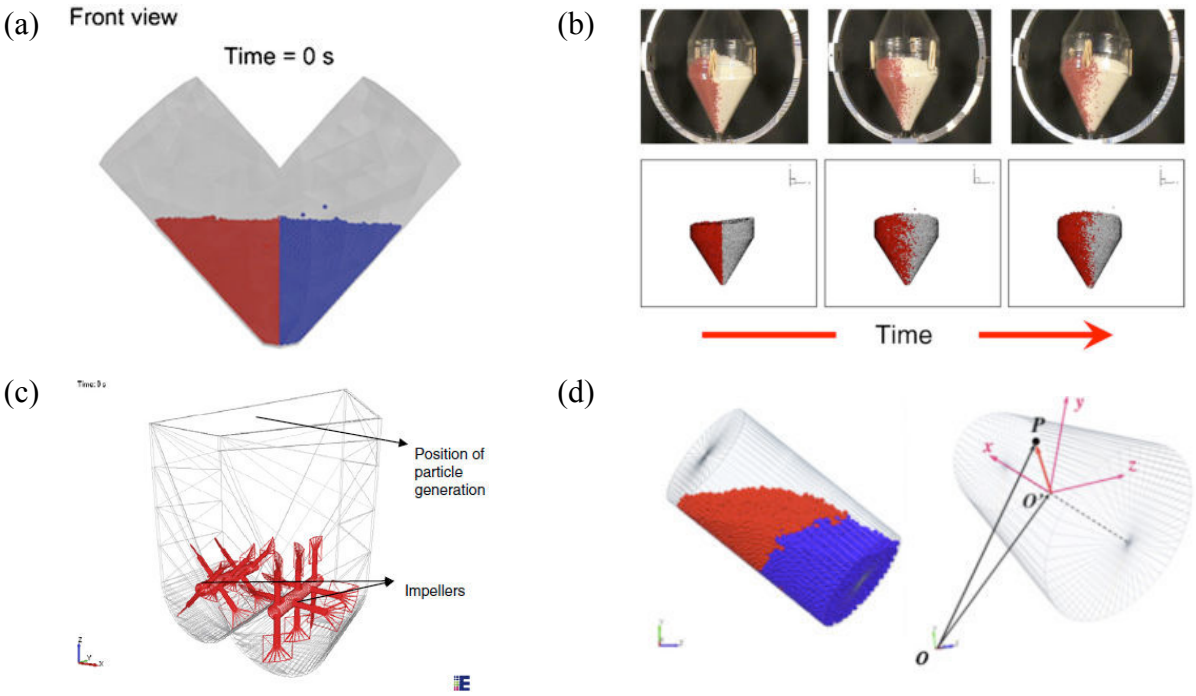

Figure I-30: Some DEM examples for batch mixers (a): V-blender simulated by Lemieux [86]; (b): Double cone mixer by Manickam [87]; (c): a paddler mixer by Hassanpour [87]; (d): Turbular mixer by Marigo et al. [89,90].

In comparison with DEM simulations for batch mixers, fewer studies have focused on DEM modeling of continuous mixing. As periodic boundary conditions have been extensively used in continuum-based solution of fluid flow and mixing for saving computational time, periodic section/slice DEM simulations of a full continuous mixer have been introduced for mixing of granular material by Dubey et al. [91]. The periodicity implies material exiting at one end of the section will enter from the other and it allows simulating an infinitely long continuous mixer with infinitely many identical sections attached on both ends of the mixer. However, inlet and outlet effects exiting in real continuous mixers cannot be computationally resolved using this periodic slice DEM approach, as stated by Sarkar and Wassgren [92,93]. The reason is that a periodic slice represents a section near the middle of the continuous mixer, away from inlet and outlet. In addition, the comparison of flow microdynamics from full mixer with periodic slice DEM simulations by Sarkar and Wassgren [94] led to the same conclusion. The work is based on the examinations of speed and velocity frequency distributions. As shown in Figure I-31, the full mixer is divided into four sections of equal axial length, section 1 corresponding to the inlet region and section 4 to the outlet region. Each section is comprised of two sets of two blades and four periodic slice models were used to simulate each of the four full mixers sections.

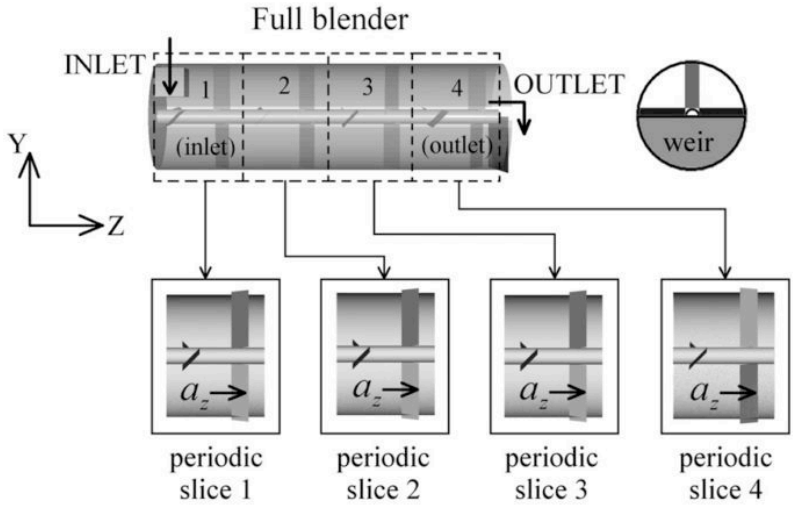

Figure I-31: Schematic of the full mixer design and corresponding periodic slice models from Sarkar and Wassgren [94].

Although DEM can be used as efficient tool, considerable limitations and challenges exist. The primary limitation is that DEM models are computationally intensive and require weeks/months of simulation, even if parallel computers are used. The computational complexity varies linearly with the number of particles and it is difficult to simulating full populations of particles (millions and billions) using conventional DEM. Recently, a hybrid DEM-Compartment model proposed by Portillo [95], hybrid DEM-PBM models proposed by Freireich et al. [96] and Sen et al. [97] and hybrid DEM-Markov models proposed by Doucet et al. [98], Tjakra et al. [99] and Trabelsi [100], demonstrated the potential for overcoming the defects of conventional DEM.

5 Studies on control strategies for particulate processes

The aim of control strategies is to ensure the stability of the process, to minimize the influence of disturbances and to optimize the overall performance. For developing a control strategy for an existing process, it is essential to analyze the process from the control engineer's viewpoint, so as to identifying three important types of variables [101].

- **Process variables (*PVs*):** variables that are measured, monitored, and controlled. The desired value of a controlled variable is referred to as its set-point.

- **Manipulated variables (*MVs*):** variables that can be adjusted in order to keep the controlled variable at or near their set-points.
- **Disturbance variables (*DVs*):** variables that affect the controlled variables but cannot be manipulated. Disturbances generally are related to changes in the operating environment of the process.

The specifications and selections of *PVs*, *MVs* and *DVs* should be based on process knowledge, experiences, and control objectives. To design control systems, two general approaches have been developed [102]:

(1) ***Traditional approach***

The control strategy is selected based on knowledge of the process, experience, and insight. After the control system is installed in the plant/process, the controller settings are adjusted.

(2) ***Model-based approach***

A dynamic model of the process is first developed that can be helpful in at least three ways: (a) it can be used as the basis for model-based controller design methods, (b) the dynamic model can be incorporated directly in the control law, and (c) the model can be used in a computer simulation to evaluate alternative control strategies and to determine preliminary values of the controller settings.

5.1 PID control and Model-based predictive control theories

5.1.1 Proportional-integral-derivative (PID) control

The PID controller has been the most popular and is by far the most applied form of feedback in use. More than 90% of all control loops are PIDs [103]. This predominance of PID control is due to its simplicity and its effectiveness in a wide range of applications.

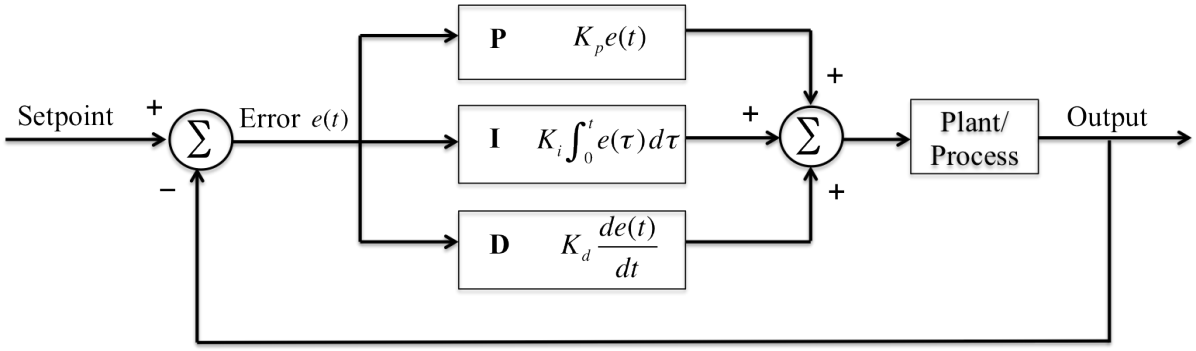

Figure I-32: Block diagram of a PID controller in a feedback loop.

Figure I-32 illustrates a block diagram of a single loop PID controller. It attempts to minimize the error (difference between the process output and the set-point) by adjusting the input of the process. The PID controller involves three actions: proportional action (denoted by P), integral action (denoted by I) and derivative action (denoted by D). The proportional action depends on the present error and the constant of proportionality is referred to the proportional gain, K_p. The integral action is for handling error based on learning from the past and the integral gain is K_i. The derivative action is a prediction of future errors and the derivative gain is K_d. The determination of K_p, K_i and K_d is well known as PID tuning. But PID tuning is usually a difficult problem, even though there are several different methods of PID tuning available [104], such as the Ziegler-Nichols tuning method, the internal model control method, and the integral square error method, etc. PID control performance can generally be improved by careful tuning, and performance may be unacceptable with poor tuning. Moreover, in order to enhance the single loop PID feedback control performance, a number of special control configurations such as cascade control, feedforward control and inferential control are often used and details can be found in the book of Spitzer [105].

5.1.2 Model-based predictive control (MBPC) strategy

Model based predictive control (MBPC) is also named model predictive control (MPC). Besides PID control, MPC is well known as the second most used advanced control technique [106] in the process industry, in which there is plant/process model to predict the future behavior of a process. A block diagram of a MPC system is shown in Figure I-33. A process model is used to predict the current values of the process output variables. The residuals, the differences between the actual and predicted outputs, serve as the feedback signal to the prediction block. The predictions are used in two types of MPC calculations: set-point

calculations and control calculations. The set points for the control calculations, also called target, are calculated from an economic optimization based on a steady-state model of the process. The set points are typically calculated each time the control calculations are performed.

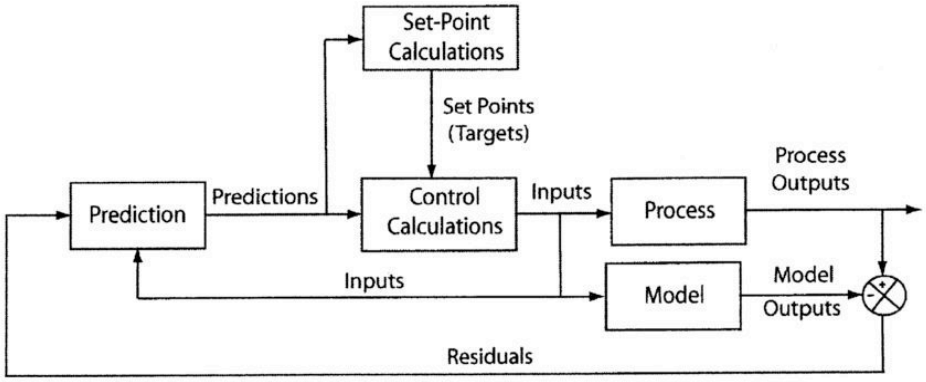

Figure I-33: Block diagram for model predictive control (MBP) [102].

The MPC calculations are based on current measurements and predictions of the future values of the output. The objective of the MPC control calculations is to determine a sequence of control moves (that is, manipulated input changes) so that the predicted response moves to the set point in an optimal manner. The actual output, predicted output, and manipulated input are shown in Figure I-34.

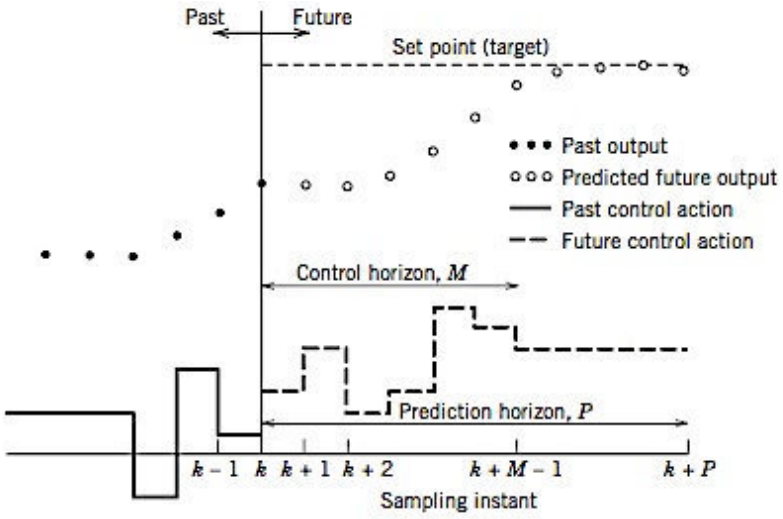

Figure I-34: Basic concept for model predictive control (MPC) [102].

At the current sampling instant *k*, the MPC strategy calculates a set of *M* values of the input. The set consist of the current input and *M-1* future inputs. The input is held constant after the *M* control moves. The inputs are calculated so that a set of *P* predicted outputs reaches the set point in an optimal manner. The control calculations are based on optimizing an objective function. The number of predictions *P* is referred to as the prediction horizon while the number of control moves *M* is called the control horizon.

Although the development and application of MPC technology was driven by industry, the main disadvantage of MPC is that it cannot be able of explicitly dealing with plant model uncertainties. A model with good predictive capability is not always available and has to be derived. The model accuracy determines the performance of MPC. On the other hand, the model was required as simple as possible to make on-line optimization feasible. It is obvious that accuracy and simplicity are often contradictory requirements.

Several recent publications provide a good introduction to applications of control technology in particulate processes. Christofides et al. [107,108] presented an overview of previously developed methods for model-based control of particulate process. Model predictive control (MPC) strategies have been frequently mentioned. Recently, MPC has been applied in several batch or continuous particulate processes, such as a batch crystallization reported by Mesbah et al. [109], a continuous crystallization studied by Shi et al. [110], a continuous drum granulation reported by Ramachandran and Chaudhury [111], a fluidized bed drying studied by Obregon et al. and continuous powder mixing discussed by Suresh et al. [112] and Ramanchandran et al. [112]. So far, few studies have focused on control loops for continuous powder mixing processes. In the following, we will present two examples.

5.2 Examples of model-based control

- **Model predictive control of a dynamic powder mixing**

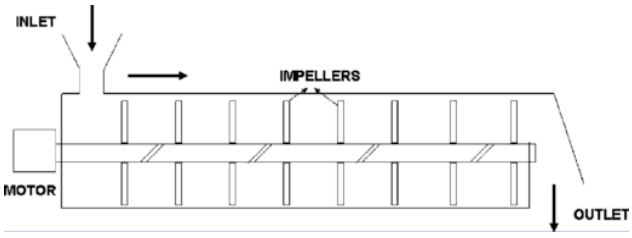

Figure I-35: Schematic of a continuous dry mixer from Suresh et al. [112].

Suresh et al. [112] presented a model for a continuous mixer (see Figure I-35). This model related the correlation between the variance reduction ratio, the blender efficiency and the various operating parameters. It was the extension and re-derivation of the previous model introduced by Williams and Rahman [59,113] using residence time distributions. The proposed model was based on the assumption that the powder mixture at the input to the mixer behaves like a Newtonian fluid for local insider the mixer barrel.

$$VRR(t)=\frac{\sigma_i^2(t)}{\sigma_o^2(t)}=\frac{\exp\left(-\frac{2w(t)}{W(t)}\right)\eta(t-1)}{\left[1-\exp\left(-\frac{w(t)}{W(t)}\right)\eta(t-1)\right]^2}\times$$
$$\left\{\sum_{j=1}^{K}\exp\left[-2j\left(\frac{w(t)}{W(t)}\right)\eta(t-j)\right]+2\sum_{j=1}^{K-1}\sum_{\mathscr{L}=j+1}^{K}\exp\left(-\frac{w(t)}{W(t)}\right)(j\eta(t-j)+\mathscr{L}\eta(t-\mathscr{L}))r_{j\mathscr{L}}\right\}^{-1} \quad \text{(I-22)}$$

$$\frac{dW(t)}{dt}=w(t)-0.3\omega(t)W_dHD\cos\varphi \quad \text{(I-23)}$$

$$\eta(t)=\begin{cases}0.126\omega^2(t)-2.25\omega(t)+11.16 & t>0\\ 0 & t\le 0\end{cases} \quad \text{(I-24)}$$

where the variables listed are defined as follow: VRR, the variance reduction ration; W, the mass in the mixer; W_1, the lower mass limit in the mixer; ω, the screw speed; w, the inlet mass flow; W_d, the pitch of the screw; H, the gap between the screw and the barrel; D, the diameter of the barrel; φ, the helix angle of the screw; η, the measure of blender efficiency; $r_{j\mathscr{L}}$, the input serial correlation coefficient; and k, the number of samples of input.

Using the dynamic mixing model presented above, a model predictive control (MPC) was implemented. The VRR and the mass in the mixer W were used as controlled variables. The inlet flow rate $w(t)$ and the rotational speed $\omega(t)$ were manipulated variables. It was assumed that there are no disturbance variables in the operation. The change in the manipulated variables were modeled using a first order actuator dynamics, as given by:

$$\frac{dw}{dt} = \frac{w_d - w}{\tau_w}, \quad \frac{d\omega}{dt} = \frac{\omega_d - \omega}{\tau_\omega} \tag{I-25}$$

where parameters w_d and ω_d are the set-points, τ_w and τ_ω are the time constants for the inlet flow rate and the rotational speed, respectively. The application of the MPC was performed using OntoMODEL, which is an ontological tool for mechanistic mathematical model management that facilitates systematic and standardizable methods for model storage, usage and solution and effective as the multifunctional platform for mathematical model-based application in pharmaceutical process and product development. The MPC controller simulation for the dynamic mixing operation described above is illustrated in Figure I-36.

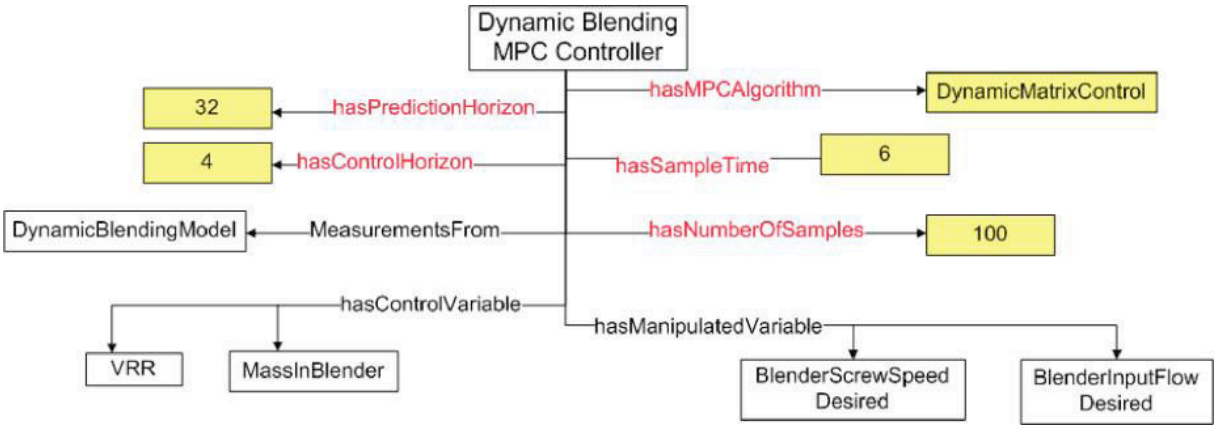

Figure I-36: Dynamic blender MPC controller instance from Suresh et al. [112].

It was found that the controller performed satisfactorily for a 10% change in the *VRR* setpoint but was rather delaying when a 10% change of the mass in the mixer (W) setpoint was initiated, due to the nonlinearity of the process model described above. It was also pointed out that this control problem may be resolved using a linearized process model with acceptable performanca or a nonlinear MPC.

- **Model-based control-loop of a continuous direct compaction process**

Ramachandran et al. [114] reported a model-based control-loop performance of a continuous direct compaction process , as shown in Figure I-37 (a), which involves multiple processing steps: powder feeding, powder mixing, tablet compaction and tablet dissoultion test. Focused on process control, the manipulated and controlled variables (MVs and CVs) for each unit

operation were illustrated in Figure I-37 (b) . The continuous mixing process studied here was the combination of powder feeding and mixing operations

(a)

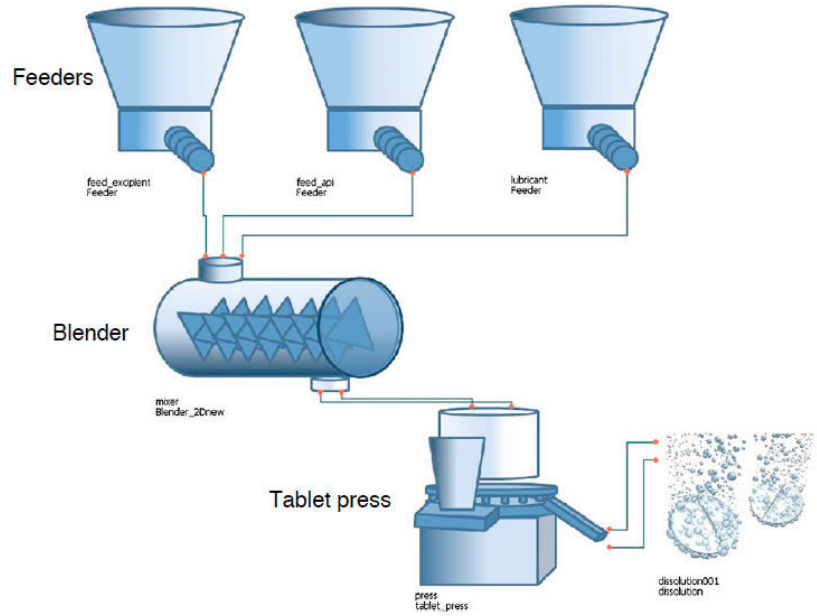

(b)

Unit operation	MV	CV
Feeders	Screw speed (rpm)	Feed rates (CPP)
Blender	Rotation rate (rpm), feed rates	Flowrate (CPP), API composition (CQA), RSD (CQA)
Tablet press	Compression and precompression forces	Weight (CQA), hardness (CQA)
Dissolution process	Hardness	Dissolution (CQA)

MV manipulated variable, *CV* controlled variable, *CPP* critical process parameter, *API* active pharmaceutical ingredient, *CQA* critical quality attribute, *RSD* relative standard deviation

Figure I-37: (a) Schematic of a direct compaction process (b) Manipulated variables (MV) and controlled variables (CV) of the various units operations indicating the important critical process parameters (CPPs) and critical quality attributes (CQAs) of tablets (or intermediate products) [114].

In the feeding operation, three feeders were implemented for the active pharmaceutical ingredient (API), excipient and lubricant, respectively. The feed rates were controlled by adjusting the screw speeds of feeders. In the mixing operation, the rotational speed and feed rates of the mixer were identified as manipulated variables; the exiting total flow rate, API composition and relative standard deviation (*RSD*) were identified as controlled variables.

The proposed control approach mainly consists of three steps : (1) to obtain control (or process) models via system identification from dynamic models, experimental data, and/or literature data, (2) formulate a suitable control structure, (3) optimal tuning of controller

parameters via a suitable control-loop performance criteria, e.g. a scaled integral time error (*ITAE*) defined as follows:

$$ITAE(\boldsymbol{p}) = \sum_{m=1}^{n_m}\sum_{z=1}^{n_z}\left\| \frac{\boldsymbol{y}_{reponse,m}(t_z,\boldsymbol{p}) - \boldsymbol{y}_{setpoint,m}(t_z)}{\boldsymbol{y}_{setpoint,m}(t_z)} t_z \right\|_1 \qquad \text{(I-26)}$$

where $\boldsymbol{p}$ represents the vector of tuning parameters for the various m controllers, z represents the number of time points and $\boldsymbol{y}$ represents the controlled variables of interest.

The mixer was modeled via a dynamic population model (PBM). The transfer function, as process models for continuous powder mixing, were obtained via system identification from PBM, experimental data, and/or literature data. Due to uncertainties present in the data, the process models will always be an inaccurate representation of the true process. For instance, a different set of transfer functions were obtained due to uncertainties in model parameters. Therefore, cases with three intensities (mild, moderate and high) of multivariable process interactions were analysed.

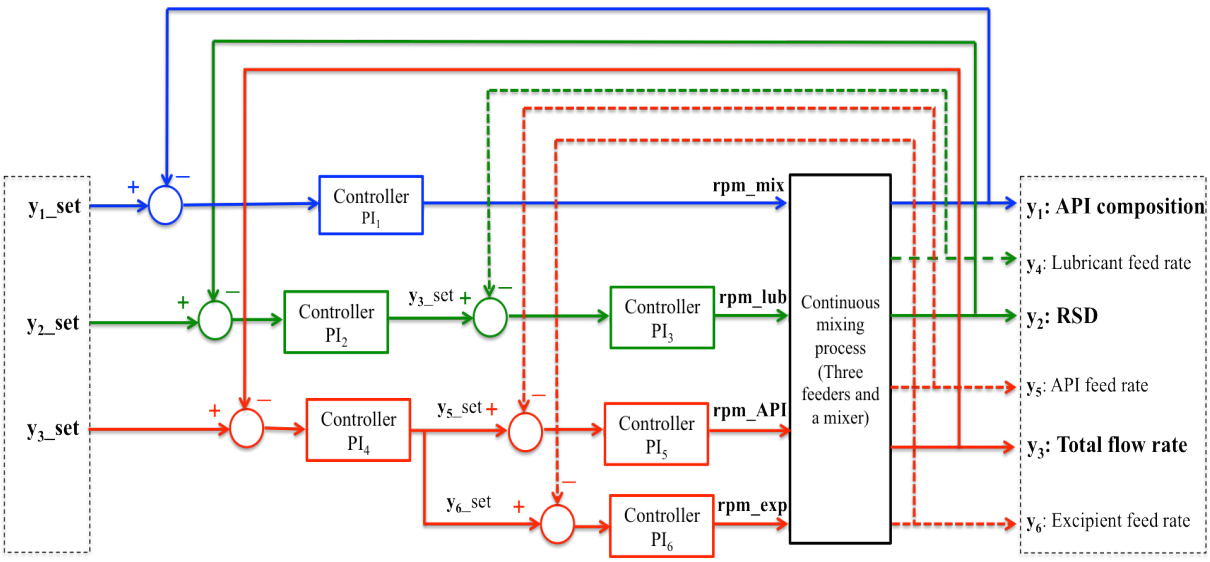

Figure I-38: Cascade control system proposed by Ramachandran et al. [114].

For each case, the same control structure was proposed, as shown in Figure I-38. API composition (y_1), relative standard deviation (y_2) and total flow rate (y_3) at the exit of the mixer were taken as master controlled variables. The control loop of API Composition (y_1) was performed using a proportional-integral (PI) controller for manipulating the mixing rotational speed (rpm_mix). The control loop of *RSD* (y_2) consisted of two PI controllers

(master and slave), where a slave loop controlled the lubricant feed rate (y_4) set point generated through a master loop that controlled by manipulating the lubricant feeder screw speed (rpm_lub). The control loop of the exit total flow rate (y_3) involved three PI controllers (one master and two slave), where a master loop was implemented to provide the feed rate set-points of API (y_5) and excipient (y_6) while two slave loops tracked y_5 and y_6 set-points by manipulating respective feeder screw speed (rpm_API and rmp_exp).

For each case, the performance of the proposed control system for set-point tracking was evaluated. In particular, the step changes in the set point have been made for analyzing the ability of the controller to track the provided set point. Simulation results showed that for mild process interactions, the set-point tracking ability of the control strategy and tuning parameters was robust. In addition, the disturbance rejection ability of the proposed control strategy was also investigated by setting stochastic disturbances (e.g. random noise) and results revealed that the control system couldn't lighten the effect of the disturbances.

6 Conclusion

Powder mixing process depends on many factors like particles properties, mixer designs, operating conditions, and mixture formulations, etc. In comparison with batch mixing, continuous powder mixing is an attractive alternative for large volume processing in industry. Studies on powder mixing in continuous mixers were reviewed, involving at-/in-/on-line measurements of mixture homogeneity by various monitoring techniques and characterizations of powder flow behavior using *VRR*, RTD, and hold-up. In addition, modeling approaches (e.g. Markov chain, DEM), were introduced to predict the behavior of powder mixing in mixers. The ultimate goal of all these studies is to understand how the critical process parameters influence the performance of continuous powder mixing. Although several control strategies were proposed for continuous particulate process, control system loops have not yet been introduced for continuous mixing in experimental set-up. Thus, this calls for further research on the developpement of control strategies for continous powder mixing process in order to ensure good performance and stability.

CHAPTER II: Materials and experimental setting

1 Materials

The two granular materials used in the experiments are fine couscous and medium couscous, provided by RICCI and FERRERO. Fine couscous was colored in black with a 10% Iodine solution and then air-dried under a fume hood. It is noted that the fine couscous particles become slightly larger and tend to form agglomerates during color processing. A sieve with a mesh opening of 1250 μm was used for pre-screening both the colored fine-grain couscous and medium-grain couscous. For the colored fine couscous, the pre-screening permits the removal of agglomerates, and the powder with particles less than 1250 μm was used as component A. For the medium-grain couscous, the powder with particles larger than 1250 μm was utilized as component B for mixing experiments.

(a)  (b) 

Figure II-1: Granular material samples: (a) component A (colored fine couscous); (b) component B (medium couscous).

The bulk behavior of powders of each component is characterized in terms of particle size distribution, density, surface state, porosity, flowability and floodability properties. These properties play an important role in powder handling and processing operations, such as feeding, transportation, mixing, compression, etc.

1.1 Particle size distribution

The particle size distribution of each component is assed by sieve analysis with a series of RESTCH sieve shakers (AS 200), for which the particles are separated on sieves of different sizes by setting vibration amplitude and sieving time.

(a)

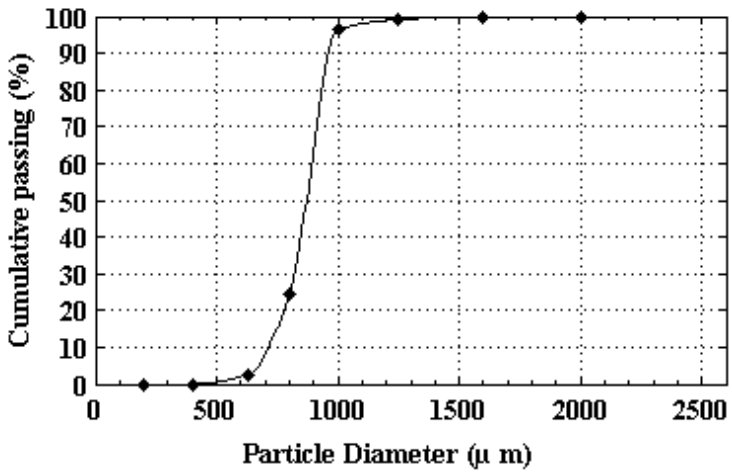

(b)

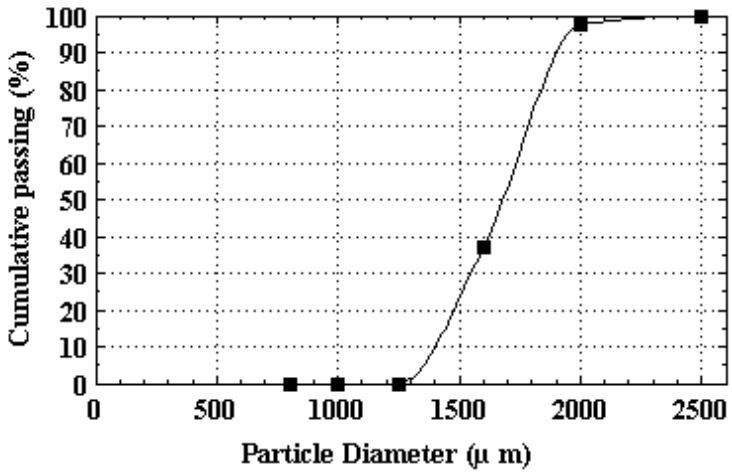

Figure II-2: Particle size distribution: (a) colored fine couscous (Component A); (b) medium couscous (Component B).

The results of size analysis of two components are respectively represented by a cumulative mass fraction curve, in which the mass proportion of particles smaller than a certain size is plotted against that size. As shown in Figure II-2 (a) and (b), component A is made up of particles of diameter between 500 μm and 1250 μm, while component B contains particles in the size range 1250–2000 μm.

From each cumulative curve, it is easy to determine particle size distribution parameters such as the d_{10}, d_{50}, and $d_{90,}$ respectively, representing 10%, 50%, and 90% of the particles finer than these sizes. In other words, the values of d_{10}, d_{50}, and d_{90} correspond to the cumulative distribution at 10%, 50% and 90%. In addition, the width of the particle size distribution can be evaluated by the "Span", which is calculated by:

$$Span = \frac{d_{90} - d_{10}}{d_{50}} \qquad \text{(II-1)}$$

The values of the key particle size distribution parameters of component A and B are illustrated in Table II-1. The spans of both components are low as 0.29, indicating that the particles are quasi-monodisperse and tend to segregate.

Table II-1: Particle size distribution parameters of component A and B.

Diameter [μm]	Component A (Colored fine couscous)	Component B (Medium couscous)
d_{10}	700	1400
d_{50}	870	1680
d_{90}	960	1900
$Span = \frac{d_{90} - d_{10}}{d_{50}}$	0.29	0.29

1.2 Particle shape and surface roughness

Particles of the two components are visualized under an optical microscope at 50 times magnification. Information about particle shape and surface roughness can be obtained from the images in Figure II-3. By comparing the two images, we can see that the particles of component B are more irregular in shape and rougher in surface.

(a) 

(b) 

Figure II-3: Particle images captured by an optical microscope: (a) particles of component A; (b) particles of component B.

1.3 Density and Porosity

- ***True (particle) density***

The true density of a solid is the average mass per unit volume, exclusive of all voids that are not fundamental part of the particle packing arrangement. Therefore, the true density of a solid is an intrinsic property. In this study, the true density of each component is determined experimentally using a helium pycnometer, for which the true volume of a solid is determined by measuring the pressure difference when a known quantity of helium under pressure is allowed to flow from a precisely known reference volume into a sample cell containing the solid material.

- ***Aerated bulk density***

Aerated bulk density is, in practical terms, the density at which the powder is in its most loosely packed form. The apparatus, for determining aerated bulk density, usually consists of a screen cover, a screen sieve, a spacer ring and a stationary chute attached to a vibrator. A Hosokawa Powder tester is used for measuring the aerated bulk density of each component studied. The powder sample is poured by a vibrating sieve and allowed to fall from a fixed height (about 25 cm) through the stationary chute into a test cup (100ml). This allows to calculate an aerated volume, and thus the aerated bulk density, given the powder mass.

- ***Tapped density***

The tapped density of a powder is the ratio of the mass of the powder to the volume occupied by the powder after tapping. The tapped density of a powder represents its random dense packing. Tapped density is measured by first gently pouring a specified mass of powder into a graduated cylinder and then tapping mechanically the cylinder against a hard surface, from a standard height (typically 15mm), by a defined number of times. In this study, the tapped density of each granular component is measured after 1500 taps.

- ***Porosity***

Porosity is also an important granular characteristic and it is defined as the fraction of the void volume over the total volume of the powder sample. Porosity can be derived directly from powder density as:

$$\varepsilon_{aerated} = \frac{\rho_{true} - \rho_{aerated}}{\rho_{true}} \text{ or } \varepsilon_{tapped} = \frac{\rho_{true} - \rho_{tapped}}{\rho_{true}} \quad \text{(II-2)}$$

Table II-2: Different types of densities of component A and B.

Density [g.cm^{-3}]	Component A	Component B
ρ_{true}	1.437	1.444
$\rho_{aerated}$	0.840	0.737
ρ_{tapped}	0.875	0.756

Table II-3: Inter-particle porosity of component A and B

Porosity	Component A	Component B
$\varepsilon_{aerated}$	0.415	0.490
ε_{tapped}	0.391	0.476

From Table II-2 it can be seen that the true density of component A is very close to that of component B, which is logical since these components are of the same nature. However, component B has lower aerated and tapped densities than component A, thereby showing a higher inter-particle porosity, as listed in Table II-3. The higher porosity of component B is mostly due to high irregular shape and surface roughness of the particles, because the "Span" of the two components are the same.

1.4 Flowability

Powder flowability refers to the ability of a powder to flow under given conditions and it is an important property in powder handling and processing operations. Therefore, evaluation of the flowability of any powder is a very important issue for many industries. To evaluate the flowability, three tests are carried out to measure:

- ***Hausner ratio (H) and Carr's index (CI)***

Hausner ratio and Carr's index (compressibility) are two closely related, empirically derived methods for assessing flowability. The two indexes are determined based on the aerated bulk density and tapped density mentioned above. Hausner ratio (H) is defined as the ratio of tapped density to aerated bulk density, given by Eq. (II-3).

$$H = \frac{\rho_{tapped}}{\rho_{aerated}} \tag{II-3}$$

For a Hausner ratio of 1.0–1.1, the powder is classified as free-flowing; 1.0–1.25, medium-flowing; 1.25–1.4, difficult-flowing; and >1.4, very-difficult-flowing.
Carr's compressibility index (*CI*) is defined as follows:

$$CI(\%) = \frac{\rho_{tapped} - \rho_{aerated}}{\rho_{aerated}} \times 100 \tag{II-4}$$

The smaller the Carr's compressibility index, the more fluidity the powder behaves. Thus, a free-flowing powder should have a low compressibility index, because the inter-particle

forces are not as significant as in a poorly-flowing powder, which implies the value of aerated bulk density is close to that of tapped density.

- ***Angle of repose (α_R)***

Angle of repose is defined as the angle of the free surface of a pile of powder to the horizontal plan. Depending on the conditions under which the pile has been poured and how the angle is measured, somewhat different values of the angle can be obtained for the same powder. The major factors influencing the angle of repose are size distribution, surface roughness of the particles, void fraction of the powder bed, and moisture content. An angle of repose of less than 38° is considered a free-flowing powder, whilst more than 55° is considered a cohesive powder.

- ***Angle of spatula (α_S)***

Angle of spatula provides an indication of the internal friction between particles. It is determined by inserting a flat blade into a pile of granular material and lifting vertically. The new angle of repose that the material forms relative to the horizontal blade surface is know as the angle of spatula (α_S). For a material to be considered free-flowing, its angle of spatula should be below 40°.

Table II-4: Granular material flowability evaluation.

Measures of flowability	Component A	Component B
H	1.042	1.026
CI (%)	4.2	2.6
α_R (°)	30.5	33.6
α_S (°)	18.4	20.3

The flowabiltiy evaluation of two granular materials is given by Table II-4, where the angle of repose and angle of spatula are measured by a Hosokawa Powder tester. All characteristic values of flowability indicate that the two components used in experiments can be classified as free-flowing materials.

1.5 Floodability

Floodability is related to the tendency of powder to flood due to interstitial gas overpressure. It assigns an estimated value to the behavior of a bulk product when it is moved after an initial state of rest (feeding, transporting, emptying containers, etc.). Two additional tests are carried out to evaluate the floodability, by measuring:

- ***Angle of fall (α_F)***

The angle of fall is obtained as the new angle of repose when the powder cone is mechanically shocked.

- ***Angle of difference (α_D)***

The angle of difference is:

$$\alpha_D = \alpha_R - \alpha_F \qquad \text{(II-5)}$$

This parameter is related to the internal cohesion of the granular particles. A powder with high angle of difference is more likely to have an unsteady floodable flow.

Table II-5: Granular material floodability evalaution.

Measures of floodability	Component A	Component B
α_F (°)	17.1	17.6
α_D (°)	13.4	16

The measurements of floodabilty for the two granular materials are shown in Table II-5. It is found that component A and B have similar floodability, since relatively close values of α_F or α_D are obtained from the two components.

2 Experimental set-up

The experimental set-up shown in Figure II-4 includes three parts: a feeding system, a continuous mixing equipment, and an on-line analysis system for powder mixture homogeneity. The feeding system is used to feed continuously the powder directly into the mixer inlet chute. This study is related to the mixing of two powder ingredients, therefore two powder feeders are used. The continuous mixer is a Gericke GCM 500, for which where the two powder ingredients fed at the inlet are continuously mixed and removed from the outlet. At the outlet of the mixer, the mixed powder is discharged through a chute and fall on a moving belt. The homogeneity of the powder mixture on the belt will be directly measured on line.

Figure II-4: Experimental set-up.

2.1 Feeding system

In the feeding system, two loss-in-weight feeders are used for the experiments to ensure a high accuracy feed rate control. As shown in Figure II-5, each feeder mainly consists of a hopper, a screw feeder, and a weighing unit. To prevent powder caking and bridging during feeding, two types of agitators (vertical and horizontal) with separate drives are respectively installed in the hopper and feeder. The material to be fed is stored in the hopper, which has an upper and lower fill level. That implies that the hopper should be refilled when the minimum fill level is reached and the refilling should be stopped when the maximum fill level is reached. In this study, the hopper is pre-filled to its upper level before starting each experiment. The feeder under the hopper has a rotating spiral screw that moves material from the hopper to the outlet of the feeder through a discharge tube. The rotational screw is driven by a separate electric motor that is controlled for adjusting the rotation speed of the screw through a variable-speed drive (VSD) model VLT 5000. The weighing unit permits the measurement of weight reduction with time during discharge, which is also instantaneous mass flow rate (or feed rate). In the feeding system, a closed-loop control is applied for continuously modifying the screw's rotational speed to compensate for the difference between the setpoint and the current measured value of the mass flow rate. This allows to ensure that the actual flow rate is maintained as close as possible to its setpoint.

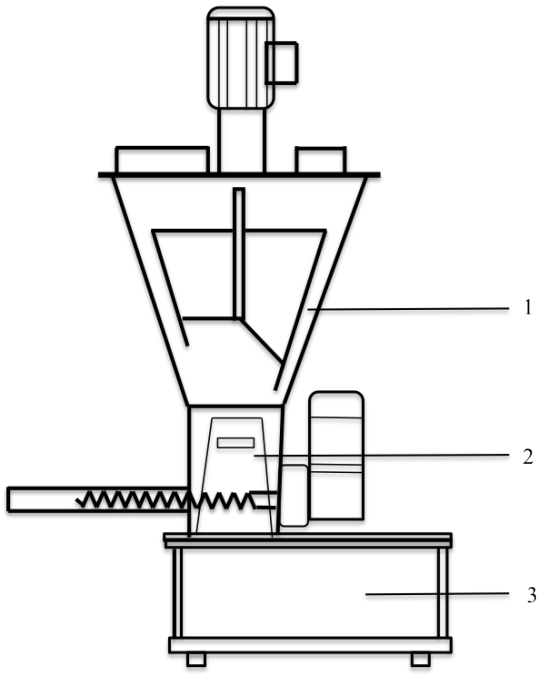

1: Hopper
2: Screw feeder
3: Weighing unit

Figure II-5: Feeding system.

2.2 Mixing system

The continuous mixing system used in this work is shown Figure II-6. It mainly comprises a horizontal convective mixer and a mixing tool in the mixer.

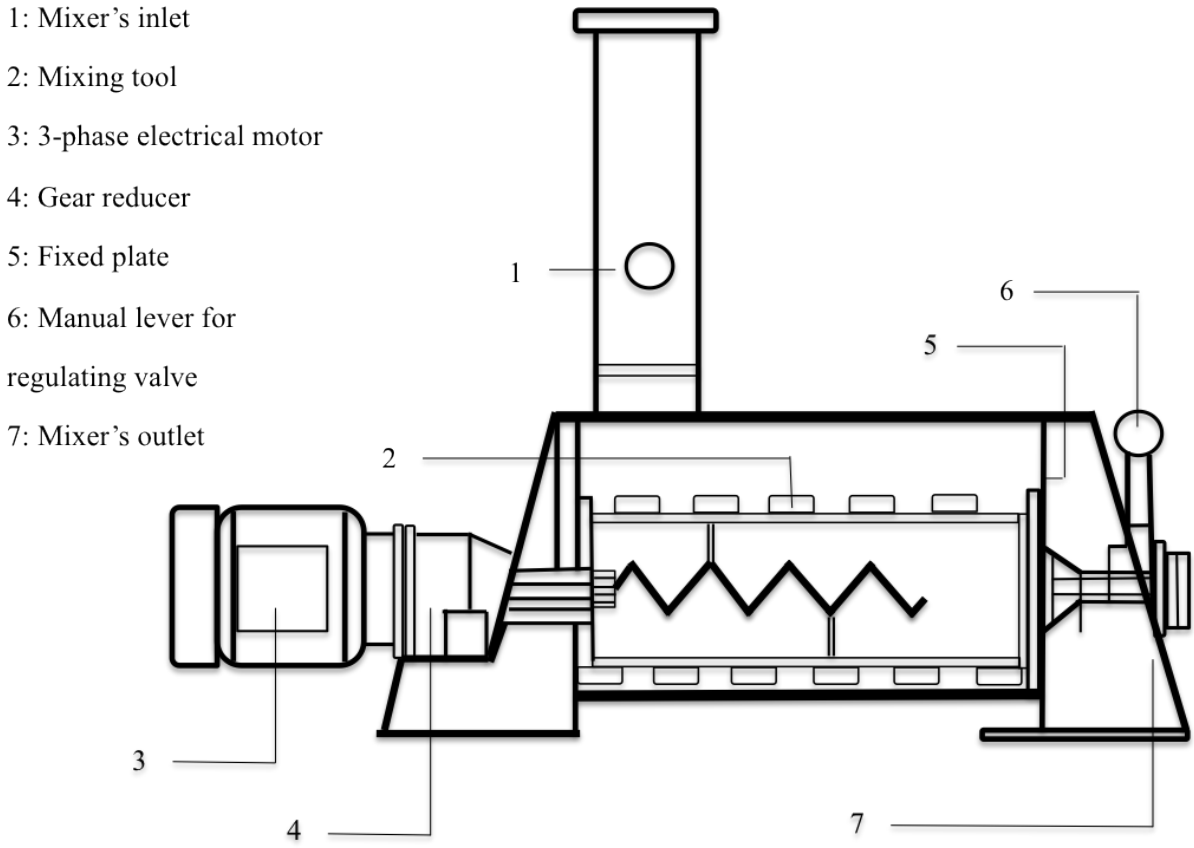

Figure II-6: Gericke GCM 500 continuous mixer.

The continuous mixer is a Gericke model GCM500. It is in semi-cylindrical of 0.5 m long, 0.615 m height and 0.2 m in diameter. A cylindrical tube with two symmetrical holes is set at the mixer's inlet and a manually adjustable valve is mounted at the mixer's outlet. Throughout the study, the outlet valve is turned to its maximum open position showing an fan-shaped exit, the surface of which is about 15 cm^2. The mixing tool (or stirring device), shown in Figure II-7, consists of a rectangular frame with five blades on each long side and two blades on each short side, which ensure radial particle dispersion inside the mixer. A screw promotes the powder's axial transport to the mixer's outlet.

Figure II-7: Mixing tool.

The mixing tool is rotated by a gear reducer driven by a 3-phase electrical motor, which is controlled by a variable-speed drive (VSD) model VLT 2800. The motor's frequency is denoted as N (Hz) and the actual rotational speed of the mixing tool is denoted as N_m (rpm). The empirical ratio between N_m (rpm) and N (Hz) is 2.6. In addition, the rotational speed of the motor is up to 60 Hz in order to avoid particulate attrition in the process.

2.3 On-line image analysis system

The on-line analysis system is for on-line monitoring the composition and the homogeneity of the powder discharged from the mixer. Actually, the implementation of the on-line analysis system has been presented by Demeyre [26] and Ammarcha [2]. It mainly consists of a green conveyor belt of 30 cm width and a digital line scan camera, as depicted in Figure II-8.

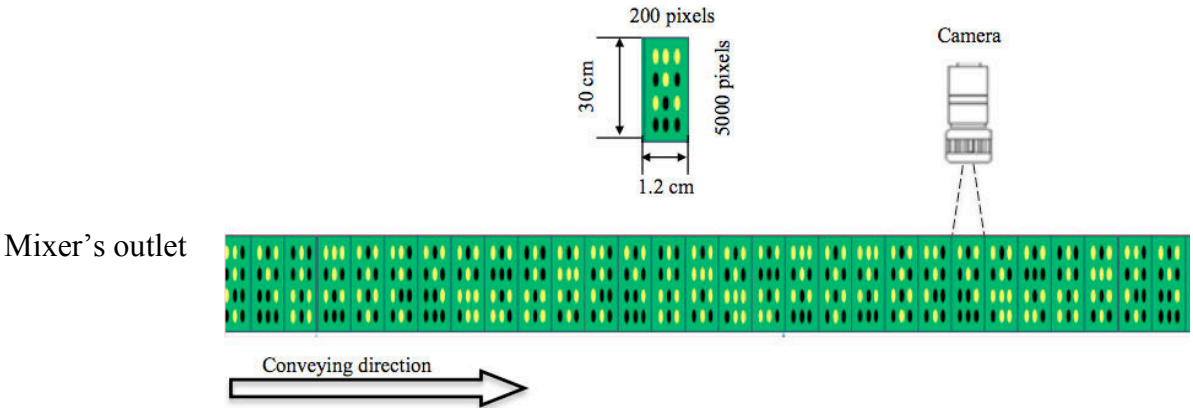

Figure II-8: On-line image analysis system at the mixer's outlet.

As shown in the figure, the powders are continuously discharge from the mixer and delivered as monolayer on the conveyor belt, the moving direction of which allows powders to pass

under a fixed camera and then to be retrieved in a container. The camera is a digital line scan camera Lord DVL 5000 T (see Figure II-9).

Figure II-9: Digital line scan camera Lord DVL 5000 T.

This camera scans one line at a time and it is usually chosen for capturing moving images. Its principal optoelectronic characteristics are listed in Table II-6.

Table II-6: Principle optoelectronic characteristics of camera DVL 5000 T.

Number of pixels	5000 pixels
Size of pixel	7 μm x 7μm
Photo-sensitive area	35 mm x 7 μm
Sensitivity	300 000 lsb/lux.s
Maximum pixel frequency	20 MHz
Maximum line frequency	3.77 KHz
Output video format	16 bits RS422
Lens mount	F-Nikon 24 x 36

This camera has a 1-D (line) CCD image sensor with a resolution of 5000 pixels. In order to exclude external light interference, the camera is set in an opaque wooden box, in which an illumination system is provided for increasing the image contrast and resolution. This helps improve the overall performance of the system. In this study, the camera is fixed in an appropriate height to ensure that the entire 30 cm width of the conveyor belt lays in the photo-sensitive area of 5000 pixels in width. This implies that each pixel represents 60 μm x 60 μm area under inspection. Because the camera scans one line at a time, the line rate of the camera should be synchronized with the moving speed of the conveyor belt in order to ensure that consecutive lines can be captured without overlap nor skip space. Every 200 consecutive lines

create an image (or frame), for which each line is composed of 5000 pixels in width. The images are continuously acquired at a rate close to 14 images per second.

3 Experimental operating system

The experimental set-up is controlled using a Labview software, which is a system design platform and development environment for a visual programming language from National Instruments (NI). The overall experimental operating system is illustrated in Figure II-10.

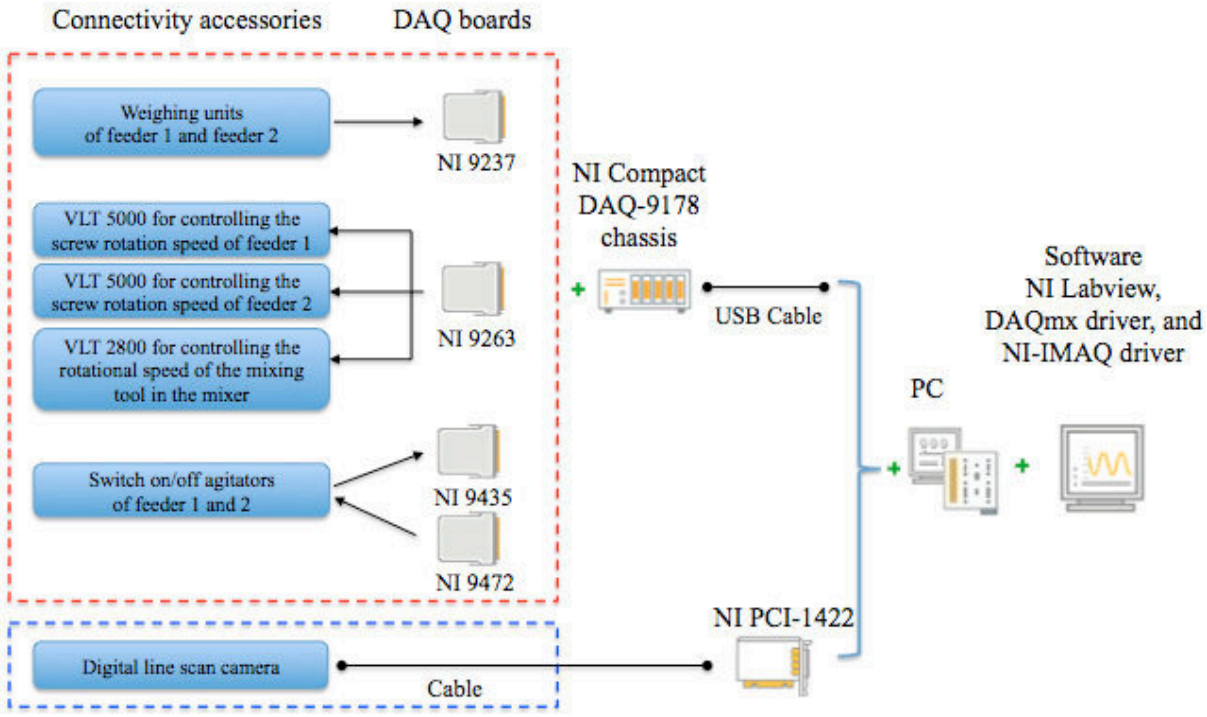

Figure II-10: Experimental operating system layout.

It can be decomposed into two main parts: (1) operating platform for the feeding and mixing systems and (2) operating platform for the on-line image analysis system.

3.1 Operating platform for the feeders and the mixer

In the feeding and mixing systems, the data acquisition device (DAQ) used is a NI Compact DAQ-9178 chassis, which includes four NI modules: source digital input module NI 9435,

source digital output module NI 9472, analog voltage input module NI 9237, and analog voltage output module NI 9263.

The module NI 9472 is used to switch on/off the agitators of the hoppers and the module NI 9435 is used to display on/off status. The module NI 9237 is connected to the weighing unit of the feeding system. The module NI 9263 is used to send the analog output voltages to three variable-speed drives of model VLT, thereby adjusting three motors' rotational speeds. The feeders are driven by VLT 5000 and the mixer is driven by VLT 2800. The executable program in Labview for running the feeders and the mixer can be summarized in Figure II-11.

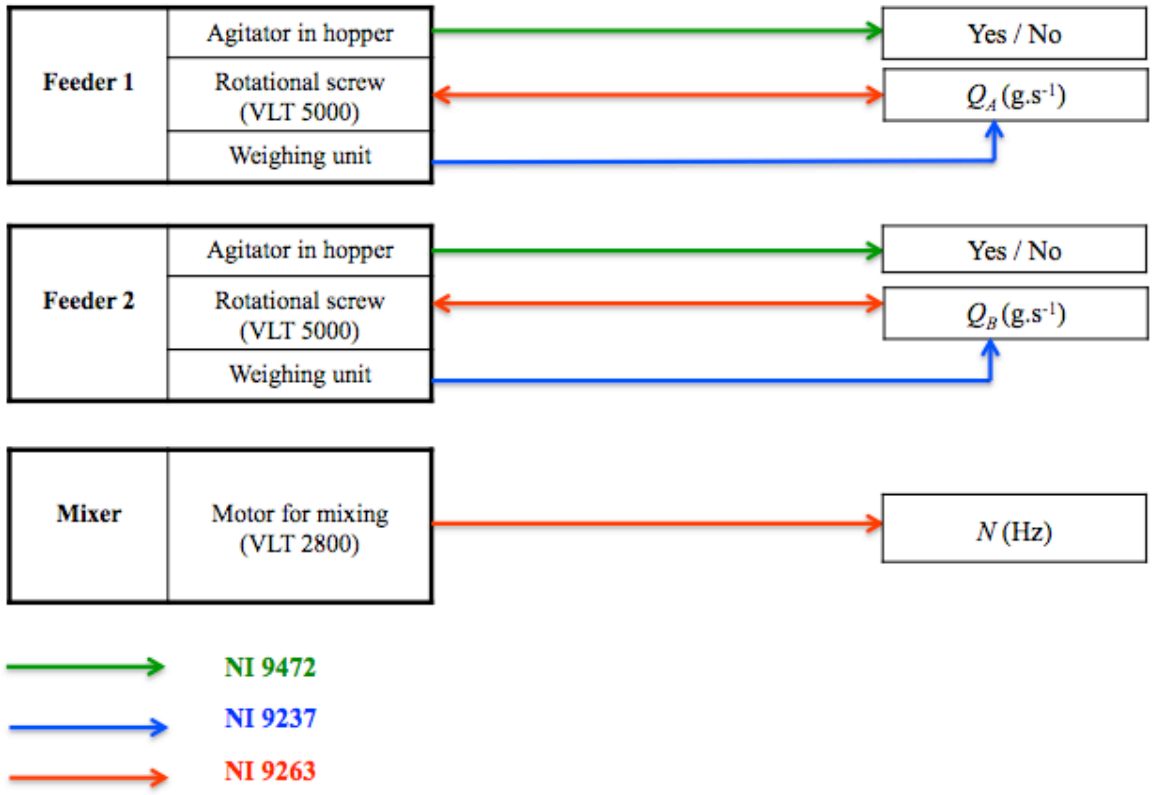

Figure II-11: Principles for driving the feeders and the mixer.

As shown in the figure, for each feeder, the on/off of the hopper's agitator is controlled by NI 9472 and the flow rate Q_A or Q_B depends on the screw's rotational speed, which is adjusted through a feedback control where the flow rate monitored by the weighing unit is compared with its setpoint. For the mixer, the motor's frequency (N) depends on the output voltage from NI 9263. The curve given in Figure II-12 shows a linear relationship between the reference voltage signal from NI 9263 and the corresponding output frequency of VLT 2800 (or motor frequency). The maximum voltage of analog output is 10 V.

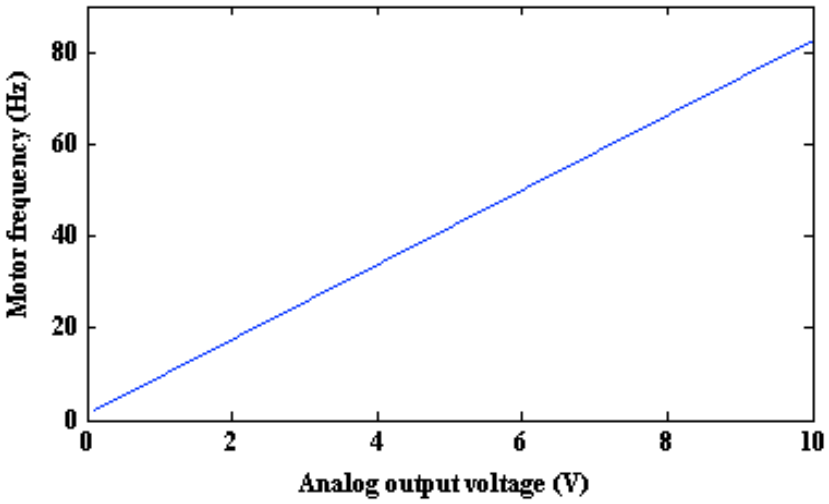

Figure II-12: Correlation curve between the analog output voltage (V) and the mixer's motor frequency (Hz).

3.2 Operating platform for the on-line image analysis system

The NI PCI-1422 board is implemented to acquire images from the digital line scan camera. This digital image acquisition board is directly controlled by NI-IMAQ driver and it performs high-speed, large-image, high-resolution digital image capture, and can capture up to 16 bits of data at a frequency of 40 MHz for a total acquisition rate of 80 MB/s. The image processing and analysis is then accomplished using the NI Vision development module in Labview. All these procedures are key to achieve the ultimate objective of determining the concentration of the component interest and the homogeneity of powder mixtures in real time.

3.2.1 Image processing and analysis

As shown in Figure II-8, we observe three different colours with naked eyes: the green of the conveyor belt, the black of component A and the light yellow of component B. The procedure for determining the percentages of surfaces occupied by component A and B, respectively, can be summarized in the following steps:

(1) Each acquired image is first saved as an 8-bit (from 0 to 255) gray-scaled image and transferred to a memory buffer with a separate number in the buffer list. It can then be extracted from the buffer list for further image processing and analysis. The buffer list follows a first-in first-out principle, outputting data in the order it arrived.

(2) In order to differentiate the object (the material to be measured) from the others being background, each gray-scaled image is then converted to a binary image in which the object has a pixel intensity of 1 (white) and the background has a pixel intensity of 0 (black). The binarization is realized using an IMAQ thresholding function, for which each pixel value in the image is compared with two specified threshold intensities (or values), the lowest pixel value and the highest pixel value. Pixel values that lay within the range of two threshold values will be set to 1 (white), while others will be set to 0 (black).

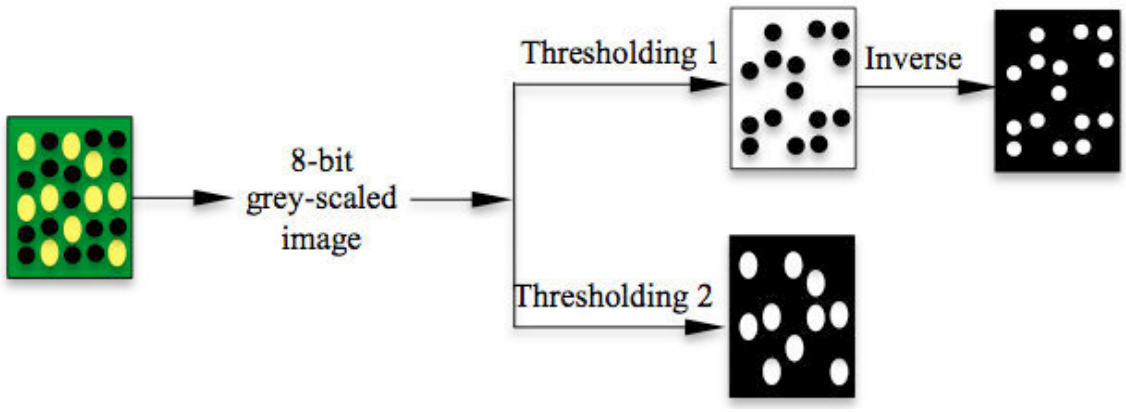

Figure II-13: Image processing and analysis for determination of the percentages of surfaces occupied by component A and B, respectively.

As shown in Figure II-13, for a given image, the percentage of the surface covered by component A ($\%S_A$) is quantified through thresholding 1 and an inverse operation. In this study, the inverse operation is newly suggested to directly measure $\%S_A$ unlike in the work of Ammarcha [2], for which $\%S_A$ is deduced from the white coverage ratio of the image binarised by thresholding 1. The percentage of the surface covered by component B ($\%S_B$) is quantified through thresholding 2. It should be noted that $\%S_A$ and $\%S_B$ are percentages corresponding to the entire surface of one image and for each image there is still a blank area that isn't covered by particles. Therefore, the composition of powder mixture assessed by the surface fraction of either component A or B is finally given as:

$$surface\ fraction\ of\ A = \frac{\%S_A}{\%S_A + \%S_B} \tag{II-6}$$

Or $$surface\ fraction\ of\ B = \frac{\%S_B}{\%S_A + \%S_B} = 1 - surface\ fraction\ of\ A \tag{II-7}$$

Once the composition of powder mixture in surface is determined, the calibration is required to estimate the corresponding mass composition. Samples of powder mixture of different compositions, 0%, 10%, 20%, 30%, 40%, 50%, 60%, 70%, 80%, 90%, and 100% of component A, have firstly been prepared. The average surface fraction of component A for each sample is then measured by spreading the powder sample as a monolayer on the moving conveyor belt under the digital line scan camera. The known mass fractions (%) of component A are finally plotted against the measured surface fractions (%) of component A. As shown in Figure II-14, a third order polynomial function has been fitted to the data points of powder mixtures for which the mass fraction of component A varies from 10% to 80%, while the inclusion of the data points of 0%, 90%, and 100% samples will cause a larger estimation error.

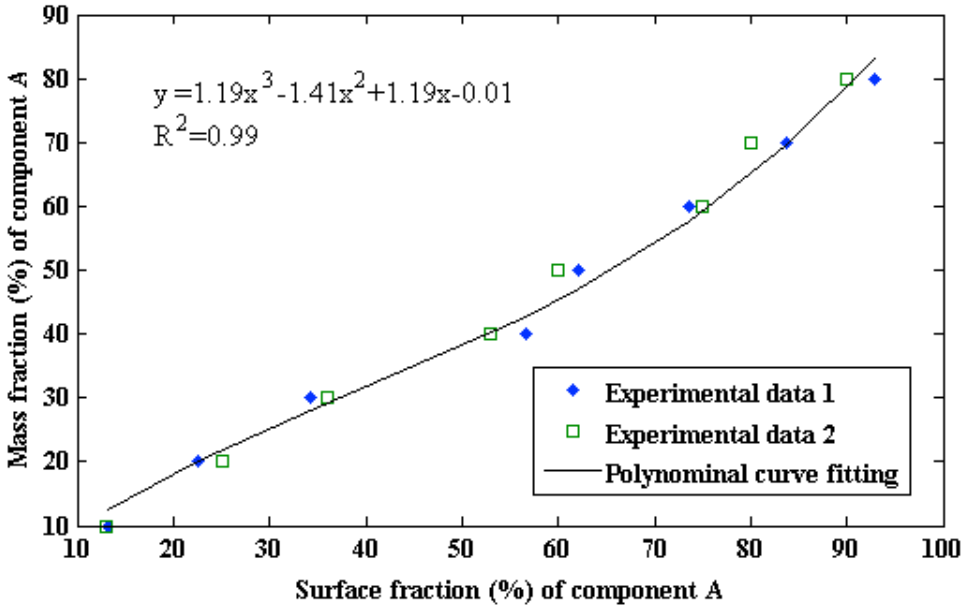

Figure II-14: Calibration curve for component A: mass fraction (%) versus surface fraction (%).

3.2.2 Computational approach for characterizing continuous mixing performance

As mentioned in Section 2.3, each image of powder mixtures represents a 30cm x 1.2cm inspection area and the image acquisition rate is 14 images/second. In this work, the size of one image is considered as the scale of scrutiny for characterizing continuous mixing performance. In addition, the weight of the powders captured in each image depends on the

mass flow rate at the mixer's outlet, which also depends on the mass inflow rate and the rotational speed of the mixer. As schematized in Figure II-15, every *n* consecutive images (or samples) are inspected as one "window". The continuous mixing performance is evaluated by quantification of powder mixtures in successive "windows" in terms of the composition as well as the homogeneity.

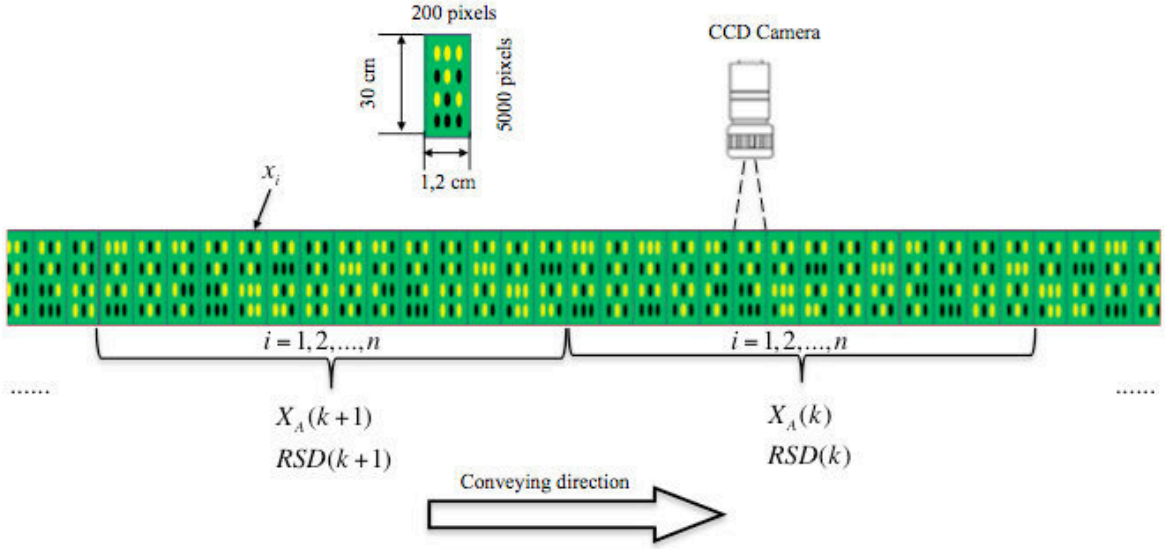

Figure II-15: Schematic representation of the scale of scrutiny and the "window" for characterizing the continuous mixing performance.

For each "window", the composition of the final mixture is estimated by calculating the mean composition of component A (X_A) and the mixing homogeneity is measured by calculating the relative standard deviation (*RSD)*. The equations are as follows:

$$X_A(k) = \frac{1}{n}\sum_{i=1}^{n} x_i(k) \qquad \text{(II-8)}$$

$$\sigma(k) = \sqrt{\frac{1}{n}\sum_{i=1}^{n}\left[x_i(k) - X_A(k)\right]^2} \qquad \text{(II-9)}$$

$$RSD(k) = \frac{\sigma(k)}{X_A(k)} \qquad \text{(II-10)}$$

Where *n* is the number of images containing in one "window", x_i is the mass fraction of component A monitored in each image, *k* is the order number of the "window" acquired at time instant *k*, and σ is the standard deviation. In this work, *n* will be fixed at 14 and this

means that the mean composition X_A and *RSD* are examined every second, because the image acquisition rate is about 14 images per second.

4 Conclusion

The first section introduces the two granular materials for mixing: component A (fine couscous colored in black) and component B (medium couscous). The materials have been characterized by physical properties, such as particle size distribution, density, flow, etc. The main difference between the two materials is found in particle size distribution. The second section gives the mechanical descriptions of the experimental equipment for the continuous powder mixing, including the feeders, the continuous mixer and the on-line image analysis system. In this work, the overall experimental set-up is operated in an automatic mode. The last section demonstrates how all instruments have been connected to a computer and controlled by the Labview software. The experimental operating system has been summarized in the two parts: the operating platform for the feeders and the mixer, and the operating platform for the on-line image analysis system. The former is related to the operating conditions of the feeders and the mixer. The latter is for the on-line measurement of the mixing performance in terms of the mean composition of component A (X_A) and the relative standard deviation (*RSD*).

CHAPTER III: New developments in the understanding of continuous powder mixing

The continuous mixer is the same as used and reported previously by Marikh [1] and Ammarcha [2]. In this work, a substantial number of experiments have been performed to deeper understand the continuous powder mixing in this equipment. The experiments are focused on studying powder flow and mixing in the mixer. An improved Markov chain model is finally obtained to predict process behaviour over a much wider range of operating conditions. In this chapter, the first section presents the method for measuring hold-ups in the mixer figured by five cells in the axial direction. Experimental results are presented and discussed in the next section. The new model development, the experimental validation and simulation studies are demonstrated in the last section.

1 Hold-up measurement

Powder hold-up weight in the continuous mixer is important because it determines the average residence time (hold-up/feed rate) of the powder, in turn affecting the quality of the mixtures [53,73]. In this study, the hold-up measurement is extended to investigate the axial mixing or dispersion of powders in the mixer. The mixer has been virtually divided into five axial cells of same length 0.1 m. As shown in Figure III-1, the stirring only lays in the first 4 cells. Cells 2, 3 and 4 each have one pair of blades allocated at two sides, and cells 1 and 5 have two pairs of blades.

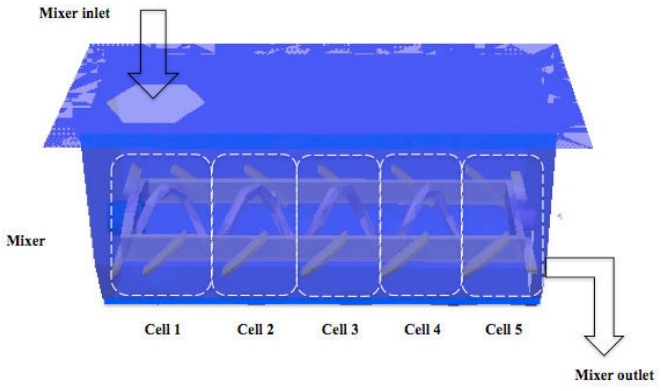

Figure III-1: Virtual division of the mixer into 5 compartments.

At the start of each experiment, the mixer is empty. At the mixer's inlet, powder is continuously fed. At the mixer's outlet, a balance is used to weigh the exiting powder thus deducing the mass outflow rate. The process is stopped when the mass outflow rate nearly reaches a constant value, indicating a steady state.

For bulk handling, the mixer is emptied at one time to measure the hold-up weight. For powder mixing, the mixer's cells are successively emptied from cell 5 to cell 1 in sequence in order to measure the hold-up in each cell. For the powder retrieved from each cell, the powder weight as well as the mixture composition is measured. When considering a mixing of two components (A and B), the mixture composition can be determined by separating the two components through a sieve of 1250 μm.

2 Experimental design and results

2.1 Experiments with bulk powder

Bulk powder flow in the continuous mixer has been extensively studied under different rotational speeds [52,54]. For a given bulk powder feed rate, an increase in rotational speed leads to a decrease in the hold-up weight as well as an acceleration to steady state. Thus, prior to the mixing experiments, the effect of bulk feed rate on the mixer's hold-up has been studied at a relatively high rotational speed (50 Hz) for each component. Experiments were done with bulk material of fine couscous (component A) or medium couscous (component B) for four different feed rates (1.67, 2.78, 4.17 and 4.86 $g.s^{-1}$).

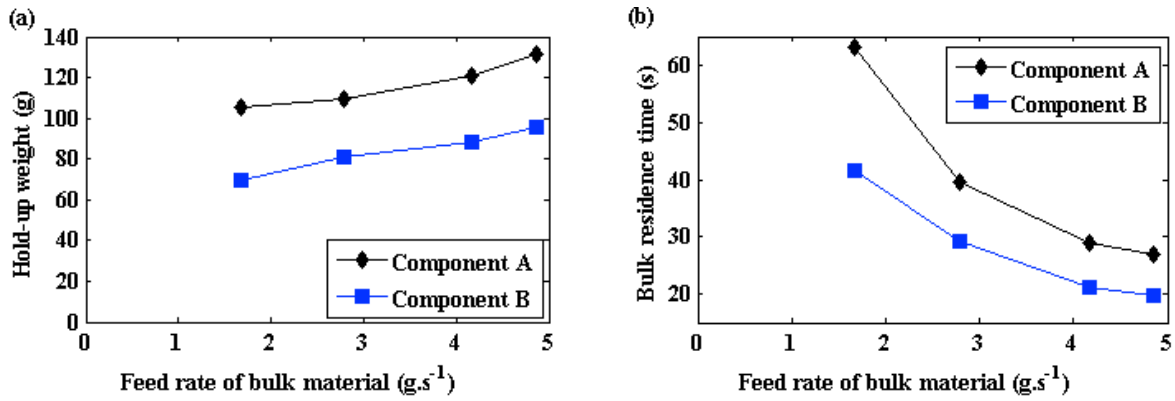

Figure III-2: Comparison of effects of bulk feed rate of component A and that of component B on (a) hold-up weight; (b) bulk residence time.

For each experiment, the hold-up was measured and the bulk residence time was also calculated. The results are presented in Figure III-2 (a) and (b). As shown in Figure III-2 (a), hold-up increases quasi-linearly with increase in feed rate for both components. In addition, for the same feed rate, hold-up is found to be higher for component A than for component B, indicating higher bulk residence time. This is mainly because particles in component A are smaller than those in component B. As shown in Figure III-2 (b) at a high rotational speed of 50 Hz, the effect of feed rate on bulk residence time decreases with increasing feed rate.

2.2 Powder mixing experiments

Thirty experiments of continuous mixing of component A and B were performed under various operating conditions, such as mixing formulation, total feed rate and rotational speed, as given in Table III-1.

Table III-1: Mixing experiments proceeding conditions.

<table>
<tr><th>Experiment N°</th><th>Mixing formulation</th><th>Total feed rate of the mixer (g.s^{-1})</th><th>Rotational speed (Hz)</th></tr>
<tr><td>1
2
3
4
5
6
7
8
9
10</td><td rowspan="10">30% A - 70% B</td><td rowspan="2">5.56</td><td rowspan="4">30</td></tr>
<tr><td rowspan="2">6.94</td></tr>
<tr><td>11
12
13
14
15
16
17
18
19
20</td><td rowspan="10">50% A - 50% B</td><td rowspan="2">8.33</td></tr>
<tr><td rowspan="2">9.72</td><td rowspan="6">50</td></tr>
<tr><td>21
22
23
24
25
26
27
28
29
30</td><td rowspan="10">70% A - 30% B</td><td rowspan="2">11.11</td></tr>
</table>

In brief, the continuous mixer was studied over the following operating ranges:

- three mixing formulations: 30% A – 70% B, 50% A – 50% B, and 70% A – 30% B;
- five total feed rates: 5.56 g.s^{-1}, 6.94 g.s^{-1}, 8.33 g.s^{-1}, 9.72 g.s^{-1} and 11.11 g.s^{-1};
- two rotational speeds : 30 Hz (medium value) and 50 Hz (high value).

In each mixing experiment, powder flow and mixing behaviour is investigated through hold-up in the whole mixer and hold-ups in the five axial cells of the mixer.

2.2.1 Hold-up in the whole mixer

Hold-up weight in the whole mixer is examined for the whole mixture as well as for each component in the mixture.

- **Hold-up of mixture**

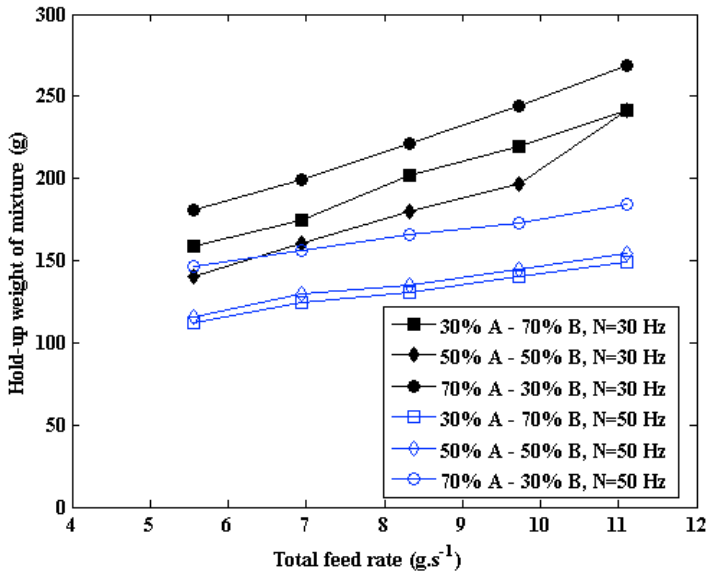

Figure III-3: Hold-up weight of mixture measured under different operating conditions.

As shown in Figure III-3, for a given set of mixing formulation and rotational speed (*N*), powder hold-up mass increases with increase in total feed rate. For a given set of total feed rate and mixing formulation, lower hold-ups are attained at the high rotational speed (50 Hz). For the same total feed rate, at either 30 or 50 Hz, hold-up is the highest for the mixing formulation of 70% A – 30% B, indicating the highest average residence time. This corresponds to higher bulk residence time for component A than for component B under the same operating condition. However, a lower mass fraction of component A in feed stream does not necessarily imply a smaller hold-up. For example, at 30 Hz, smaller hold-ups are found for 50% A – 50% B than for 30% A – 70% B, while at 50 Hz, very close hold-ups are found.

- **Hold-ups of component A and B**

(a) *30% A – 70% B* (b) *50% A – 50% B* (c) *70% A – 30% B*

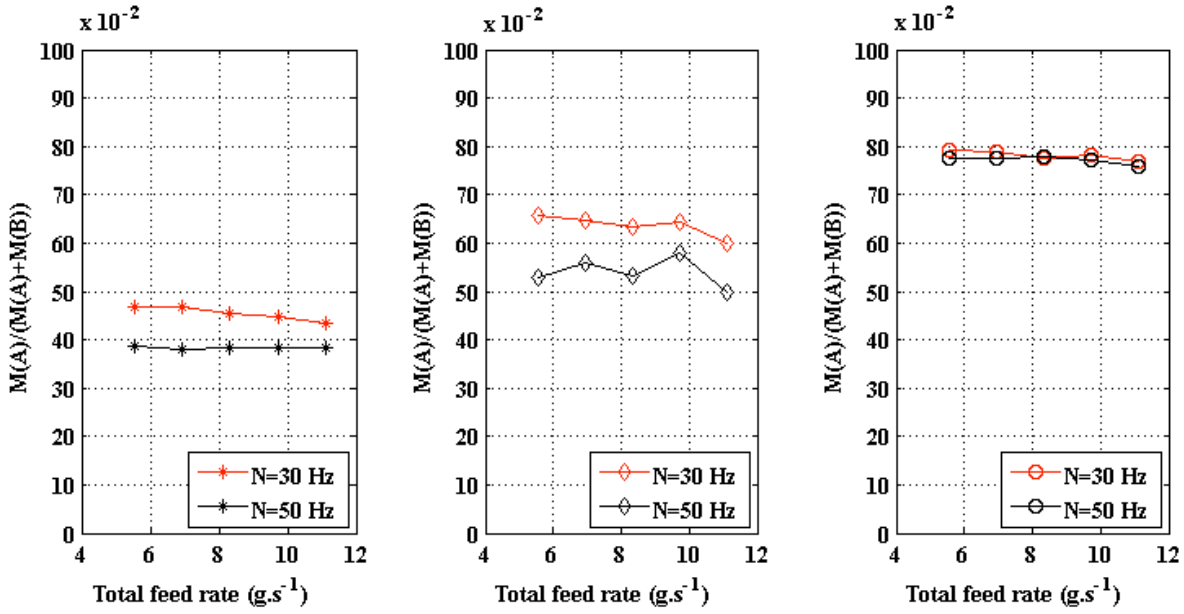

Figure III-4: Composition analysis of hold-up in the whole mixer: (a) 30% A – 70% B; (b) 50% A – 50% B; (c) 70% A – 30% B.

The separation of the two components in the whole mixer has been realised by sieving. $M(A)$ and $M(B)$ refer to the powder weights of component A and B, respectively. The mass fraction of component A in the whole hold-up weight was calculated by $M(A)/(M(A)+M(B))$. As shown in Figure III-4, for either mixing formulation, the mass fraction of component A is always larger than the desired fraction of component A, indicating segregation due to faster moving of component B (medium couscous) compared to component A (fine couscous). For 30% A – 70% B and 50% A – 50% B, the high rotational speed (50 Hz) helps to reduce the intensity of segregation and it can be seen from lower value of $M(A)/(M(A)+M(B))$. While for 70% A – 30% B, the rotational speed has little influence on $M(A)/(M(A)+M(B))$.

Hold-up weight has been empirically expressed as a function of rotational speed at different flow rates (or feed rates) [52,54]. However, this function is more often focused on understanding powder bulk flow rather than powder mixing. In this study, based on experimental data of continuous mixing of the components A and B, the following empirical

relationships are proposed to link the hold-up of each component with the studied process parameters, such as mixing formulation, total feed rate and rotational speed of the mixer.

(1) Empirical expression of hold-up of component A

The hold-up weight of component A in the entire mixer, denoted by $M(A)$, has been expressed as follows:

$$M(A) = a_1 x_A^{b_1} Q^{c_1} N^{d_1} \qquad \text{(III-1)}$$

where x_A is the mass fraction of component A in the feed stream, Q is the total feed rate of the mixer ($g.s^{-1}$), and N is the rotational speed (Hz). The unknown parameters a_1, b_1, c_1, and d_1 have been determined by least square fitting. The minimization of the square error between the predicted and experimental data of $M(A)$ was achieved with a_1 = 1124, b_1 = 1, c_1 = 0.5 and d_1 = –0.75.

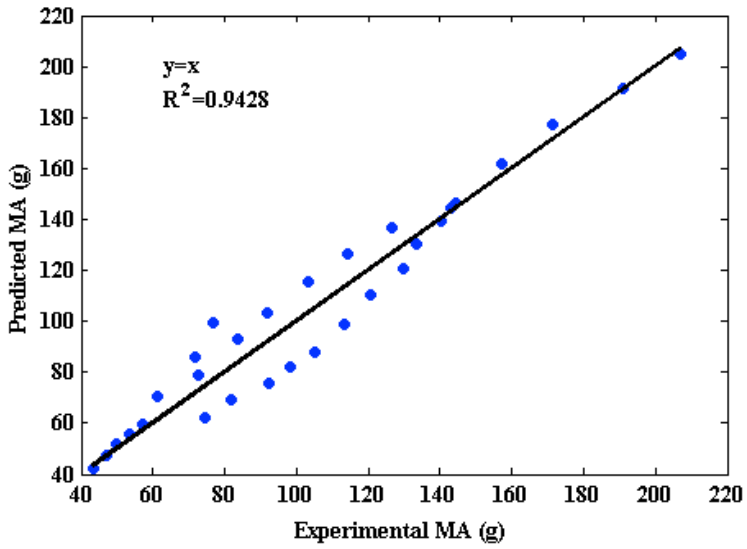

Figure III-5: Quality of prediction of Eq. (III-1) for the hold-up of component A in the whole mixer.

The plot of the predicted versus experimental $M(A)$ is shown in Figure III-5. A good linear correlation was found between the predicted and experimental $M(A)$, as the R^2 = 0.943.

(2) Empirical expression of hold-up of component B

The hold-up weight of component B in the whole mixer, denoted by $M(B)$, has been expressed as follows:

$$M(B) = a_2(1 - x_A)^{b_2} Q^{c_2} N^{d_2} \qquad \text{(III-2)}$$

where (1- x_A) is the mass fraction of component B in the feed stream, Q is the total feed rate of the mixer (g.s^{-1}), and N is the rotational speed (Hz). The unknown parameters a_2, b_2, c_2 and d_2 have also been determined by least square fitting. The minimization of the square error between the predicted and experimental data of $M(B)$ was achieved with a_2 = 294, b_2 = 1, c_2 = 0.5, and d_2 = –0.5.

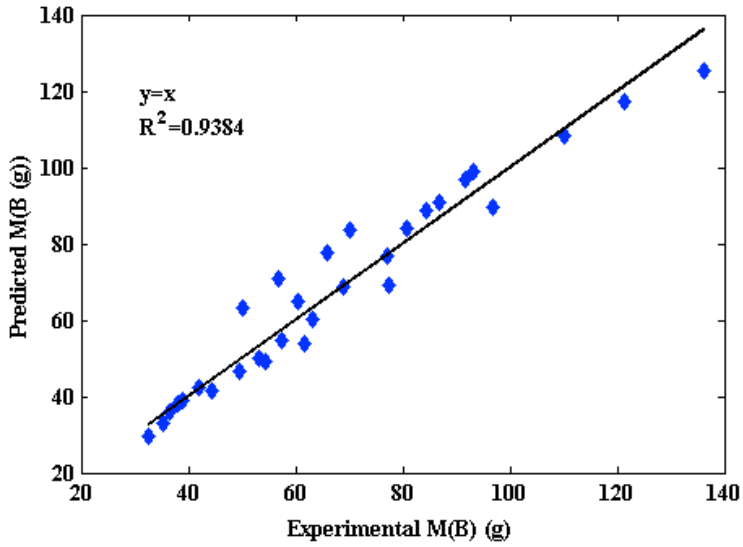

Figure III-6: Quality of prediction of Eq. (III-2) for the hold-up of component B in the whole mixer.

Figure III-6 shows a good linear relationship (R^2 = 0.938) between the predicted and experimental $M(B)$.

In conclusion, Eq. (II-1) and Eq. (III-2) have been proposed to express hold-up weight of component A and B, respectively, as a function of mixing formulation, total feed rate and

rotational speed. The parameters of the two equations have been experimentally estimated using least square fitting.

2.2.2 Hold-ups in the five cells of the mixer

In the following, the hold-up profiles of component A and B in the mixer will be discussed from the subdivision into five axial cells.

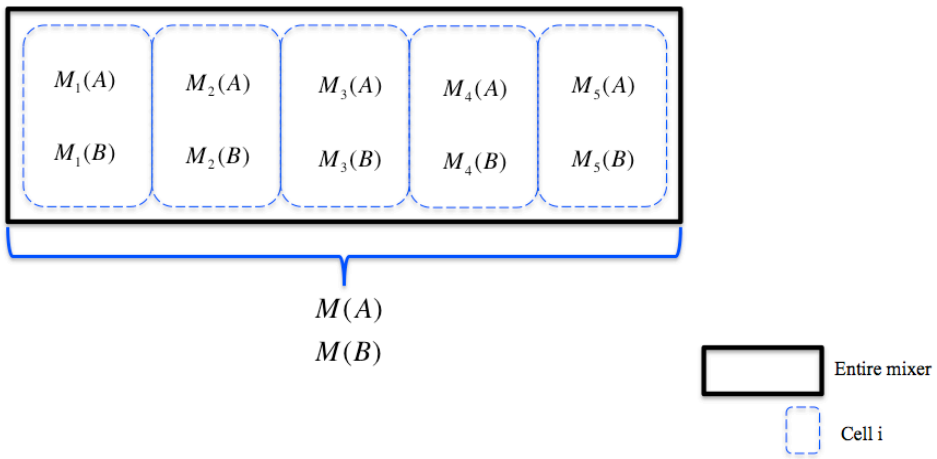

Figure III-7: Mass distribution of powders in the five virtual cells of the mixer.

The distribution of the masses of component A and B in the five cells is shown schematically in Figure III-7. $M_i(A)$ represents the hold-up mass of component A in the cell i and $M_i(B)$ represents the hold-up mass of component B in the cell i. $M(A)$ and $M(B)$ are the whole hold-up masses of component A and B in the mixer, respectively, calculated as

$$M(A) = \sum_{i=1}^{5} M_i(A) \qquad \text{(III-3)}$$

$$M(B) = \sum_{i=1}^{5} M_i(B) \qquad \text{(III-4)}$$

For each mixing experiment, $M_i(A)/M(A)$ and $M_i(B)/M(B)$ have been calculated to assess the relative hold-up mass distributions of component A and B, respectively.

- **Relative hold-up weight distribution of component A –** $M_i(A)/M(A)$

(a) *Mixing of 30% A – 70% B*

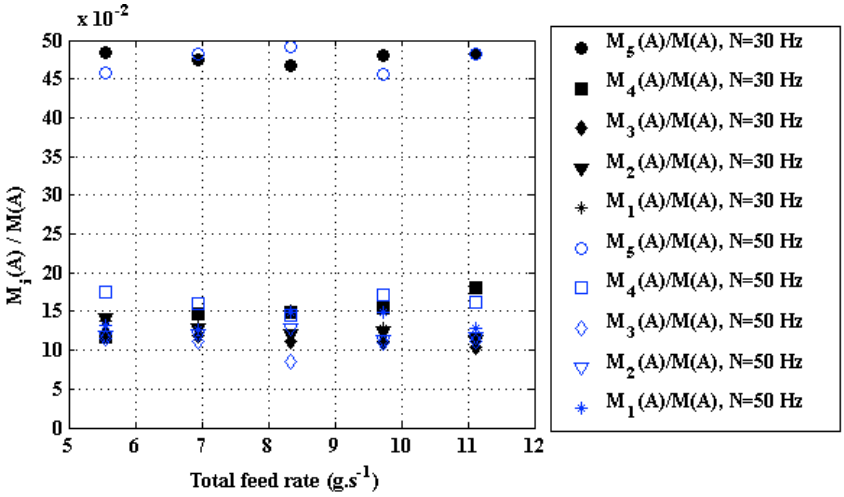

(b) *Mixing of 50% A – 50% B*

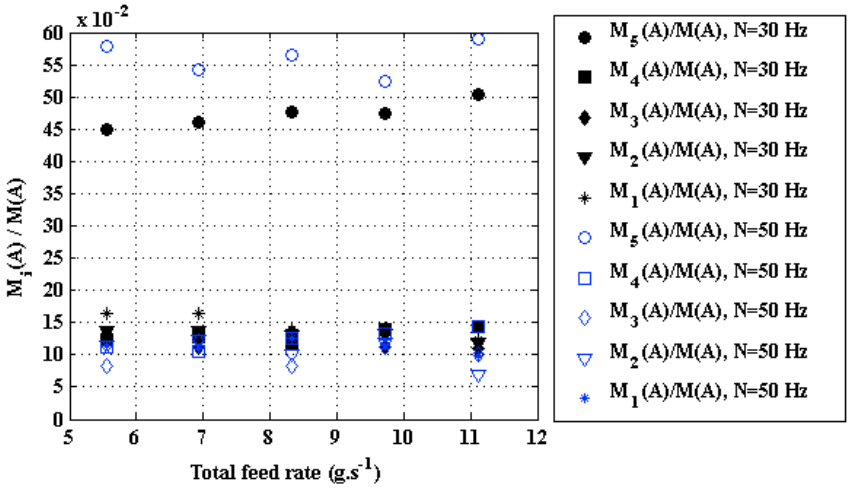

(c) *Mixing of 70% A – 30% B*

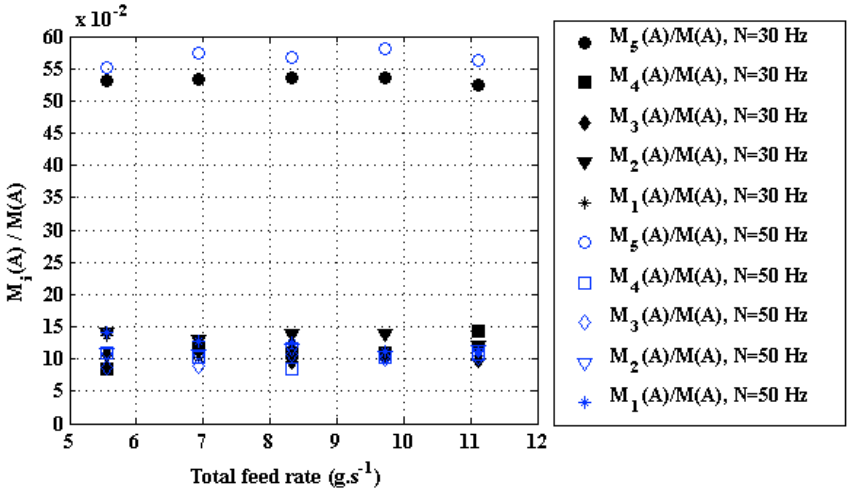

Figure III-8: Relative hold-up weight distribution of component A in the continuous mixer divided into 5 cells: (1) mixing experiments of 30% A – 70% B; (2) mixing experiments of 50% A – 50% B; (3) mixing experiments of 70% A - 30% B.

The plots of $M_i(A)/M(A)$ versus total feed rate of the mixer are shown in Figure III-8 for three mixing formulations: 30% A – 70% B, 50% A – 50% B and 70% A – 30% B. In Figure III-8 (a), for a given cell *i*, $M_i(A)/M(A)$ is found to be roughly independent of total feed rate and similar profiles of $M_i(A)/M(A)$ are observed from mixing experiments at 30 Hz and 50 Hz. When comparing the results from each cell, we find that the values of $M_i(A)/M(A)$ for the first four cells (i = 1, 2, 3, and 4) are very close to each other, around 10%, while those for the last cell (i = 5), next to the mixer's outlet, are nearly up to 50%. Similar results are obtained for the two other mixing formulations, as seen from Figure III-8 (a) and (b). This indicates that $M_i(A)/M(A)$, is little influenced by the mixing formulation. All experimental data of $M_5(A)$ have been plotted versus those of $M(A)$, as shown in Figure III-9. All these results imply that, for a given cell *i*, there exists a linear relationship between $M_i(A)$ and $M(A)$ and the observation from the 5th cell is different from the first four cells.

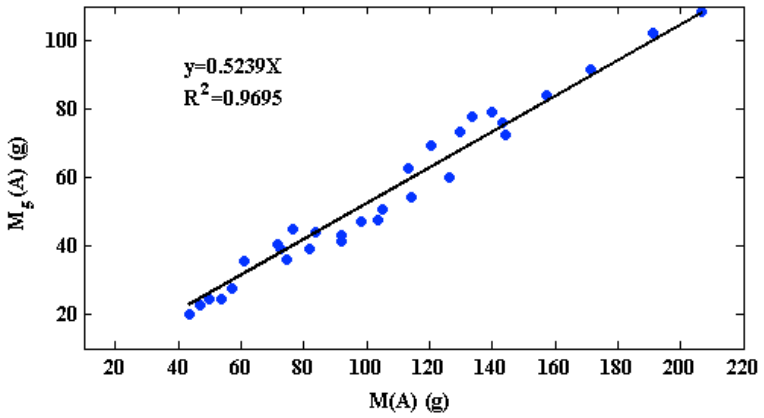

Figure III-9: Evidence of an empirical linear relationship between $M_5(A)$ and $M(A)$.

$$M_5(A) = 52.4\% M(A) \qquad \text{(III-5)}$$

$M_5(A)/M(A)$ has been estimated by a linear regression, as shown in Eq. (III-5). This empirical equation shows that, at steady state, there is 52.4% of whole mass of component A in the 5th cell of the mixer, indicating 38,6% in the other cells. The values of $M_i(A)/M(A)$ for i=1,2,3,4, can be estimated to be 11.9%, since the experimental data of $M_i(A)/M(A)$ are almost the same for the first four cell.

The same analysis has been performed for hold-up mass distribution of component B.

- **Relative hold-up weight distribution of component B –** $M_i(B)/M(B)$

(a) *Mixing of 30% A – 70% B*

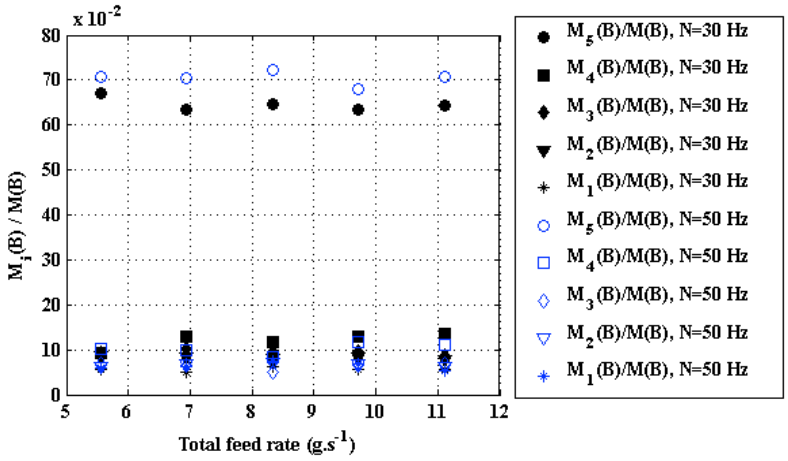

(b) *Mixing of 50% A – 50% B*

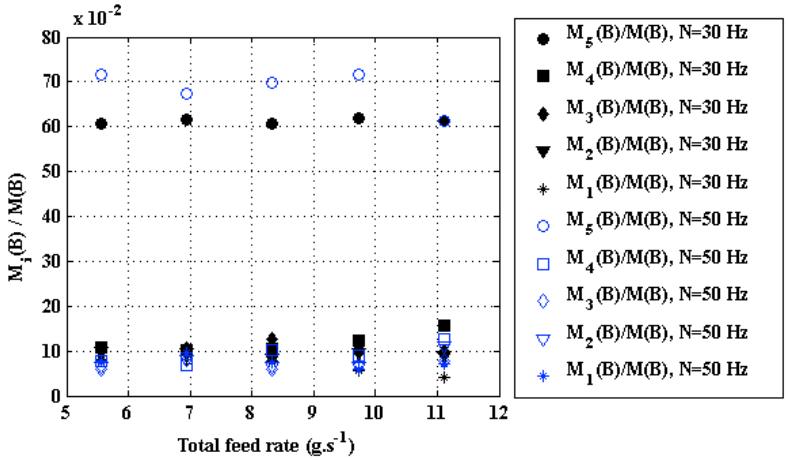

(c) *Mixing of 70% A – 30% B*

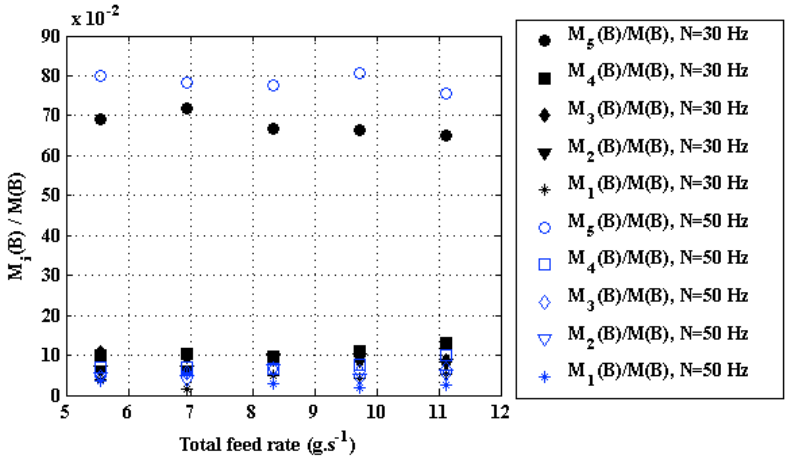

Figure III-10: Relative hold-up weight distribution of component B in the continuous mixer divided into 5 cells: (1) mixing experiments of 30% A – 70% B; (2) mixing experiments of 50% A – 50% B; (3) mixing experiments of 70% A - 30% B.

As seen from Figure III-10, experimental results of $M_i(B)/M(B)$ are similar for three different mixing formulations. For any given mixing formulation, changes in total feed rate has almost no influence on $M_i(B)/M(B)$ and the values of $M_i(B)/M(B)$ for the first four cells are very different from the 5th cell, where there is no screw and the wall effect is pronouced. The linear relation between $M_5(B)$ and $M(B)$ has been confirmed by plotting the experimental data and using a regression coefficient (R^2) of 0.96.

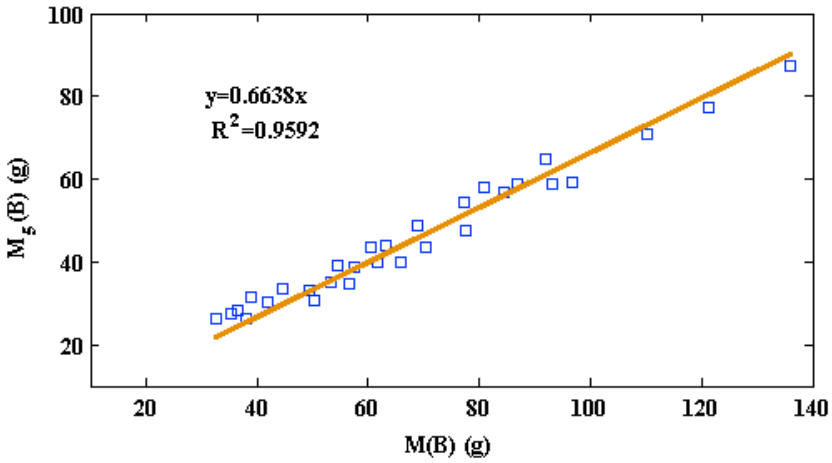

Figure III-11: Empirical linear relationship between $M_5(B)$ and $M(B)$.

The empirical expression shown below has been obtained.

$$M_5(B) = 66.4\% M(B) \qquad \text{(III-6)}$$

This shows that, at steady state, there are 66.4% of whole mass of component B in the 5th cell of the mixer and 38,6% in the other cells. The values of $M_i(B)/M(B)$ for i=1,2,3,4, can be estimated to be 8.4%, since the experimental data of $M_i(B)/M(B)$ are almost the same for the first four cell.

In conclusion, the measurements of hold-up mass distribution of component A and B, evaluated by $M_i(A)/M(A)$ and $M_i(B)/M(B)$ show that, for each component, there exist linear relationships between the hold-up mass in each individual cell and the whole hold-up mass in the mixer. With the empirical linear relationships, $M_i(A)$ and $M_i(B)$ can finally be

estimated, since $M(A)$ and $M(B)$ have been expressed as functions of the different operating conditions, shown in Eq. (III-1) and Eq. (III-2), respectively.

3 Improved Markov chain modelling and experimental validation of continuous powder mixing

3.1 Improved Markov chain Modelling for mixing of two powder components

Also concerned with the continuous mixing of two powder components, the previous work of Ammarcha [2] has proposed to model the process by two Markov chains, for which each Markov chain corresponds to each component. However, few results have been presented to illustrate the determinations of critical model parameters. In this work, the modelling principle using two Markov chains need to be improved by intergrating the empirical expressions of hold-up weights of component A and B in the whole mixer and the relative hold-up weight distributions of both components..

The model contains five cells for the mixer and one cell at the outlet of the mixer corresponding to the absorbing state. Two Markov chains have been used to describe powder mass evolutions of component A and B, respectively, as illustrated in Figure III-12.

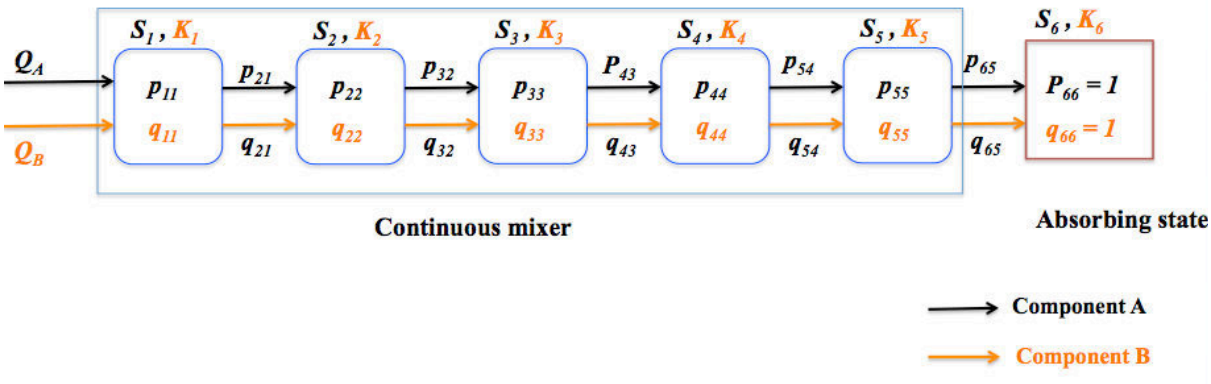

Figure III-12: A two Markov chain scheme for describing flow dynamics of component A and B in the continuous mixer.

The process is observed in discrete moments of time with the sampling time Δt. The evolutions of the state (or mass) vectors for component A and B are described by the following matrix formulas:

$$\begin{bmatrix} S_1(n+1) \\ S_2(n+1) \\ S_3(n+1) \\ S_4(n+1) \\ S_5(n+1) \\ S_6(n+1) \end{bmatrix} = \begin{bmatrix} p_{11}(n) & 0 & 0 & 0 & 0 & 0 \\ p_{21}(n) & p_{22}(n) & 0 & 0 & 0 & 0 \\ 0 & p_{32}(n) & p_{33}(n) & 0 & 0 & 0 \\ 0 & 0 & p_{43}(n) & p_{44}(n) & 0 & 0 \\ 0 & 0 & 0 & p_{45}(n) & p_{55}(n) & 0 \\ 0 & 0 & 0 & 0 & p_{65}(n) & p_{66}(n) \end{bmatrix} \begin{bmatrix} S_1(n)+Q_A\Delta t \\ S_2(n) \\ S_3(n) \\ S_4(n) \\ S_5(n) \\ S_6(n) \end{bmatrix} \quad \text{(III-7)}$$

$$\begin{bmatrix} K_1(n+1) \\ K_2(n+1) \\ K_3(n+1) \\ K_4(n+1) \\ K_5(n+1) \\ K_6(n+1) \end{bmatrix} = \begin{bmatrix} q_{11}(n) & 0 & 0 & 0 & 0 & 0 \\ q_{21}(n) & q_{22}(n) & 0 & 0 & 0 & 0 \\ 0 & q_{32}(n) & q_{33}(n) & 0 & 0 & 0 \\ 0 & 0 & q_{43}(n) & q_{44}(n) & 0 & 0 \\ 0 & 0 & 0 & q_{45}(n) & q_{55}(n) & 0 \\ 0 & 0 & 0 & 0 & q_{65}(n) & q_{66}(n) \end{bmatrix} \begin{bmatrix} K_1(n)+Q_B\Delta t \\ K_2(n) \\ K_3(n) \\ K_4(n) \\ K_5(n) \\ K_6(n) \end{bmatrix} \quad \text{(III-8)}$$

In Eq. (III-7), Q_A is the mass flow rate of component A; $S_i(n+1)$ is the mass of component A in cell *i* after *n* transitions; $p_{ii}(n)$ and $p_{(i+1)i}(n)$ are respectively the probabilities of component A to stay in cell *i* and to move from cell *i* to cell *i+1* during the n^{th} transition; $p_{ii}(n) = 1 - p_{(i+1)i}(n)$ and $p_{66}(n) = 1$ because there is no backward flow for the last cell.

In Eq. (III-8), Q_B is the mass flow rate of component B; $K_i(n+1)$ is the mass of component B in cell *i* after *n* transitions; $q_{ii}(n)$ and $q_{(i+1)i}(n)$ are respectively the probabilities of component B to stay in cell *i* and to move from cell *i* to cell *i+1* during the n^{th} transition; $q_{ii}(n) = 1 - q_{(i+1)i}(n)$ and $q_{66}(n) = 1$.

Since the model is used to predict the continuous mixing process during two phases: (1) start stage and (2) steady state, the transition probabilities $p_{(i+1)i}(n)$ as well as $q_{(i+1)i}(n)$ should be identified for the two phases. During start stage, it is assumed that the transition probabilities for each component vary linearly with the corresponding powder mass in the mixer as evidenced by Ammarcha [2]. The transition probability $p_{(i+1)i}(n)$ or $q_{(i+1)i}(n)$ is zero when the mass of corresponding powder component is zero in cell *i*. While, at steady state, the transition probabilities are kept constant, denoted as $p_{(i+1)i\,max}$ and $q_{(i+1)i\,max}$, because the mass of each component in each cell equals to its stationary hold-up weight.

For component A, the transition probability $p_{(i+1)i}(n)$ can be expressed as a function of $S_i(n)$ representing the mass of component A in cell i = 1, 2, 3, 4 or 5 at every transition. As given in Eq. (III-9), $M_i(A)$ is the hold-up mass of component A in cell i and $p_{(i+1)i\,max}$ is the transition probability at steady state, which depends on cell i, Q_A, Δt and $M_i(A)$, and can be calculated from Eq. (III-10).

$$p_{(i+1)i}(n) = \begin{cases} 0, & for\ S_i(n) = 0 \\ \dfrac{p_{(i+1)i\,max}}{M_i(A)} S_i(n), & for\ 0 < S_i(n) < M_i(A) \\ p_{(i+1)i\,max}, & for\ S_i(n) = M_i(A) \end{cases} \quad \text{(III-9)}$$

$$p_{(i+1)i\,max} = \begin{cases} \dfrac{Q_A \Delta t}{M_i(A) + Q_A \Delta t}, & for\ i = 1 \\ \dfrac{Q_A \Delta t}{M_i(A)}, & for\ i = 2,3,4,5 \end{cases} \quad \text{(III-10)}$$

For component B, the transition probability $q_{(i+1)i}(n)$ can be expressed as a function of $K_i(n)$ representing the mass of component B in cell i = 1, 2, 3, 4 or 5 at every transition. As given in Eq. (III-11), $M_i(B)$ is the hold-up mass of component B in cell i and $q_{(i+1)i\,max}$ is the transition probability at steady state, which depends on cell i, Q_B, Δt and $M_i(B)$, and can be calculated from Eq. (III-12).

$$q_{(i+1)i}(n) = \begin{cases} 0, & for\ K_i(n) = 0 \\ \dfrac{q_{(i+1)i\,max}}{M_i(B)} K_i(n), & for\ 0 < K_i(n) < M_i(B) \\ q_{(i+1)i\,max}, & for\ K_i(n) = M_i(B) \end{cases} \quad \text{(III-11)}$$

$$q_{(i+1)i\,max} = \begin{cases} \dfrac{Q_B \Delta t}{M_i(B) + Q_B \Delta t}, & for\ i = 1 \\ \dfrac{Q_B \Delta t}{M_i(B)}, & for\ i = 2,3,4,5 \end{cases} \quad \text{(III-12)}$$

The above equations indicate that the determinations of transition probabilities are fundamentally linked to $M_i(A)$ and $M_i(B)$. Thus, the prediction performance of the Markov chain model mainly depends on whether $M_i(A)$ and $M_i(B)$ can be estimated for different operating conditions. As stated in Section 2, the prediction of $M_i(A)$ can be performed using the empirical expression of $M(A)$ and the empirical linear relationships between $M_i(A)$ and $M(A)$. The similar prediction can be made for $M_i(B)$. Implementing these empirical expressions, the algorithm for the improved Markov chain model can be summarised as Figure III-13.

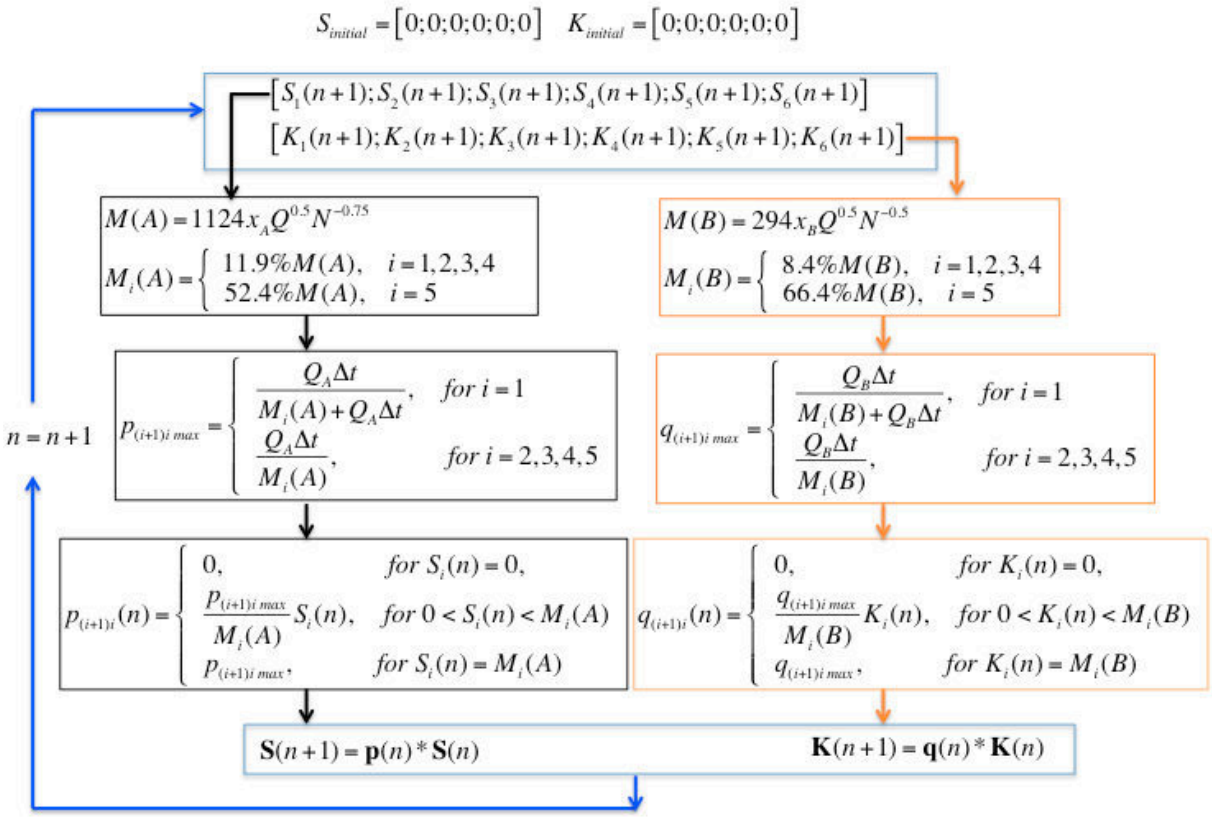

Figure III-13: Algorithm of iterative calculation for the two Markov chains.

Since there is no powder in the mixer at the start of the mixing operation, the initial states for component A and B can be taken as the zero vectors. The gathering of the two Markov chains allows us to calculate the concentration (or mass fraction) of either component at the mixer's outlet. For instance, the concentration of component A during n^{th} transition $x(n)$ can be calculated as:

$$x(n) = \frac{S_6(n+1) - S_6(n)}{\left[S_6(n+1) - S_6(n)\right] + \left[K_6(n+1) - K_6(n)\right]} \quad \text{(III-13)}$$

The simulations for continuous mixing of the two powder components were performed in Matlab (see the program in Annex 1). The transition time Δt has been set at 0.1 second. To compare simulation results with experimental data, the Markov chain model has been used to predict four process outputs:

(1) Mean concentration X of component A

$$X_A(k) = \frac{1}{10}\sum_{i=1}^{10} x_i(k) \quad \text{(III-14)}$$

X_A at time instant k is the mean value of x for 10 consecutive samples.

(2) Relative standard deviation *RSD*

$$RSD(k) = \frac{\sqrt{\frac{1}{10}\sum_{i=1}^{10}[x_i(k) - X_A(k)]^2}}{X_A(k)} \quad \text{(III-15)}$$

The *RSD* is calculated to quantify the homogeneity over 10 consecutive samples.

(3) Whole powder mass in 6th cell (or absorbing state) M_6 (g)

$$M_6(n) = S_6(n) + K_6(n) \quad \text{(III-16)}$$

(4) Outflow rate of the mixer Q_{out} (g.s^{-1})

$$Q_{out}(n) = \frac{M_6(n+1) - M_6(n)}{\Delta t} \quad \text{(III-17)}$$

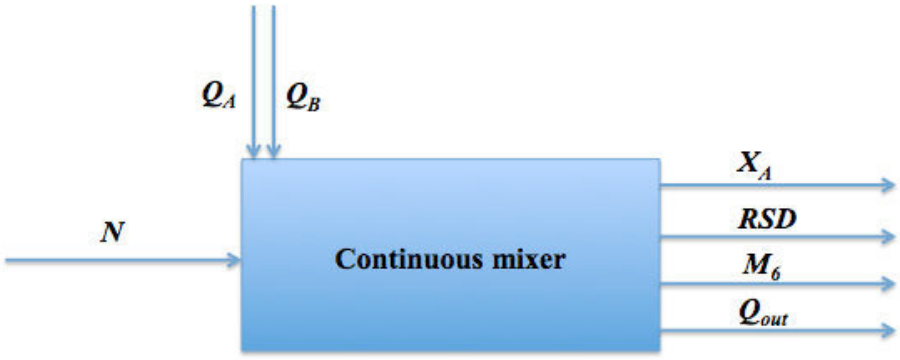

Figure III-14: General structure of the continuous mixer simulator.

To summarise, the process simulator contains three inputs and four outputs, as shown in Figure III-14. The inputs are the rotational speed of the mixer N, the flow rates of Q_A and Q_B. The outputs are the mean concentration X_A, the relative standard deviation RSD, the whole powder mass obtained at the outlet M_6 and the mass outflow rate of the mixer Q_{out}.

3.2 Reliability study of the model

The reliability of the model has been examined by experimental tests of continuous mixing of component A and B under three different operating conditions as follows:

(1) Constants N, Q_A and Q_B
(2) Constants flow rate Q_A, Q_B with a step change in rotational speed N
(3) Constants N and Q_B with a step change in flow rate Q_A

There is no powder in the mixer at the start of each experiment. It is also worth noting that experimental measurements of X_A, RSD, M_6, and Q_{out} were performed not tightly next to the mixer's outlet but at a distance of 84 cm. The time delay is about 5 s, because the moving speed of the conveyor belt at the outlet is 16.8 $cm.s^{-1}$. However, simulation results were obtained tightly next to the mixer's outlet. Measurements during the first 5 s were removed from experimental data in order to be consistent with those obtained from the simulations.

3.2.1 An example for constant operating conditions

Both flow rates of component A an B were fixed at 4.5 $g.s^{-1}$ and the rotational speed of the mixer was kept at 30 Hz. As shown in Figure III-15, the experimental data of X_A, *RSD*, M_6 and O_{out} were plotted against time and compared with the simulation results.

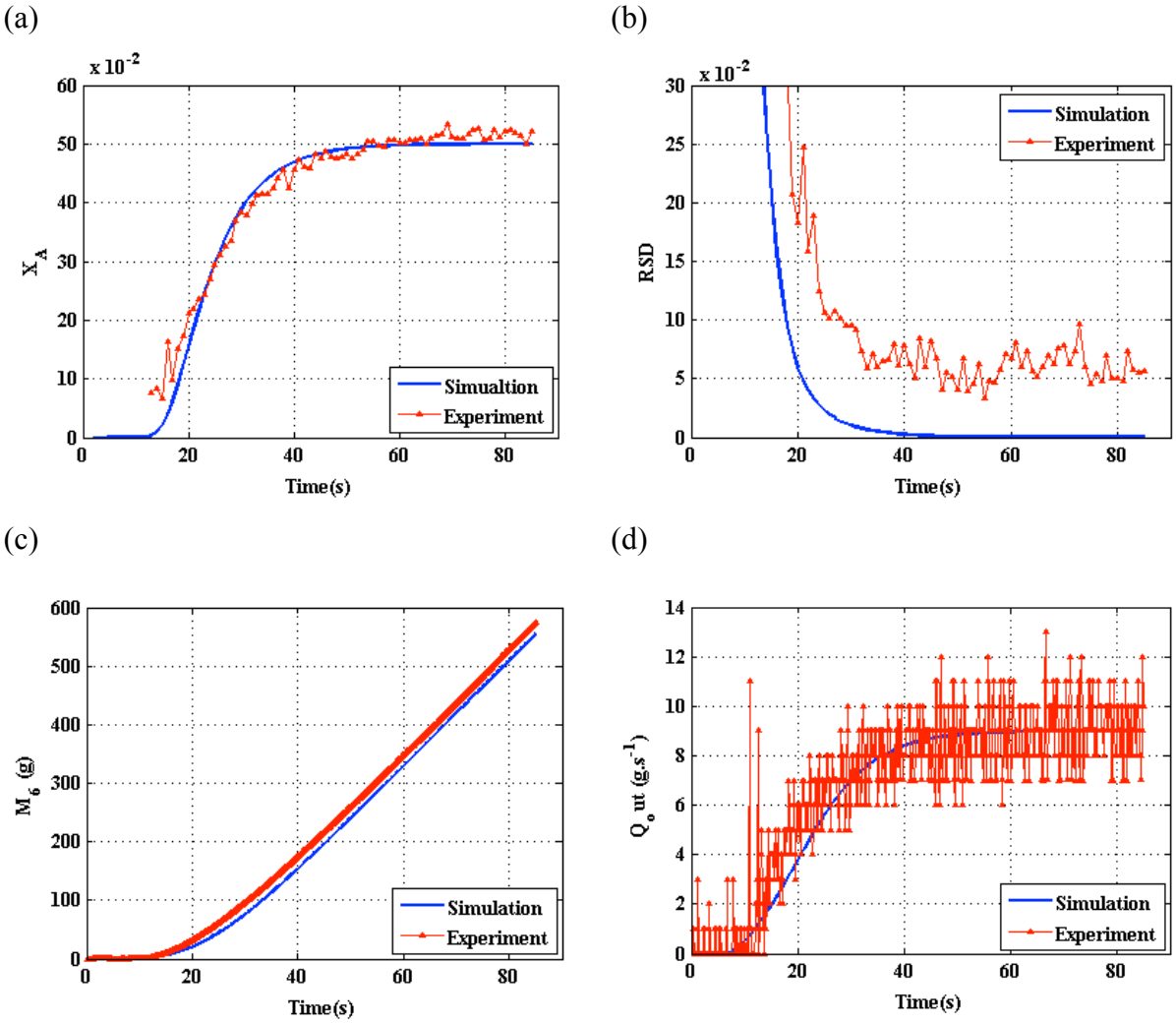

Figure III-15: Comparison of simulated results with experimental data for constant experimental conditions Q_A=Q_B=4.5 $g.s^{-1}$ and N=30 Hz: plots of (a) X_A, (b) *RSD*, (c) M_6 and (d) Q_{out}.

In Figure III-15 (a), the mean concentration of component A has been well predicted, although a little difference was found at the early start phase. The X_A reached around its target value 50% after 60 s. Figure III-15 (b) shows that before 40 s, both experimental and predicted *RSD*s were significantly reduced during the transitory period. However, simulated *RSD* has been underestimated, as it can be seen from experimental values of *RSD* greater than 5% while predicted values of *RSD* are approaching zero after 40 s. Figure III-15 (c) and (d) show good agreement between measured and predicted M_6 and Q_{out}. After about 80 s, the

mixing reached the steady state because the mass outflow rate of the mixer Q_{out} nearly equals to the total feed rate of 9 $g.s^{-1}$.

3.2.2 An example for step change in rotational speed of the mixer

The mixing was started at a fixed rotational speed (50 Hz). Both flow rates Q_A and Q_B were set at 4.17 $g.s^{-1}$. At the moment of 100 s, the rotational speed was changed to 30 Hz by a negative step.

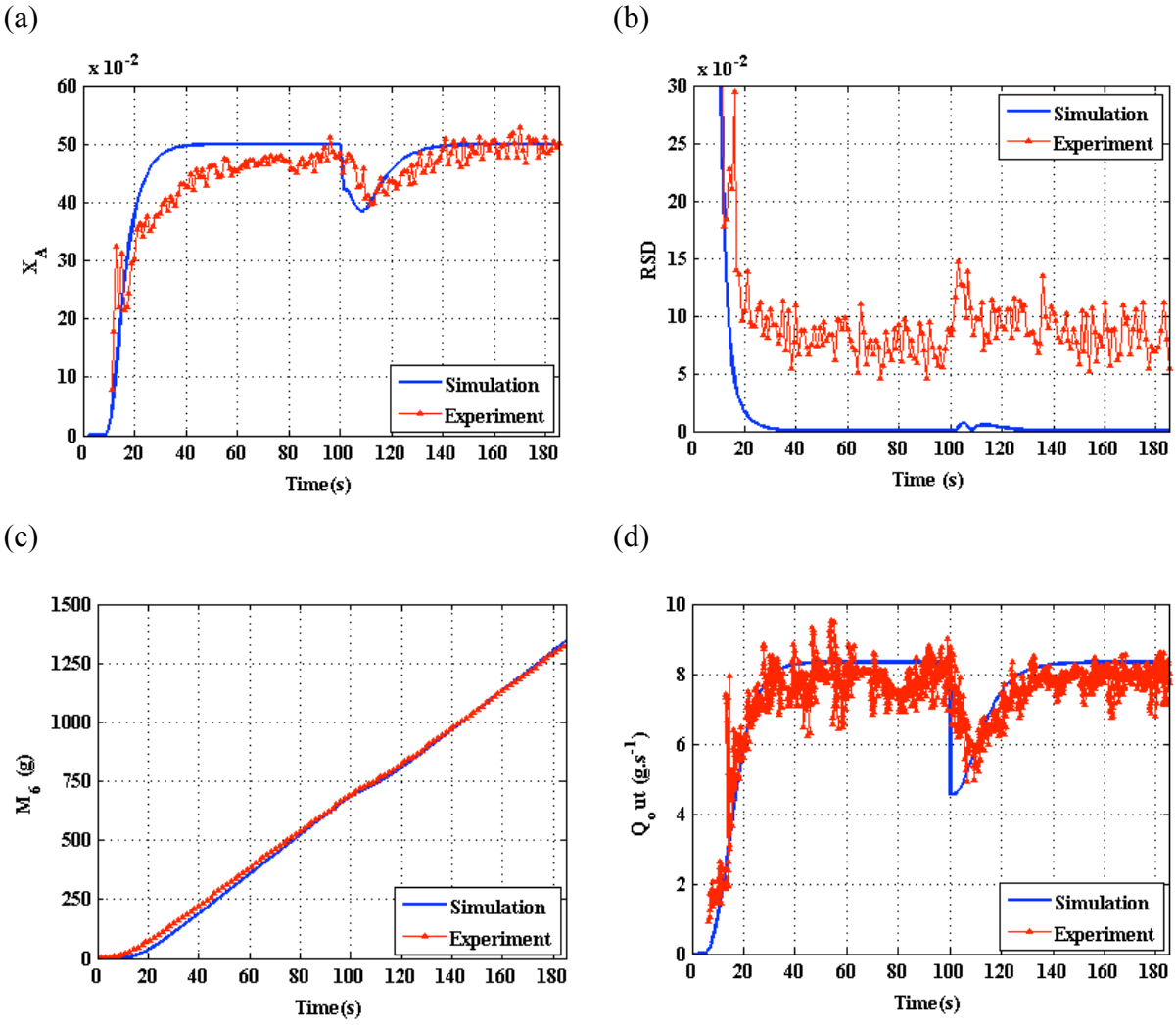

Figure III-16: Validation result for a step change in rotational speed: plots of predicted vs. experimentally measured (a) X_A, (b) *RSD*, (c) M_6 and (d) Q_{out}.

In Figure III-16 (a), at 100 s, the measured X_A tended to be stable around 50%. Both experimental and predicted X_A shows that the change in rotational speed from 50 to 30 Hz led to a time period X_A decline and the X_A finally reached the original stable concentration of

component A. From Figure III-16 (b), the *RSD* was experimentally increased immediately after the negative step change in *N* but the increase of *RSD* was not very significant. The predicted *RSD*s was relatively smaller than those calculated from the experiment. Figure III-16 (c) and (d) show that M_6 and Q_{out} were well predicted by the model. At around 60 s, Q_{out} approximately equals to the total feed rate, indicating a steady state. The decrease in rotational speed at 100 s led to a time period Q_{out} slowdown and the Q_{out} finally returned to its original stable outflow rate.

3.2.3 An example for step change in flow rate

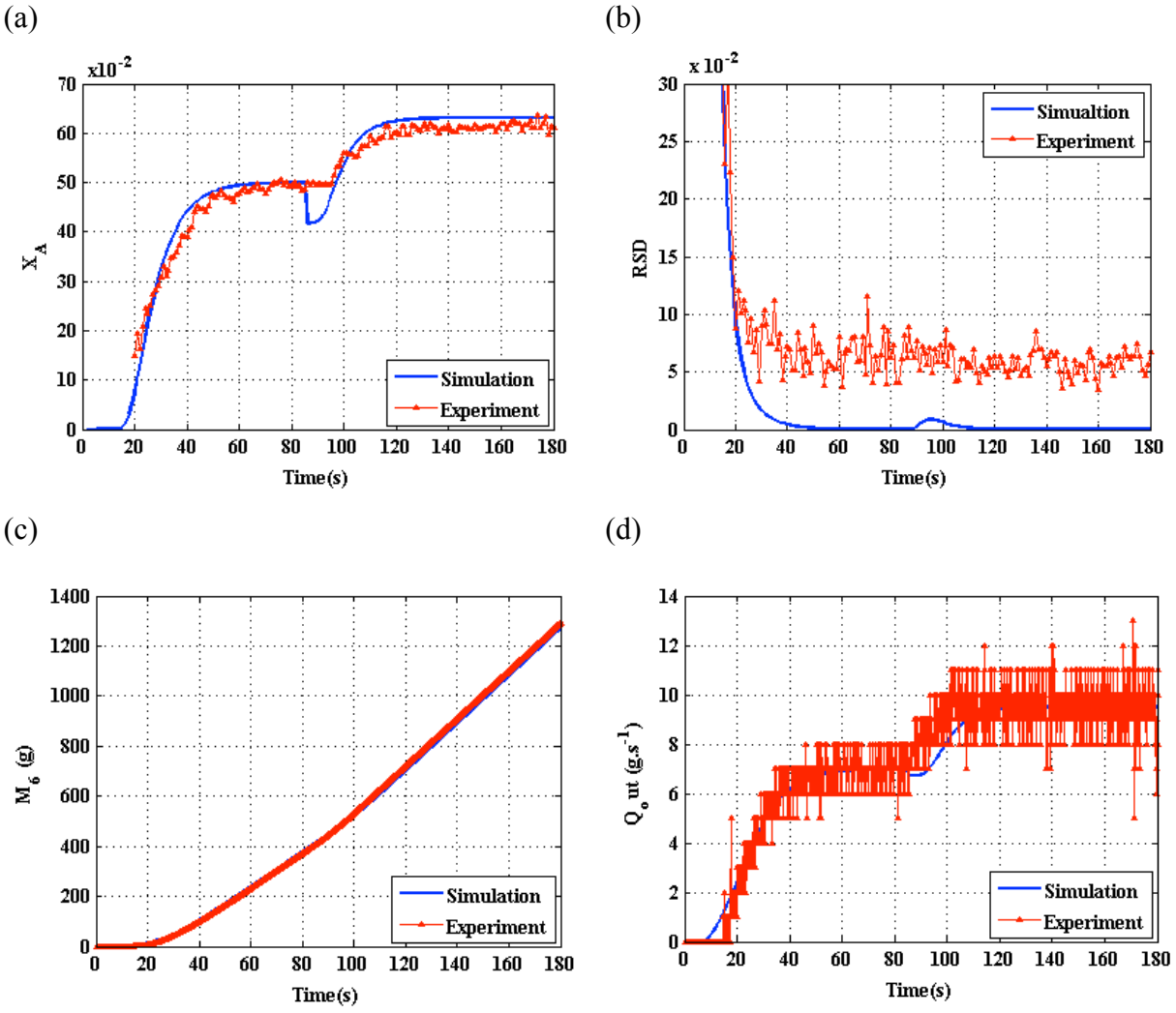

Figure III-17: Validation result for a step change in flow rate: plots of predicted vs. experimentally measured (a) X_A, (b) *RSD*, (c) M_6 and (d) Q_{out}.

During the mixing, the rotational speed *N* was set at 30 Hz. Both flow rates Q_A and Q_B were initially set at 3.5 $g.s^{-1}$. At the moment of 85 s, a step change from 3.5 to 6 $g.s^{-1}$ was applied

in the flow rate of component A. The plots of X_A as a function of time in Figure III-17 (a) show that roughly same trends were found between experimental and predicted X_A, except for the instantaneous decline of predicted X_A at 85 s. Two possible analyses can be listed here trying to explain: (1) If the error is come from the model, it may be attributed to the model assumptions, the non-considered process parameters, and unmeasurable even unavoidable disturbances in the real plant. (2) If the error is come from the measurements, it implies that the instantaneous change in X_A may not be detected by the monitoring technique used in the study, or the instantaneous change may be weaker or even disappeared due to powder transport from the mixer's outlet to the moving belt. At least, from about 95 s, the same increasing of X_A has been obtained from both experimental and simulation results. From Figure III-17 (b), relatively small values of predicted *RSD* show that the model cannot be used to estimate the variability in the concentration between samples taken per second. In Figure III-17 (c) and (d), little difference was found between experimental and simulation results in terms of M_6 and Q_{out}. The profiles of Q_{out} show that the mixing has been achieved at steady state at 85 s and the Q_{out} increased and finally became stable due to the increase in Q_A.

In conclusion, the experimental validation for the three examples shows that the improved model provides satisfactory prediction results for the mean concentration of component A X_A, the powder mass collected at the mixer's outlet M_6, and the mass outflow of the mixer Q_{out}, except for the relative standard deviation *RSD*. This might come from: (1) *RSD* is a variable very sensitive to change in operating conditions, even if change is extremely small. (2) The simulations have been performed for ideal operating conditions and they have not yet taken account into actual uncertainties such as fluctuations in flow rates, unmeasurable even unavoidable disturbances.

3.3 Simulation studies

Since the prediction of hold-up mass for each component, as an important part in the Markov chain model, has been presented as a function of mixing formulation, total feed rate and rotational speed, various simulations were performed to study the influence of the three operating parameters.

Simulation studies were classified into two categories:

(1) Influence of rotational speed and total feed rate at a constant mixing formulation;

(2) Influence of rotational speed and mixing formulation at a constant feed rate.

3.3.1 Influence of rotational speed and total feed rate at a constant mixing formulation

The mixing formulation of components A and B was fixed at 50% - 50%. The simulations were performed under two different rotational speeds (30 an 50 Hz) for three total feed rates (7, 9, and 11 $g.s^{-1}$, respectively). The influence has been analysed from the predicted mean concentration of component A X_A and the predicted outflow of the mixer Q_{out}, respectively.

(a)

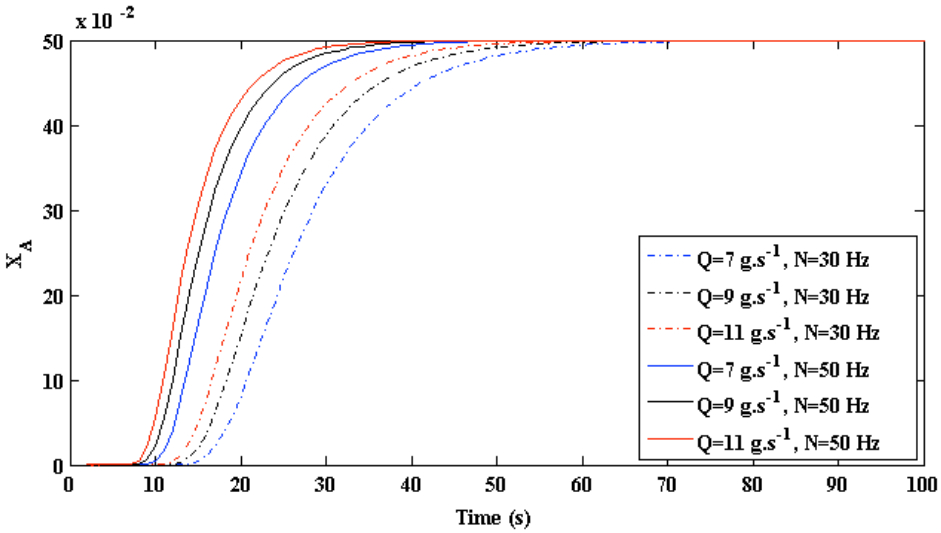

(b)

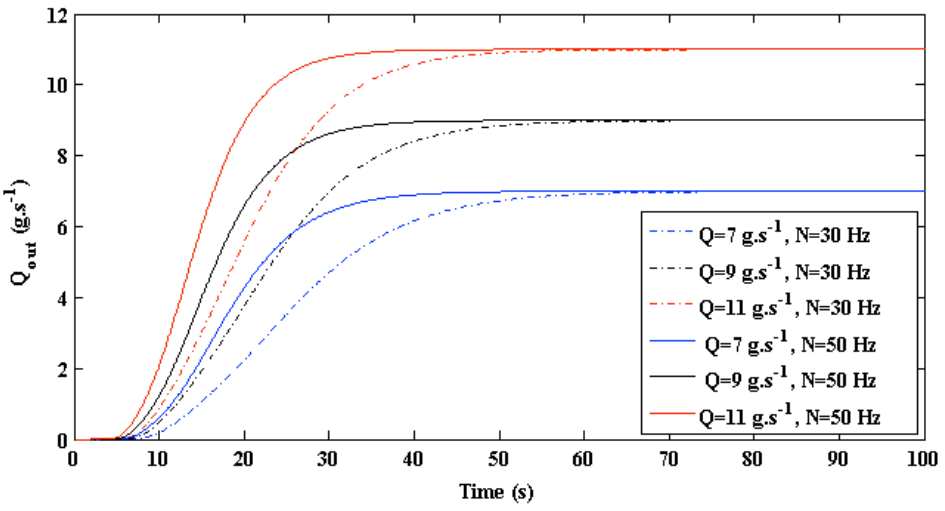

Figure III-18: Influence of rotational speed and total feed rate: (a) plots of X_A; (b) plots of Q_{out}.

In Figure III-18, both X_A and Q_{out} are plotted as a function of time. The three colours correspond to the three feed rate. The dash-dotted lines and solid lines correspond to 30 and 50 Hz, respectively. As shown in Figure III-18 (a), for either total feed rate, the mean concentration of component A rises much faster at high rotational speed. At either 30 or 50

Hz, as total feed rate increased, X_A rises faster to reach the target value. From Figure III-18 (b), the time required to reach steady state can be determined for each simulation, because we can consider the process reaches steady state when the outflow rate equals to the feed rate of the mixer. As seen from the figure, the final stable value of Q_{out} depends on the total feed rate while the time required to reach steady state is more influenced by rotational speed. Steady state was achieved at around 40 s for N=50 Hz while around 60 s for N=30 Hz. This indicates increasing in rotational speed allows achieving steady state more rapidly.

3.3.2 Influence of rotational speed and mixing formulation at a constant total feed rate

(a)

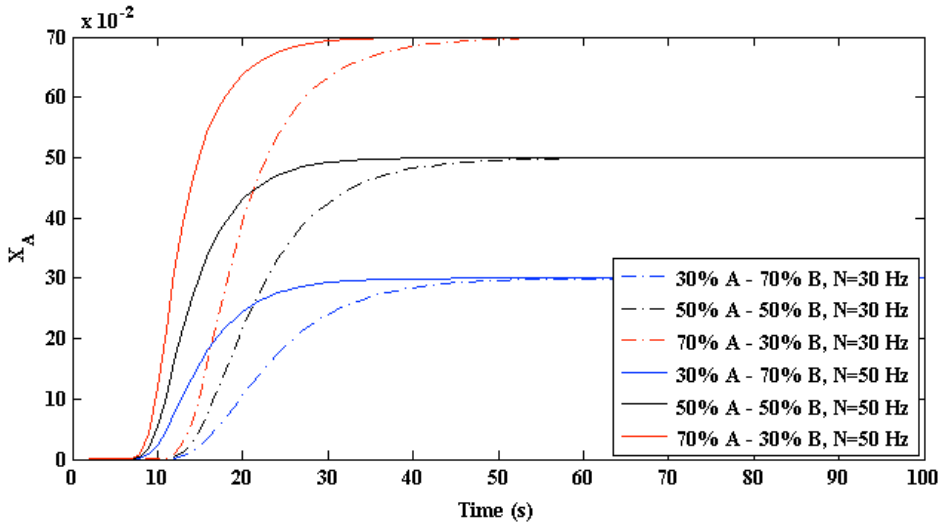

(b)

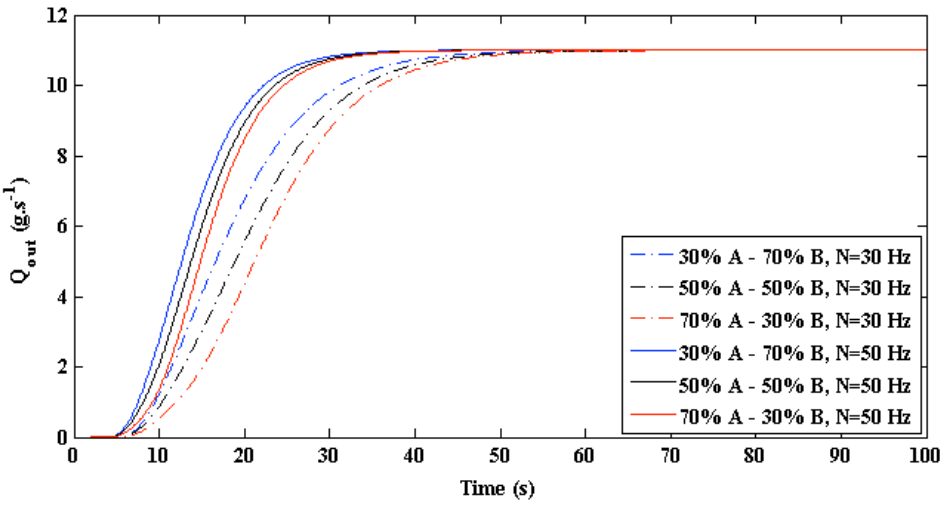

Figure III-19: Influence of rotational speed and mixing formulation: (a) plots of X_A; (b) plots of Q_{out}.

The total feed rate was fixed at 11 $g.s^{-1}$. The simulations were performed under two different rotational speeds (30 an 50 Hz) for three mixing formulations (30% A – 70% B, 50% A – 50% B, and 70% A – 30% B, respectively). The influence has been also analysed from the predicted mean concentration X_A and the predicted outflow of the mixer Q_{out}, respectively.
In Figure III-19, both X_A and Q_{out} are plotted as a function of time. The three colours correspond to the three mixing formulations. The dash-dotted lines and solid lines correspond to 30 and 50 Hz, respectively. As shown Figure III-19 (a), for either mixing formulation, the mean concentration of component A rises faster at high rotational speed (50 Hz). As seen from Figure III-19 (b), for either mixing formulation, Q_{out} rises more rapidly at high rotational speed (50 Hz), indicating that X_A reaches the expected concentration faster at 50 Hz. The time required to reach steady state is more influenced by rotational speed, since steady state was achieved at around 40 s for N=50 Hz while around 60 s for N=30 Hz. Under the same rotational speed and total feed rate, the mixing formulation has little influence on the time required to reach steady state.

4 Conclusion

The first section has proposed a method of powder hold-up measurement, for which the continuous mixer is divided into five cells in the axial direction and powder hold-up mass is detailed for each cell. The second section focuses on the experimental results. Firstly, bulk experiments for both components A and B were performed to study bulk powder flow in the continuous mixer. The results show that under the same operating condition component A has a higher hold-up mass in the mixer than component B. Secondly, mixing experiments of the two components were carried out by varying a set of operating conditions, such as mixing formulation, total feed rate and rotational speed of the mixer. For each experiment, powder flow and mixing behaviour was examined from the entire mixer and the individual cells of the mixer. For the entire mixer, the whole hold-up masses of component A and B, denoted as $M(A)$ and $M(B)$, were empirically expressed as a function of the operating parameters. For the individual cells of the mixer, the hold-up masses of component A and B, denoted as $M_i(A)$ and $M_i(B)$, were described as a linear function of $M(A)$ and $M(B)$, respectively. In the last section, continuous mixing of component A and B has been modelled using two Markov chains, one for each component. The model has been improved by using the

empirical functions related to hold-ups of each component, such as $M(A)$, $M(B)$, $M_i(A)$ and $M(B)$. The improved model was validated by comparing simulation results with experimental data in terms of mean concentration of component A X_A, the relative standard deviation *RSD*, the whole powder mass obtained at the outlet M_6 and the mass outflow rate of the mixer Q_{out}. The results of experimental validation show that the model can be used to predict X_A, M_6 and Q_{out}, except for *RSD*, which quantifies the homogeneity of samples per second. In addition, several simulations were performed to study the effects of operating conditions, such as rotational speed, total feed rate and mixing formulation. The simulation results of X_A and Q_{out} show that: (1) for a constant composition mixing, increasing in either rotational speed or total feed rate allows achieving steady state more rapidly. However, the impact of rotational speed is greater. (2) for a constant total feed rate, the influence of rotational speed is also more important than that of mixing formulation. Mixing achieves steady state more rapidly at higher rotational speed. A decrease in mass fraction of component A in feed stream reduces the time required to reach steady state.

CHAPTER IV: The design and implementation of PID controllers in a continuous mixing process

In powder mixing process that requires a high degree of accuracy in product composition, such as pharmaceutical and food industries, the continuous processing can be a troublesome proposition in practice because of a lack of knowledge in both process understanding and control. Therefore, deeper process understanding and real-time control systems are crucial to reduce or even avoid off-specification products due to manufacturing failure.

For the continuous powder mixing process presented in this work, the following issues will be discussed.

(1) Why the process needs to be controlled? What are the process variables that need to be controlled?

(2) What are the process variables important to achieve good control?

(3) Is there any control strategy available for this process?

1 Process analysis for continuous powder mixing from a control point of view

Figure IV-1: The continuous powder mixing process described by a “black box” model.

The continuous powder mixing process can be represented by a “black box” model as shown in Figure IV-1. The important process inputs consist of the rotational speed of the mixer (N) and the flow rates of the two components (Q_A and Q_B). The important process outputs, referring to as the controlled variable, consist of the mean concentration of component A (X_A) and the relative standard deviation (RSD). The process outputs are directly influenced by the process inputs.

The reason why the presented process needs to be controlled is illustrated by the following experimental observations. Two experiments were carried out. Each experiment contains two stages. At the first stage, both experiments were started at 30 Hz with an equivalent flow rates Q_A and Q_B (4.5 g.s^{-1}). At the second stage (after 85 s), both flow rates Q_A and Q_B were changed to 5.68 g.s^{-1} and the rotational speed N for experiment 1 was kept at 30 Hz while for experiment 2 the N was changed to 38 Hz.

At the mixer's inlet, since the flow rates of the two components have been controlled by the loss-in-weight mechanism, the actual Q_A and Q_B were well followed with random fluctuations, as shown in Figure IV-2.

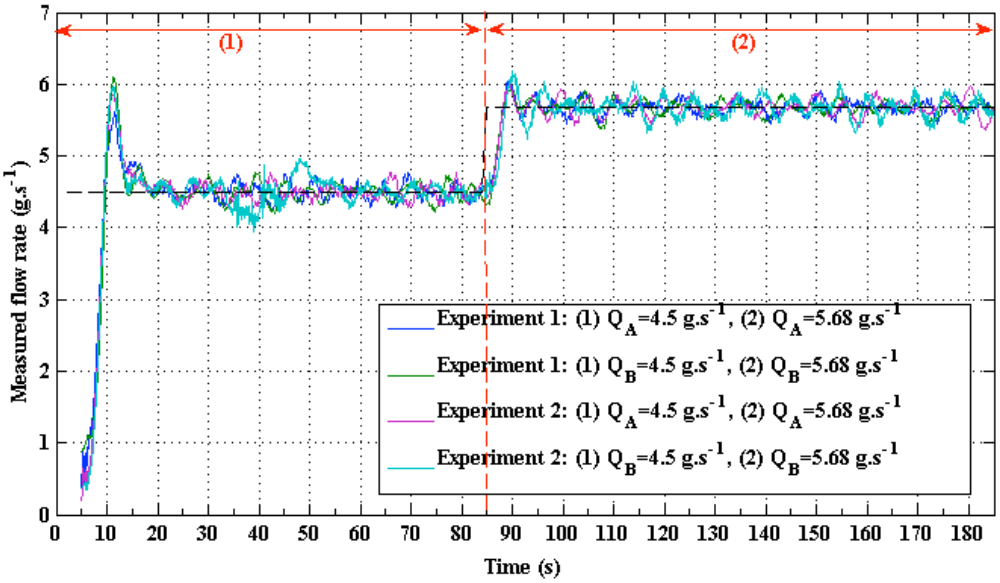

Figure IV-2: Experimental observations of the flow rates of the two components.

The experimental results of the mean concentration at the mixer's outlet are shown as follows.

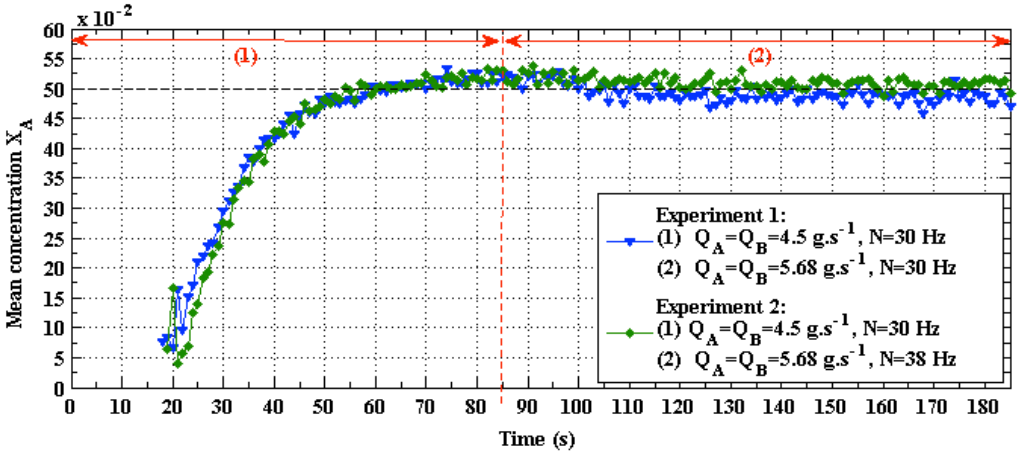

Figure IV-3: Experimental results of the mean concentration X_A.

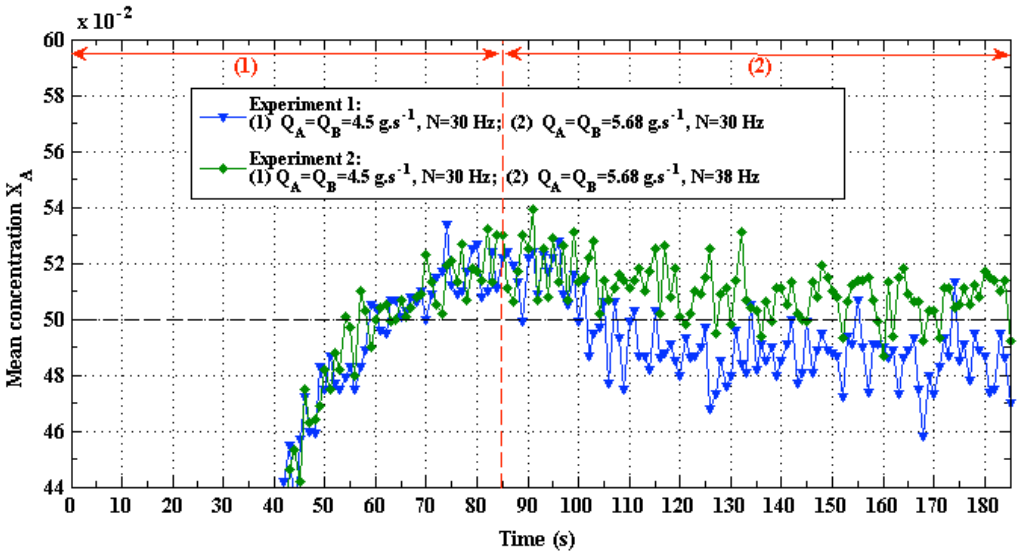

Figure IV-4: Enlargement in region around 50% of the measured mean concentration X_A.

As zoomed in Figure IV-4, for both experiments, the values of the mean concentration greater than the expected concentration 50% have been observed at the end of the first stage. At the second stage, the mean concentrations obtained from experiment 2 are mostly below 50%.

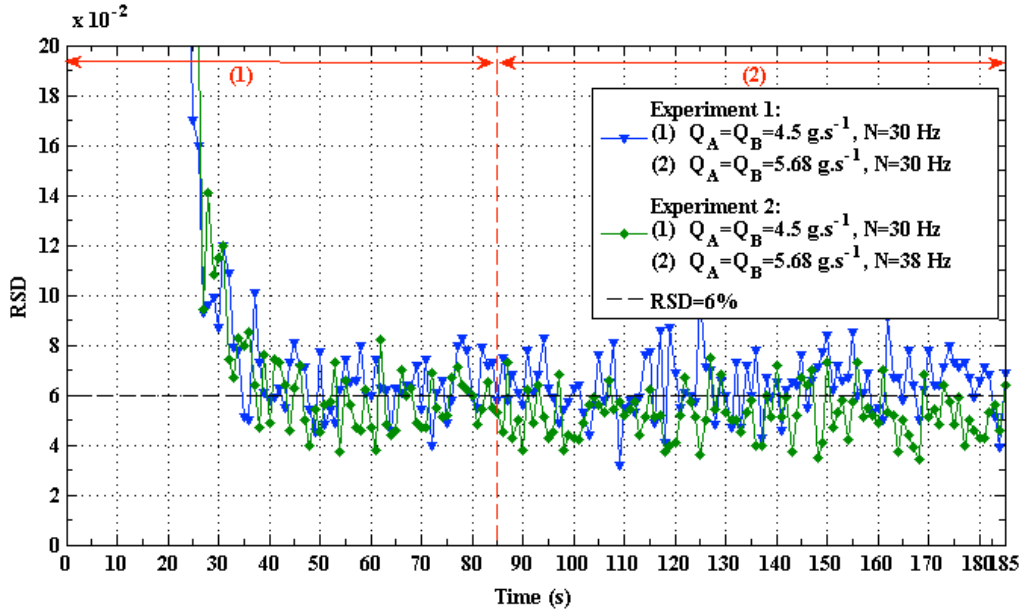

Figure IV-5: An example of experimental results of the relative standard deviation *RSD*.

In addition, as seen from Figure IV-5, many relative standard deviations obtained from experiment 1 exceed 6%, which is the label claim in the pharmaceutical industry.

In summary, the poor or unstable responses of the outputs X_A and *RSD* show that powder mixing in the continuous mixer should be controlled in order to ensure satisfactory mixture quality. Accordingly, the next step refers to the identification of the manipulated variable(s). In this work, the rotational speed N has been considered as the manipulated variable. The following three points are listed to confirm the choice.

(1) As part of the process inputs, the flow rates of the two components can be well controlled by the feeding system, as shown in Figure IV-2. In addition, the two flow rates directly affect the setpoint of the mean concentration.

(2) As shown in Figure IV-4 and Figure IV-5, after the same proportion increase in Q_A and Q_B, better mixing performance has been obtained through the positive step change in the rotational speed N from 30 to 38 Hz. Moreover, the responses to a negative step change in N have also been examined.

(a)

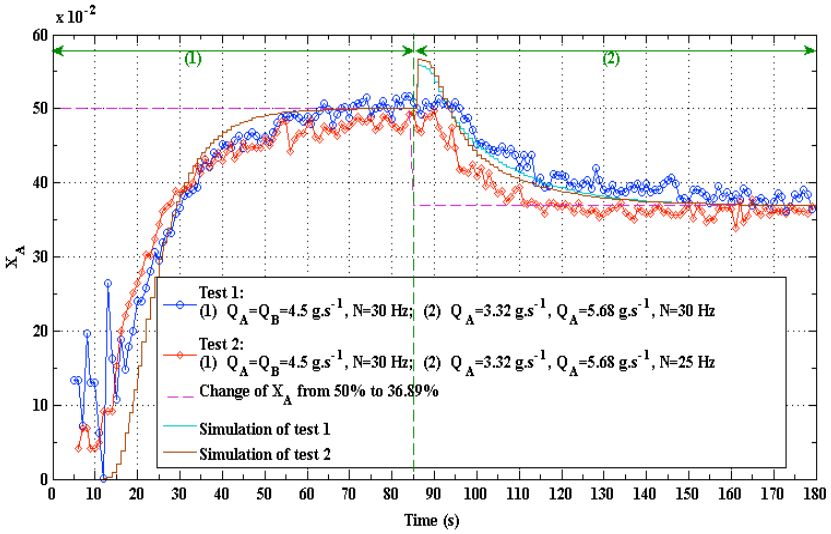

(b)

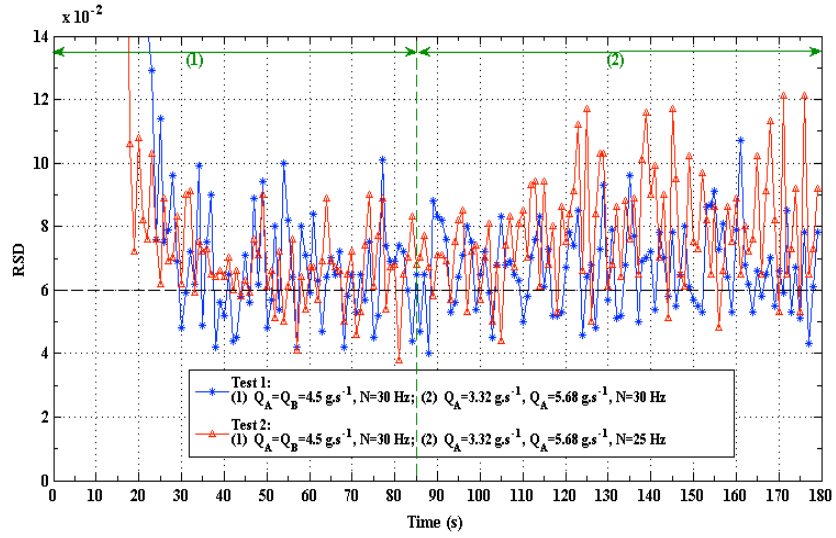

Figure IV-6: An example of measurements of (a) X_A and (b) *RSD*.

Two tests were performed. For both tests, the desired mean concentration decreased from 50% to 36.89% at 85 s due to a step change in Q_A from 4.5 to 3.32 g.s^{-1} and a step change in Q_B from 4.5 to 5.68 g.s^{-1}. The rotational speed N was kept at 30 Hz for test 1 while for test 2 a negative step change in N from 30 to 25 Hz occurred at 85 s. As seen from Figure IV-6 (a), both experimental and simulation results indicate that the negative step change in N is favourable for a rapid transition of the mean concentration X_A from 50% to 36.89% and the effect observed from experimental result is quite evident. This means that lower rotational speed does not always lead longer transition time to achieve the desired mixture concentration. While from Figure IV-6 (b), higher values of the relative standard deviation *RSD* have been obtained after the negative step change N compared to the rotational speed N maintained at 30 Hz in test 1.

(3) As illustrated in chapter II, for given flow rates of the two components, a higher rotational speed gives rise to an increase of mean concentration more rapidly (until to the desired value) during mixer start. However, the rotational speed N could not always keep at the highest value, due to high energy use, attrition phenomena, fluidized flow regime, etc.

2 Closed-loop control design for the process

During the last few years, both PID and model-predictive control systems for continuous powder-based processing have been suggested and discussed. However, no attempt has been made to implement a control system in a real plant continuous mixer. In this work, the implementation of a proportional-integral-derivative (PID) controller in the pilot continuous mixer has been realised using the PID Control Toolkit in Labview software package. PID control has been proposed as a first step of experimental control strategy, due to its easily implementation in practice and wide-use in the process industries. In the following, a single loop PID feedback control scheme is designed for either the mean concentration X_A or the relative standard deviation *RSD*.

2.1 Mean concentration control

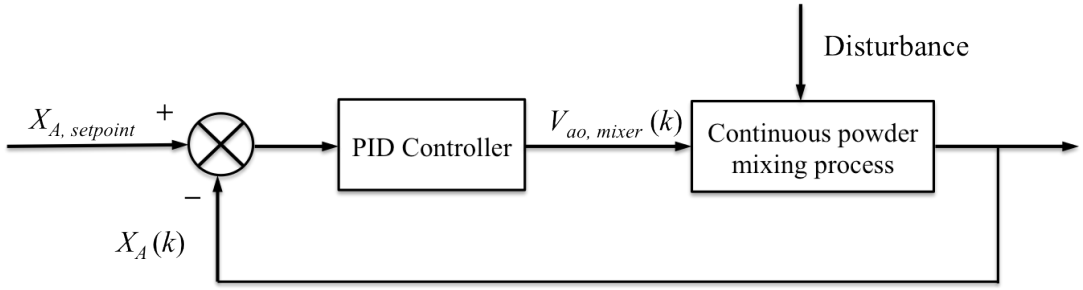

Figure IV-7: Closed-loop control of the mean concentration at the mixer's outlet.

In Figure IV-7 , $X_{A,\ setpoint}$ represents the desired mean concentration of component A, and $X_A\ (k)$ represent the current measured mean composition at the mixer's outlet, where k is the discretised time. $V_{ao,\ mixer}$ is the analog output voltage used to rotate the engine. In this closed-loop, the mean concentration X_A is considered as the controlled variable and $V_{ao,\ mixer}$ is taken as the immediate actuator, which in turn adjusts the rotational speed of the engine N. The final actuator N can be easily determined using the linear relationship reported in Figure II-12. The actuator $V_{ao,\ mixer}$ setting is calculated on the basis of the deviation from the setpoint of the mean concentration of component A, using a PID algorithm included in Labview.

$$e_{X_A}(k) = X_{A,\ setpoint} - X_A(k) \tag{IV-1}$$

$$V_{ao}(k) = K_c\left[e_{X_A}(k) + \frac{1}{T_i}\sum_{i=1}^{k}\left[\frac{e_{X_A}(i) + e_{X_A}(i-1)}{2}\right]\Delta t - \frac{T_d}{\Delta t}(X_A(k) - X_A(k-1))\right] \tag{IV-2}$$

Where Δt is the sampling time that will be set to 1 s in the following, since the controlled variable mean concentration X_A has been measured every second. e_{X_A} is the deviation from the setpoint of the mean concentration of component A. K_c is the controller gain, T_i is the integral time in minutes and T_d is the derivative time in minutes. The three parameters are the basic parameters of a PID controller.

2.2 Relative standard deviation control

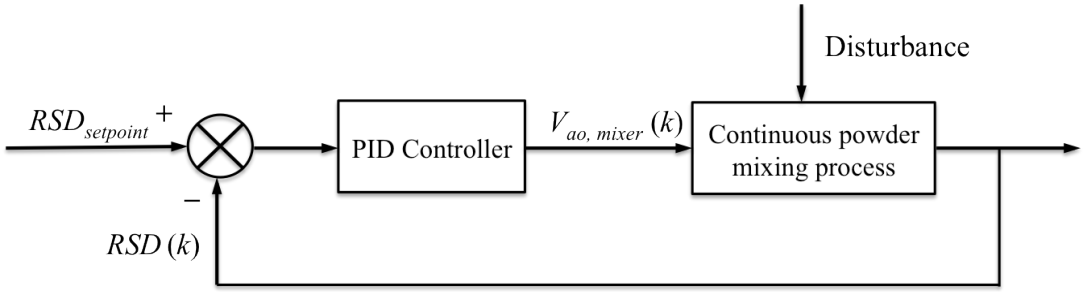

Figure IV-8: Closed-loop control of *RSD* at the mixer's outlet.

The relative standard deviation *RSD* is identified as the controlled variable since it is an important variable to quantify the homogeneity of the powder at the mixer's outlet. In the control scheme of *RSD*, the rotational speed of the engine *N* is also considered as the final actuator and it is calculated from $V_{ao,\ mixer}$, which is directly generated through a PID controller, as shown in Figure IV-8. $RSD_{setpoint}$ represents the desired value of the relative standard deviation and *RSD (k)* represents the current measured *RSD* at the mixer's outlet. The actuator $V_{ao,\ mixer}$ setting is calculated on the basis of the deviation from the setpoint of the *RSD*, using a PID algorithm included in Labview.

$$e_{RSD}(k) = RSD_{setpoint} - RSD(k) \tag{IV-3}$$

$$V_{ao}(k) = K_c\left[e_{RSD}(k) + \frac{1}{T_i}\sum_{i=1}^{k}\left[\frac{e_{RSD}(i) + e_{RSD}(i-1)}{2}\right]\Delta t - \frac{T_d}{\Delta t}(RSD(k) - RSD(k-1))\right] \tag{IV-4}$$

Where Δt is the sampling time that will also be set to 1 s in the following. e_{RSD} is the deviation from the setpoint of *RSD*. K_c, T_i and T_d are three parameters of the PID controller.

2.3 Implementation of PID in the pilot plant continuous mixer

As presented in Chapter II, the process contains two operating platforms: one for the feeding system and the mixer, another for the on-line image analysis system. The two operating platforms have been integrated into one programme through two while loops in parallel. The measurement results of X_A and *RSD* obtained from the loop of on-line image analysis have been introduced into the running loop of the mixer by creating local variables for X_A and *RSD*. The detailed information can be found in Annexe 2 including two block diagrams.

Focused on the control of the mixer, there are three alternative regulations for the rotational speed of the engine *N*.

(1) The rotational speed of the engine *N* keeps at the initial value, if there is no PID control for the mixer. This is referred to as an open-loop control.

(2) The rotational speed of the engine *N* is regulated by the closed-loop control of the mean concentration X_A.

(3) The rotational speed of the engine *N* is regulated by the closed-loop control of the relative standard deviation *RSD*.

(a)

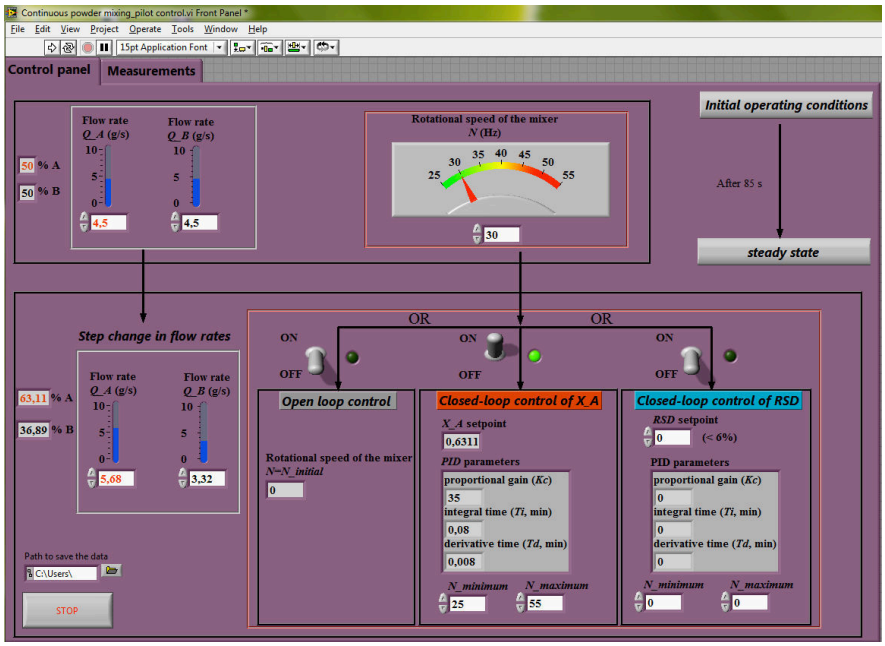

(b)

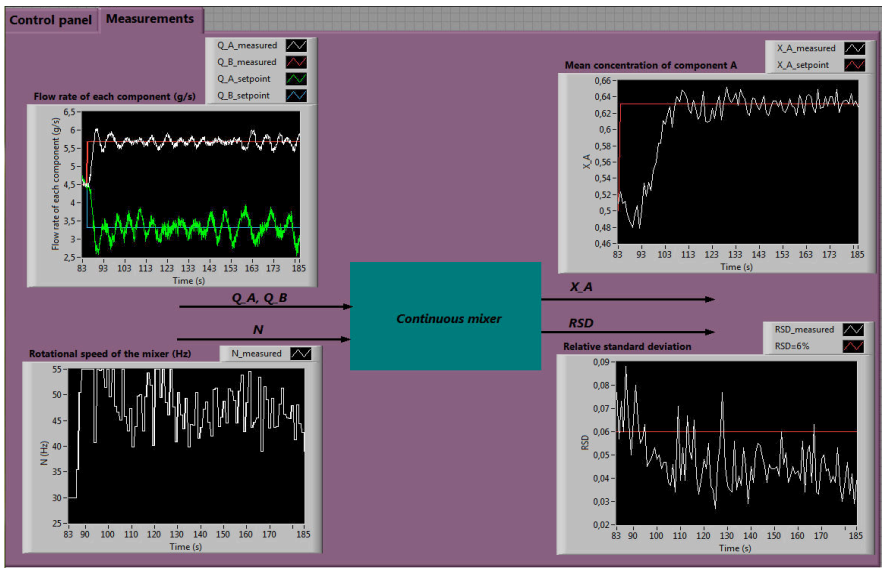

Figure IV-9: Graphic user interface of Labview: (a) control panel; (b) display panel for measurement results.

Figure IV-9 illustrates an example of the mean concentration X_A control. As seen from the figure, the operating procedure can be summarized. First of all, the initial process operating conditions including Q_A, Q_B and N should be defined. Once the process nearly attains steady state, the Q_A and Q_B can be redefined and the rotational speed of the engine N can be manipulated by one of the three regulation choices. In addition, an appropriate limit should be addressed to the rotational speed when there is a closed-loop control.

2.4 Performance criteria

The impact of proposed control loops on the continuous mixer's efficiency has been evaluated using the mean concentration and the *RSD* as performance criteria.

2.4.1 Mean concentration criteria

Prior to mixing homogeneity, the mean composition of powder mixtures at the outlet should be examined to evaluate the continuous mixer performance. The control objective is to rapidly attain the desired mean composition, which also means the error between the desired and measured mean composition should be minimized in time. Therefore, the integral absolute error (*IAE*), the integral square error (*ISE*) and the integral of time-weighted absolute error (*ITAE*) are used to evaluate the mixer's efficiency in terms of mean concentration X_A. They are calculated as follows:

$$ISE = \sum_{k=1}^{n} \left[e(k) \right]^2 \Delta t \qquad \text{(IV-5)}$$

$$IAE = \sum_{k=1}^{n} \left| e(k) \right| \Delta t \qquad \text{(IV-6)}$$

$$ITAE = \sum_{k=1}^{n} t_k \left| e(k) \right| \Delta t \qquad \text{(IV-7)}$$

Where Δt is the sampling time and *e(k)* is the error between the desired and actual measured values of mean composition X_A, at time instant k.

The three indices quantify the errors with respect to time through different ways. The *ISE* is similar to the *IAE*, but with more weight given to the magnitude of large errors, while the *ITAE* puts a heavy penalty on errors that persist for long periods of time.

2.4.2 RSD criteria

In the continuous process, an effective control strategy can significantly increase the number of qualified products on a continuous production line. In terms of *RSD*, the number of samples of the *RSD* less than 6% will be quantified during control stage.

2.5 Tuning of PID parameters

In order to obtain satisfactory control performance, PID parameters (K_c, T_i and T_d) in control loop of either X_A or *RSD* need to be tuned.

2.5.1 PID tuning for mean concentration X_A control

The commonly used method for PID tuning such as Ziegler-Nichols is a method based on the step response. The step response reveals how the controlled variable reacts to a step change in the manipulated variable. In this context, the controlled variable refers to the mean concentration X_A and the manipulated variable refers to the rotational speed of the engine N. As seen from Figure IV-10, for both simulations, the positive step change in rotational speed N at 85 s led to an increase of X_A after which X_A finally reached its original stable concentration. The responses of X_A to the step change in N are completely different from the results of the traditional step test for which the process response moving from one steady state to a new steady state. Therefore, the step response method is not applicable to this case. It seems that the PID parameters can only be tuned by a number of control experiences. While tuning of controllers implemented in a real plant is a challenging task because it often demands time-consuming and costly experiments. Thus, the X_A control based on the process model has been proposed as preliminary guidance for PID tuning. The question then arises whether the designed closed-loop schemes can be applied to the process model previously presented in Chapter III.

(a)

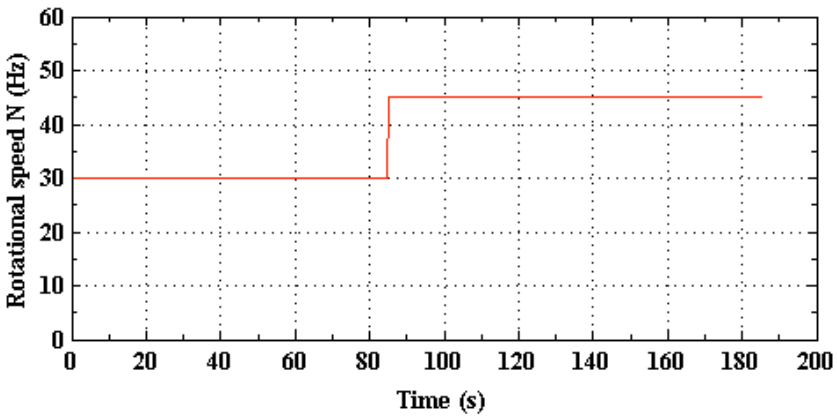

(b)

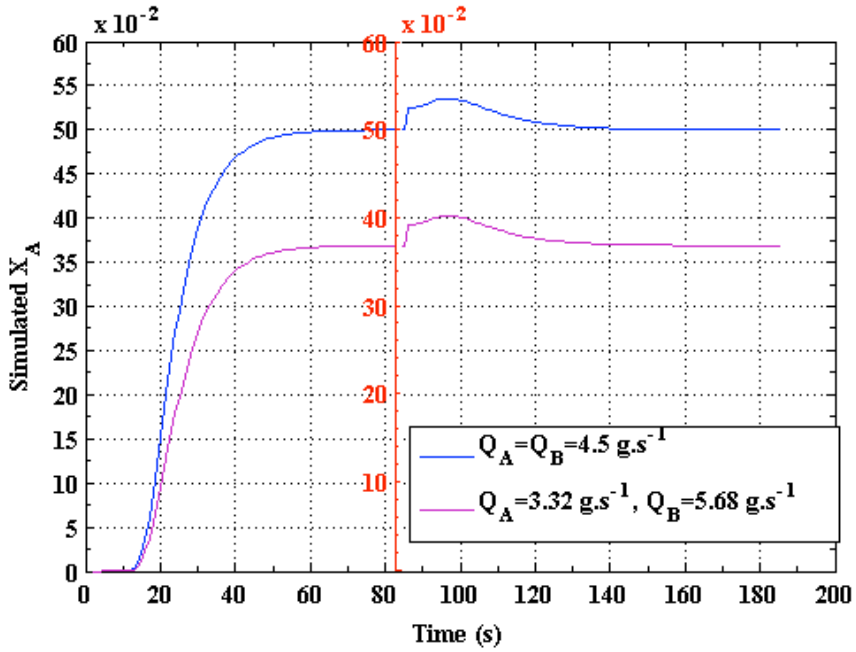

Figure IV-10: Simulated step response test: (a) positive step change in rotational speed N from 30 to 45 Hz (b) responses to the step change for the mixing 50% A – 50% B with Q_A=Q_B=4.5 g.s^{-1} and the mixing 36.89% A – 63.11% B with Q_A =3.32 g.s^{-1} and Q_B=5.68 g.s^{-1}.

The improved Markov chain model has been re-programmed in Labview and the same PID controller has also been integrated into the model. According to the source of the flow rates, two different simulation models have been presented as follows:

(1) Simulation Markov chain model using theoretical values of the flow rates Q_A and Q_B;

(2) Simulation Markov chain model taking into account the actual fluctuations in the flow rates Q_A and Q_B.

The detailed information about X_A control based on the model can be found in Annex 3.

As an example, the performance of X_A control using a PID controller setting of K_c=35, T_i=0.08 min and T_d=0.008 min has been examined both experimentally and via Markov chain simulations. In this example, the initial operating conditions were Q_A=Q_B=4.5 g.s^{-1} and N=30 Hz. At 85 s, Q_A was changed to 5.68 g.s^{-1} and Q_B was changed to 3.32 g.s^{-1}, which in turn decreased the setpoint of X_A from 50% to 63.11%. The closed-loop control of X_A was then used for set-point tracking.

(a)

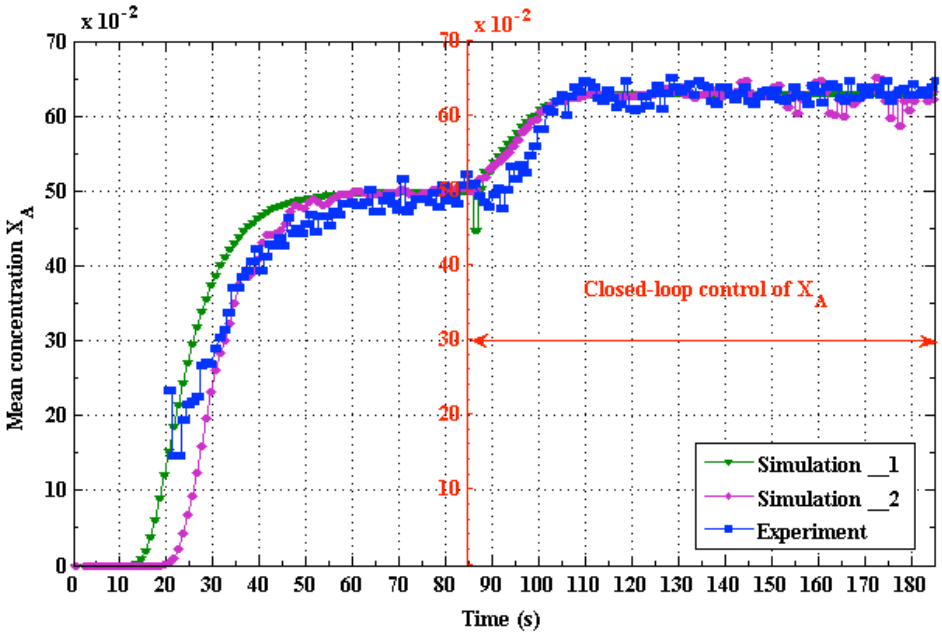

(b)

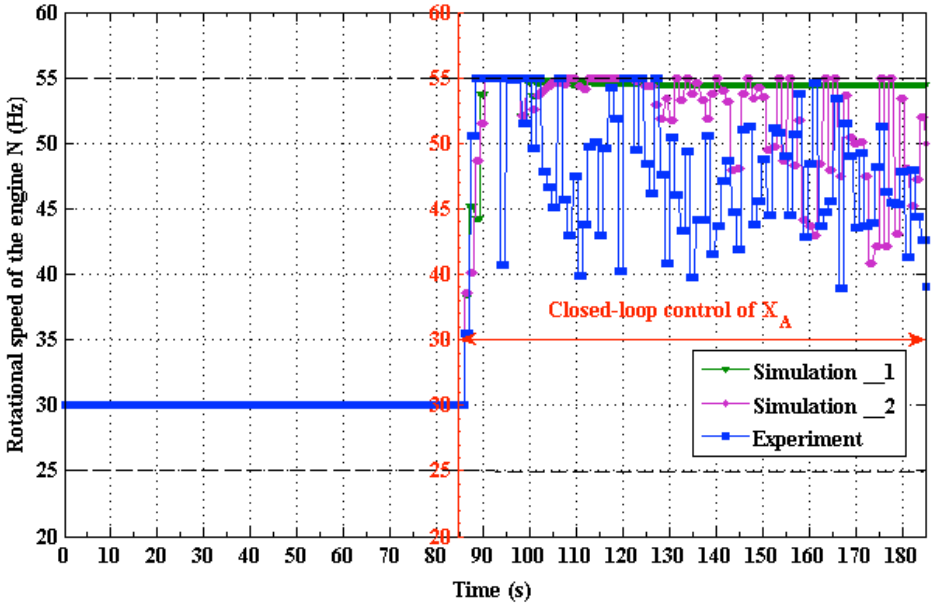

Figure IV-11: Comparison of model results with experimental results for X_A control: (a) mean concentration X_A; (b) rotational speed of the engine N.

Simulation_1 refers to the simulation using theoretical values of the flow rates. Simulation _2 refers to the simulation taking account into the fluctuations in the flow rates Q_A and Q_B, as shown in Figure IV-12.

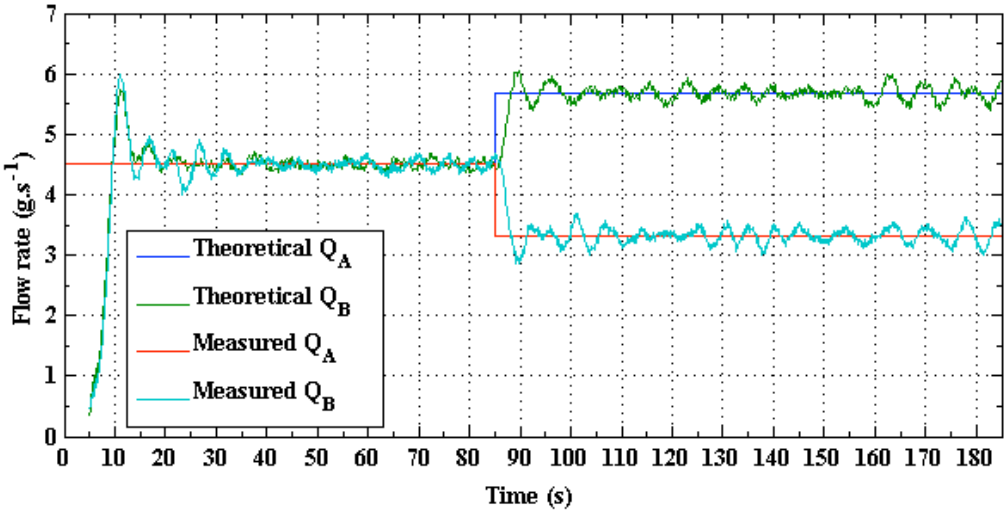

Figure IV-12: Theoretical values and experimental data of the flow rates Q_A and Q_B.

From Figure IV-11 differences can be observed between simulation and experimental results, particularly for the regulation of the rotational speed N during the control phase after 85 s. This is probably due to the model uncertainty related to unmeasured (or rather badly estimated) disturbances. In comparison to simulation_1, the X_A and N profiles of simulation _2 are closer to those obtained from the experiment.

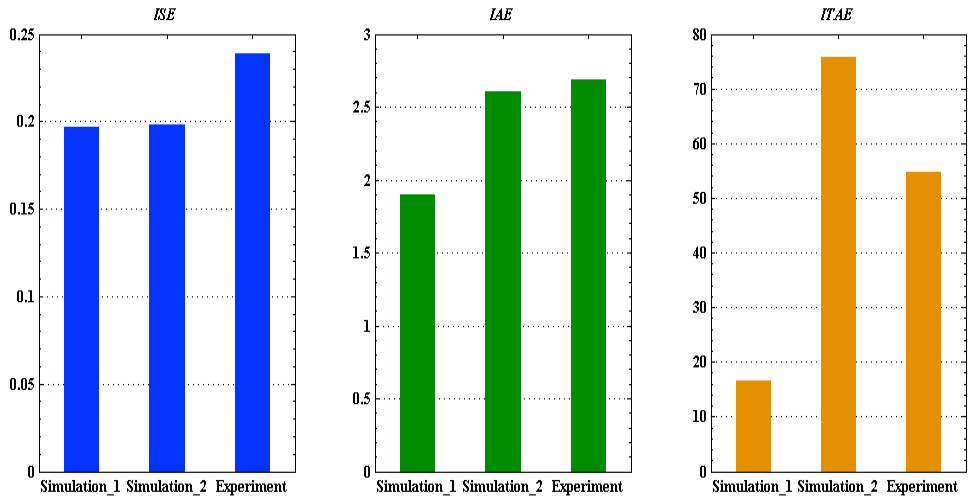

Figure IV-13: Performance comparison of simulated and experimental results by calculating *ISE*, *IAE* and *ITAE*.

This indicates that in order to improve the quality and accuracy of the prediction model the fluctuations in the flow rates Q_A and Q_B should be taken into account, particularly for the purpose of closed-loop control. This also can be concluded from the evaluation of X_A control performance through *ISE*, *IAE* and *ITAE*. As shown in Figure IV-13, the values of *ISE*, *IAE* and *ITAE* obtained from simulation_2 are closer to the experimental results, particularly for *IAE*.

However, the mass flow rates have not yet been studied from a modelling viewpoint. The actual fluctuations in the flow rates have been added to the model using the experimentally measured flow rates.

2.5.2 PID tuning for relative standard deviation RSD control

For *RSD* control, the tuning of PID parameters have been directly accomplished by control experiments of *RSD*, since the presented model cannot be used to predict the variability in the concentration over 14 consecutive samples experimentally. In particular, the *RSD* control is based on a closed-loop while the performance evaluation of *RSD* is directly related to a pharmaceutical limit less than 6% rather than the *RSD* setpoint, which should be set to a value smaller than 6%.

In summary, for the closed-loop of X_A, different PID settings are firstly tested via simulation and the performances are then evaluated and compared. PID settings giving optimal performance are finally tested in the closed-loop experiements. Possible adjustment of PID settings may be made according to experimental results. While, for the closed-loop control of *RSD*, different PID settings are directly tested in experiments.

3 Conclusion

In this chapter, we have analysed the continuous powder mixing process from a control point of view. The process control demand has been illustrated by several experimental results. The mean concentration X_A and the relative standard deviation *RSD* have been identified as the important controlled variables for the assessment of the continuous mixer's efficiency. The rotational speed of the mixer *N* has been identified as the important manipulated variable and this decision has also been justified. A simplified PID control has been proposed to control

either the mean concentration or the relative standard deviation. The implementation of a PID controller in a pilot scale continuous mixer has finally been realised using Labview. The performance criteria in terms of the mean concentration X_A and the relative standard deviation *RSD* have been defined to evaluate closed-loop control performance. The tuning of PID parameters, as an important step towards good control, has been discussed. For the closed-loop control of mean concentration X_A, a PID tuning based on the process model has been proposed as the preliminary guidance for further PID tuning through control experiments. While for the closed-loop control of relative standard deviation *RSD*, a number of *RSD* control experiments have been required for PID tuning, since the presented process model has not yet been enough accurate for the *RSD* prediction.

CHAPTER V: Control case studies

1 Case study design

We focus on the performance assessment of closed-loops subjected to step changes in flow rates Q_A and Q_B. Four case studies have been designed according to possible step changes in Q_A and Q_B, as shown in Table V-1.

Table V-1: The four cases studied.

	Q_A (g.s^{-1})	Q_B (g.s^{-1})	Control system
Case 1	Positive step change (from 4.5 to 5.68)	Negative step change (from 4.5 to 3.32)	Closed-loop (X_A or *RSD*)
Case 2	Negative step change (from 4.5 to 3.32)	Positive step change (from 4.5 to 5.68)	Closed-loop (X_A or *RSD*)
Case 3	Positive step change (from 4.5 to 5.68)	Positive step change (from 4.5 to 5.68)	Closed-loop (X_A or *RSD*)
Case 4	Negative step change (from 4.5 to 3.32)	Negative step change (from 4.5 to 3.32)	Closed-loop (X_A or *RSD*)

From an industrial viewpoint, the study of case 1 and 2 aims at contributions to control the process when requiring a change in mixture composition during the production while no change in the total production volume. Case 3 corresponds to an increase in continuous production volume and case 4 correspond to a decrease in continuous production volume.

The overall control procedure is summarized in Figure V-1. In each case, the continuous mixing process is experimentally started at 50%, with component A and B, both flow rates at 4.5 g.s^{-1}. The rotational speed of the engine N is initially set to 30 Hz. Once the continuous mixing process reaches steady state, the closed-loop of either X_A or *RSD* is implemented and the defined step changes in flow rates are performed simultaneously. Each experiment is totally run for 185 s with a step changes implemented at t=85 s after steady state is achieved. Consequently, the control time lasts 100 s because it should be counted from the moment

when the corresponding PID controller starts working. In addition, the duration of 100 s is chosen because the time is long enough to ensure the achievement of a new steady state under open-loop operation. Moreover, the closed-loop performance of either X_A or *RSD* is compared against open-loop operation, which refers to the mixer running in "manual mode". In open-loop operation, the rotational speed of engine is kept at 30 Hz.

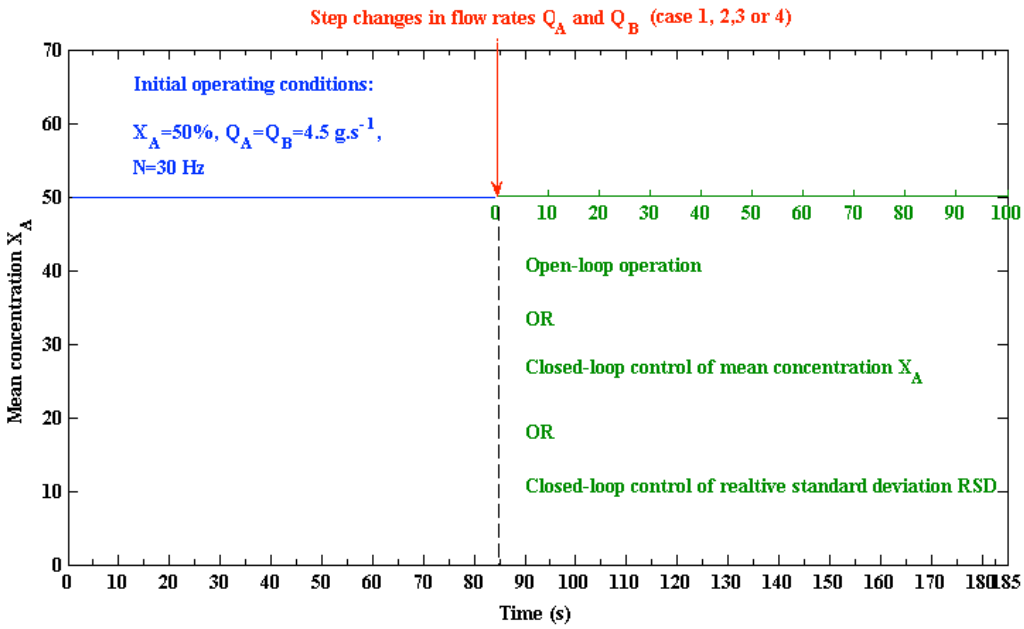

Figure V-1: The design of control procedure.

The mixing composition 50% A – 50% B is selected as the starting point, because this mixture is the most commonly studied in previous work of Marikh [1] and Ammarcha [2] using the continuous mixer. In all control experiments, the maximum rotational speed of engine is set at 55 Hz, since higher rotational speeds lead to particle breakage/attrition on component B, particles of diameter larger than 1250 μm. This remark is outlined in the present work as well as in [2].

As shown in Table V-1, in case 1 and 2, the magnitudes of step change in set-points of mean composition in component A are +13.11% and −13.11%, respectively, whereas total flow rates at the mixer inlet are kept constant. In case 3 and 4, the setpoints of X_A are kept constant, whereas total flow rates are changed due to the same magnitude increase or decrease of both components. Two main reasons that can be listed to explain these designs are: (1) a tolerance of ±7.5% is acceptable for mean content in pharmaceutical industry, and the magnitudes of ±13.11% facilitates enlarging control effects; (2) mixtures after introducing step changes in

flow rates are still in the range of 30%–70%, in which experiments were performed for modelling the process, as given Table III-1.

2 Case study 1

In all experimental studies, the flow rates of both component A and B at the mixer's inlet have been investigated, because well controlled flow rates are prerequisites for obtaining the desired mixing efficiency. Figure V-2 gives an example of experimentally obtained mass flow rates in response to step changes in Q_A and Q_B.

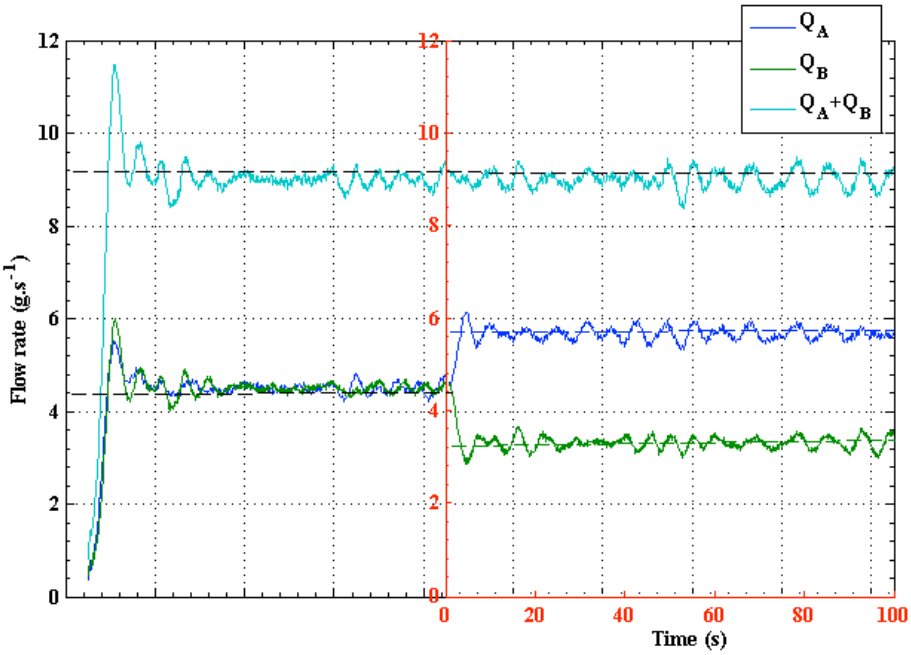

Figure V-2: Flow rate responses to a positive step change in Q_A and a negative step change in Q_B without changing the total feed rate.

The step changes in Q_A and Q_B result a step change in the mean composition X_A from 50% to 63.11% and the total feed rate $Q_A + Q_B$ keeps at 9 $g.s^{-1}$ the same as for the starting stage. In addition, small random fluctuations around the desired values can be observed in both flow rates, although loss-in-weight feeders are used to feed the continuous mixer.

2.1 Closed-loop control of mean concentration X_A

First, the simulated closed-loop of X_A has been used to tune PID parameters. The theoretical step changes in Q_A and Q_B have been considered in the model. The rotational speed of the engine N has been limited in the range of 25−55 Hz.

(1) Tuning of P controller

Prior to PID controller, Labview PID controller has been used as P controller by appropriate setting of $T_i \rightarrow \infty$ and $T_d = 0$. Three values of the proportional gain K_c were tested. The performances of the three P controllers have been evaluated by calculating *ISE*, *IAE* and *ITAE*, and compared with that of open-loop operation. As shown in Table V-2, P controller of $K_c = 35$ performs better than two other P controllers, whereas X_A controlled by P controllers seems to be worse than that obtained in open-loop operation.

Table V-2: Results of P tuning based on the model.

	ISE	*IAE*	*ITAE*
Open-loop	0.497	3.818	53.837
P controller ($K_c = 25$)	0.541	4.53	96.88
P controller ($K_c = 35$)	0.392	4.255	98.86
P controller ($K_c = 45$)	0.471	4.452	115.407

(2) Tuning of PI controller

Then, Labview PID controller has been used as PI controller by setting of $T_d = 0$. Keeping K_c at 35, three values of T_i were examined. The performances of PI controllers have been evaluated as given in Table V-3. It is found that the PI setting of $K_c = 35$ and $T_i = 0.08$ min gives the best performance.

Table V-3: Results of PI tuning based on the model

	ISE	*IAE*	*ITAE*
Open-loop	0.497	3.818	53.837
PI controller ($K_c = 35$, $T_i = 0.02$ min)	0.193	1.852	15.645
PI controller ($K_c = 35$, $T_i = 0.08$ min)	0.187	1.807	15.107
PI controller ($K_c = 35$, $T_i = 0.14$ min)	0.208	2.111	21.508

(3) Tuning of PID controller

Using K_c = 35 and T_i = 0.08 min, Labview PID controller has been tuned by varying T_d. Smaller errors were obtained from PID setting of K_c = 35, T_i = 0.08 min, T_d = 0.008 min, as shown in Table V-4.

Table V-4: Results of PID tuning based on the model

	ISE	*IAE*	*ITAE*
Open-loop	0.497	3.818	53.837
PID controller (K_c = 35, T_i = 0.08 min, T_d = 0.002 min)	0.197	1.897	16.489
PID controller (K_c = 35, T_i = 0.08 min, T_d = 0.008 min)	0.194	1.86	15.82
PID controller (K_c = 35, T_i = 0.08 min, T_d = 0.02 min)	0.295	3.815	122.993

In summary, from previous P/PI/PID tuning based on the simulated closed-loop of X_A, it can be seen that K_c = 35 and T_i = 0.08 min are proper values if a PI controller is used, and K_c = 35, T_i = 0.08 min and T_d = 0.008 min are proper values if a PID controller is used. Therefore, the two sets PI(D) parameters have been tested in the experimental closed-loop of X_A.

Figure V-3 (a) shows the PI/PID closed-loop responses of mean composition in component A at the mixer's outlet, and they are also compared to the open-loop response of X_A. Clearly, the PI/PID controller drives the controlled X_A to its new setpoint in a significantly shorter time than the one required in an open-loop operation. Slightly smaller oscillations at the final steady state can be observed in the proposed PID control. As shown in Figure V-3 (b), the PI/PID closed-loop of mean concentration X_A provide lower *RSD* values, which means better mixing homogeneity, as compared to the open-loop. For Figure V-3 (b), the percentage of samples of *RSD* value less than 6% is quantified as the ratio of RSD < 6%. Figure V-3 (c) shows the rotational speed N adjusted through the PI/PID controller. In the closed-loop control, high values of the rotational speed N have been generated at the beginning and then the values vary between 35 and 55 Hz.

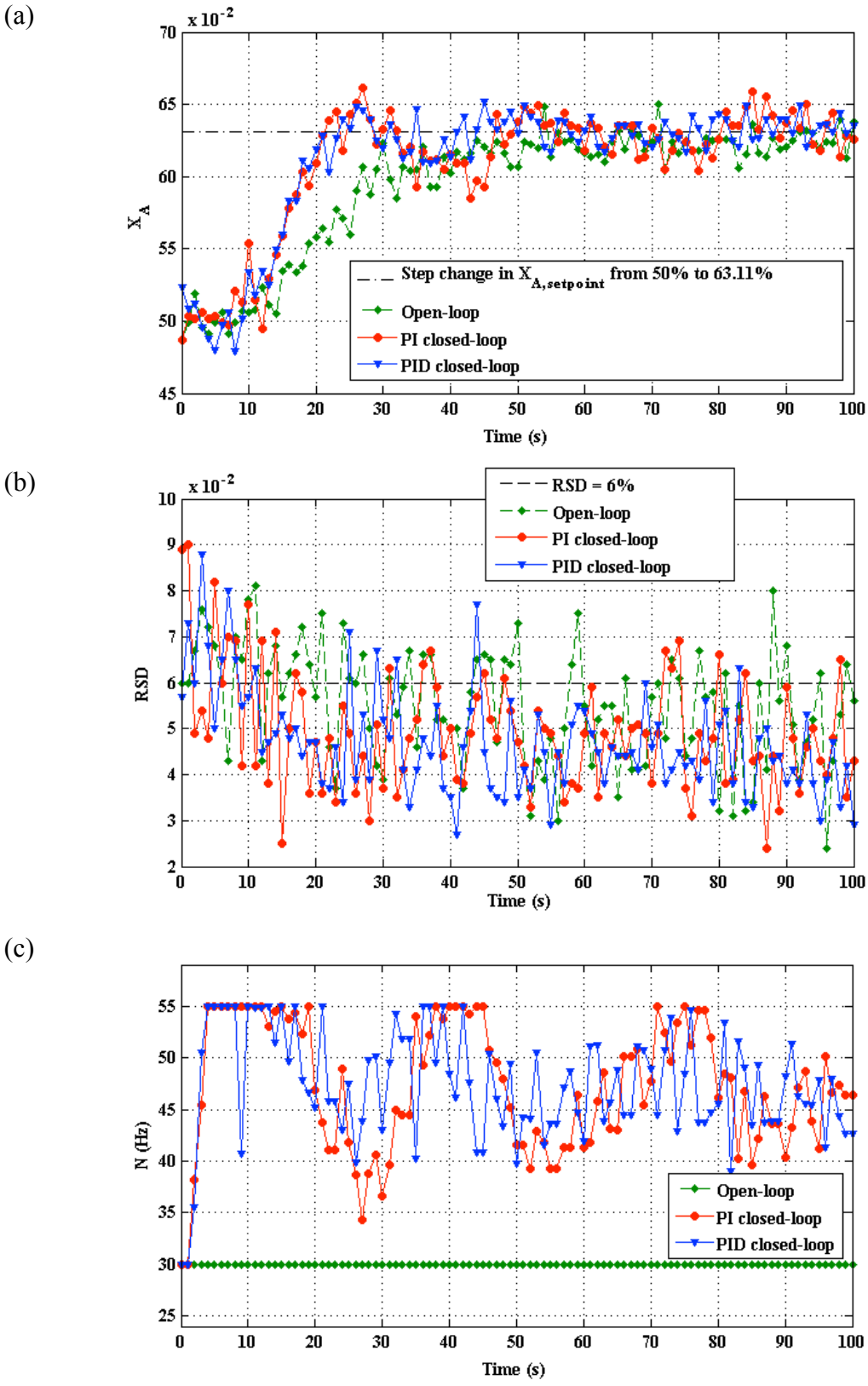

Figure V-3: Experimental results from PI/PID closed-loop control of mean concentration X_A in case 1: (a) mean composition X_A, (b) relative standard deviation *RSD*, (c) rotational speed of the engine *N*.

The mixing performance has been quantified as shown in Table V-5. By comparing the *ISE*, *IAE*, *ITAE* values of the PI/PID closed-loop to the open-loop, it can be found that the PID closed-loop of X_A exhibits the best mixing performance in terms of both X_A and *RSD*.

Table V-5: Performance assessment results from experiments of closed-loop control of X_A in case 1.

	ISE	*IAE*	*ITAE*	*Ratio of RSD < 6%*
Open-loop	0.329	3.783	87.614	56 / 101
PI closed-loop	0.241	3.001	74.204	80 / 101
PID closed-loop	0.239	2.687	54.815	87 / 101

When we turn back to the simulation results of *ISE*, *ITAE* and *ITAE*, significant differences of *IAE* and *ITAE* can be observed between simulation and experiments. This is because the fluctuations in flow rates have not been taken into account in the model which has been used for P/PI/PID tuning. The corresponding PI/PID control simulations including the actual measured flow rates have also been performed.

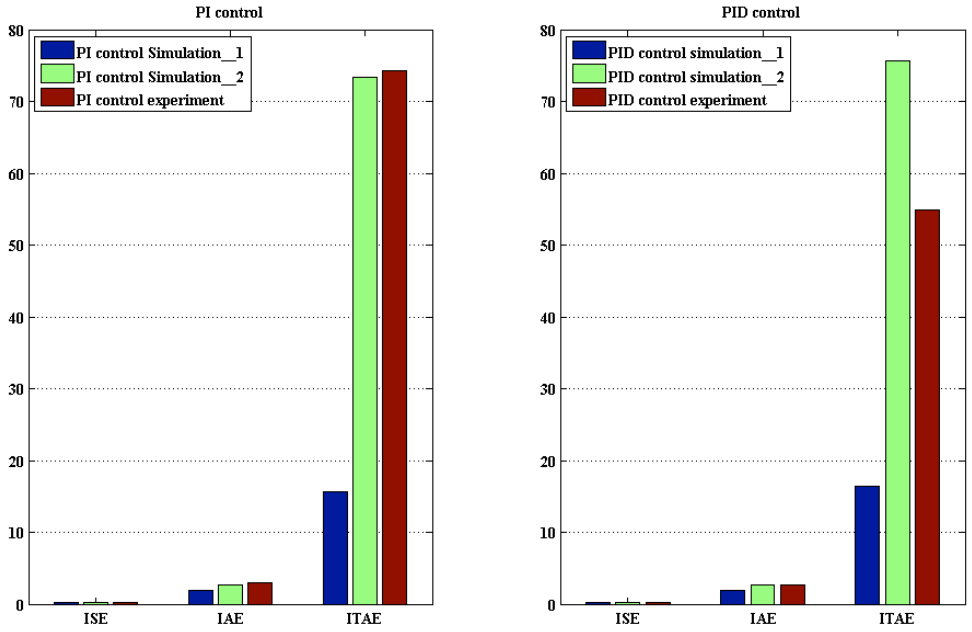

Figure V-4: Comparison of simulated values with measured values for the mean concentration performance criteria *ISE*, *IAE* and *ITAE*.

Simulation_1 and simulation_2 refer to control simulation without and with actual flow rate fluctuations, respectively. As can been seen from Figure V-4, for either the PI or the PID control, the *IAE* and *ITAE* obtained from simulation_2 are more closer to the experimental data compared to those obtained from simulation_1. This indicates that flow rate fluctuations, even if they are very small, play an important role in the reliability and accuracy of the model-based control study.

2.2 Closed-loop control of *RSD*

Since *RSD* could not be accurately predicted from the presented model so far, the PID controller in the closed-loop of *RSD* has been directly tuned by experiments. The *RSD* setpoint is an important starting point in the closed-loop control of RSD. For powder mixing, values less than 6% need to be used as *RSD* setpoints, as *RSD* is required to be less than 6% in the pharmaceutical industry. In this case, the closed-loop performance of *RSD* has been studied for the *RSD* setpoints of 4% and 3%, respectively.

A PID setting of K_c = 28, T_i = 0.08 min, T_d = 0.008 min has been tested and the experimental results have been depicted in Figure V-5. In Figure V-5 (a), the *RSD* setpoint of 4% leads to a negative effect on the mean concentration X_A, as can be seen from the measured X_A, which has finally exceeded the desired value. While from Figure V-5 (b), it seems that the *RSD* profile obtained from the *RSD* setpoints of 4% is better. For the *RSD* setpoint of 4%, the final excessive X_A and better *RSD* profile can be attributed to a large increase in the rotational speed at later times, as shown in Figure V-5 (c).

Table V-6: Performance assessment results from experiments of closed-loop control of *RSD* with the *RSD* setpoints of 4% and 3% in case 1.

	ISE	*IAE*	*ITAE*	*Ratio of RSD < 6%*
Open-loop	0.329	3.783	87.614	56 / 101
RSD setpoint = 4%	0.306	4.316	162.717	83 / 101
RSD setpoint = 3%	0.411	4.272	94.25	61 / 101

As can be seen from Table V-6, similar mixer performance has been obtained from the open-loop and the *RSD* setpoint of 3%. The *RSD* setpoint of 4% has provide a higher ratio of *RSD* < 6% but large deviations in the mean concentration X_A.

(a)

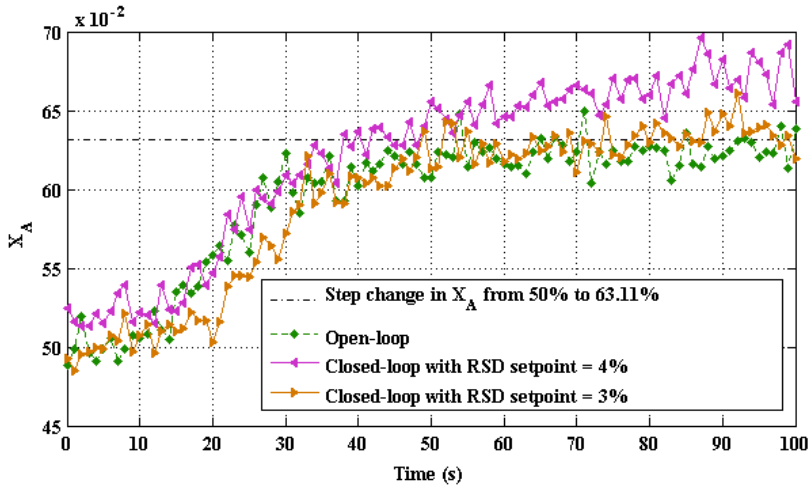

(b)

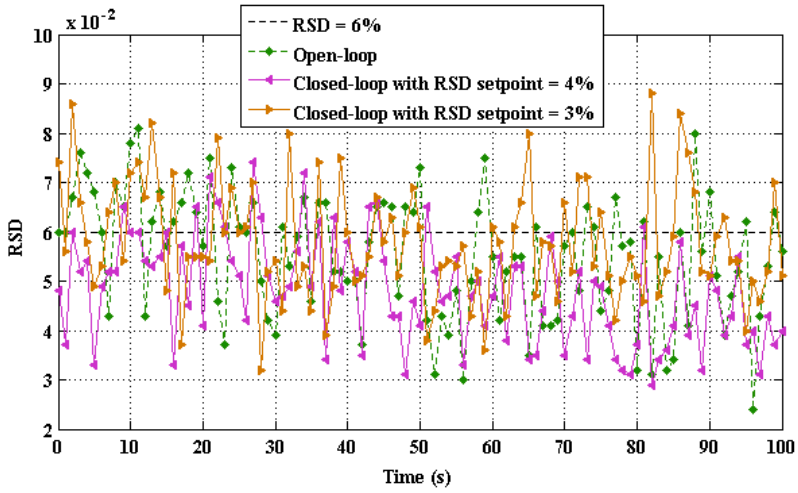

(c)

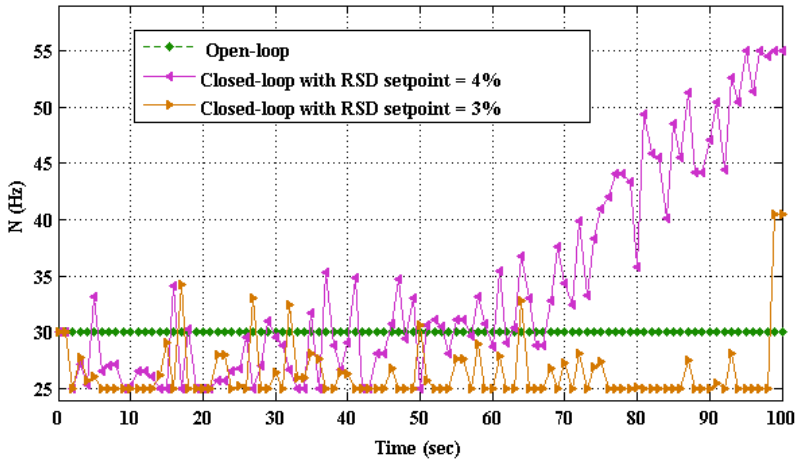

Figure V-5: Experimental results from closed-loop of *RSD* with the *RSD* setpoints of 4% and 3% in case 1: (a) mean composition X_A, (b) relative standard deviation *RSD*, (c) rotational speed of the engine *N*.

In summary, the above-mentioned control parameters (e.g. $RSD_{setpoint}$ and PID parameters) need to be modified in order to be effective.

As previously observed from *RSD* setpoint of 3%, the setting of controller parameters caused poorly control of the mixer performance in terms of *RSD* as well as X_A, since the rotational speeds approximately the minimum limit generated. Therefore, a negative value of the controller gain (K_c) has been proposed to reverse the regulation direction of the rotational speed of the engine. Then, a PID setting of K_c = −28, T_i = 0.05 min, T_d = 0.008 min has been tested in the closed-loop of *RSD* with the setpoint of 3%.

(a)

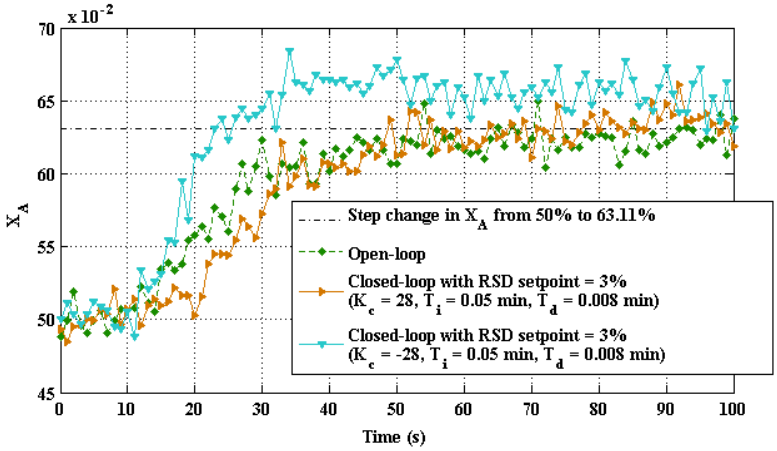

(b)

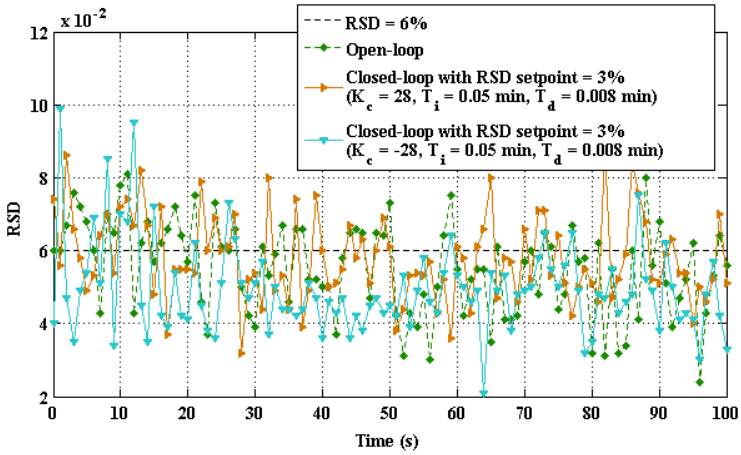

(c)

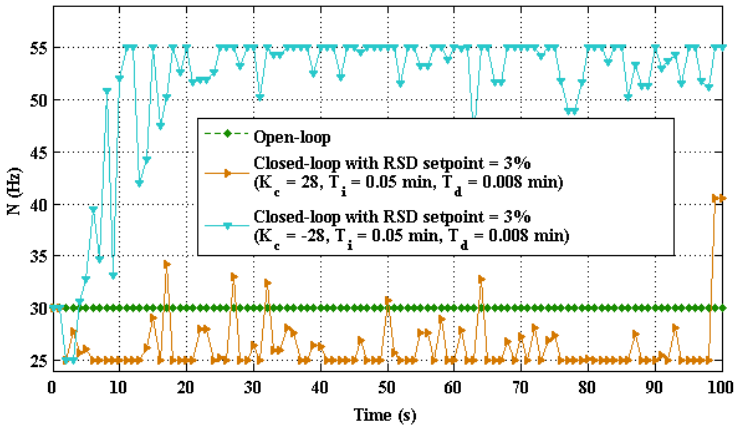

Figure V-6: Experimental results from closed-loop of *RSD* with negative controller gain in case 1: (a) X_A, (b) *RSD*, (c) *N*.

As shown in Figure V-6 the negative controller gain of –28 contributes to a faster X_A response to the step changes in flow rates, but the mean concentration becomes stable around 65%, about 2% higher than the ideal value. If the 2% exceeding is acceptable in practice, we consider that the negative controller gain in the closed-loop can improve the mixer performance due to lower values of *RSD* obtained at the mixer's outlet, as shown in Figure V-6 (b). However, from a theoretical point of view for the control, the negative controller gain is unsatisfactory for the mean concentration due to larger values of *ISE*, *IAE* and *ITAE* as given in Table V-7. This could be attributed to the excessive rotational speeds approximately 55 Hz, as depicted in in Figure V-6 (c).

Table V-7: Performance assessment results from experiments of closed-loop control of *RSD* with negative controller gain in case 1.

	ISE	*IAE*	*ITAE*	*Ratio of RSD < 6%*
Open-loop	0.329	3.783	87.614	56 / 101
RSD setpoint = 3% (K_c = 28, T_i = 0.05 min, T_d = 0.008 min)	0.411	4.272	94.250	61 / 101
RSD setpoint = 3% (K_c = –28, T_i = 0.05 min, T_d = 0.008 min)	0.311	4.272	131.619	86 / 101

Hence, the negative controller gain of –28 has been tested again by setting the upper limit of the rotational speed at 48 Hz. As can be seen from Figure V-7 (a), the upper limit of *N* at 48 Hz provides a fast X_A response (as compared to the open-loop) without too much overshoot (as compared to the control under the upper limit of *N* at 55 Hz). The *RSD* responses and the regulation of *N* are shown in Figure V-7 (b) and (c), respectively.

Table V-8: Performance assessment results from experiments of closed-loop control of *RSD* under different limits of the manipulated variable *N* in case 1.

	ISE	*IAE*	*ITAE*	*Ratio of RSD < 6%*
No control loop	0.3294	3.7825	87.6144	56 / 101
$N \in [25, 55]$ (K_c = -28, T_i = 0.05 min, T_d = 0.008 min)	0.311	4.272	131,6188	86 / 101
$N \in [25, 48]$ (K_c = -28, T_i = 0.05 min, T_d = 0.008 min)	0.3155	3.3953	82.9138	76 / 101

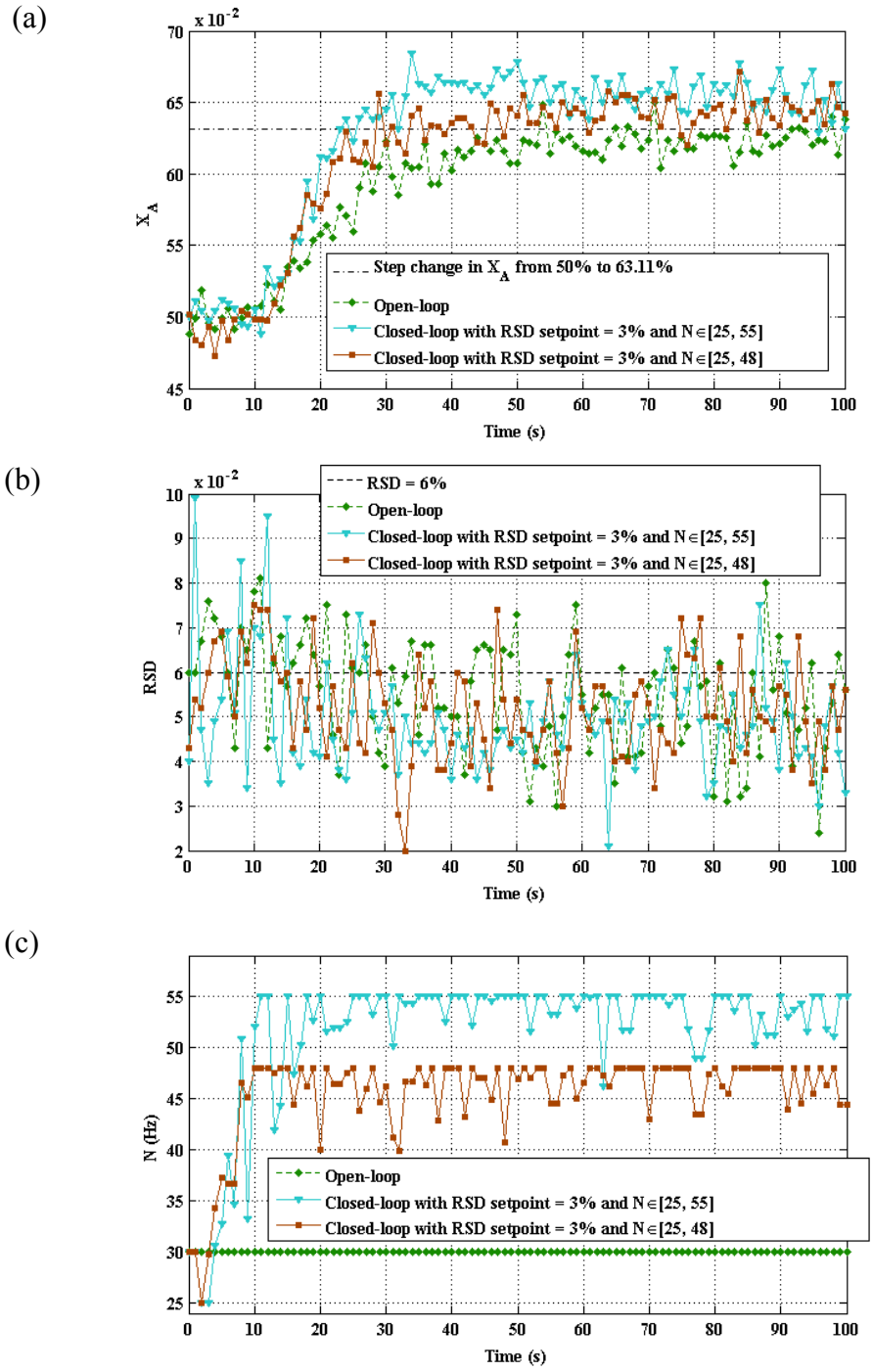

Figure V-7: Experimental results from closed-loop of *RSD* under different limits of the manipulated variable *N* in case 1: (a) mean composition in component X_A, (b) relative standard deviation *RSD*, (c) rotational speed of the engine *N*.

Table V-8 compares the mixer performance by calculating *ISE*, *IAE*, *ITAE* and ratio of RSD <6 %. It can be seen that, for the closed-loop control of *RSD*, the PID setting of K_c = –28, T_i = 0.08 min, T_d = 0.008 min with the *N* manipulated in the range of 25–48 Hz is more appropriate to achieve an overall improvement in the mixing, although the effect of control on the mean concentration is not very significant.

2.3 Conclusion

Among the tested PI/PID controller settings, the setting of K_c = 35, T_i = 0.08 min and T_d = 0.008 min for closed-loop control of X_A gives a better performance when the rotational speed of the engine N is limited in the range of 25–55 Hz, and the setting of $RSD_{setpoint}$ =3%, K_c = 25, T_i = 0.08 min and T_d = 0.008 min for closed-loop control of RSD gives a better performance when the rotational speed of the engine N is limited in the range of 25–48Hz. In comparison to the open-loop operation, both control settings show an improvement of mixing performance in terms of X_A as well as RSD. The rotational speeds generated from both control settings also show that when there is a step change in X_A from 50% to 63.11% due to the step changes in Q_A and Q_B, the overall process can be adequately controlled by the rotational speeds rapidly increased at the beginning and then varied between certain bounds.

3 Case study 2

In case 2, the desired mean composition X_A is changed from 50% to 36.89% due to a step change in Q_A from 4.5 to 3.32 g.s^{-1} and a step change in Q_B from 4.5 to 5.68 g.s^{-1}. The total feed rate Q_A + Q_B keeps at 9 g.s^{-1}. Figure V-8 shows an example of experimentally obtained flow rates at the mixer's inlet in response to the step changes in both Q_A and Q_B.

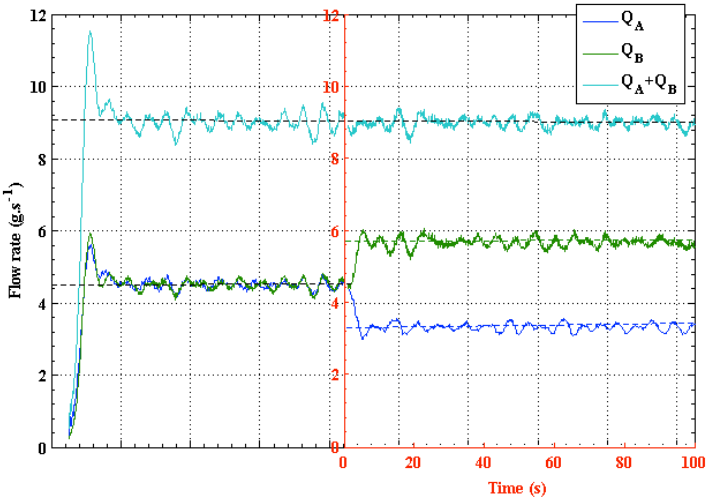

Figure V-8: Flow rate responses to a negative step change in Q_A and a positive step change in Q_B without changing the total feed rate.

3.1 Closed-loop control of mean concentration X_A

Two experiments are firstly performed for two different settings of PI/PID controller parameters as follows:

Setting 1: $K_c = 35$, $T_i = 0.08$ min, $T_d = 0$ min.
Setting 2: $K_c = 35$, $T_i = 0.08$ min, $T_d = 0.008$ min.

The two controller settings are selected because they have been previously studied in case 1 and some improvements have been obtained.

In case 2, the open-loop responses are also illustrated and compared to closed-loop responses, as shown in Figure V-9. Figure V-9 (a) shows the responses of mean concentration X_A at the mixer's outlet. As shown in the figure, similar results are obtained from the three experiments. Long lag time is present before X_A starts to decrease. Figure V-9 (b) shows the evolutions of *RSD*. The regulation of the rotational speed N through the PI/PID controllers is shown in Figure V-9 (c). The rotational speed of the engine N is mainly regulated below 30 Hz under the controller setting 1 and it is varied between 25 and 38 Hz under the controller setting 2.
The performance assessment results are summarized in Table V-9. In terms of *ISE*, *IAE* and *ITAE* criterions, the continuous mixing is slightly better for the controller setting 2 and the derivative action provides slightly lower values of *ISE*, *IAE* and *ITAE*. In terms of *RSD* criterion, the continuous mixing operated in the closed-loop is worse than that in the open-loop, because a lower ratio of *RSD* < 6% is obtained from both controller settings. The results show that the overall process performance is negatively influenced by the two controller settings.

Table V-9: Performance assessment results from experiments of closed-loop control of X_A with controller settings 1 and 2 in case 2.

	ISE	*IAE*	*ITAE*	*Ratio of RSD < 6%*
Open-loop	0.460	4.981	131.940	33 / 101
Setting 1	0.551	5.532	158.599	18 / 101
Setting 2	0.448	4.569	116.966	16 / 101

(a)

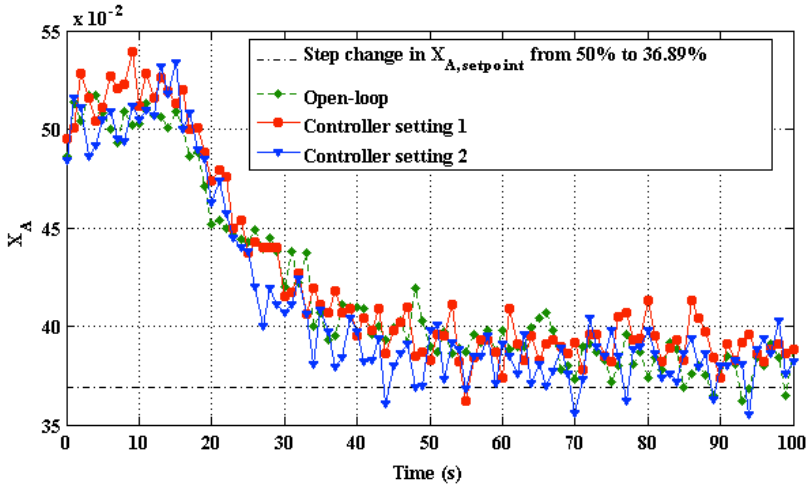

(b)

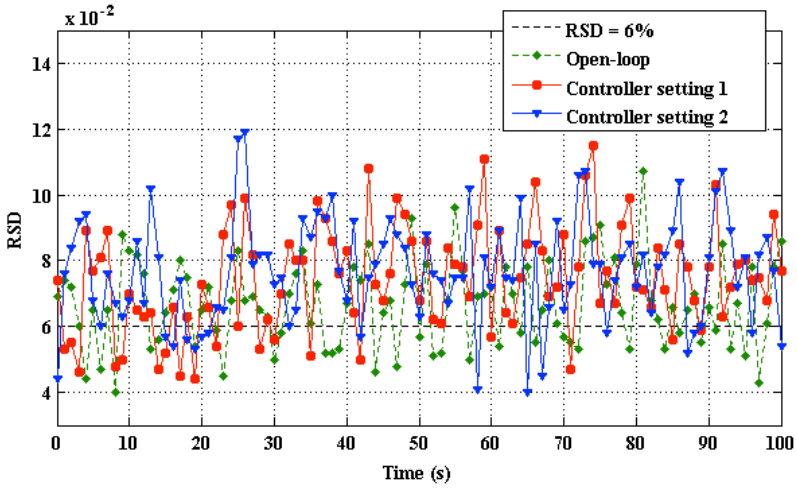

(c)

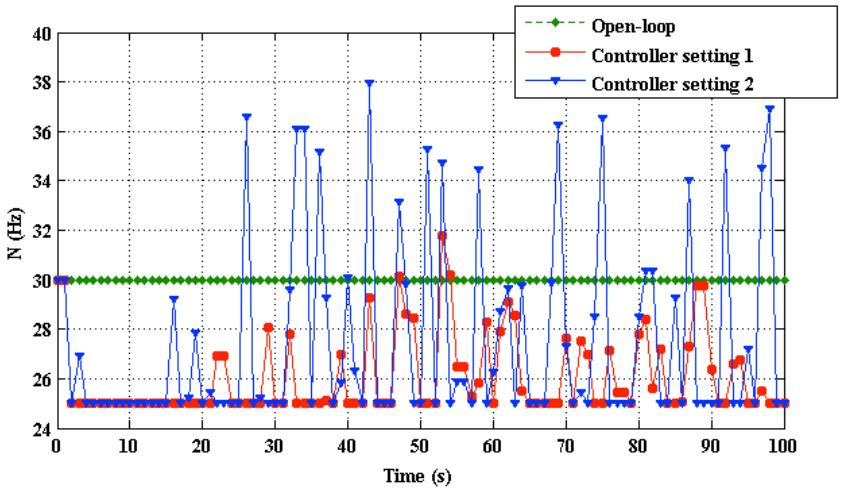

Figure V-9: Experimental results from closed-loop of X_A with controller settings 1 and 2 in case 2: (a) mean concentration X_A, (b) relative standard deviation *RSD*, (c) rotational speed of the engine *N*.

The following retuned PID controller parameters are applied:

Retuned setting 1: $K_c = 40$, $T_i = 0.1$ min, $T_d = 0.009$ min.

Retuned setting 2: $K_c = -35$, $T_i = 0.08$ min, $T_d = 0.008$ min

(a)

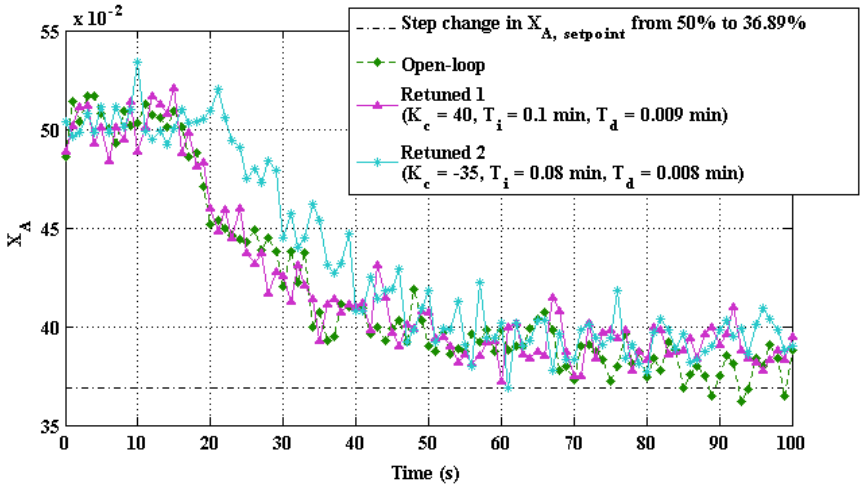

(b)

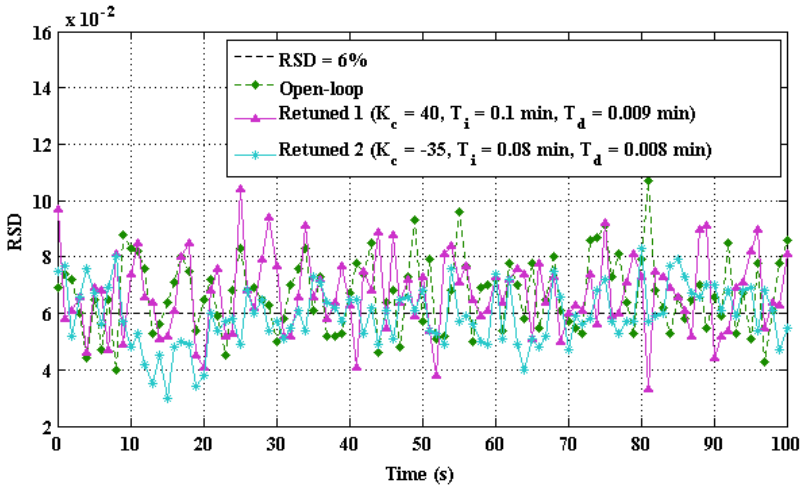

(c)

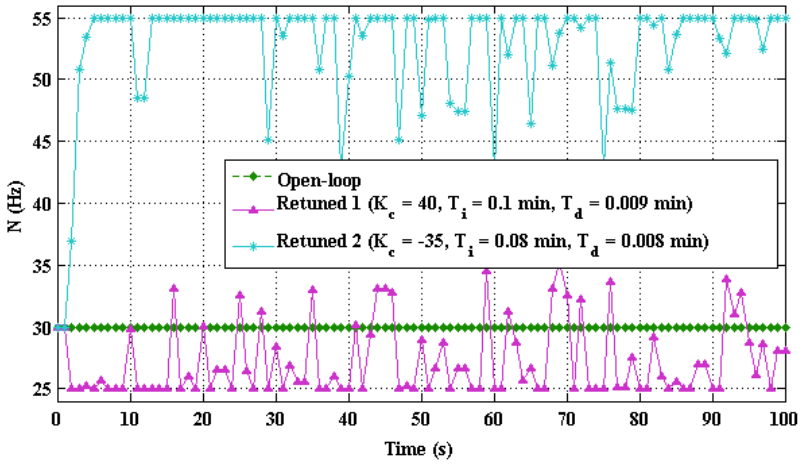

Figure V-10: Experimental results from closed-loop of X_A with controller retuned 1 and 2 in case 2: (a) mean concentration X_A, (b) relative standard deviation *RSD*, (c) rotational speed of the engine *N*.

As shown in Figure V-10, for the retuned 2, due to the generated higher rotational speeds, the response of the mean composition at the mixer's outlet is delayed more severely whereas the mixing homogeneity is improved, which can be seen from the ratios of RSD < 6% listed in Table V-10. In conclusion, it is found that the feedback control purpose is not yet reached by using the retuned controller settings in the closed-loop control of X_A.

Table V-10: Performance assessment results from experiments of closed-loop control of X_A with controller retuned 1 and 2 in case 2.

	ISE	*IAE*	*ITAE*	*Ratio of RSD < 6%*
Open-loop	0.460	4,981	131,940	33 / 101
Retuned 1	0,460	5,207	154,959	29 / 101
Retuned 2	0,625	6,339	196,771	55 / 101

3.2 Closed-loop control of *RSD*

This section attempts to find a good parameter setting for the closed-loop control of *RSD*. The following three sets of control parameters are studied:

Setting 1: $RSD_{setpoint}$ = 3%, K_c = 28, T_i = 0.05 min, T_d = 0.008 min.
Setting 2: $RSD_{setpoint}$ = 3%, K_c = -28, T_i = 0.05 min, T_d = 0.008 min.
Setting 3: $RSD_{setpoint}$ = 3%, K_c = 15, T_i = 0.05 min, T_d = 0 min.

Where the setting 2 has previously presented a good closed-loop performance of *RSD* in case 1. As shown in Figure V-11 (a), the X_A profile obtained from setting 2 has a relatively slower decreasing before attaining the new steady state, compared to those obtained from the other experiments. This can be attributed to the difference in manipulation of the actuator. As shown in in Figure V-11 (c), in term of the rotational speed, the *N* approximately 25 Hz and little variations are found for setting 1 and 3, whereas the *N* approximately 55 Hz for setting 2.

(a)

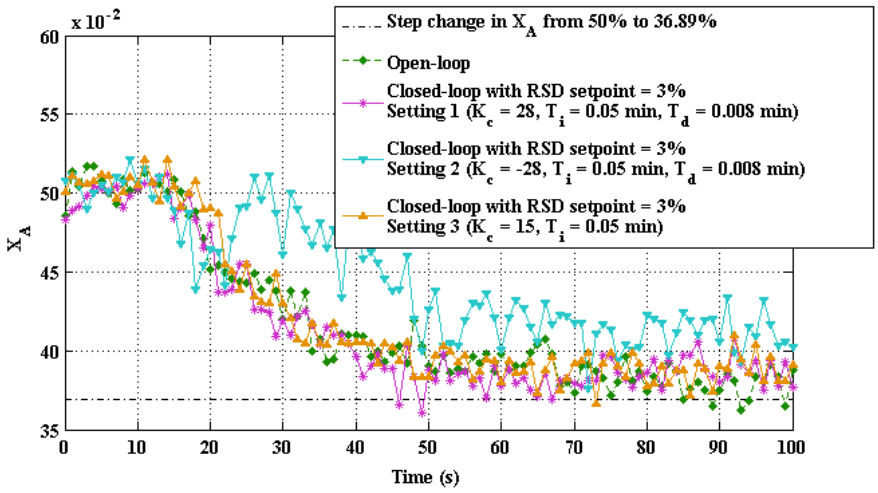

(b)

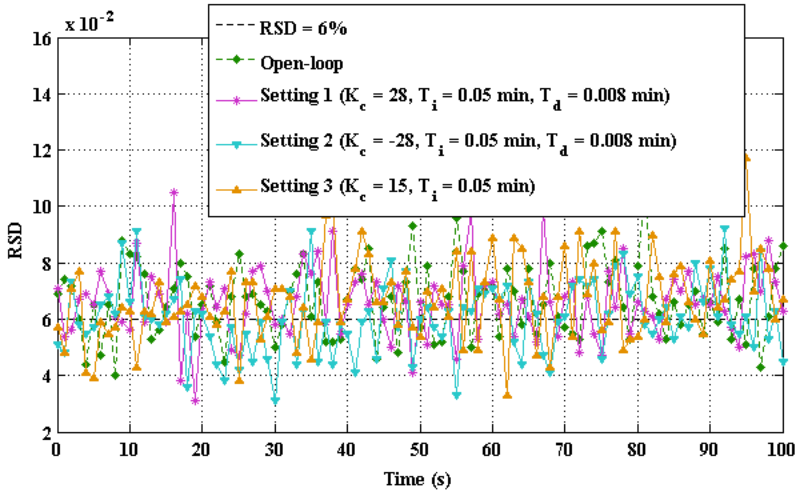

(c)

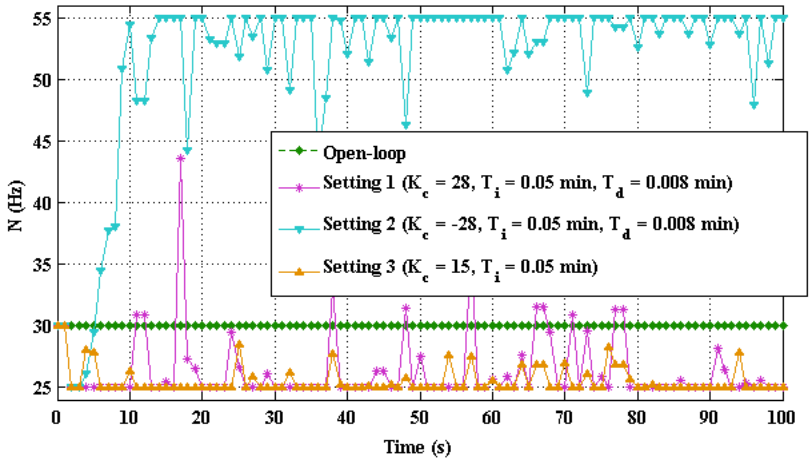

Figure V-11: Experimental results from closed-loop of *RSD* with the *RSD* setpoint of 3% in case 2: (a) mean concentration X_A, (b) relative standard deviation *RSD*, (c) rotational speed of the engine *N*.

The calculation results of the mixing performance indices are given in Table V-11 for each experiment. In comparison to the open-loop, setting 1 has smaller values of the *ISE*, *IAE* and *ITAE* and setting 2 has a larger value of the ratio of *RSD* < 6%.

Table V-11: Performance assessment results from experiments of closed-loop control of *RSD* with the *RSD* setpoint of 3% in case 2.

	ISE	*IAE*	*ITAE*	*Ratio of RSD < 6%*
Open-loop	0.460	4.981	131.940	33 / 101
Setting 1	0.414	4.655	128.240	29 / 101
Setting 2	0.745	7.730	290.590	47 / 101
Setting 3	0.491	5.229	147.777	32 / 101

None of the three settings used in the closed-loop control of *RSD* is able to decrease the *ISE*, *IAE* and *ITAE* as well as to increase the ratio of *RSD* < 6%. Since the *RSD* curves in Figure V-11 (b) show that experimental *RSD* values are still far away from the *RSD* setpoint defined as 3%, a new *RSD* setpoint at 5% is proposed for retuning. The control parameters are retuned as follows:

Retuned 1: $RSD_{setpoint}$ = 5%, K_c = 28, T_i = 0.05 min, T_d = 0.008 min.
Retuned 2: $RSD_{setpoint}$ = 5%, K_c = 8, T_i = 0.05 min, T_d = 0.008 min.

The retuned results are also compared with the open-loop. As shown in Figure V-12 (a), the transient time for achieving the new $X_{A,setpoint}$ is slightly shorter under retuned 1. As shown in Figure V-12 (c), retuned 1 provides greater and more frequent variations in the rotational speed of the engine compared to retuned 2. From Table V-12, smaller values of the *ISE*, *IAE* and *ITAE* obtained from retuned 1 indicate an improvement for the X_A setpoint tracking, while smaller values of the ratio of *RSD* < 6% obtained from returned 1 and 2 indicate poorer mixing homogeneity at the mixer's outlet.

Table V-12: Performance assessment results from experiments of closed-loop control of *RSD* with the *RSD* setpoint of 5% in case 2.

	ISE	*IAE*	*ITAE*	*Ratio of RSD < 6%*
Open-loop	0.460	4.981	131.940	33 / 101
Retuned 1	0.358	3.904	89.180	22 / 101
Retuned 2	0.590	5.955	178.463	29 / 101

(a)

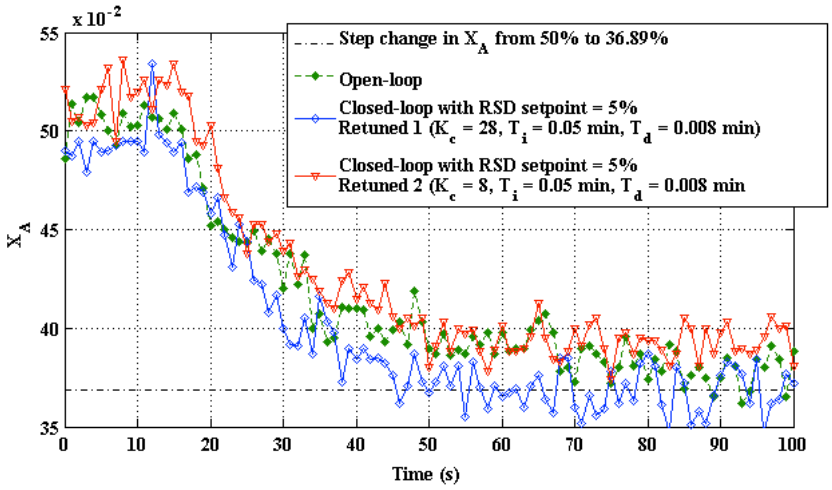

(b)

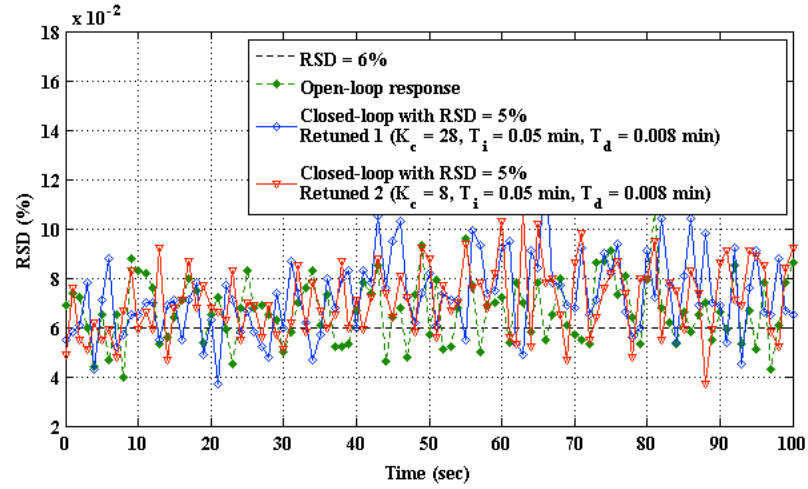

(c)

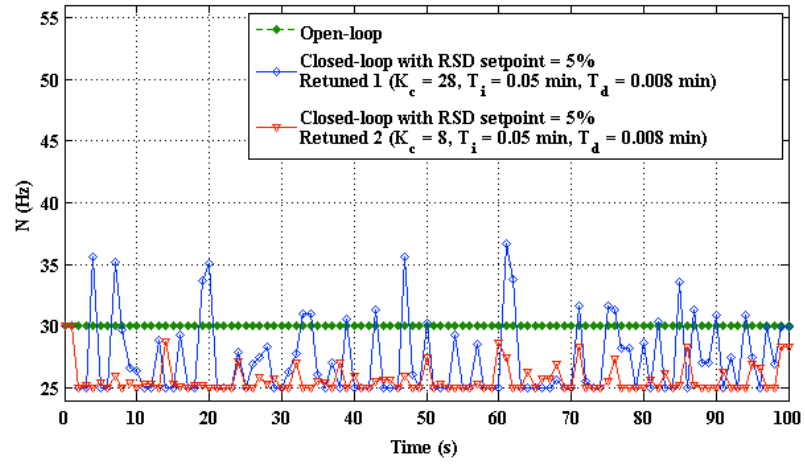

Figure V-12: Experimental results from closed-loop of *RSD* with the *RSD* setpoint of 5% in case 2: (a) mean concentration X_A, (b) relative standard deviation *RSD*, (c) rotational speed of the engine *N*.

3.3 Conclusion

None of the settings used for closed-loop control of X_A or *RSD* allow controlling the mixing performance in terms of X_A and *RSD* at the same time. The outputs of the manipulated variable N from all settings show that when the setpoint of X_A is changed from 50% to 32.89% due to the step changes in Q_A and Q_B, the rotational speeds consistently adjusted above 30 Hz lead to negative effects on X_A while the rotational speeds consistently adjusted below 30 Hz lead to negative effects on *RSD*.

4 Case study 3

In case 3, the Q_A and Q_B are simultaneously changed from 4.5 to 5.68 $g.s^{-1}$. From the experimental measurements of Q_A and Q_B at the mixer's inlet, as shown in Figure V-13, it can be seen that the step changes in Q_A and Q_B are well tracked by the loss-in-weight feeders. In this case, the process control aims to maintain the mixing composition as well as to improve the mixing homogeneity.

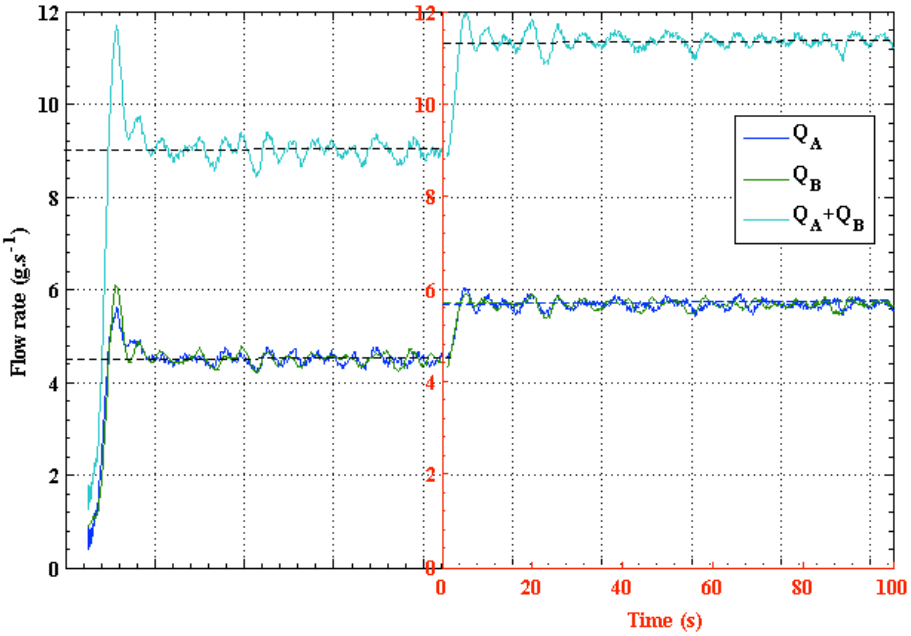

Figure V-13: Flow rate responses to a positive step change in both Q_A and Q_B without changing the mixture composition.

4.1 Closed-loop control of mean concentration X_A

The PID setting of K_c = 35, T_i = 0.08 min, T_d = 0.008 min is examined under the closed-loop control of X_A. The rotational speed of the engine N is limited in the range of 25−55 Hz.

(a)

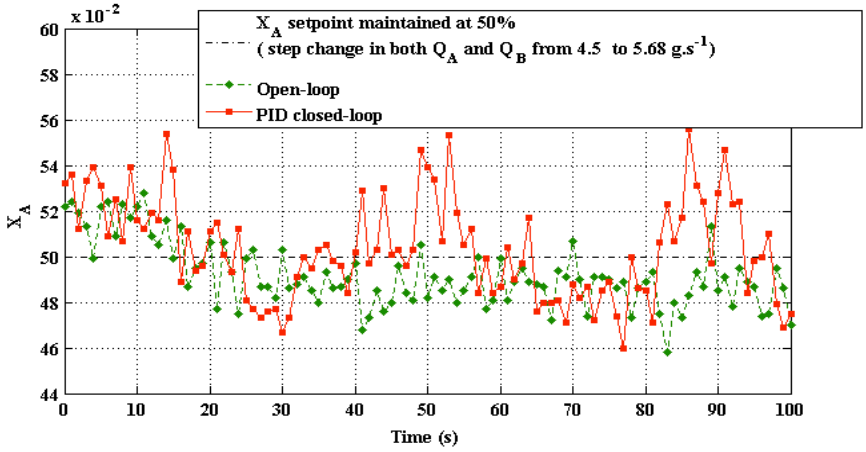

(b)

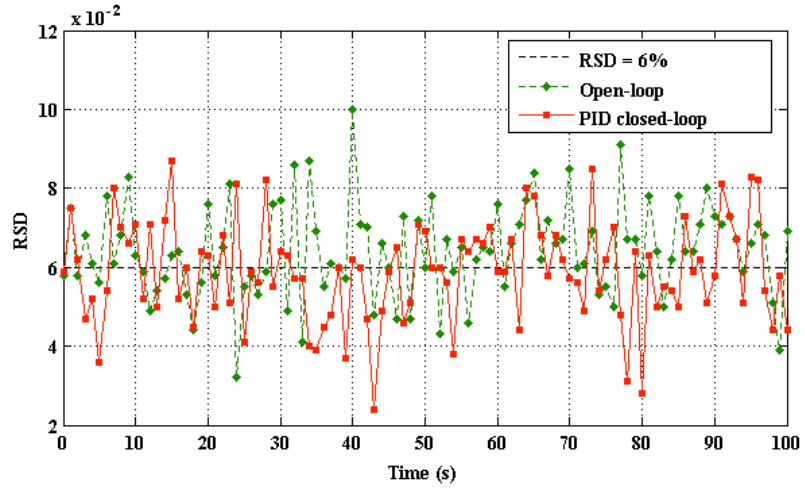

(c)

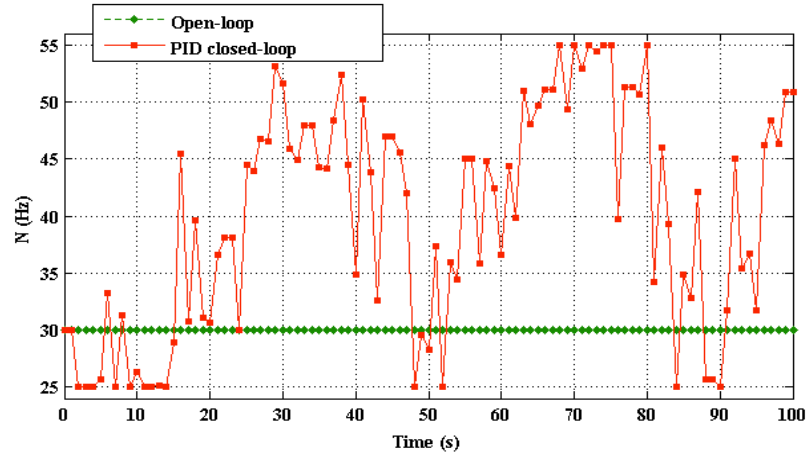

Figure V-14: Experimental results from closed-loop of X_A in case 3: (a) mean concentration X_A, (b) relative standard deviation RSD, (c) rotational speed of the engine N.

As shown in Figure V-14 (a), the mixing performance in term of X_A, under the tested control setting, becomes unstable with considerable variations around the X_A setpoint at 50%. From Figure V-14 (b), smaller values of *RSD* can be obtained from the closed-loop control of X_A. As shown in Figure V-14 (c), the tested control setting provides large adjustments of the rotational speed within the constraints given.

The mixing performance under the closed-loop control is evaluated and compared to the open-loop, as shown in Table V-13. For the tested control setting, larger values of the *ISE*, *IAE* and *ITAE* indicate a worse control of X_A, while a higher ratio of RSD < 6% indicates an improvement in *RSD*.

Table V-13: Performance assessment results from experiments of closed-loop control of X_A in case 3.

	ISE	*IAE*	*ITAE*	*Ratio of RSD < 6%*
Open-loop	0.026	1.407	72.258	35 / 101
PID closed-loop	0.05	1.789	89.37	53 / 101

4.2 Closed-loop control of *RSD*

The following control settings are experimentally examined under closed-loop control of *RSD*.

Setting 1: $RSD_{setpoint}$ = 5%, K_c = 28, T_i = 0.05 min, T_d = 0.008 min, $N \in [25, 55]$
Setting 2: $RSD_{setpoint}$ = 4%, K_c = 38, T_i = 0.05 min, T_d = 0.008 min, $N \in [25, 55]$
Setting 3: $RSD_{setpoint}$ = 3%, K_c = -28, T_i = 0.05 min, T_d = 0.008 min, $N \in [25, 48]$

The *RSD* setpoints for the three settings are 5%, 4% and 3%, respectively. The rotational speeds of the engine for setting 1 and 2 have the same constraints: $N \in [25, 55]$, while the upper *N* constraint for setting 3 is set at 48 Hz.

The outputs of the process X_A and *RSD* and the rotational speed *N* are plotted versus time in Figure V-15 (a), (b) and (c), respectively. The rotational speed of the engine is differently

manipulated under different control parameters. As shown in Figure V-15 (c), setting 1 and 2 generate the rotational speeds varying between 25 and 40 Hz, while setting 3 generates the rotational speeds rapidly increased and finally varying between 40 and 48 Hz.

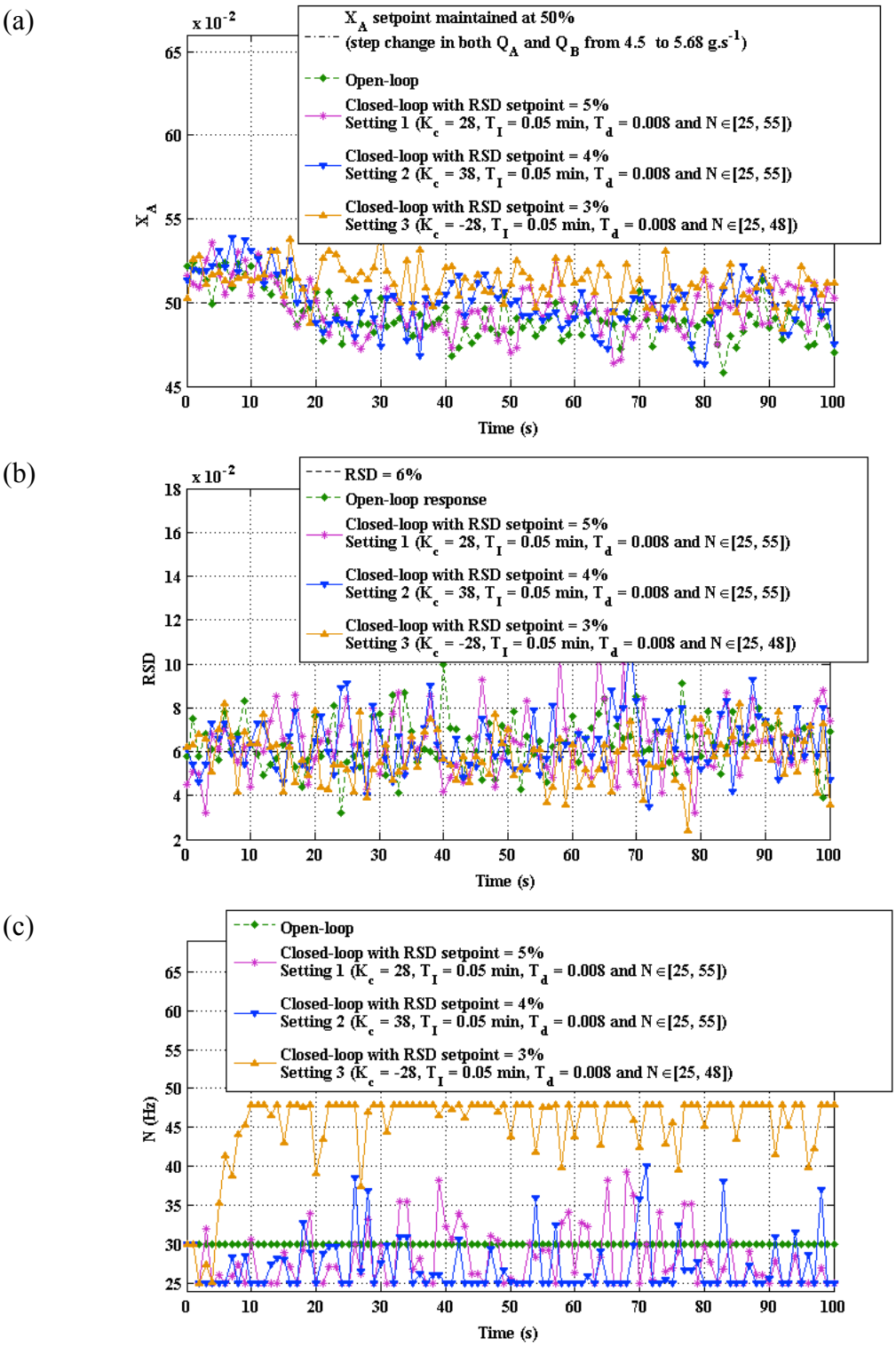

Figure V-15: Experimental results from closed-loop of *RSD* in case 3: (a) mean concentration X_A, (b) relative standard deviation *RSD*, (c) rotational speed of the engine *N*.

The mixing performance under each control setting is evaluated and compared to that of open-loop operation, as shown in Table V-14. In comparison to the open-loop, each control setting brings smaller values of the *ISE*, *IAE* and *ITAE* and a higher ratio of *RSD* < 6%. The overall process performance is slightly improved by any one of the three control settings. The control of X_A is more significant by setting 1 and 2 and the control of *RSD* is more efficient by setting 3.

Table V-14: Performance assessment results from experiments of closed-loop control of *RSD* in case 3.

	ISE	*IAE*	*ITAE*	*Rate of RSD < 6%*
Open-loop	0.026	1.407	72.258	35 / 101
Setting 1	0.023	1.237	56.707	40 / 101
Setting 2	0.025	1.245	54.451	43 / 101
Setting 3	0.028	1.385	60.17	55 / 101

4.3 Conclusion

When there is a same positive step change in Q_A and Q_B, the continuous mixing process is slightly controlled by the last three settings under closed-loop control of *RSD*. And the corresponding outputs of the actuators show that the mixing homogeneity *RSD* can be better improved by the rotational speeds consistently adjusted above 30 Hz while the mean concentration setpoint can be potentially tracked by the rotational speeds consistently adjusted below 30 Hz.

5 Case study 4

In case 4, the flow rates Q_A and Q_B are simultaneously decreased from 4.5 to 3.32 $g.s^{-1}$. Figure V-16 shows experimental results of Q_A and Q_B at the mixer's inlet after the step changes.

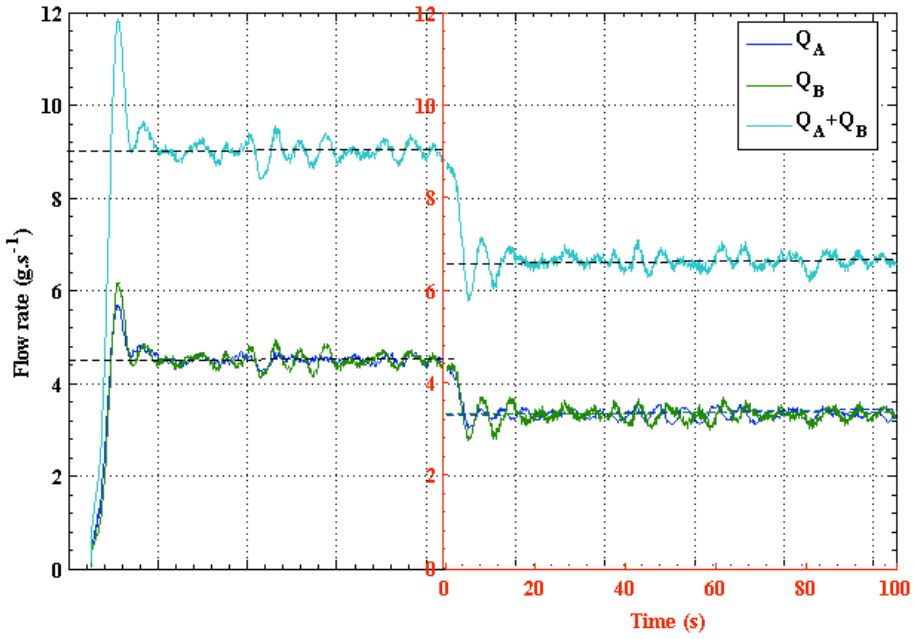

Figure V-16: Flow rate responses to a negative step change in both Q_A and Q_B without changing the mixture composition.

5.1 Closed-loop control of mean concentration X_A

The implementation of closed-loop control of X_A is discussed for the control settings as follows:

Setting 1: $K_c = 35$, $T_i = 0.08$ min, $T_d = 0.008$ min, $N \in [25, 55]$.

Setting 2: $K_c = 35$, $T_i = 0.08$ min, $T_d = 0.008$ min, $N \in [20, 50]$.

The same controller parameters but different actuator constraints are imposed on the two settings.

As shown Figure V-17 (a), for both open-loop and setting 1, the X_A values obtained at the mixer's outlet are mostly above the desired value of 50%, while for setting 2, the X_A curve versus time shows strong oscillations around 50%. For each experiment, the *RSD* versus time profile taken at the mixer's outlet is depicted in Figure V-17 (b). Different profiles of rotational speed N are generated using different control parameters, as shown Figure V-17 (c).

(a)

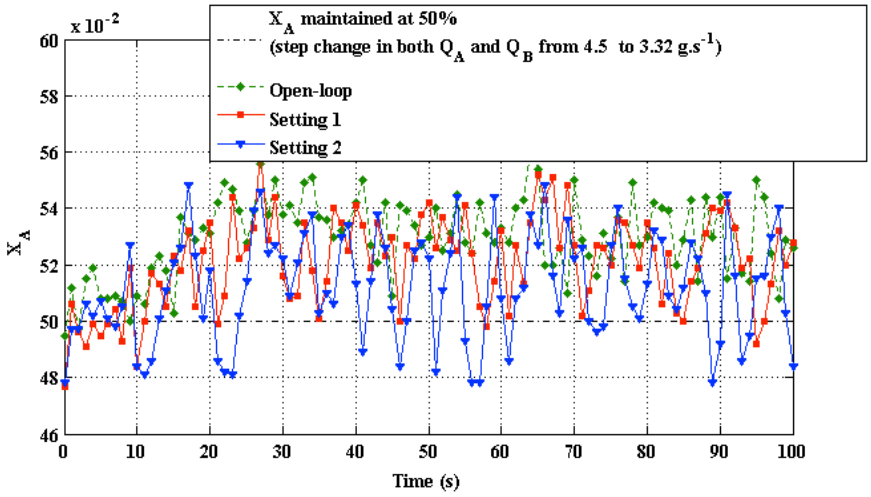

(b)

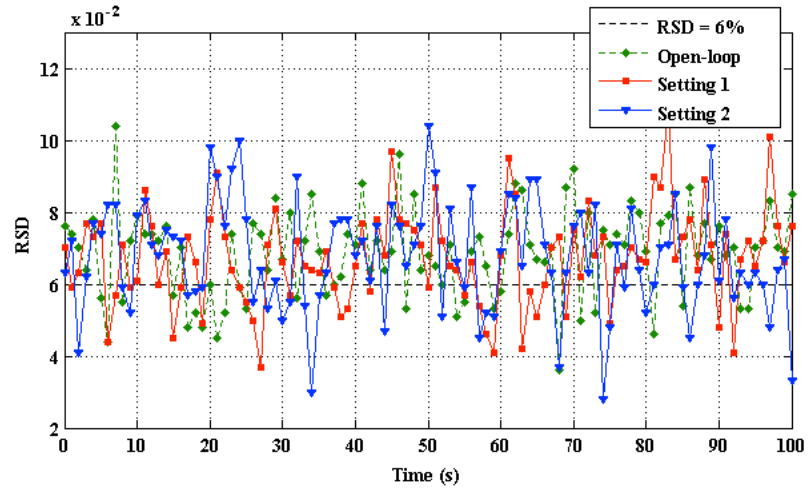

(c)

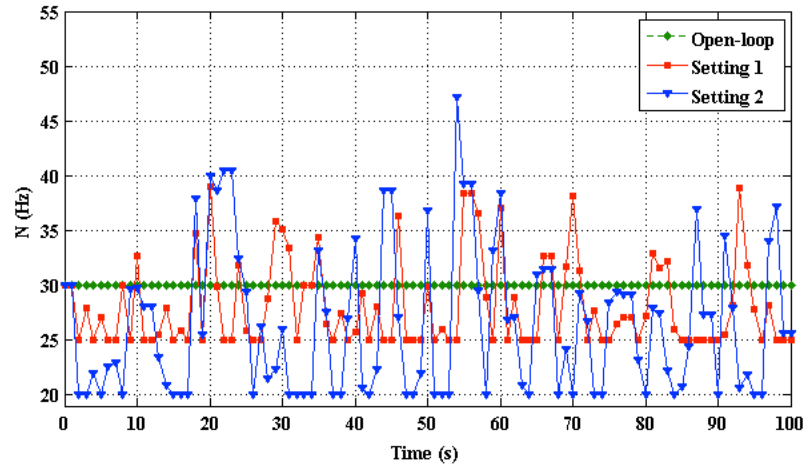

Figure V-17: Experimental results from closed-loop of X_A in case 4: (a) mean concentration X_A, (b) relative standard deviation *RSD*, (c) rotational speed of the engine *N*.

As shown in Table V-15, compared to the open loop operation, setting 1 and 2 provide smaller values of the *ISE*, *IAE*, and *ITAE*, whereas little different values of the ratio of RSD < 6%. These results indicate that setting 1 and 2 for closed-loop control of X_A present notable improvements in the mean composition rather than the *RSD*.

Table V-15: Performance assessment results from experiments of closed-loop control of X_A in case 4.

	ISE	*IAE*	*ITAE*	*Rate of RSD < 6%*
Open-loop	0.109	3.004	158.345	25 / 101
Setting 1	0.07	2.239	120.68	28 / 101
Setting 2	0.049	1.8	93.988	29 / 101

5.2 Closed-loop control of *RSD*

The closed-loop control of *RSD* is discussed for the two settings as follows:

Setting 1: $RSD_{setpoint}$ = 4%, K_c = 28, T_i = 0.05 min, T_d = 0.008 min, $N \in [25, 55]$
Setting 2: $RSD_{setpoint}$ = 3%, K_c = 28, T_i = 0.05 min, T_d = 0.008 min, $N \in [22, 55]$

For the two settings, the PID controller parameters are the same and the *RSD* setpoints are 4% and 3%, respectively. In addition, in the setting 1 the actuator (N) is limited in the range of 25−55 Hz whereas in the setting 2 it is limited in the range of 22−55 Hz.

As shown in Figure V-18 (a), for each experiment, the mean compositions at the final steady state exceed the X_A setpoint of 50%. In particular, the maximum X_A measured from setting 1 is up to about 57%. As shown in Figure V-18 (b), for each experiment, the *RSD* measured at the mixer's outlet is varied between 3% and 12%. From Figure V-18 (c), for setting 1, the rotational speed N is manipulated between 25 and 36 Hz, whereas for setting 2, it is manipulated between 22 and 30 Hz, mainly due to its lower minimum limit.

(a)

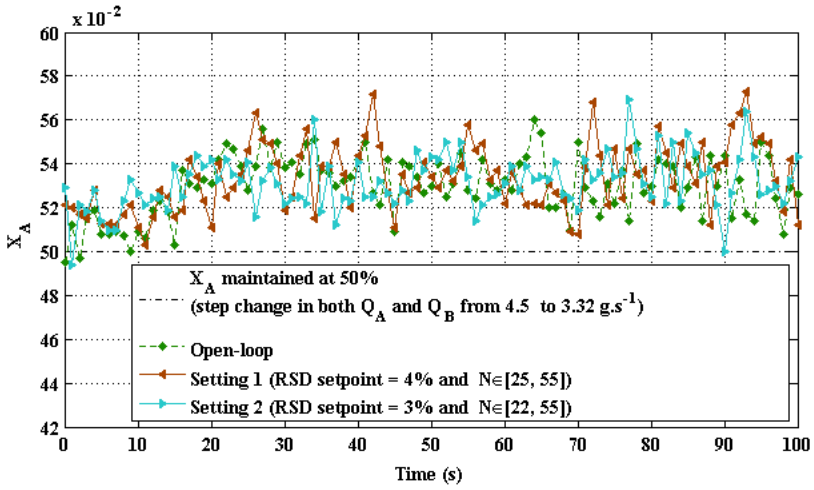

(b)

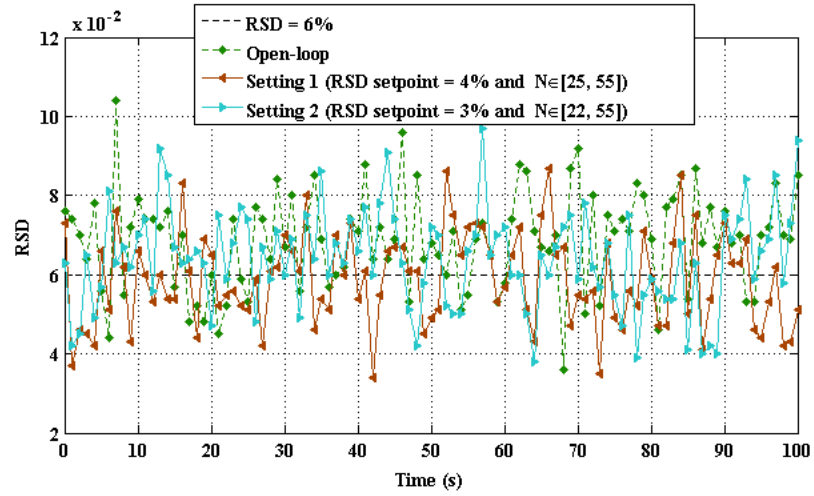

(c)

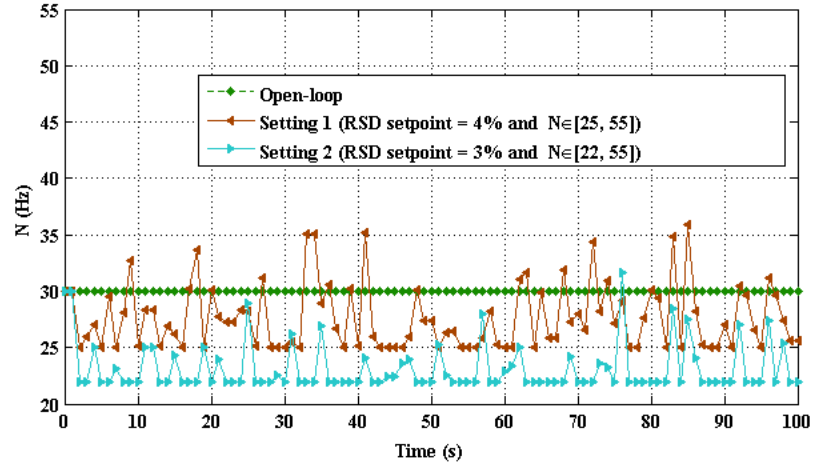

Figure V-18: Experimental results from closed-loop of *RSD* in case 4: (a) mean concentration X_A, (b) relative standard deviation *RSD*, (c) rotational speed of the engine *N*.

As given in Table V-16, the mixing performance for each experiment is quantified and compared to open-loop operation. Values of the *ISE*, *IAE* and *ITAE* of both settings are

greater than those of the open-loop, which indicate that the applied control settings cannot reduce the effect of the flowrate disturbances on the mean concentration. However, both settings under closed-loop control of *RSD* show improvements in the mixing homogeneity, indicated by higher ratios of *RSD* < 6% compared to the open-loop.

Table V-16: Performance assessment results from experiments of closed-loop control of *RSD* in case 4.

	ISE	*IAE*	*ITAE*	*Ratio of RSD < 6%*
Open-loop	0.109	3.004	158.345	25 / 101
Setting 1	0.136	3.362	184.204	51 / 101
Setting 2	0.114	3.157	168.267	34 / 101

5.2.1 Conclusion

When there is a same negative step change for Q_A and Q_B, a PID setting used for closed-loop control of X_A shows positive effects on X_A but little effects on *RSD*, while a PID setting used for closed-loop control of *RSD* shows positive effects on *RSD* but little effects on X_A. The outputs of the manipulated variable *N* show that the mean concentration setpoint can be better tracked by the rotational speeds adjusted in large amplitudes (around 30 Hz) while the mixing homogeneity *RSD* can be better improved by the rotational speeds adjusted between 25 and 35 Hz.

6 Study of the influence of the starting rotational speed *N*

As presented above, the rotational speed of the engine *N* is initially fixed at 30 Hz before introducing the load disturbances. An alternative initial rotational speed of 40 Hz will now be used to exercise a possible influence of this value. The subjected step changes in the flow rates Q_A and Q_B are the same as those in case 1, which in turn leads to a step change in X_A from 50% to 63.11%.

Like in case 1, good control results are obtained from the control settings as follows:

Setting for closed-loop of X_A:

$$K_c = 35,\ T_i = 0.08 \text{ min and } T_d = 0.008 \text{ min},\ N \in [25, 55].$$

Setting for closed-loop of *RSD*:

$$RSD_{setpoint} = 3\%,\ K_c = 25,\ T_i = 0.08 \text{ min and } T_d = 0.008 \text{ min},\ N \in [25, 48].$$

So the two control settings are respectively examined under $N_{initial}$ = 40 Hz. The experimental results are also compared to those obtained from the case 1 with $N_{initial}$ = 30 Hz.

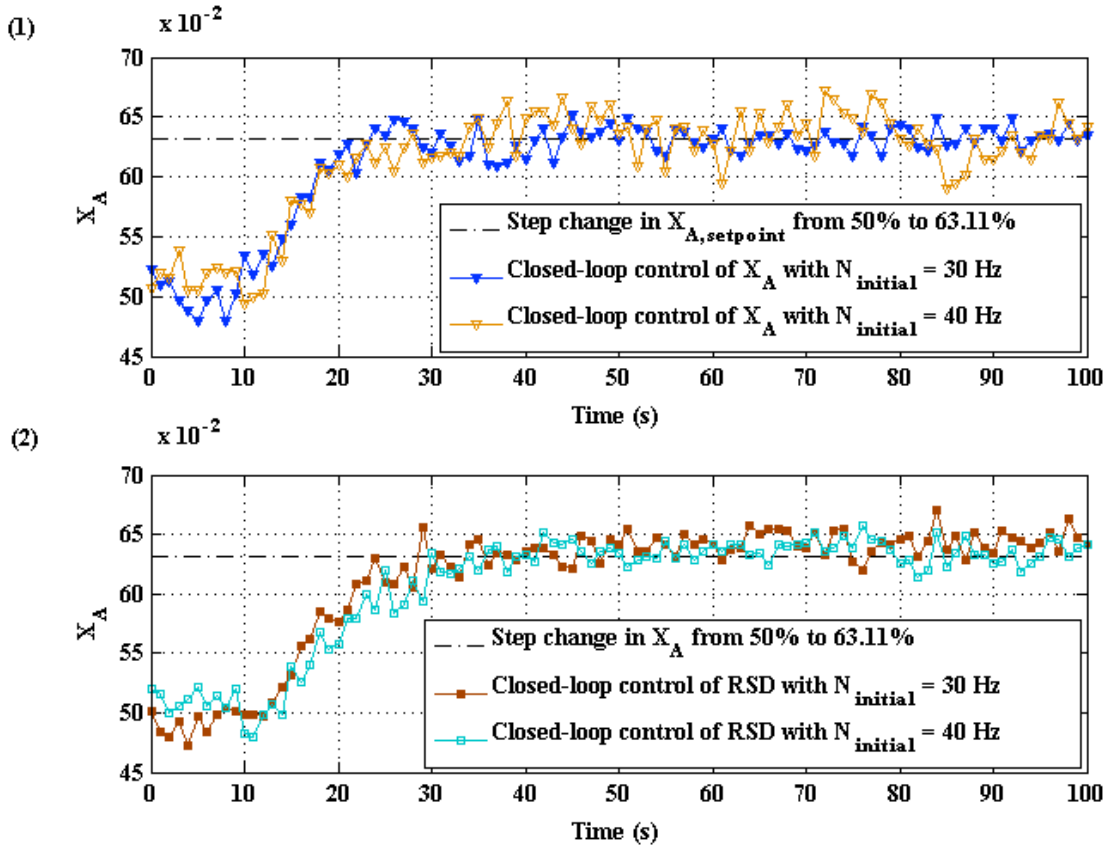

Figure V-19: Plots of X_A: (1) closed-loop control of X_A starting with N=30 Hz and N=40 Hz, respectively; (2) closed-loop control of *RSD* starting with N=30 Hz and N=40 Hz, respectively.

As shown in Figure V-19, similar X_A profiles are obtained from closed-loop of X_A as well as RSD. As shown in Figure V-20 (1), for closed-loop control of X_A, the *RSD* profile of $N_{initial}$ = 30 Hz is better than that of $N_{initial}$ = 40 Hz, contrary to the RSD profiles obtained from closed-loop control of *RSD*, as shown in Figure V-20 (2).

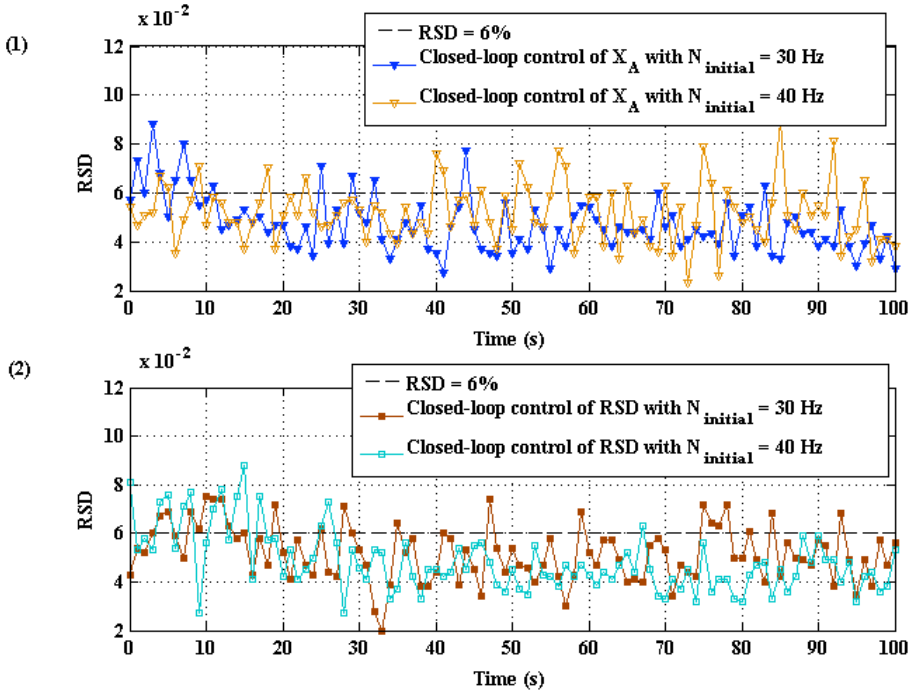

Figure V-20: Plots of *RSD*: (1) closed-loop control of X_A starting with N=30 Hz and N=40 Hz, respectively; (2) closed-loop control of *RSD* starting with N=30 Hz and N=40 Hz, respectively.

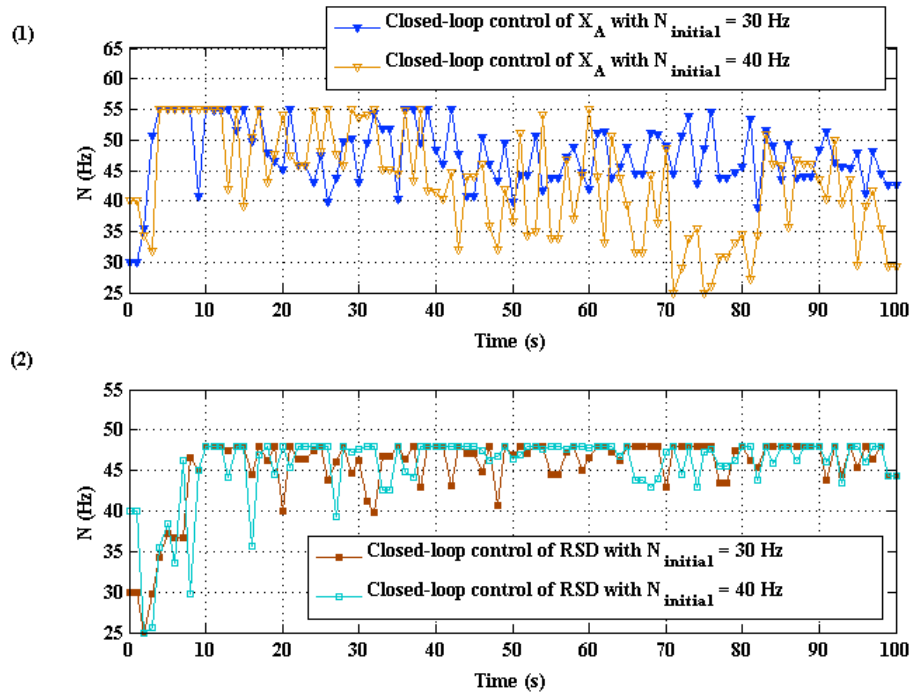

Figure V-21: Plots of the rotational speed N: (1) closed-loop control of X_A starting with N=30 Hz and N=40 Hz, respectively; (2) closed-loop control of *RSD* starting with N=30 Hz and N=40 Hz, respectively.

The overall adjustments of the rotational speed of the engine N in closed-loop control of X_A are very strong than those in closed-loop of *RSD*, as depicted in Figure V-21.

Table V-17: Comparison of process performances obtained from closed-loop control of X_A starting with N=30 Hz and N=40 Hz.

	ISE	*IAE*	*ITAE*	*Rate of RSD < 6%*
Closed-loop of X_A (N_{initial} = 30 Hz)	0.239	2.687	54.815	87 / 101
Closed-loop of X_A (N_{initial} = 40 Hz)	0.231	3.145	90.838	79 / 101

From Table V-17, in closed-loop control of X_A, the mixing performance obtained under $N_{initial}$ = 40 Hz is little less than that obtained under $N_{initial}$ = 30 Hz, since larger values of the *ISE*, *IAE* and *ITAE* and a lower ratio of RSD < 6% are observed under $N_{initial}$ = 40 Hz. It is possible due to the notable decreases in the rotational speed during the time t=70 and 80 second.

Table V-18: Comparison of process performances obtained from closed-loop control of *RSD* starting with N=30 Hz and N=40 Hz.

	ISE	*IAE*	*ITAE*	*Rate of RSD < 6%*
Closed-loop of *RSD* (N_{initial} = 30 Hz)	0.316	3.395	82.914	76 / 101
Closed-loop of *RSD* (N_{initial} = 40 Hz)	0.297	3.249	69.039	88 / 101

From Table V-18, in closed-loop control of *RSD*, the $N_{initial}$ = 40 Hz shows a better mixing performance than the $N_{initial}$ = 30 Hz, since smaller values of the *ISE*, *IAE* and *ITAE* and a higher ratio of RSD < 6% are observed under $N_{initial}$ = 40 Hz.

In summary, the influence of the starting rotational speed on the mixing performance depends on the implemented control scheme and the effect will not be very significant if the control parameters are well tuned under the corresponding control loop.

7 Conclusion

In this chapter, the proposed control loop has been studied in four different cases, which correspond to different step changes in flow rates of the two components at the mixer's inlet. From an industrial point of view, case 1 and 2 correspond to a change in the mixture composition without changing the total production volume, while case 3 and 4 correspond to an increase/decrease in production volume. Continuous mixing has been controlled in terms of either mean concentration X_A or relative standard deviation *RSD*. The performance of the closed-loop control of either X_A or *RSD* has been evaluated using both X_A and *RSD* performance criteria, such as *ISE*, *IAE*, *ITAE* and ratio of $RSD < 6\%$. In each case, control efficiency has been determined by comparing the performance of closed-loop control of either X_A and *RSD* with that of open-loop operation, for which the rotational speed was kept constant at the initial value 30 Hz. In case 1, a PID controller for closed-loop control of either X_A or *RSD* has been found to be well tuned to improve the mixer's performance in terms of both mean concentration and mixing homogeneity. The outputs of the manipulated variable show that a rapid increase in the rotational speed at the beginning of control contributes to achieve a new steady state rapidly when there is an increase in mass fraction of component A in the mixture. In other case, different control settings (PID controller parameters, the *RSD* setpoint, and the constraints of the manipulated variable *N*) have also been experimentally tested and discussed. The results show that since either X_A or *RSD* has been considered the controlled variable in closed-loop control, most of the tested PID settings allow improving mixing performance in terms of either the X_A or the *RSD* and the improvement of one output variable (X_A or *RSD*) often accompanies with a negative impact on another output variable. Hence, the coupling of the two control loops should be considered in further studies.

GENERAL CONCLUSION

This work has been concerned with a new development in understanding of a pilot continuous powder mixing process from a practical control point of view. The implementation of a simplified regulatory control system (PID) in a pilot scale continuous mixer has been presented and considered as an initial step toward the development of an efficient real-time control of continuous powder mixing processes. The mixing of powders of two components with different size distributions has been considered. The pilot process mainly consists of two loss-in-weight feeders, a Gericke GCM 500 continuous mixer and a previously developed on-line monitoring system of mixture quality. The synchronization control of the three individual parts has been realised using Labview.

Without giving much importance to the interactions of the material in the blender, the continuous mixer has been analysed from a “black box” model, for which the flow rates of each component and the rotational speed of the mixer are the input variables, while the mean concentration and the relative standard deviation of the mixture are output variables indicating the mixing efficiency. Due to the complex effects of the inputs, the process control study has been started with new developments in the understanding of continuous powder mixing. The continuous mixer has been virtually divided into 5 compartments. Hold-up weight and relative hold-up distribution in the whole mixer have been experimentally investigated for each component under different operating conditions, including the mixing formulation, the total feed rate and the rotational speed. Empirical correlations for each component have been proposed and determined to describe the hold-up weight and the relative hold-up distribution in the whole mixer as a function of operating conditions. The model involves two Markov chains, for which one chain corresponds to one component. The model has been completed based on the investigations on hold-ups. The comparison of experimental and simulation results demonstrate that the improved process model could be used to predict the profiles of the mean concentration and the mass outflow rate of the mixer, but is mainly non-predictive for the relative standard deviation.

For what concerns control process, the motivation to develop a control system for the presented continuous mixer has been first illustrated by several experimental examples. The results show that an effective control system is highly needed due to the instability problems

and strict regulatory constraints in terms of mixture quality. The control can be performed by adjustment of the important input variables looking at the powder mixtures flowing out from the continuous mixer, due to an on-line image analysis technique available for the measurement of mixture quality. Since the two flow rates as process inputs can be experimentally well controlled by the loss-in-weight mechanism applied in the two feeders and, on the other hand, in the literature the rotational speed of the mixer is commonly considered as a very important process variable, the rotational speed of the mixer has been considered as the manipulated variable in the process control system. This decision has also been justified by several step change experiments. As an initial step towards the experimental control of a pilot continuous mixer, a simple proportional-integral-derivative (PID) control has been proposed and designed to control either the mean concentration or the relative standard deviation. The implementation of a PID controller in a pilot scale continuous mixer has been realised using Labview, by which the feeding system and the measuring system for mixture quality have been incorporated in a single platform to enable data communication with the PID controller for the mixer. Two performance criteria in terms of both mean concentration and relative standard deviation have been proposed to evaluate the performance of closed-loop control of either the mean concentration or the relative standard deviation. For instance, in term of the mean concentration, the integral square error (*ISE*), the integral absolute error (*IAE*), and the integral of time-weighted absolute error (*ITAE*) have been used to evaluate the mixer's performance. In term of the *RSD*, the number of samples of the *RSD* less than 6% has been quantified during the control.

The control performance is strongly influenced by the tuning of PID parameters. In this work, the commonly used tuning based on step response method couldn't be applied due to the special process responses to step changes in the manipulated variable. Thereby, a PID tuning based on the process model has been proposed to avoid extensive experiments. The improved process model has then been re-programmed in Labview in order to use a PID controller, which can be equally used in real control experiments. For closed-loop control of mean composition, PID parameters have been preliminary tunned based on the process model and then tested or retuned in mean composition control experiments. While for closed-loop control of relative standard deviation, PID parameters have been directly tuned by relative standard deviation control experiments, since the presented model has not yet been enough accurate to predict *RSD* profiles.

The closed-loop control of either the mean concentration or the relative standard deviation has finally been studied in four different cases. The four cases include different step changes in flow rates of the two components. In general, they correspond to two possible industrial demands during the process such as a change in mixture composition without changing the production volume and an increase/decrease in production volume. For either closed-loop control in each case, the control efficiency has been evaluated by comparing the closed-loop control with the open-loop operation for which there is no adjustment on the rotational speed of the engine. In case 1, for either the mean concentration control or the relative standard deviation control, a proper PID controller setting has been found to be efficient for controlling the mean concentration as well as the *RSD*. While in other cases, PID controller settings have been found to be efficient for only the controlled variable in the closed-loop control. For instance, in closed-loop control of mean concentration, mean concentration will be controlled but not *RSD*, while in closed-loop control of *RSD*, *RSD* will be controlled but not mean concentration. This indicates that further control study should be carried out to couple the two closed-loop controls.

In conclusion, several remarks can be outlined.

(1) For the proposed control, the PID tuning is a critical step to obtain a good control performance. To date, we have not yet found a systematic approach for the tuning of PID parameters due to special responses to step changes in the manipulated variable. As presented above, in order to avoid extensive experiments, the PID tuning for closed-loop control of the mean concentration has been preliminarily performed with a model-based PID control. The comparison of control simulations of the mean concentration with and without the actual fluctuations in flow rates has shown that the reliability of the presented model can be improved by taking into account the fluctuations. However, the model taking into account the actual flow rate fluctuations still couldn't be used to predict the *RSD*, mainly due to unmeasured disturbances. Therefore, a further improvement on the model is required in order to provide the possibility of the *RSD* prediction.

(2) The control performance for this process has been influenced not only by the PID parameters but also by many other process parameters, such as the lower and upper limits of the manipulated variable, the sampling time, the applied control type (for mean concentration or *RSD*), the load disturbance type, the type of changes in flow rates (step change,

impulsion…), etc. The four cases studied in this work correspond to several different step changes in flow rates. Clearly, more work is needed to study the influences of these process parameters on the control loop.

(3) In particular, for the closed-loop control of the relative standard deviation, the *RSD* setpoint has a direct influence on the process control. As in the pharmaceutical industry, the *RSD* is required to be less than 6%, the sample will be considered as satisfactory if its *RSD* is less than 6%, while from a control point view, the *RSD* will be controlled looking at the error between the *RSD* setpoint and the measured RSD. Therefore, there is still a doubt that if it is reasonable to control RSD by a classical closed-loop control.

REFERENCES

[1] K. Marikh, Mélange des poudres en continu dynamique et modélisation, Université de Toulouse, 2003.

[2] C. Ammarcha, Mélange des poudres en continu : modèles dynamiques et caractérisation en ligne, Université de Toulouse, 2010.

[3] M. Rhodes, Principles of Powder Technology, Wiley, Great Britain, 1993.

[4] M. Rhodes, Introduction to Particle Technology, Second, Wiley, Great Britain, 1998.

[5] R. Weinekötter, H. Gericke, Mixing of solids, Kluwer Academic Publishers, Netherlands, 2000.

[6] N. Harnby, M.F. Edwards, A.W. Nienow, Mixing in the process industries, Second, Butterworth-Heinemann Ltd, Great Britain, 1992.

[7] P. Edward L, A.-O. Victor A, K. Suzanne M, Handbook of Industrial Mixing, Wiley, United States of America, 2004.

[8] P.V. Danckwerts, The definition and measurement of some characteristics of Mixtures, Appl.Sci.Research. 3 (1952) 279–296.

[9] A.E. Sawoniak, K.F. Shalansky, P.J. Zed, R. Sunderji, Formulary Considerations Related to Warfarin Interchangeability, 55 (2002) 215–218.

[10] P.M.C. Lacey, Developments in the theory of particle mixing, Journal of Applied Chemistry. 4 (1954) 257–268.

[11] K.R. Poole, R.F. Taylor, G.P. Wall, Mixing powders to fine-scale homogeneity : studies of batch mixing, Trans. Inst. Chem. Eng. 42 (1964) T305–T315.

[12] H.. Rose, A suggested equation relating to the mixing of powders and its application to the study of the performance of certain types of machines, Trans. Inst. Chem. Eng. 37 (1959) 47–64.

[13] M.D. Ashton, F.H.. Valentin, The mixture of powders and particles in industrial mixers, Trans. Inst. Chem. Eng. 44 (1966) T166–T188.

[14] P.V. Danckwerts, Continuous flow systems, Chemical Engineering Science. 2 (1953) 1–13.

[15] P.V. Danckwerts, Theory of mixtures and mixing., Research. 6 (1953) 355–361.

[16] J. Gyenis, Assessment of mixing mechanism on the basis of concentration pattern, Chemical Engineering and Processing: Process Intensification. 38 (1999) 665–674.

[17] Guidance for Industry Guidance for Industry PAT — A Framework for Innovative Pharmaceutical, (2004).

[18] F.J. Muzzio, P. Robinson, C. Wightman, D. Brone, Sampling practices in powder blending, International Journal of Pharmaceutics. 155 (n.d.) 153–178.

[19] H. Wu, M. Tawakkul, M. White, M. a. Khan, Quality-by-Design (QbD): An integrated multivariate approach for the component quantification in powder blends, International Journal of Pharmaceutics. 372 (2009) 39–48.

[20] www.fda.gov/cder/OPS/PAT.htm, (n.d.).

[21] S. Muerza, H. Berthiaux, S. Massol-Chaudeur, G. Thomas, A dynamic study of static mixing using on-line image analysis, Powder Technology. 128 (2002) 195–204.

[22] A. Realpe, C. Velázquez, Image processing and analysis for determination of concentrations of powder mixtures, Powder Technology. 134 (2003) 193–200.

[23] H. Berthiaux, V. Mosorov, L. Tomczak, C. Gatumel, J.F. Demeyre, Principal component analysis for characterising homogeneity in powder mixing using image processing techniques, Chemical Engineering and Processing: Process Intensification. 45 (2006) 397–403.

[24] L. Obregón, C. Velázquez, Discrimination limit between mean gray values for the prediction of powder concentrations, Powder Technology. 175 (2007) 8–13.

[25] C. André, J.F. Demeyre, C. Gatumel, H. Berthiaux, G. Delaplace, Dimensional analysis of a planetary mixer for homogenizing of free flowing powders: Mixing time and power consumption, Chemical Engineering Journal. 198-199 (2012) 371–378.

[26] J.F. Demeyre, Caractérisation de l'homogénéité de mélange de poudres et de l'agitation en mélangeur Triaxe, Institut National Polytechnique de Toulouse, 2007.

[27] J.G. Rosas, M. Blanco, A criterion for assessing homogeneity distribution in hyperspectral images. Part 1: homogeneity index bases and blending processes., Journal of Pharmaceutical and Biomedical Analysis. 70 (2012) 680–90.

[28] J.R. Ferraro, K. Nakamoto, Introductroy Raman Spectroscopy, Academic Press, 1994.

[29] H.W. Siesler, Y. Ozaki, S. Kawata, H.M. Heise, Near-Infrared Spectroscopy: Principles, Instruments, Applications, Allemand, 2002.

[30] J.C. Dobrowolski, G.J. Strzemecki, M.H. Jamróz, Theory of the intensian method, Chemometrics and Intelligent Laboratory Systems. 15 (1992) 39–50.

[31] A. Savitzky, M.J.E. Golay, Smoothing and Differentiation of Data by Simplified Least Squares Procedures., Analytical Chemistry. 36 (1964) 1627–1639.

[32] R.J. Barnes, M.S. Dhanoa, S.J. Lister, Standard Normal Variate Transformation and De-trending of Near-Infrared Diffuse Reflectance Spectra, Applied Spectroscopy. 43 (1989) 772–777.

[33] T. Isaksson, T. Næs, The Effect of Multiplicative Scatter Correction (MSC) and Linearity Improvement in NIR Spectroscopy, Applied Spectroscopy. 42 (1988) 1273–1284.

[34] M. Howard, J. Workman, Chemometrics in Spectroscopy, Academic Press, 2007.

[35] P. Matousek, M.D. Morris, eds., Emerging Raman Applications and Techniques in Biomedical and Pharmaceutical Fields, Springer Berlin Heidelberg, 2010.

[36] D.M. Koller, a. Posch, G. Hörl, C. Voura, S. Radl, N. Urbanetz, et al., Continuous quantitative monitoring of powder mixing dynamics by near-infrared spectroscopy, Powder Technology. 205 (2011) 87–96.

[37] T.R.M. De Beer, C. Bodson, B. Dejaegher, B. Walczak, P. Vercruysse, a Burggraeve, et al., Raman spectroscopy as a process analytical technology (PAT) tool for the in-line monitoring and understanding of a powder blending process., Journal of Pharmaceutical and Biomedical Analysis. 48 (2008) 772–9.

[38] C. Bodson, W. Dewé, P. Hubert, L. Delattre, Comparison of FT-NIR transmission and UV-vis spectrophotometry to follow the mixing kinetics and to assay low-dose tablets containing riboflavin., Journal of Pharmaceutical and Biomedical Analysis. 41 (2006) 783–90.

[39] L. Martínez, A. Peinado, L. Liesum, G. Betz, Use of near-infrared spectroscopy to quantify drug content on a continuous blending process: Influence of mass flow and rotation speed variations, European Journal of Pharmaceutics and Biopharmaceutics. (2013).

[40] S.S. Sekulic, H.W. Ward, D.R. Brannegan, E.D. Stanley, C.L. Evans, S.T. Sciavolino, et al., On-line monitoring of powder blend homogeneity by near-infrared spectroscopy., Analytical Chemistry. 68 (1996) 509–13.

[41] S.S. Sekulic, J. Wakeman, P. Doherty, P.A. Hailey, Automated system for the on-line monitoring of powder blending processes using near-infrared spectroscopy. Part II. Qualitative approaches to blend evaluation., Journal of Pharmaceutical and Biomedical Analysis. 17 (1998) 1285–309.

[42] A.U. Vanarase, M. Järvinen, J. Paaso, F.J. Muzzio, Development of a methodology to estimate error in the on-line measurements of blend uniformity in a continuous powder mixing process, Powder Technology. (2013).

[43] C. Ravn, E. Skibsted, R. Bro, Near-infrared chemical imaging (NIR-CI) on pharmaceutical solid dosage forms-comparing common calibration approaches., Journal of Pharmaceutical and Biomedical Analysis. 48 (2008) 554–61.

[44] A.S. El-hagrasy, H.R. Morris, F.D. Amico, R.A. Lodder, J.K.D. Iii, Near-Infrared Spectroscopy and Imaging for the Monitoring of Powder Blend Homogeneity, 90 (2001) 1298–1307.

[45] B.E.N. Lewis, L.H. Kidder, NIR Chemical Imaging as a Process Analytical Tool, (2004) 107–111.

[46] R.C. Lyon, D.S. Lester, E.N. Lewis, E. Lee, L.X. Yu, E.H. Jefferson, et al., Near-infrared spectral imaging for quality assurance of pharmaceutical products: analysis of tablets to assess powder blend homogeneity., AAPS PharmSciTech. 3 (2002) E17.

[47] B.J. Westenberger, C.D. Ellison, A.S. Fussner, S. Jenney, R.E. Kolinski, T.G. Lipe, et al., Quality assessment of internet pharmaceutical products using traditional and non-traditional analytical techniques., International Journal of Pharmaceutics. 306 (2005) 56–70.

[48] Z. Wu, O. Tao, X. Dai, M. Du, X. Shi, Y. Qiao, Monitoring of a pharmaceutical blending process using near infrared chemical imaging, Vibrational Spectroscopy. 63 (2012) 371–379.

[49] J.M. Amigo, J. Cruz, M. Bautista, S. Maspoch, J. Coello, M. Blanco, Study of pharmaceutical samples by NIR chemical-image and multivariate analysis, TrAC Trends in Analytical Chemistry. 27 (2008) 696–713.

[50] C. Cairós, J.M. Amigo, R. Watt, J. Coello, S. Maspoch, Implementation of enhanced correlation maps in near infrared chemical images: application in pharmaceutical research., Talanta. 79 (2009) 657–64.

[51] M.L. Hamad, C.D. Ellison, M.A. Khan, R.C. Lyon, Drug product characterization by macropixel analysis of chemical images., Journal of Pharmaceutical Sciences. 96 (2007) 3390–401.

[52] K. Marikh, H. Berthiaux, C. Gatumel, V. Mizonov, E. Barantseva, Influence of stirrer type on mixture homogeneity in continuous powder mixing: A model case and a pharmaceutical case, Chemical Engineering Research and Design. 86 (2008) 1027–1037.

[53] A.U. Vanarase, F.J. Muzzio, Effect of operating conditions and design parameters in a continuous powder mixer, Powder Technology. 208 (2011) 26–36.

[54] C. Ammarcha, C. Gatumel, J.L. Dirion, M. Cabassud, V. Mizonov, H. Berthiaux, Predicting bulk powder flow dynamics in a continuous mixer operating in transitory regimes, Advanced Powder Technology. 23 (2012) 787–800.

[55] M. Sen, R. Singh, A. Vanarase, J. John, R. Ramachandran, Multi-dimensional population balance modeling and experimental validation of continuous powder mixing processes, Chemical Engineering Science. 80 (2012) 349–360.

[56] A.U. Vanarase, M. Alcalà, J.I. Jerez Rozo, F.J. Muzzio, R.J. Romañach, Real-time monitoring of drug concentration in a continuous powder mixing process using NIR spectroscopy, Chemical Engineering Science. 65 (2010) 5728–5733.

[57] Y. Gao, A. Vanarase, F. Muzzio, M. Ierapetritou, Characterizing continuous powder mixing using residence time distribution, Chemical Engineering Science. 66 (2011) 417–425.

[58] J.P. Beaudry, Blender efficiency, Chemical Engineering. 55 (1948) 112–113.

[59] J.C. Williams, M.A. Rahman, Prediction of the performance of continuous mixers for particulate solids using residence time distributions Part I. Theoretical, Powder Technology. 5 (1972) 87–92.

[60] R. Weineikötter, L. Reh, Continuous mixing of fine particles, Particle & Particle Systems Characterization. 12 (1995) 46–53.

[61] P.M. Portillo, M.G. Ierapetritou, F.J. Muzzio, Effects of rotation rate, mixing angle, and cohesion in two continuous powder mixers—A statistical approach, Powder Technology. 194 (2009) 217–227.

[62] P.M. Portillo, A.U. Vanarase, A. Ingram, J.K. Seville, M.G. Ierapetritou, F.J. Muzzio, Investigation of the effect of impeller rotation rate, powder flow rate, and cohesion on powder flow behavior in a continuous blender using PEPT, Chemical Engineering Science. 65 (2010) 5658–5668.

[63] Y. Gao, F. Muzzio, M. Ierapetritou, Characterization of Feeder Effects on Continuous Solid Mixing Using Fourier Series Analysis, 57 (2011).

[64] A. Tamir, Applications of Markov Chains in Chemical Engineering, Elsevier Science, 1998.

[65] Y. Oyama, K. Ayaki, Studies on the Mixing of Particulate Solids, Chemical Engineering. 20 (1956) 148–155.

[66] L.T. Fan, S.H. Shin, Stochastic diffusion model of non-ideal mixing in a horizontal drum mixer, Chemical Engineering Science. 34 (1979) 811–820.

[67] R.H. Wang, L.T. Fan, Axial Mixing of Grains in a Motionless Sulzer (Koch) Mixer, Industrial & Engineering Chemistry Process Design and Development. 15 (1976) 381–388.

[68] R.H. Wang, L.T. Fan, Stochastic modeling of segregation in a motionless mixer, Chemical Engineering Science. 32 (1977) 695–701.

[69] H.G. Dehling, C. Dechsiri, T. Gottschalk, P.C. Wright, A.C. Hoffinann, A stochastic model for mixing and segregation in slugging fluidized beds, Powder Technology. 171 (n.d.) 118–125.

[70] Harris A.T., Thorpe R.B., Davidson J.F., Stochastic modelling of the particle residence time distribution in circulating fluidised bed risers, Chemical Engineering Science. 57 (2002) 18.

[71] M. Aoun-Habbachea, M. Aounb, H. Berthiaux, V. Mizonovc, An experimental method and a Markov chain model to describe axial and radial mixing in a hoop mixer, Powder Technology. 128 (n.d.) 159–167.

[72] H. Berthiaux, K. Marikh, V. Mizonvo, D. Ponomarev, E. Barantzeva, Modeling Continuous Powder Mixing by Means of the Theory of Markov Chains, Particulate Science and Technology. 22 (2004) 379–389.

[73] K. Marikh, H. Berthiaux, V. Mizonov, E. Barantseva, D. Ponomarev, Flow Analysis and Markov Chain Modelling to Quantify the Agitation Effect in a Continuous Powder Mixer, Chemical Engineering Research and Design. 84 (2006) 1059–1074.

[74] K. Sommer, Continuous powder mixing, in: In Proceeding of 1st International Particle Forum, Denver, 1994: pp. 343–349.

[75] K. Sommer, Mixing of particulate solids, KONA Powder Part. 14 (1996) 73–78.

[76] V. Kehlenbeck, K. Sommer, Modeling of the mixing process of very fine powders in a continuous dynamic mixer, in: Fourth International Conference on Conveying and Handling of Particulate Solids, 2003: pp. 26–31.

[77] D. Ramkrishna, Population Balances, Academic Press, San Diego, 2000.

[78] M. Sen, R. Ramachandran, A multi-dimensional population balance model approach to continuous powder mixing processes, Advanced Powder Technology. 24 (2013) 51–59.

[79] F. Bertrand, L. -a. Leclaire, G. Levecque, DEM-based models for the mixing of granular materials, Chemical Engineering Science. 60 (2005) 2517–2531.

[80] P.A. Cundall, O.D.L. Strack, A discrete numerical model for granular assemblies, Géotechnique. 29 (1979) 47–65.

[81] R. Bharadwaj, Using DEM to Solve Bulk Material Handling Problems | AIChE, CEP. (2012) 54–58.

[82] D. Scharpf, D. Ph, Simulation of Particulate Solids Handling and Processing Operations Using the Discrete Element Method, (n.d.).

[83] F. Bertrand, T. Gange, E. Desaulniers, D. Vidal, R.E. Hayes, Simulation of the consolidation of paper coating structures: probabilistic versus deterministic models, Computers & Chemical Engineering. 28 (2004) 2595–2604.

[84] H. Hertz, Über die berührung fester elastischer körper, Für Die Reine Und Angewandte Mathematik. (1882) 156–171.

[85] Y.C. Zhou, B.D. Wright, R.Y. Yang, B.H. Xu, A.B. Yu, Rolling friction in the dynamic simulation of sandpile formation, Physica A: Statistical Mechanics and Its Applications. 269 (1999) 536–553.

[86] M. Lemieux, G. Léonard, J. Doucet, L.-A. Leclaire, F. Viens, J. Chaouki, et al., Large-scale numerical investigation of solids mixing in a V-blender using the discrete element method, Powder Technology. 181 (2008) 205–216.

[87] S.S. Manickam, R. Shah, J. Tomei, T.L. Bergman, B. Chaudhuri, Investigating mixing in a multi-dimensional rotary mixer: Experiments and simulations, Powder Technology. 201 (2010) 83–92.

[88] A. Hassanpour, H. Tan, A. Bayly, P. Gopalkrishnan, B. Ng, M. Ghadiri, Analysis of particle motion in a paddle mixer using Discrete Element Method (DEM), Powder Technology. 206 (2011) 189–194.

[89] M. Marigo, D.L. Cairns, M. Davies, a. Ingram, E.H. Stitt, Developing mechanistic understanding of granular behaviour in complex moving geometry using the Discrete Element Method, Powder Technology. 212 (2011) 17–24.

[90] M. Marigo, M. Davies, T. Leadbeater, D.L. Cairns, a Ingram, E.H. Stitt, Application of Positron Emission Particle Tracking (PEPT) to Validate a Discrete Element Method (DEM) Model of Granular Flow and Mixing in the Turbula Mixer., International Journal of Pharmaceutics. 446 (2013) 46–58.

[91] A. Dubey, A. Sarkar, M. Ierapetritou, C.R. Wassgren, F.J. Muzzio, Computational Approaches for Studying the Granular Dynamics of Continuous Blending Processes, 1 - DEM Based Methods, Macromolecular Materials and Engineering. 296 (n.d.) 290–307.

[92] A. Sarkar, C.R. Wassgren, Simulation of a continuous granular mixer: Effect of operating conditions on flow and mixing, Chemical Engineering Science. 64 (2009) 2672–2682.

[93] A. Sarkar, C. Wassgren, Continuous blending of cohesive granular material, Chemical Engineering Science. 65 (2010) 5687–5698.

[94] A. Sarkar, C.R. Wassgren, Comparison of flow microdynamics for a continuous granular mixer with predictions from periodic slice DEM simulations, Powder Technology. 221 (2012) 325–336.

[95] P.M. Portillo, F.J. Muzzio, M.G. Ierapetritou, Hybrid DEM-Compartment Modeling Approach for Granular Mixing, 53 (2007) 119–128.

[96] B. Freireich, J. Li, J. Litster, C. Wassgren, Incorporating particle flow information from discrete element simulations in population balance models of mixer-coaters, Chemical Engineering Science. 66 (2011) 3592–3604.

[97] M. Sen, A. Chaudhury, R. Singh, J. John, R. Ramachandran, Multi-scale flowsheet simulation of an integrated continuous purification–downstream pharmaceutical manufacturing process, International Journal of Pharmaceutics. (2013) 1–10.

[98] J. Doucet, N. Hudon, F. Bertrand, J. Chaouki, Modeling of the mixing of monodisperse particles using a stationary DEM-based Markov process, Computers & Chemical Engineering. 32 (2008) 1334–1341.

[99] J.D. Tjakra, J. Bao, N. Hudon, R. Yang, Modeling collective dynamics of particulate systems under time-varying operating conditions based on Markov chains, Advanced Powder Technology. (2013).

[100] I. Trabelsi, Simulation numérique de l'écoulement et mélange granulaires par des éléments discrets ellipsoïdaux, Université Tunis El-Manar and Institut Nationale Polytechnique de Toulouse, 2013.

[101] D.E. Seborg, D.A. Mellichamp, T.F. Edgar, F.J.D. III, Process Dynamics and Control, Wiley, 2010.

[102] S.Y. Nof, ed., Springer Handbook of Automation, Springer Berlin Heidelberg, 2009.

[103] K.J. Åström, T. Hägglund, The future of PID control, Control Engineering Practice. 9 (2001) 1163–1175.

[104] O. Lequin, M. Gevers, M. Mossberg, E. Bosmans, L. Triest, Iterative feedback tuning of PID parameters: comparison with classical tuning rules, Control Engineering Practice. 11 (2003) 1023–1033.

[105] D.W. Spitzer, Advanced Regulatory Control: Applications and Techniques, First Edit, Momentum Press, New York, NY, 2009.

[106] M. Jelali, Control performance management in industrial automation assessment, diagnosis and improvement of control loop performance, (2013).

[107] P.D. Christofides, M. Li, L. Mädler, Control of particulate processes: Recent results and future challenges, Powder Technology. 175 (2007) 1–7.

[108] P.D. Christofides, N. El-Farra, M. Li, P. Mhaskar, Model-based control of particulate processes, Chemical Engineering Science. 63 (2008) 1156–1172.

[109] A. Mesbah, J. Landlust, A.E.M. Huesman, H.J.M. Kramer, P.J. Jansens, P.M.J. Van den Hof, A model-based control framework for industrial batch crystallization processes, Chemical Engineering Research and Design. 88 (2010) 1223–1233.

[110] D. Shi, N.H. El-Farra, M. Li, P. Mhaskar, P.D. Christofides, Predictive control of particle size distribution in particulate processes, Chemical Engineering Science. 61 (2006) 268–281.

[111] R. Ramachandran, A. Chaudhury, Model-based design and control of a continuous drum granulation process, Chemical Engineering Research and Design. 90 (2012) 1063–1073.

[112] P. Suresh, S.-H. Hsu, G. V. Reklaitis, V. Venkatasubramanian, OntoMODEL: Ontological Mathematical Modeling Knowledge Management in Pharmaceutical Product Development, 2: Applications, Industrial & Engineering Chemistry Research. 49 (2010) 7768–7781.

[113] J.C. Williams, M.A. Rahman, Prediction of the performance of continuous mixers for particulate solids using residence time distributions: Part II. Experimental, Powder Technology. 5 (1972) 307–316.

[114] R. Ramachandran, J. Arjunan, A. Chaudhury, M.G. Ierapetritou, Model-Based Control-Loop Performance of a Continuous Direct Compaction Process, Journal of Pharmaceutical Innovation. 6 (2011) 249–263.

ANNEX 1

Markov chain simulations in Matlab

Function 1

```
function[t,M_6,c_A,S,K,Q_out,t_s,X_A,RSD]=Mixing_modeling_constant(Q_A,Q_B,N,dt,n,
S,K)

%%%%%%%%%%%%%%%%%%%%%%%%Variable Description%%%%%%%%%%%%

%<<<<<<<<<<<<<<<<<<<<<<<<Input variables<<<<<<<<<<<<<<<<<<<<<<<<<<<<<<<<<<<<

%Q_A:     Mass inflowrate of component A [g.s^(-1)]
%Q_B:     Mass inflowrate of component B [g.s^(-1)]
%N:       Rotational speed [Hz]
%dt:      Transition time [s], in this work, dt=0.1 second
%n:       Process time [s]
%S:    Vector of mass of component A in each cell of Markov chain
%.................S=[S(1); S(2); S(3); S(4); S(5); S(6)].....................
%----------------Initial S=[0; 0; 0; 0; 0; 0]-----------------------------
%K:    Vector of mass of component B in each cell of Markov chain
%.................K=[K(1); K(2); K(3); K(4); K(5); K(6)].....................
%----------------Initial K=[0; 0; 0; 0; 0; 0]-----------------------------

%>>>>>>>>>>>>>>>>>>>>>>>>Output variables>>>>>>>>>>>>>>>>>>>>>>>>>>>>>>>>>>>>

%t:        Vector of time in every 0.1 second
t=zeros((n/dt),1);
%M_6:      Vector of mass retrieved in 6th cell (M6)
M_6=zeros((n/dt),1);
%M_6_A:    Vector of mass retrieved in 6th cell (M6(A))
M_6_A=zeros((n/dt),1);
%M_6_B:    Vector of mass retrieved in 6th cell (M6(B))
M_6_B=zeros((n/dt),1);
%c_A:      Vector of concentration of component A every 0.1 second
c_A=zeros((n/dt),1);
%Q_out:    Vector of the outflow of the mixer
 %t_s:      Vector of time in seconds
t_s=zeros(n,1);
%X_A:      Vector of mean composition of component A in seconds
X_A=zeros(n,1);
%RSD:      Vector of RSD in seconds
RSD=zeros(n,1);
%S:    Vector of mass retrieved of component A in each cell of Markov chain
%.................S=[S(1); S(2); S(3); S(4); S(5); S(6)].....................

%K:    Vector of mass retrieved of component B in each cell of Markov chain
```

```
%...............K=[K(1); K(2); K(3); K(4); K(5); K(6)]...................
%""""""""""""""""""""""""""""""""""""""""""""""""""""""""""""""""""""""""""""""""""""""""""""""""""""""""
%Q:      Feed rate of the mixer: Q=Q_A+Q_B [g.s^(-1)]
Q=Q_A+Q_B;
%x_A:    The mixing formulation of component A: x_A=Q_A/Q
x_A=Q_A/Q;
%DeltaQ_A:   Inflow mass of component A during a transition time [g]
DeltaM_A=Q_A*dt;
%DeltaQ_B:   Inflow mass of component B during a transition time [g]
DeltaM_B=Q_B*dt;
%""""""""""""""""""""""""""""""""""""""""""""""""""""""""""""""""""""""""""""""""""""""""""""""""""""""""

%=============Hold-up mass of component A in the entire mixer==============
%****************M(A)=a1*x_A^b1*Q^c1*N^d1******************************
M_A=1182.26*(x_A)^1*Q^0.5*N^(-0.766);

%=============Hold-up mass of component B in the entire mixer==============
%****************M(B)=a2*(1-x_A)^b2*Q^c2*N^d2***************************
M_B=260.64*(1-x_A)^1*Q^0.5*N^(-0.469);

%============Hold-ups of component A in each cell of the mixer===============
Smax=[M_A*0.12;M_A*0.12;M_A*0.12;M_A*0.12;M_A*0.52];

%============hold-ups of component B in each cell of the mixer===============
Kmax=[M_B*0.085;M_B*0.085;M_B*0.085;M_B*0.085;M_B*0.66];


%============Matrix of transition probabilities at steady state==================

%*********************Component A*************************************
P_A_max=[1-DeltaM_A/(Smax(1)+DeltaM_A) 0 0 0 0 0
     DeltaM_A/(Smax(1)+DeltaM_A) 1-DeltaM_A/Smax(2) 0 0 0 0
     0 DeltaM_A/Smax(2) 1-DeltaM_A/Smax(3) 0 0 0
     0 0 DeltaM_A/Smax(3) 1-DeltaM_A/Smax(4) 0 0
     0 0 0 DeltaM_A/Smax(4) 1-DeltaM_A/Smax(5) 0
     0 0 0 0 DeltaM_A/Smax(5) 1];

%*********************Component B*********************************
P_B_max=[1-DeltaM_B/(Kmax(1)+DeltaM_B) 0 0 0 0 0
     DeltaM_B/(Kmax(1)+DeltaM_B) 1-DeltaM_B/Kmax(2) 0 0 0 0
     0 DeltaM_B/Kmax(2) 1-DeltaM_B/Kmax(3) 0 0 0
     0 0 DeltaM_B/Kmax(3) 1-DeltaM_B/Kmax(4) 0 0
     0 0 0 DeltaM_B/Kmax(4) 1-DeltaM_B/Kmax(5) 0
     0 0 0 0 DeltaM_B/Kmax(5) 1];
for i=1:n/dt
   t(i)=i*0.1;
   p=zeros(5,1);
   q=zeros(5,1);
%=========Determination of transition probabilities for component A and B====
   for j=1:5
```

```
      if  S(j)==0
         p(j)=0;
      elseif S(j)<Smax(j)
         p(j)=P_A_max(j+1,j)/Smax(j)*S(j);
      else
         p(j)=P_A_max(j+1,j);
      end
      if  K(j)==0
         q(j)=0;
      elseif K(j)<Kmax(j)
         q(j)=P_B_max(j+1,j)/Kmax(j)*K(j);
      else
         q(j)=P_B_max(j+1,j);
      end
   end
%===============Matrix of transition probabilities for component A=========
%************************P_A*****************************************
*
   P_A=[1-p(1) 0 0 0 0 0
     p(1) 1-p(2) 0 0 0 0
     0 p(2) 1-p(3) 0 0 0
     0 0 p(3) 1-p(4) 0 0
     0 0 0 p(4) 1-p(5) 0
     0 0 0 0 p(5) 1];

%===============Matrix of transition probabilities for component B=========
%************************P_B*****************************************
*
   P_B=[1-q(1) 0 0 0 0 0
     q(1) 1-q(2) 0 0 0 0
     0 q(2) 1-q(3) 0 0 0
     0 0 q(3) 1-q(4) 0 0
     0 0 0 q(4) 1-q(5) 0
     0 0 0 0 q(5) 1];

%====================Markov chain for component A=======================
  S=P_A*[S(1)+DeltaM_A;S(2);S(3);S(4);S(5);S(6)];
%============================M6(A)=================================
  M_6_A(i)=S(6);

%====================Markov chain for component B=======================
  K=P_B*[K(1)+DeltaM_B;K(2);K(3);K(4);K(5);K(6)];
%============================M6(B)=================================
  M_6_B(i)=K(6);
%==Composition of component A in powder mixtures for every transition time========
  if i==1
c_A(i)=M_6_A(i)/(M_6_A(i)+M_6_B(i));
  else
c_A(i)=(M_6_A(i)-M_6_A(i-1))/((M_6_A(i)-M_6_A(i-1))+(M_6_B(i)-M_6_B(i-1)));
  end
```

```
%==============Mass retrieved of components A and B in 6th cell================
%************************M6=M6(A)+M6(B)*********************************
   M_6(i)=M_6_A(i)+M_6_B(i);

end

%********************** Calculations of X_A and RSD **********************

for k=1:n
   t_s(k)=k;
   sum_c_A=0;
   for v=1:1/dt
      sum_c_A=sum_c_A+c_A((k-1)*1/dt+v);
   end
   X_A(k)=sum_c_A/(1/dt);
   a=(k-1)*1/dt+1;
   b=k*1/dt;
   RSD(k)=std(c_A(a:b),1)/X_A(k);
end

%########################## Four figures ########################################

% plot X_A versus time
figure(1);
plot(t_s, X_A)
xlabel('Time(s)');
ylabel('X_A');
% plot RSD versus time
figure(2);
plot(t_s,100*RSD);
xlabel('Time(s)');
ylabel('RSD');
 % plot M_6 versus time
figure(3);
plot(t,M_6)
xlabel('Time(s)');
ylabel('M_6 (g)');
% plot  Q_out versus time
figure(4);
Q_out=diff(M_6)./diff(t);
plot(t(2:end),Q_out);
xlabel('Time(s)');
ylabel('Q_out (g.s^{-1
```

Function 2

```
function[t,M_6,c_A,S,K,Q_out,t_s,X_A,RSD]=Mixing_modeling_step_change(Q_A,Q_B,N,
dt,n,S,K)

%%%%%%%%%%%%%%%%%%%%%%%%%%Variable Description%%%%%%%%%%%%%


%<<<<<<<<<<<<<<<<<<<<<<<<<Input variables<<<<<<<<<<<<<<<<<<<<<<<<<<<<<

%Q_A:     Vector of mass inflow rate of component A [g.s^(-1)]
%------------------------Q_A=[Q_A_1; Q_A_2]-------------------------------
%Q_B:     Vector of mass inflow rate of component B [g.s^(-1)]
%------------------------Q_B=[Q_B_1; Q_B_2]-------------------------------
%N:       Vector of rotational speed [Hz]
%-------------------------N=[N_1; N_2]-----------------------------------
%dt:      Transition time [sec], in this work, dt=0.1 second
%n:       Vector of process time [sec]
%-------------------------n=[n1; n2]-------------------------------------
%np:      Total process time [sec]
%-------------------------np=n1+n2---------------------------------------
np=n(1)+n(2);

%S:    Vector of mass of component A in each cell of Markov chain
%.................S=[S(1); S(2); S(3); S(4); S(5); S(6)].....................
%----------------Initial S=[0; 0; 0; 0; 0; 0]-----------------------------

%K:    Vector of mass of component B in each cell of Markov chain
%.................K=[K(1); K(2); K(3); K(4); K(5); K(6)].....................
%----------------Initial K=[0; 0; 0; 0; 0; 0]-----------------------------

%>>>>>>>>>>>>>>>>>>>>>>>>Output variables>>>>>>>>>>>>>>>>>>>>>>>>>>>>>>

%t:       Vector of time in every 0.1 second
t=zeros((np/dt),1);
%M_6:      Vecotr of mass retrieved in 6th cell (M6)
M_6=zeros((np/dt),1);
%M_6_A:    Vector of mass retrieved in 6th cell (M6(A))
M_6_A=zeros((np/dt),1);
%M_6_B:    Vector of mass retrieved in 6th cell (M6(B))
M_6_B=zeros((np/dt),1);
%c_A:      Vector of concentration of component A every 0.1 second
c_A=zeros((np/dt),1);
%Q_out:    Vector of the corresponding outflow of the mixer
%t_s:      Vector of time in seconds
t_s=zeros(np,1);
%X_A:      Vector of mean composition of component A in seconds
X_A=zeros(np,1);
%RSD:      Vector of RSD in seconds
RSD=zeros(np,1);
```

```
%------------------------------------------------------------------------

Q=zeros(2,1);
x_A=zeros(2,1);
DeltaM_A=zeros(2,1);
DeltaM_B=zeros(2,1);
%------------------------------------------------------------------------

for lp=1:2
%""""""""""""""""""""""""""""""""""""""""""""""""""""""""""""""""""""""""""""""""""""""""""""
%Q:      Feed rate of the mixer: Q=Q_A+Q_B [g.s^(-1)]
Q(lp)=Q_A(lp)+Q_B(lp);

%x_A:    The mixing formulation of component A: x_A=Q_A/Q
x_A(lp)=Q_A(lp)/Q(lp);

%DeltaQ_A:   Inflow mass of component A during a transition time [g]
DeltaM_A(lp)=Q_A(lp)*dt;

%DeltaQ_B:   Inflow mass of component B during a transition time [g]
DeltaM_B(lp)=Q_B(lp)*dt;
%""""""""""""""""""""""""""""""""""""""""""""""""""""""""""""""""""""""""""""""""""""""""""""

%=============Hold-up mass of component A in the entire mixer================
%****************M(A)=a1*x_A^b1*Q^c1*N^d1*****************************
M_A=1182.26*(x_A(lp))^1*Q(lp)^0.5*N(lp)^(-0.766);

%=============Hold-up mass of component B in the entire mixer==============
%****************M(B)=a2*(1-x_A)^b2*Q^c2*N^d2***************************
M_B=260.4*(1-x_A(lp))^1*Q(lp)^0.5*N(lp)^(-0.469);

%============Hold-ups of component A in each cell of the mixer=================
Smax=[M_A*0.12;M_A*0.12;M_A*0.12;M_A*0.12;M_A*0.52];

%============Hold-ups of component B in each cell of the mixer=================
Kmax=[M_B*0.085;M_B*0.085;M_B*0.085;M_B*0.085;M_B*0.66];

%============Matrix of transition probabilities at steady state==================

%*********************Component A***************************************
P_A_max=[1-DeltaM_A(lp)/(Smax(1)+DeltaM_A(lp)) 0 0 0 0 0
    DeltaM_A(lp)/(Smax(1)+DeltaM_A(lp)) 1-DeltaM_A(lp)/Smax(2) 0 0 0 0
    0 DeltaM_A(lp)/Smax(2) 1-DeltaM_A(lp)/Smax(3) 0 0 0
    0 0 DeltaM_A(lp)/Smax(3) 1-DeltaM_A(lp)/Smax(4) 0 0
    0 0 0 DeltaM_A(lp)/Smax(4) 1-DeltaM_A(lp)/Smax(5) 0
    0 0 0 0 DeltaM_A(lp)/Smax(5) 1];
```

```
%**********************Component B*****************************************
P_B_max=[1-DeltaM_B(lp)/(Kmax(1)+DeltaM_B(lp)) 0 0 0 0 0
      DeltaM_B(lp)/(Kmax(1)+DeltaM_B(lp)) 1-DeltaM_B(lp)/Kmax(2) 0 0 0 0
      0 DeltaM_B(lp)/Kmax(2) 1-DeltaM_B(lp)/Kmax(3) 0 0 0
      0 0 DeltaM_B(lp)/Kmax(3) 1-DeltaM_B(lp)/Kmax(4) 0 0
      0 0 0 DeltaM_B(lp)/Kmax(4) 1-DeltaM_B(lp)/Kmax(5) 0
      0 0 0 0 DeltaM_B(lp)/Kmax(5) 1];

 for i=1:n(lp)/dt
  if lp==1
   t(i)=i*dt;
  else
     t(n(1)/dt+i)=(n(1)/dt+i)*dt;
  end
   p=zeros(5,1);
   q=zeros(5,1);
%==========Determination of transition probabilities for component A and B==========
   for j=1:5
      if  S(j)==0
         p(j)=0;
      elseif S(j)<Smax(j)
         p(j)=P_A_max(j+1,j)/Smax(j)*S(j);
      else
         p(j)=P_A_max(j+1,j);
      end
      if  K(j)==0
         q(j)=0;
      elseif K(j)<Kmax(j)
         q(j)=P_B_max(j+1,j)/Kmax(j)*K(j);
      else
         q(j)=P_B_max(j+1,j);
      end
   end
%===============Matrix of transition probabilities for component A==============
%**************************P_A*****************************************
   P_A=[1-p(1) 0 0 0 0 0
      p(1) 1-p(2) 0 0 0 0
      0 p(2) 1-p(3) 0 0 0
      0 0 p(3) 1-p(4) 0 0
      0 0 0 p(4) 1-p(5) 0
      0 0 0 0 p(5) 1];

%===============Matrix of transition probabilities for component B==============
%**************************P_B*****************************************
   P_B=[1-q(1) 0 0 0 0 0
      q(1) 1-q(2) 0 0 0 0
      0 q(2) 1-q(3) 0 0 0
      0 0 q(3) 1-q(4) 0 0
      0 0 0 q(4) 1-q(5) 0
      0 0 0 0 q(5) 1];
```

```
%=====================Markov chain for component A=====================
  S=P_A*[S(1)+DeltaM_A(lp);S(2);S(3);S(4);S(5);S(6)];

%=====================Markov chain for component B=====================
  K=P_B*[K(1)+DeltaM_B(lp);K(2);K(3);K(4);K(5);K(6)];

  if lp==1
%============================M6(A)================================
     M_6_A(i)=S(6);
%============================M6(B)================================
     M_6_B(i)=K(6);
%=============Mass retrieved of components A and B in 6th cell=============
%**********************M6=M6(A)+M6(B)*******************************
     M_6(i)=M_6_A(i)+M_6_B(i);
  else
     M_6_A(n(1)/dt+i)=S(6);
     M_6_B(n(1)/dt+i)=K(6);
     M_6(n(1)/dt+i)=M_6_A(n(1)/dt+i)+ M_6_B(n(1)/dt+i);
  end

%==Composition of component A in powder mixtures for every transition time==========
 if lp==1
  if i==1
  c_A(i)=M_6_A(i)/(M_6_A(i)+M_6_B(i));
  else
  c_A(i)=(M_6_A(i)-M_6_A(i-1))/((M_6_A(i)-M_6_A(i-1))+(M_6_B(i)-M_6_B(i-1)));
  end
 else
  c_A(n(1)/dt+i)=(M_6_A(n(1)/dt+i)-M_6_A(n(1)/dt+i-1))/((M_6_A(n(1)/dt+i)-
M_6_A(n(1)/dt+i-1))+(M_6_B(n(1)/dt+i)-M_6_B(n(1)/dt+i-1)));
 end
end
end


%######################## Calculations of X_A and RSD ########################

for k=1:np
   t_s(k)=k;
   sum_c_A=0;
   for v=1:1/dt
      sum_c_A=sum_c_A+c_A((k-1)*1/dt+v);
   end
   X_A(k)=sum_c_A/(1/dt);
   a=(k-1)*1/dt+1;
   b=k*1/dt;
   RSD(k)=std(c_A(a:b),1)/X_A(k);
end
```

```
%######################## Four figures ###################################

% plot X_A versus time
figure(1);
plot(t_s, X_A)
xlabel('Time(s)');
ylabel('X_A');
% plot RSD versus time
figure(2);
plot(t_s,100*RSD);
xlabel('Time(s)');
ylabel('RSD');
 % plot M_6 versus time
figure(3);
plot(t,M_6)
xlabel('Time(s)');
ylabel('M_6 (g)');
% plot  Q_out versus time
figure(4);
Q_out=diff(M_6)./diff(t);
plot(t(2:end),Q_out);
xlabel('Time(s)');
ylabel('Q_out (g.s^{-1})');
```

ANNEX 2

Control system programmed in Labview – User graphical interface (1)

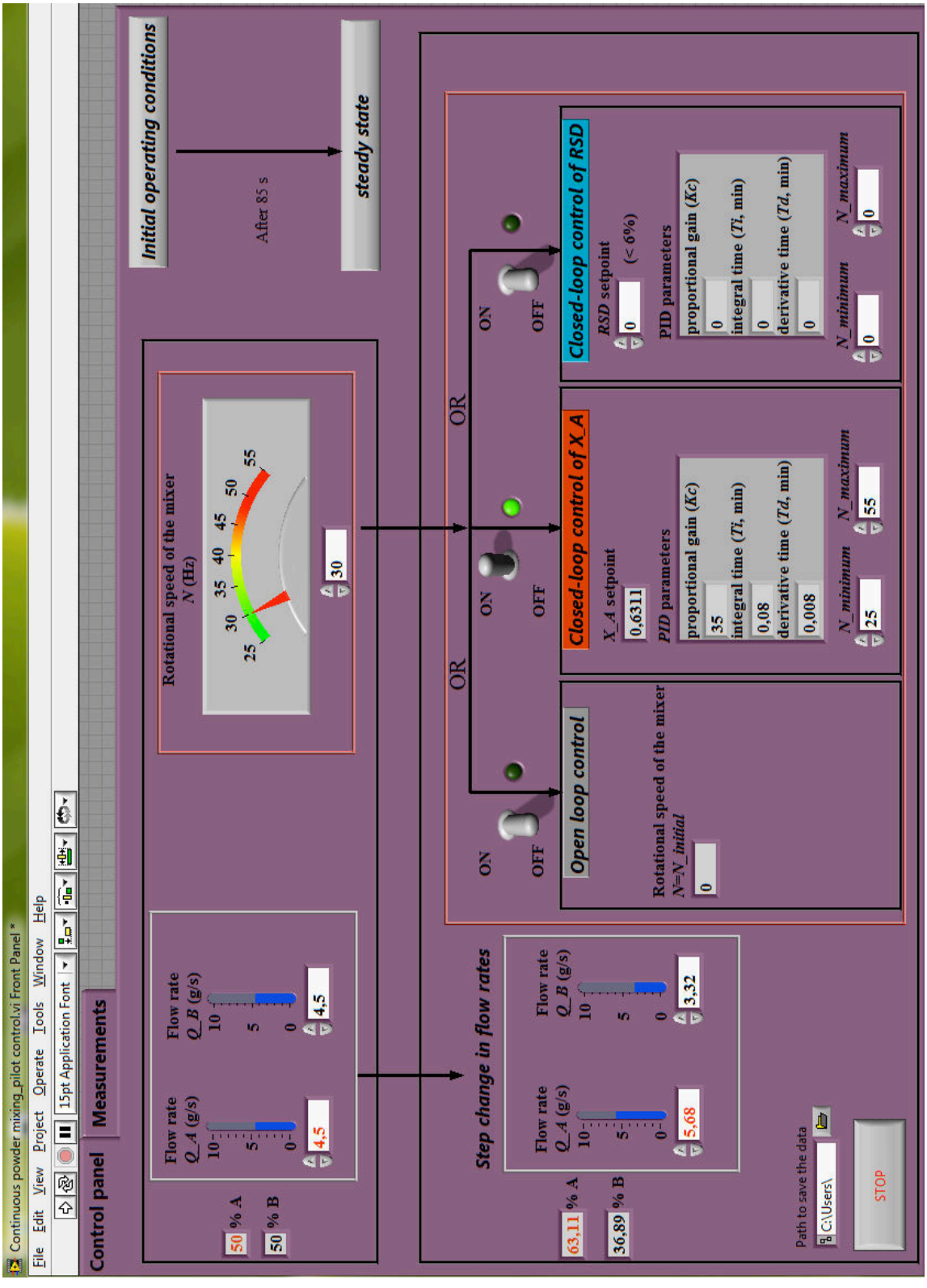

Control system programmed in Labview – User graphical interface (2)

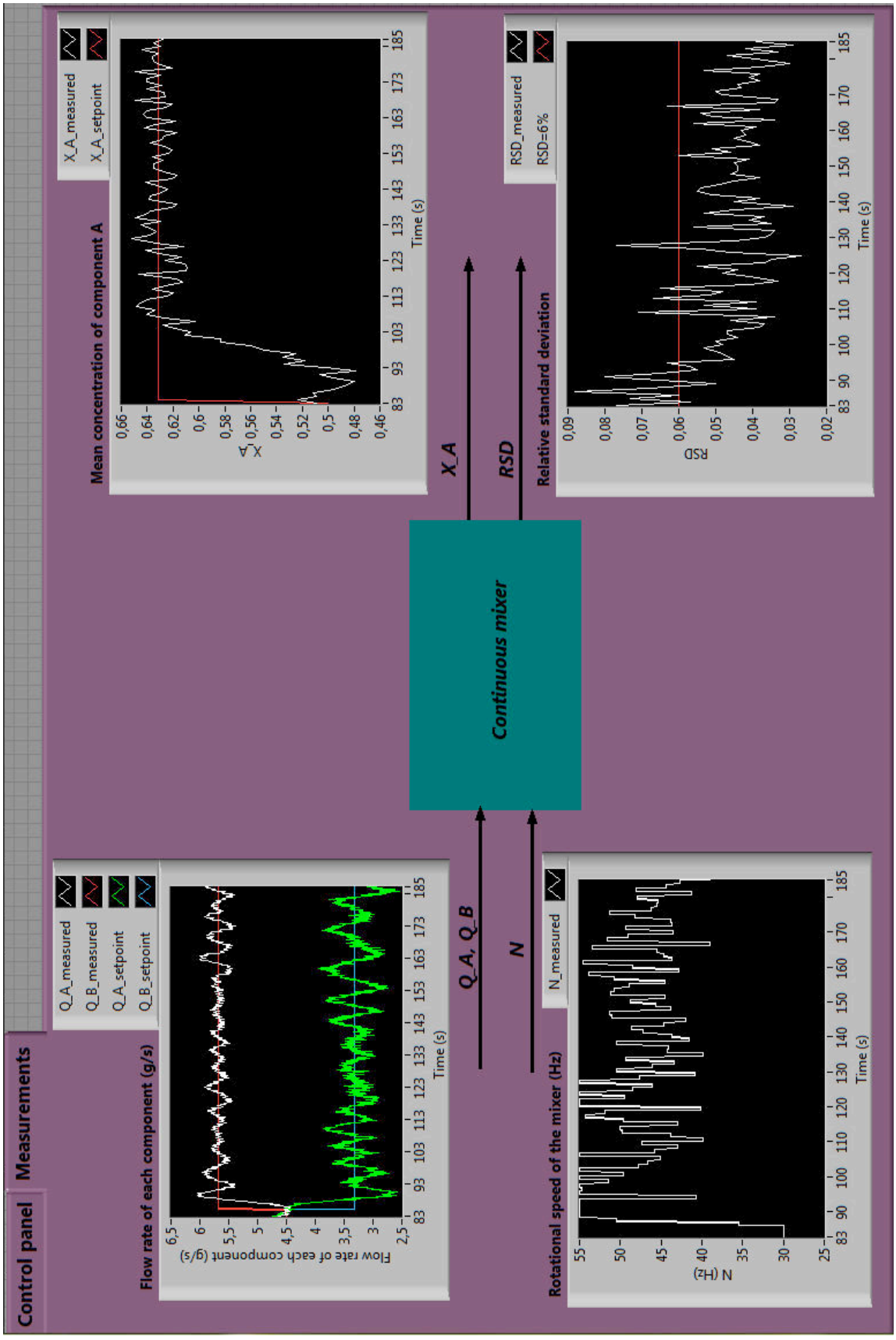

Control system programmed in Labview – Block program (1)

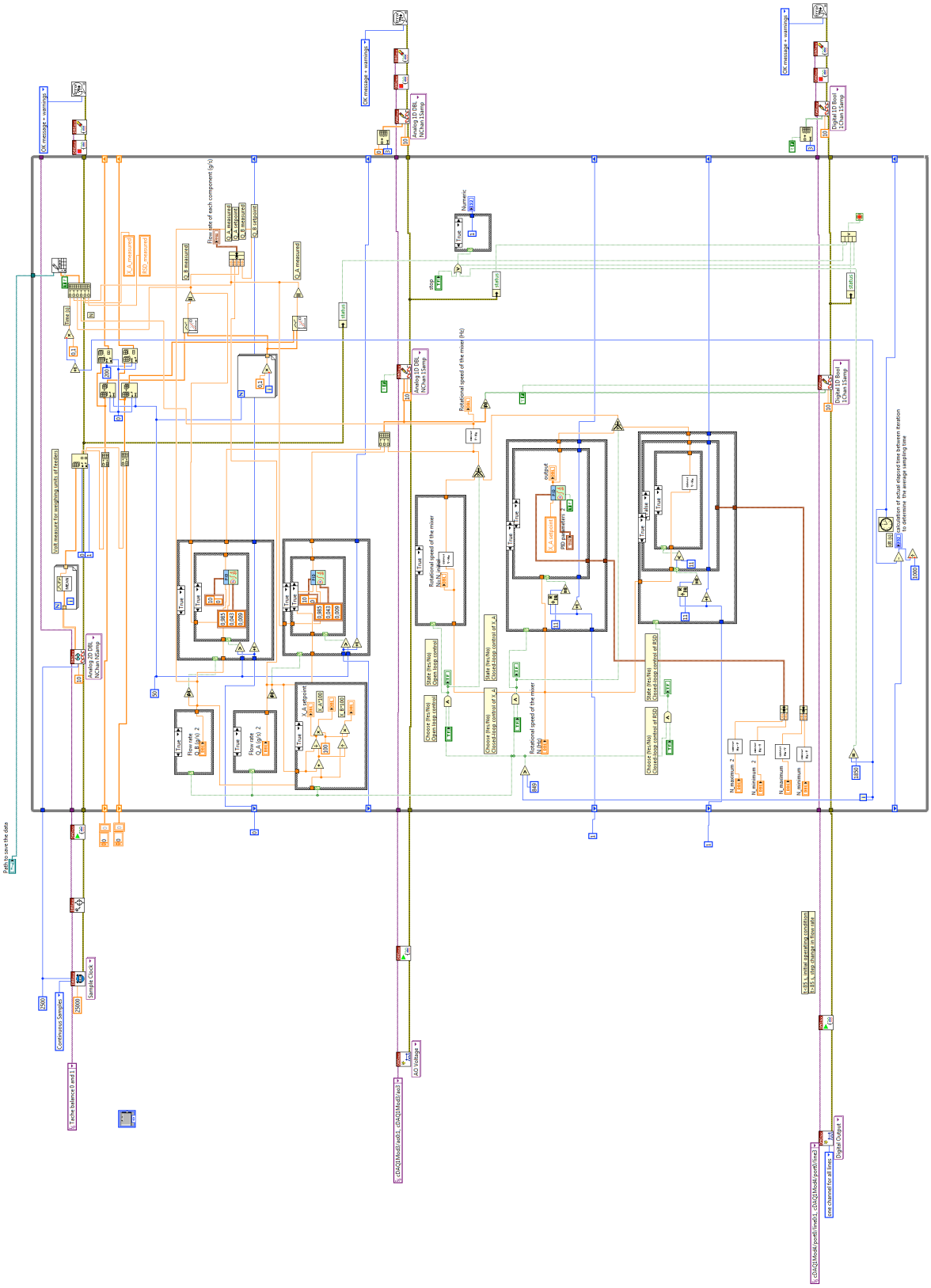

Control system programmed in Labview – Block program (2)

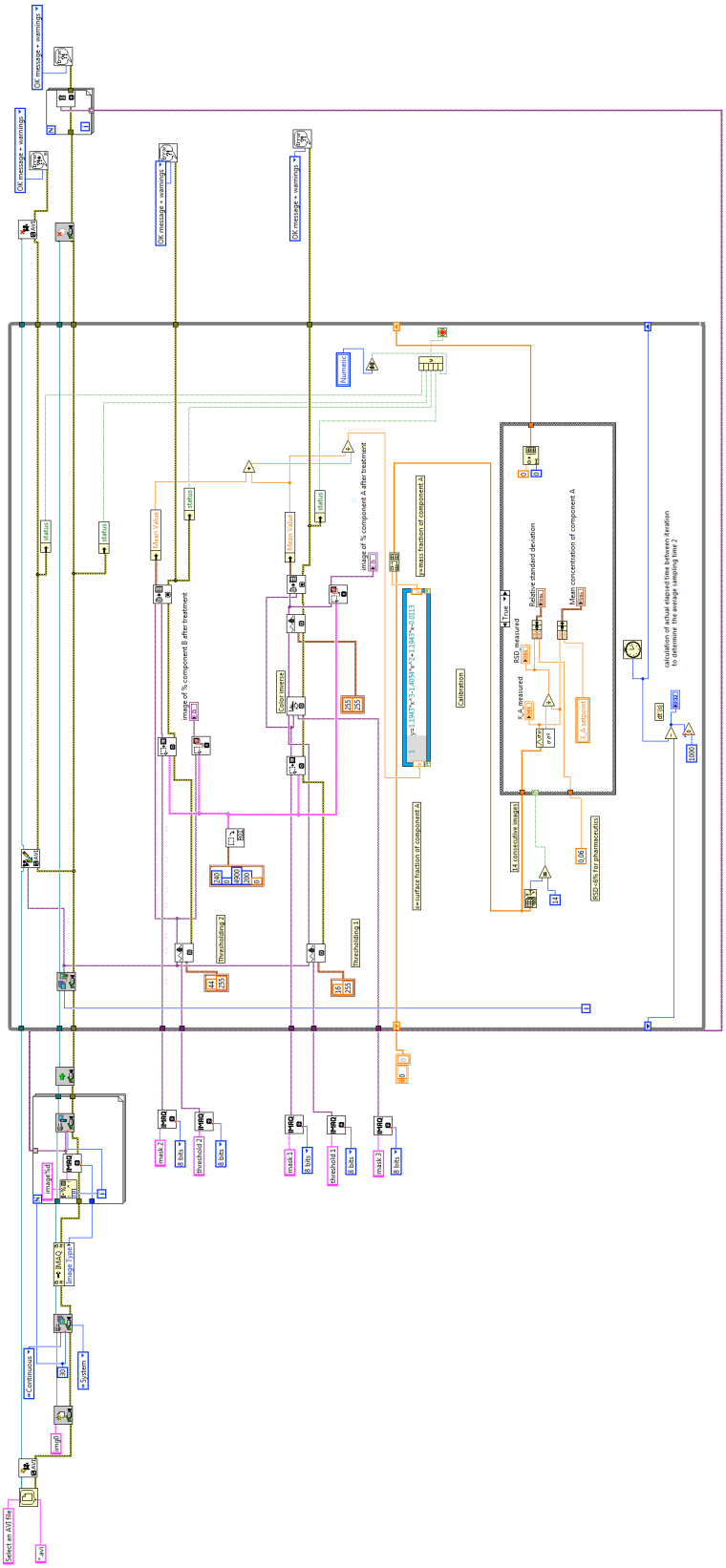

ANNEX 3

Markov chain model including a PID controller programmed in Labview

(1) Markov chain model programmed in Labview

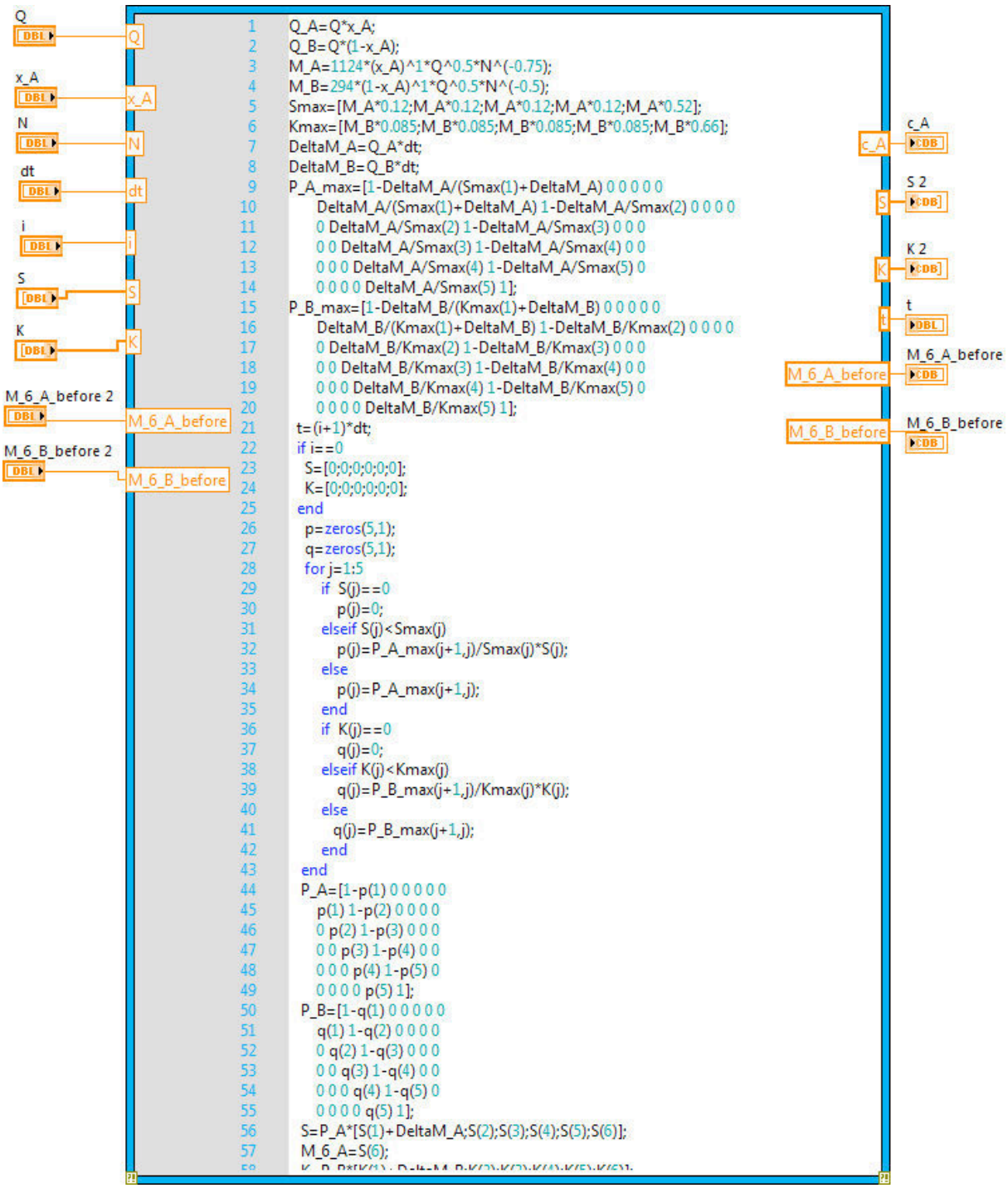

(2) Simulation Markov chain model using theoretical values of the flow rates Q_A and Q_B

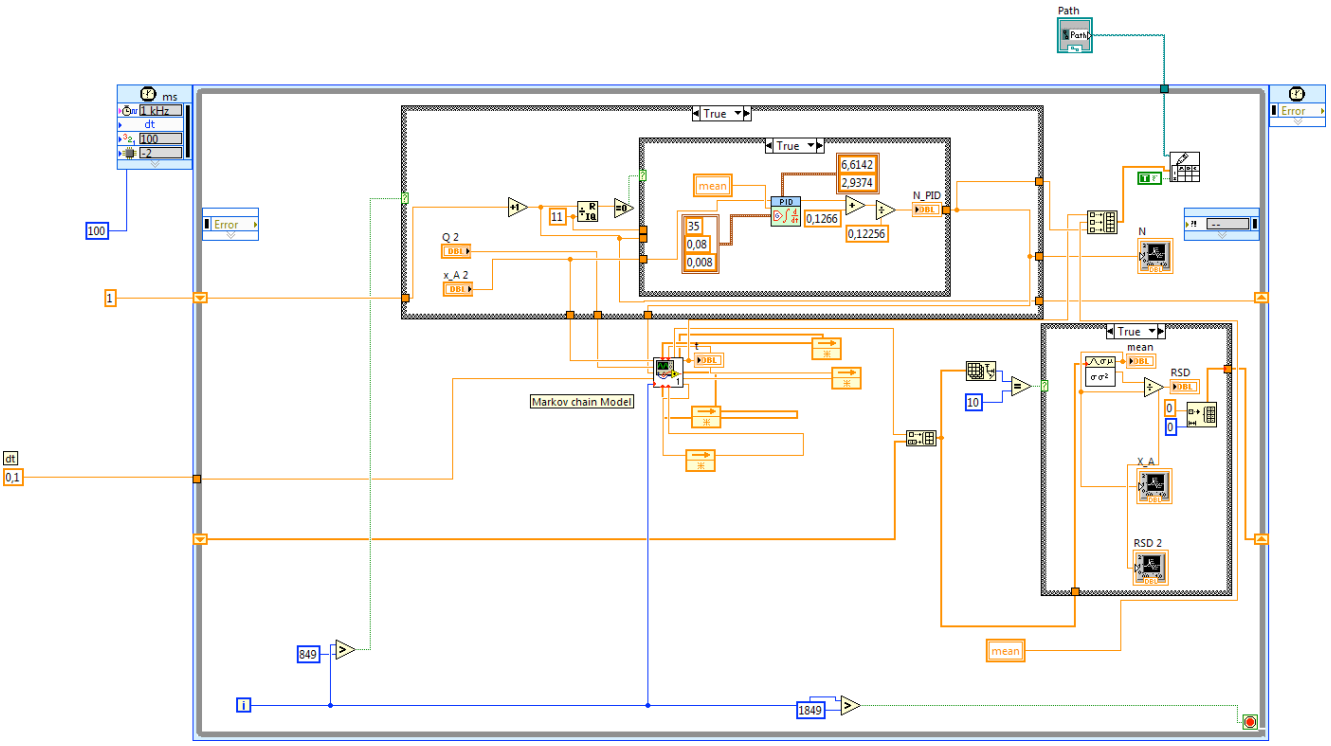

(3) Simulation Markov chain model taking into account the actual fluctuations of the flow rates Q_A and Q_B

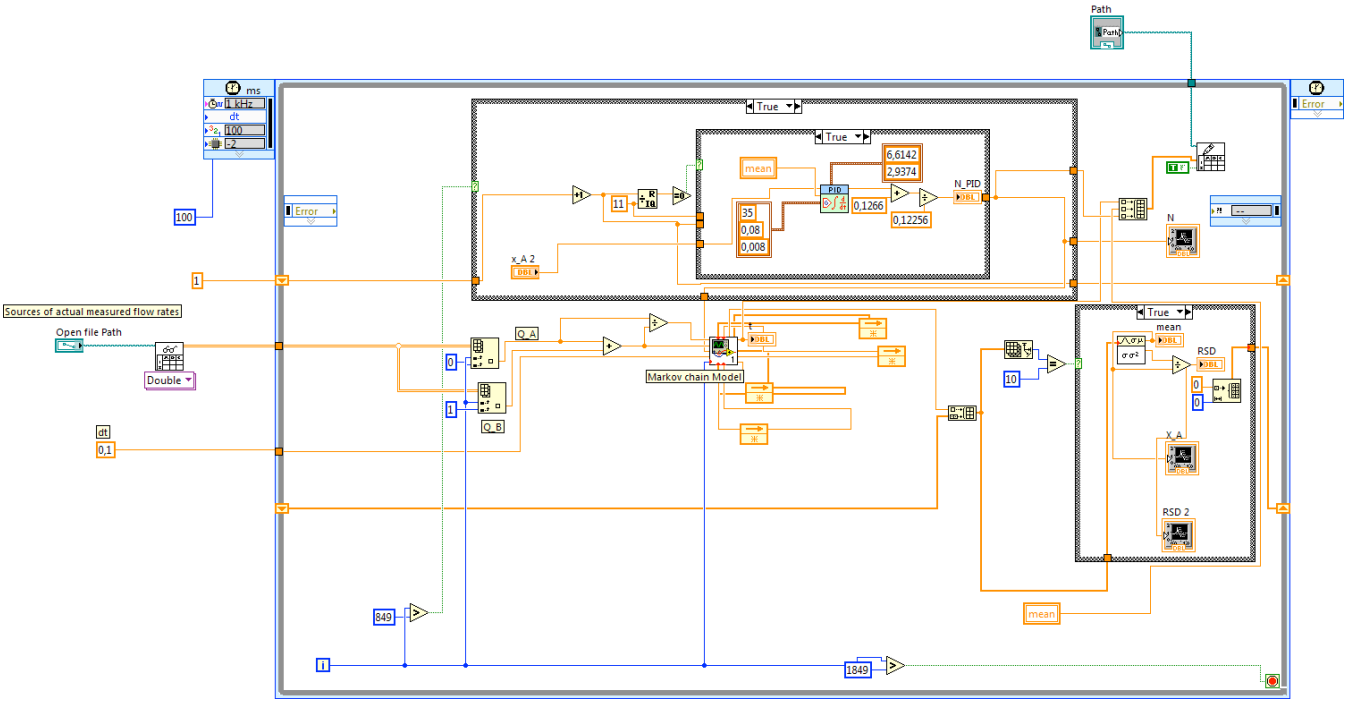

LISTS OF TABLES

LISTS OF FIGURES

NOMENCLATURE

CI	Carr's index (%)
e_{RSD}	deviation in *RSD* between the setpoint and the measured
e_{X_A}	deviation in mean concentration of component A between the setpoint and the measured
H	Hausner ratio
IAE	integral absolute error
$ITAE$	integral of time-weighted absolute error
ISE	integral square error
k	time instant
K_c	proportional gain of a PID controller
$K_i(n+1)$	mass of component B in cell i after n transitions in Markov chains
$M(A)$	hold-up weight of component A in the entire mixer (g)
$M(B)$	hold-up weight of component B in the entire mixer (g)
$M_i(A)$	hold-up weight of component A in the cell i =1,2,…,5 of the mixer (g)
$M_i(B)$	hold-up weight of component B in the cell i =1,2,…,5 of the mixer (g)
M_6	whole powder mass obtained at the mixer's outlet
$M_i(A)/M(A)$	relative hold-up weight distribution of component A
$M_i(B)/M(B)$	relative hold-up weight distribution of component B
N	rotational speed of the engine (Hz)
$p_{(i+1)i}(n)$	probability of component A to move from cell i to cell $i+1$ during the n^{th} transition
$p_{(i+1)i\,max}$	transition probability of component A at steady state
$q_{(i+1)i}(n)$	probability of component B to move from cell i to cell $i+1$ during the n^{th} transition
$q_{(i+1)i\,max}$	transition probability of component B at steady state
Q_A	mass flow rate of component A ($g.s^{-1}$)
Q_B	mass flow rate of component B ($g.s^{-1}$)

$Q_{out}(n)$	outflow rate of the mixer after *n* transitions ($g.s^{-1}$)
r	distance between two samples
$R(r)$	autocorrelation function
RSD	relative standard deviation
S_A	percentage of surface covered by component A (%)
S_B	percentage of surface covered by component B (%)
$S_i(n+1)$	mass of component A in cell *i* after *n* transitions in Markov chains
T_d	derivative time of a PID controller (min)
T_i	integral time of a PID controller (min)
$V_{ao,\ mixer}$	analog output voltage used to rotate the engine (V)
VRR	variance reduction ratio
X_A	mean concentration of component A in every *n* consecutive samples

Greek letters

ρ_{true}	true particle density ($g.cm^{-3)}$
$\rho_{aerated}$	aerated bulk density ($g.cm^{-3}$)
ρ_{tapped}	tapped density ($g.cm^{-3}$)
σ^2	variance of a mixture
σ_0^2	upper limiting variance (completely segregated) of a binary mixture
σ_R^2	lower limiting variance (randomly mixed) of a binary mixture
σ_{in}^2	variance in concentration at the mixer's inlet
σ_{out}^2	variance in concentration n at the mixer's outlet
ε	porosity of particle system
Δt	time interval for simulation or transition duration for Markov chain or sampling time of PID controllers (s)
α_D	angle of difference of a granular material (°)
α_F	angle of fall of a granular material (°)
α_R	angle of repos of a granular material (°)
α_S	angle of spatual of a granular material (°)

ABSTRACT

Powder mixing is an essential operation in various industrial fields, such as pharmaceuticals, agro-food, cements, etc. Continuous powder mixing, as an alternative to conventional batch mixing, has attracted a lot of interest mainly due to its capacity in handling high volume manufacturing. This work aims at the contribution to the implementation of process control applications for powder mixing in a pilot-scale continuous mixer. Prior to developing process control strategies, new developments have been presented for better understanding continuous mixing of two components. Hold-up weight and relative hold-up weight distribution of each component in the whole mixer have been experimentally investigated under different operating conditions. An improved Markov chain model has been finally presented to predict the mean concentration of the mixtures obtained at the mixer's outlet. The implementation of a proportional-integral-derivative (PID) controller has been experimentally performed as an initial attempt to real-time control the homogeneity of the mixture produced. The rotational speed of the stirrer, identified as an important deciding factor towards the mixer's efficiency, has been considered as the manipulated variable. The closed-loop control is based on either the mean concentration or the relative standard deviation. The performances of the proposed closed-loops have been evaluated for continuous mixing subjected to step changes in feed rates of the mixer. Four case studies have been defined and presented. The main challenge in the process control system is the tuning of PID parameters. The performance of closed-loop control of either the mean concentration or the relative standard deviation has been compared to open-loop operation.

Key words: Continuous powder mixing, Implementation, Process control, Markov chain, PID controller, Closed-loop control

TITRE: Contribution à l'implémentation d'un système de contrôle-commande pour mélange de poudres en continu

RESUME

Le mélange de poudres est une opération essentielle dans divers domaines industriels, tels que les produits pharmaceutiques, agro-alimentaires, ciments, etc. Le mélange de poudres en continu, comme alternative intéressante au mélange conventionnel en batch, suscite beaucoup d'intérêt surtout en raison de sa capacité à gérer de grands volumes de production. Ce travail vise à contribuer à l'implémentation des applications de contrôle-commande. Avant de développer des stratégies de contrôle-commande, de nouveaux développements ont été présentés pour mieux comprendre le mélange continu de deux composants. La masse retenue et la répartition relative de la masse retenue de chaque composant dans le mélangeur ont été étudiées et prédites sous les différentes conditions opératoires. L'amélioration d'un modèle basé sur les chaînes de Markov a été finalement présentée pour prédire la concentration moyenne des mélanges obtenus à la sortie du mélangeur. L'implémentation d'un contrôleur PID a été expérimentalement réalisée comme une première tentative pour contrôler en temps réel l'homogénéité du mélange produit. La vitesse de rotation du mobile d'agitation, identifiée comme un facteur important influençant l'efficacité du mixer, a été considérée comme la variable manipulée. La commande en boucle fermée est basée soit sur la concentration moyenne, soit sur le coefficient de variation. Les performances des boucles fermées proposées ont été évaluées pour le mélange continu subi à des changements d'échelon dans les débits d'alimentation du mélangeur. Quatre études de cas ont été définies et présentées. Le défi principal dans le système de contrôle-commande est le réglage des paramètres PID. La performance de commande en boucle fermée soit de la concentration moyenne, soit du coefficient de variation a été comparée à l'opération en boucle ouverte.

Mots clés: Mélange de poudres en continu, Implémentation, Contrôle-commande, Chaînes de Markov, Contrôleur PID, Commande en boucle fermée